technische universität dortmund

MAX-PLANCK-INSTITUT FÜR MOLEKULARE PHYSIOLOGIE

A cell fusion interaction network during the mating of *Saccharomyces cerevisiae*

Dissertation

zur Erlangung des akademischen Grades
eines Doktors der Naturwissenschaften
der Fakultät für Chemie und Chemische Biologie
der Technischen Universität Dortmund

(Dr. rer. nat.)

Angefertigt in der
Abteilung für Strukturbiochemie am
Max-Planck-Institut für molekulare Physiologie

Vorgelegt von

Angela Hagemeier

Juli 2023

Erstgutachter: **Prof. Dr. Stefan Raunser**

Abteilung für Strukturbiochemie

Max-Planck-Institut für molekulare Physiologie

Fakultät für Chemie und Chemische Biologie

Technische Universität Dortmund

Zweitgutachter: **Prof. Dr. Stefan Westermann**

Arbeitsgruppe Molekulare Genetik I

Zentrum für Medizinische Biotechnologie, Essen

Fakultät für Biologie

Universität Duisburg-Essen

Die vorliegende Arbeit wurde in der Arbeitsgruppe von Dr. Matias Hernandez in der Abteilung für Strukturbiochemie am Max-Planck-Institut für molekulare Physiologie unter der Leitung von Prof. Dr. Stefan Raunser im Zeitraum Juni 2019 bis März 2023 erstellt.

Datum des Einreichens der Arbeit: 12.07.2023

Table of contents

TABLE OF CONTENTS

List of figures

List of tables

Abbreviations

Table 1: Abbreviations used in this study.

Abbrevation	Meaning
Aa	Amino acids
Amp	Ampicillin
APS	Ammonium persulfate
BHK	Baby hamster kidney
BiFC	Bimolecular fluorescence complementation
bp	Base pairs
C-GFP	C-terminal split GFP
Ca^{2+}	Calcium ions
ConA-647	Concanavalin A, Alexa Fluor 647 conjugate
ConA-Tet	Concanavalin A Tetramethylrhodamine
DAPI	4',6-Diamidino-2-phenyl-indol-dihydrochlorid
DMSO	Dimethyl sulfoxide
DNA	Deoxyribonucleic acid
dNTP	Deoxynucleotide triphosphate
DO	Drop out
Dol-P	Dolichol phosphate
Dol-PP	Dolichol pyrophosphate
E. coli	*Escherichia coli*
EDTA	Ethylenediaminetetraacetic acid
eGFP	Enhanced green fluorescent protein
ER	Endoplasmic reticulum
et al.	et alia
FAST	Fusion-associated small transmembrane
FM4-64	(*N*-(3-Triethylammoniumpropyl)-4-(6-(4-(diethylamino)phenyl)hexatrienyl)pyridinium dibromide)
gDNA	Genomic DNA
GEF	Guanine nucleotide exchange factor
GOI	Gene of interest
gp	Glycoprotein
GPCR	G protein-coupled receptor
GPI-AP	Glycosyl-phosphatidylinositol anchored protein
GTP	Guanosine triphosphate
HA	Hemagglutinin
His	Histidine

HOG	High osmolarity glycerol
Ig	Immunoglobulin
kb	Kilo base pair
kDa	Kilo daltons
LACS	Low affinity Ca^{2+} influx system
LB	Lysogeny Broth
LDs	Lipid droplets
Leu	Leucine
LiAC	Lithium acetate
Lys	Lysin
MAPK	Mitogen activated protein kinase
MES	2-(N-morpholino)ethanesulfonicacid
Met	Methionine
min	Minute(s)
mM	Milli molar
mNG	mNeonGreen
MW	Molecular weight
N-GFP	N-terminal split GFP
NaF	Sodium fluoride
NaN3	Sodium azide
OD_{600}	Optical density at 600 nm
ORF	Open reading frame
PAGE	Polyacrylamide gel electrophoresis
PBS	Phosphate Buffered Saline
PCR	Polymerase chain reactions
PEG	Polyethylen glycol
pH	Potentia hydrogenii
PIC	Protease inhibitor cocktail
PMSF	Phenylmethyl sulfonylfluoride
RT	Room temperature
SC	Standard Complete
SD-URA	Standard Defined-Uracil
SDS	Sodium dodecyl sulfate
SE	Sterol ester
sec	Seconds
SORB	Sorbitol
ssDNA	Single stranded DNA
TAG	Triacylglycerol
TAF	Tris-HCl (pH 7.4), NaN3, NaF in PBS

TCA	Trichloracetic acid
TEMED	Tetramethylethylenediamene
TMD	Transmembrane domain
Tris	Tris(hydroxymethyl)-aminomethane
Ura	Uracil
WT	Wild type
YPD	Yeast extract peptone dextrose
ZP	Zona pellucida
β-ME	β-mercaptoethanol

Abstract

Cell-cell fusion is essential for sexual reproduction and occurs when the lipid membranes of two distinct cells merge into one continuous bilayer. While in recent years some general aspects have been uncovered, the underlying molecular mechanism remains poorly understood. Mating of haploid *Saccharomyces cerevisiae* cells of the opposite sex provides an ideal model system to study plasma membrane (PM) fusion in eukaryotic organisms. In this work, a multicolor flow cytometry assay based on fluorescent complementation (BiFC) of split-GFP was adapted to screen a customized yeast knockout library (YKO) for fusion defects. In total, 28 mutants were identified that exhibited fusion levels at least as defective as Δ*prm1*, a known regulator of this step. Like Δ*prm1*, the majority displayed a bilateral fusion defect.

The remaining part of the work focused on an in-depth analysis of select gene of interest (GOI) mutants. Investigations of synergistic relationships in *trans* revealed an interaction network operating during PM fusion involving at least four independent yet partially overlapping fusion pathways. Previously two pathways with *ERG6* and *PRM1* have been reported. *VMA2,* a gene encoding a subunit of the vacuolar membrane ATPase (V-ATPase), was revealed in this work to operate on a third pathway. The findings show that the V-ATPase i) promotes cell fusion indirectly by acidifying endomembrane organelles, ii) facilitates both cell wall (CW) remodeling and PM fusion stages approximately equally, and iii) synergistically interacts with 12 other genes identified in this study. *CAX4* was identified to operate on the fourth pathway and the only novel gene found to synergize with *PRM1*. Further investigations revealed that Prm1p was less abundant in a Δ*cax4* sensitized background, while its localization is not affected.

Finally, this work discovered that several subunits of the RNA polymerase II mediator complex are involved in promoting early and late stages of yeast mating. The deletion of subunits leads to varying degrees of defects in cell pairing and pheromone secretion as well as CW remodeling and PM fusion. Together, these findings suggest that the mediator complex acts as a master regulator of cell fusion perhaps by synchronizing the expression of mating genes needed at crucial time points starting from the digestion of the CW up to the merging of the PMs.

Zusammenfassung

Die Zell-Zell-Fusion ist ein essentieller Prozess für die sexuelle Fortpflanzung. Dabei verschmelzen die Lipidmembranen zweier verschiedener Zellen zu einer kontinuierlichen Doppelmembran. Einige generelle Aspekte wurden in den letzten Jahren aufgedeckt, jedoch bleibt der zugrunde liegende molekulare Mechanismus nach wie vor wenig verstanden. Der Paarungsprozess von haploiden *Saccharomyces cerevisiae*-Zellen unterschiedlicher Geschlechter eignet sich als ideales Modellsystem für die Erforschung von Plasmamembran(PM-)fusion in eukaryontischen Organismen. In dieser Arbeit wurde mit Hilfe eines Mehrfarben-Durchflusszytometrie-Assays basierend auf Fluoreszenzkomplementierung (BiFC) von Split-GFP eine individualisierte Hefe-deletionsbibliothek (YKO) auf Fusionsdefekte untersucht. Dabei wurden 28 Mutanten identifiziert die mindestens so defekt waren wie Δ*prm1*, ein bekannter Regulator dieses Schritts. Wie Δ*prm1* wies die Mehrheit einen bilateralen Fusionsdefekt auf.

Der verbleibende Teil der Arbeit befasste sich eingehend mit der Analyse einer Mutanten-bibliothek ausgewählter Gene. Die Untersuchungen synergistischer Beziehungen in *trans* deckten ein Interaktionsnetzwerk auf, das bei der PM-Fusion aktiv ist. Dieses umfasst mindestens vier unabhängige, sich jedoch teilweise überschneidende Fusionspfade. Bisher wurden zwei dieser Pfade mit *ERG6* und *PRM1* beschrieben. *VMA2*, ein Gen, welches für eine Untereinheit der Vakuolarmembran-ATPase (V-ATPase) kodiert, wurde in dieser Arbeit als dritter Pfad identifiziert. Die Ergebnisse zeigen, dass die V-ATPase i) die Zellfusion indirekt durch Ansäuerung von Endomembranorganellen begünstigt, ii) den Umbau der Zellwand (CW) und die PM-Fusion in etwa gleichem Maße fördert und iii) synergistisch mit 12 anderen in dieser Studie identifizierten Genen interagiert. *CAX4* agiert auf dem vierten Pfad und ist das einzige neu identifizierte Gen, das mit *PRM1* synergiert. Weitere Untersuchungen ergaben, dass Prm1 in einem Δ*cax4* sensibilisierten Hintergrund weniger stark exprimiert wird, jedoch die Lokalisierung unbeeinträchtigt ist.

Diese Arbeit zeigt außerdem, dass mehrere Untereinheiten des RNA-Polymerase-II-Mediator-Komplexes an der Förderung früher und später Stadien der Hefepaarung beteiligt sind. Die Deletion von Untereinheiten führt zu unterschiedlich ausgeprägten Defekten in der Zellpaarung und Pheromonsekretion sowie beim CW-Umbau und der PM-Fusion. Zusammengenommen deuten diese Ergebnisse darauf hin, dass der Mediator-Komplex als Hauptregulator der Zellfusion fungiert, indem er möglicherweise die Expression von Paarungsgenen synchronisiert, die zu entscheidenden Zeitpunkten benötigt werden, beginnend mit der Verdauung der CW bis hin zur Verschmelzung der PMs.

1. Introduction

1.1 Diverse spectrum of membrane fusion

Membrane fusion is characterized by the merger of two distinct lipid bilayers into one continuous bilayer allowing internal content mixing. It is an ubiquitous event occurring between cellular compartments or between cellular compartments and the plasma membrane enabling cargo transfer or exocytosis. Fusion can also occur between enveloped viruses with the host cell membrane to gain access to the cytosol, or between two cells, which is an essential process for organ development and sexual reproduction. Chapter 1 will provide an overview about a basic concept of membrane fusion and specialized proteins, called fusogens, mediating this process. Examples of fusogens in diverse cellular systems will be described while one section will be dedicated to the fungal eukaryote *S. cerevisiae*, as it is the model system used in this work to study plasma membrane fusion between cells during sexual reproduction.

1.2 Membrane fusion via a hemifusion stalk pore formation

Although the requirements might differ for intracellular, extracellular or viral-cell fusion, the general aspects of the fusion process seem to be similar. Initially, the target membranes are brought in close proximity. Because of opposing electrostatic forces between the charged lipid bilayers and steric crowding from membrane bound proteins, the closest distance between apposing membranes is no closer than 10-20 nm [1]. Since bringing the membranes together is an energetically costly event, a fusion pore is unlikely to be directly formed simply by pulling [1-3]. Instead, fusion is thought to proceed through a hemifusion intermediate. Originally, a stalk-mechanism was proposed in which the proximal monolayers of apposing membranes merge into an hourglass shape (**Figure 1**). This structure gave the model its name and represents the lowest energy structure between the partially fused membranes [4, 5]. Radial expansion of the stalk leads to the formation of a hemifusion diaphragm in which the distal leaflets form a new bilayer separating the luminal contents [1-3]. Destabilization of the hemifusion diaphragm then leads to the opening and expansion of a fusion pore, completing the fusion process [1, 6].

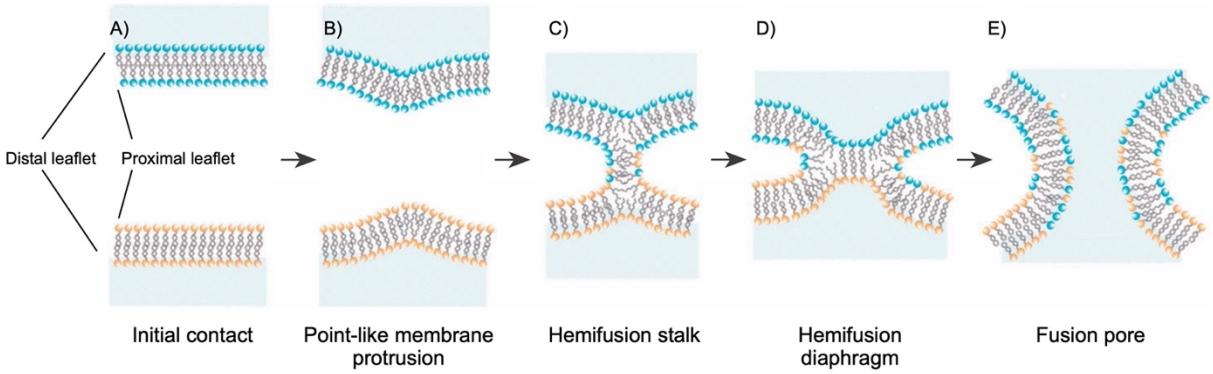

Figure 1: Membrane fusion occurs via a hemifusion stalk pore formation. A) Pre-fusion events bring membranes in close proximity. B) A point-like membrane protrusion establishes the first contact. C) Hemifusion stalk formation with fused proximal leaflets and unfused distal leaflets. D) Stalk expansion results in the formation of a hemifusion diaphragm with merged inner distal leaflets. E) Disruption of the hemifused single bilayer leads to formation of a fusion pore followed by luminal content mixing. The fusion process of two separated lipid compartments into one is complete. Figure adapted from Marsden et al., 2011 [3].

1.3 Fusogens mediate membrane fusion in cells

Spontaneous and uncontrolled fusion of membranes would lead to unstable membrane structures. High kinetic energy barriers need to be overcome to make fusion an energetically favorable process [7]. Fusogens act at the final distance of about 10 nm between apposing membranes and surmount the energetically demanding tasks of dehydration of polar head groups, allowing hemifusion stalks and fusion pore opening and expansion [8]. Three criteria define a *bona fide* biological fusogen: i) it is expressed at the appropriate place and time of membrane merger, ii) its fusogenic activity is essential for the process, and iii) it is sufficient to mediate fusion in membranes that would usually not fuse [7-10]. Fusogens can either act bilaterally, meaning its presence is required on both fusing membranes, or unilaterally, meaning its presence is sufficient on only one of the fusing membranes and can be further distinguished between heterotypic or homotypic [8, 11]. Heterotypic fusogens mediate fusion between two dissimilar types of membranes such as an endosomal membrane with a Golgi membrane, whereas homotypic fusogens mediate fusion between two similar membranes, like vacuole-to-vacuole fusion [11].

Hitherto, only a select few fusogens mediating cell-cell fusion have been identified. Among them, the EFF-1 and AFF-1 proteins in *Caenorhabditis elegans* (*C. elegans*) involved in organ

and tissue formation, the Myomerger and Myomixer mediating myoblast fusion in vertebrates and Syncytins enabling placenta trophoblast fusion. So far, only HAP2 was identified to mediate gamete fusion in plants, algae and protists, and more recently the IZUMO1 in vertebrates. However, the fusogenic machinery promoting membrane merger during sexual reproduction in fungi remains elusive, including whether it is composed of a single protein or a protein complex. Since so little is known about the composition of the fusogenic machinery across different organisms, it is important to identify them and uncover their common ancestry to elucidate when they mechanistically diverged to adjust to their biological environments [8, 12].

Well-studied *bona fide* fusogens include the viral fusogen Hemagglutinin HA2 subunit from the influenza virus, and the soluble N-ethylmaleimide-sensitive factor attachment protein receptor (SNARE) proteins mediating intracellular membrane fusion. With these two case studies, a basic understanding on the principles of how fusogens fuse their membranes can be obtained and will be further described in the following sections.

1.3.1 Virus-cell fusion: Influenza hemagglutinin HA2

By fusing the viral membrane with the cell membrane, enveloped viruses release their genetic material in the cytosol and infect their target cells. Over the years, four classes of viral fusogens have been identified based on their 3D-structure in the pre- and/ or post-fusion formation [13-15]. Class I viral fusogens comprise of α-helical hairpin and are found e.g. in the human immunodeficiency virus (HIV) gp41 and influenza viruses. Class II fusogens are mostly composed of ß-sheets and are found in the dengue virus glycoprotein. Class III fusogens are defined by a structural combination of both class I and class II fusogens, as found in rabies virus G glycoprotein. Differently from the previous classes, class IV fusogens are composed of fusion-associated small transmembrane (FAST) proteins that are encoded by non-enveloped reoviruses [14]. Beside FAST proteins which follow a distinct fusion mechanism not through a hemifusion state and do not contain a fusion peptide, the other three classes are believed to share a similar mechanism of fusion (**Figure 2**). Most of the viral fusogens are activated by conformational changes following specific on-cue triggers such as exposure to low pH within the endocytic pathway, binding to a (co-)receptor of the target cell, or a combination of both [16]. Such conformational changes lead to exposure of a hydrophobic fusion peptide or

amphiphilic fusion loop that permits interaction with lipid bilayers. This interaction causes destabilization of the membrane, a process that is sufficient to overcome the kinetic barriers to initiate a fusion stalk [14].

The Hemagglutinin (HA) subunit from the influenza virus is an example for a well characterized class I viral fusogen. In crystallographic studies it was shown that HA assembles into a homo-trimeric protein composed of α-helices. Initially, the inactive precursor of the trimeric glycoprotein, designated as HA0, requires proteolytic processing by a host-cell protease to produce a complex consisting of a HA1 and HA2 subunit. The virus gains access to the host cell by binding of the HA1 domain to a receptor located on the host cell. After cellular uptake into endosomal compartments, the low pH shift causes a conformational change in which HA2 exposes a N-terminal hydrophobic fusion peptide. The fusion peptide extends out, forms a pre-hairpin structure and inserts into the target membrane. The extended structure then foldbacks into a hairpin-like structure that pulls the viral and target membrane together via a hemifusion intermediate stalk that results in pore opening and expansion [17, 18]. For influenza virus, it was shown that a truncated fusogen with a mutation in its trans-membrane domain (TMD) region of the fusion peptide results in a hemifusion arrest, demonstrating that the full-length protein is required [8, 19, 20]. This suggests that TMDs not only serve as a membrane anchor, but also play an active role in the transition between hemi-fusion and full-fusion stages [19, 20].

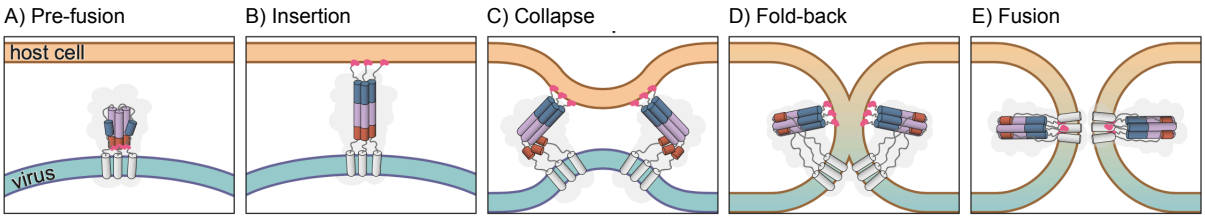

Figure 2: Schematic of class I viral membrane fusion. A) Pre-fusion state. B) Receptor-binding or acidic pH triggers a conformational change leading to the exposure of a hydrophobic fusion peptide. The fusion peptide extends out, forms a pre-hairpin structure and inserts into the target membrane. C) Insertion-induced membrane collapse. D) A foldback of the extended structure pulls the membranes in close proximity. E) Fusion pore formation and expansion via a hemifusion intermediate. Figure adapted from Ebel et al., 2022 [21]

1.3.2 Intracellular membrane fusion: SNARE proteins

The key players in mediating intracellular membrane fusion and exocytosis within the eukaryotic secretory pathway are SNARE (Soluble NSF Attachment Protein Receptor) proteins. SNAREs are a superfamily of small fusion proteins that are composed of a conserved SNARE motif that consists of 60-70 amino acids arranged in heptad repeats, one trans-membrane domain at the C-terminal end that is connected to the motif by a linker and a non-conserved more variable N-terminal domain [22, 23]. Initially, SNAREs were classified according to their subcellular localization either into v-SNAREs located on the vesicle membrane, or t-SNAREs located on the apposing target membrane. Later, based on their structural features SNAREs were re-classified into R- or Q-SNAREs depending on whether they contained an arginine (R) or glutamine (Q) on a highly-conserved residue of the motif [22].

Unlike viral fusogens, SNAREs are bilateral fusogens that promote fusion between heterotypic membranes (**Figure 3**) [22]. Typically, three α-helix domains from Q-SNAREs and one from R-SNAREs form a complex that assembles into a coiled coil four helical bundle. The assembly occurs in a zippering-like fashion starting at the N-terminus towards the TMDs at the C-terminus, generating a strong pulling force [7, 22, 23]. As shown for the viral fusogen HA2, perturbations in the SNARE complex can lead to a hemi-fusion arrest in which the outer leaflets are merged while the inner leaflets are not [24, 25].

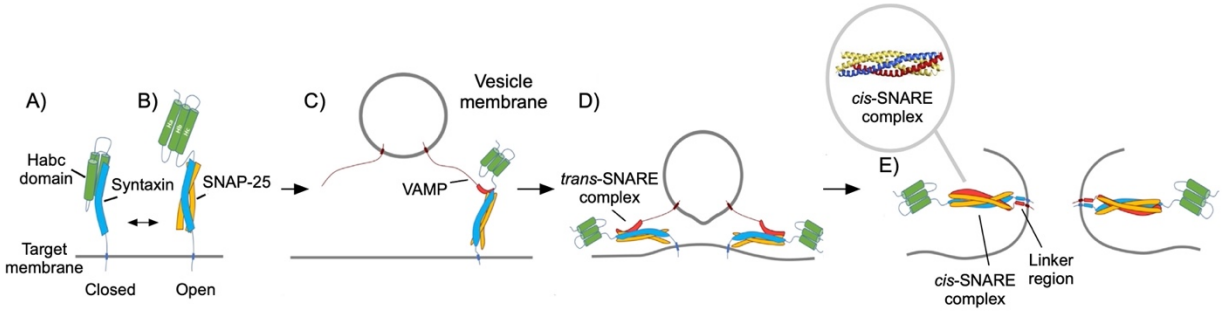

Figure 3: Schematic of SNARE-mediated membrane fusion. A, B) Syntaxin undergoes a conformational change, shifting from a closed to an open state. It then binds with two additional Q-SNARE motifs to form a pre-complex of Q-SNARE proteins. C, D) Formation of a tight SNARE complex by "zipping" towards the transmembrane domains to overcome increasing repulsion forces. E) The generated pulling force brings the membranes together, which then fuses through a hemi-fusion intermediate. Figure adapted from Yoon & Munson, 2018 [26].

1.4 Cell-cell fusion

Cell-cell fusion is an essential physiological process for sculping organs such as muscles and bones and for fusing gametes in sexually reproducing organisms. A dysfunction of this process can therefore lead to pathological conditions such as myo- and osteopathy, infertility or even cancer [11]. This emphasizes the importance of understanding the underlying mechanism driving this process.

Compared to viral-cell fusion and intracellular membrane fusion, fusion between cells is more complex. Before fusing their membranes, cells usually undergo three pre-fusion stages: i) in response to extracellular or intracellular stimuli cells differentiate into fusion competent cells; ii) cells that are destined to fuse recognize each other and iii) adhere tightly. At the end, the two apposing membranes are closely positioned within a ~10 nm distance [11, 27]. Recent understanding about how cells fuse their plasma membranes has been demonstrated by the identification of certain fusogens in diverse organisms, of which some will be further described in the following sections.

1.4.1 Epithelial fusion in *C. elegans*: EFF-1 and AFF-1

In the nematode worm *Caenorhabditis elegans (C. elegans)*, a variety of epithelial cell fusion events occur such as fusion of the hypodermis, pharynx, vulva and excretory glands. About one third of mononucleated syncytial cells were found to fuse and generate multinucleated cells that initiates the formation of syncytia [28]. Through genetic screens, the genes epithelial fusion failure 1 (*EFF-1*) and its paralog anchor fusion failure 1 (*AFF-1*) were identified as essential for fusion. Both encode for type I transmembrane glycoproteins and cause a fusion block in its absence leading to defects in sculpting of organs and tissues in embryos and larvae [8, 29, 30].

The fusogenic activity of both *EFF-1* and *AFF-1* was demonstrated by ectopic expression in *C. elegans* embryos which induces fusion of epithelial cells that would normally not fuse. Also, in insect or mammalian cultured cells fusion is induced when *EFF-1* or *AFF-1* are ectopically expressed [10, 30-32]. Furthermore, the replacement of the fusogenic glycoprotein in pseudotyped vesicular stomatitis virus (VSV) with *AFF-1* resulted in fusion with the host

membrane when either *EFF-1* or *AFF-1* were present on the host cell as well. This indicates that *EFF-1* and *AFF-1* follow a bilateral requirement and can act either homo-or heterotypically in *trans* via a similar fusion mechanism [8, 32, 33].

1.4.1.1 EFF-1 shares structural homology to viral class II fusogens

Interestingly, the crystal structure of the ectodomain of Eff1 was shown to share structural homology to the post-fusion hairpin conformation of viral class II fusion proteins. EFF-1 however differentiates from viral fusogens in some aspects: i) its presence is necessary on both fusing membranes and ii) it lacks a hydrophobic fusion loop enabling the insertion into the target membrane. Instead, a fusion mechanism was proposed in which EFF-1 brings the membrane in close proximity in a zipper-like manner such as observed in SNAREs (**Figure 4**) [8, 32]. Taken together, this indicates that both EFF-1 and viral class II fusogens share a common ancestry but have diverged mechanistically to adapt to specific biological scenarios [8].

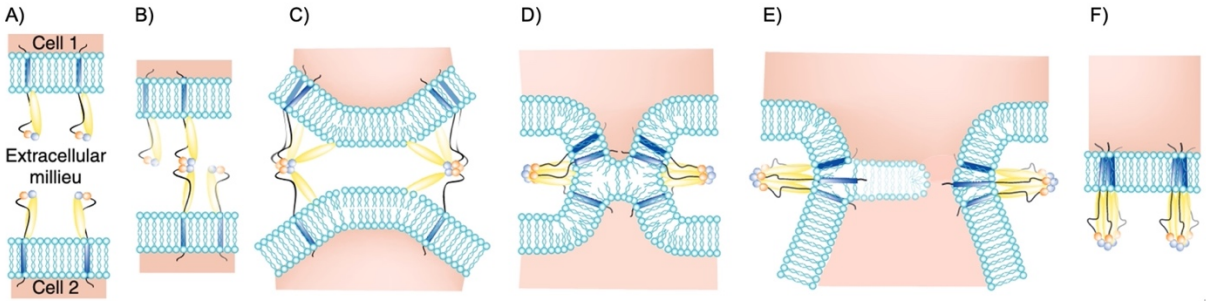

Figure 4: Schematic of EFF-1 induced membrane fusion in *C. elegans*. a) *EFF-1* is expressed on both fusing membrane as monomers. b) Initial contact induces assembly into trimers bringing the membranes closer together. c) Fold back of the EFF-1 trimer in a zippering-like fashion causes hemifusion. d) Initial fusion pore formation. e) Fusion pore expansion and cytoplasmic content mixing. f) Post-fusion state. Figure taken from Palfreyman & Jorgensen, 2015 [34].

1.4.2 Myoblast fusion in vertebrates: Myomaker and Myomerger

Myoblast fusion is essential for skeletal muscle development and regeneration. Merger of individual myoblasts leads to formation of multinucleated myotubes, a process that is regulated by two muscle-specific proteins: Myomaker and Myomerger/Myomixer/Minion [35, 36]. Myomaker, a seven-pass transmembrane (TM) protein, was the first identified. In its absence, myoblasts fail to form syncytia in mice in cultured cells [35]. Expression of Myomaker was shown to induce fusion between muscle cells and fibroblasts, whereas fibroblasts failed to

fuse among themselves. This implied that additional myogenic factors are required to mediate this process [35, 36]. Later, Myomerger/Myomixer/Minion was identified by three independent groups to induce fusion in fibroblasts when co-expressed with Myomaker [37-39]. Myomerger is a small single-pass TM protein with a fusogenic extracellular C-terminus (ectodomain). As its primary sequence differs from classical fusogens with long extracellular domains, Myomerger has been proposed to mediate fusion in a similar fashion to FAST proteins (section 1.3.1) [40, 41] .

Further investigations revealed that Myomaker is required on both fusing membranes, whereas Myomerger is only required on one. This suggested that both are acting at different steps in fusion, in which Myomaker acts upstream for gaining of fusion competence and Myomerger downstream conferring fusogenic activity [37-39]. Evidence for this hypothesis was provided via an assay that monitored lipid- and content mixing of myoblasts lacking either Myomaker or Myomerger [42]. This assay allowed to distinguish between hemifused, in which only the lipids of the outer leaflet have mixed, from initial fusion pore formation and opening allowing content mixing. Indeed, Myomaker promotes hemifusion competence even in the absence of Myomerger. However, without the presence of Myomerger, cells arrest as a hemifused intermediate. In contrast, Myomerger has no effect on hemifusion. Instead, it initiates membrane stress that induces cell fusion even in the absence of Myomaker. Moreover, applying membrane stress was sufficient to initiate pore formation and compensate for the lack of Myomerger.

Therefore, it is proposed that unlike viral fusogens and EFF-1 in which only one protein is mediating fusion, myoblast fusion requires the presence of at least two distinct proteins. Myomaker for hemifusion formation and Myomerger for downstream fusion events including pore formation, opening and expansion [42]. This step-wise mechanism is likely to serve as an additional regulatory checkpoint assuring proper cell fusion during organ sculpting, an evolutionary strategy developed in higher organisms [38, 42].

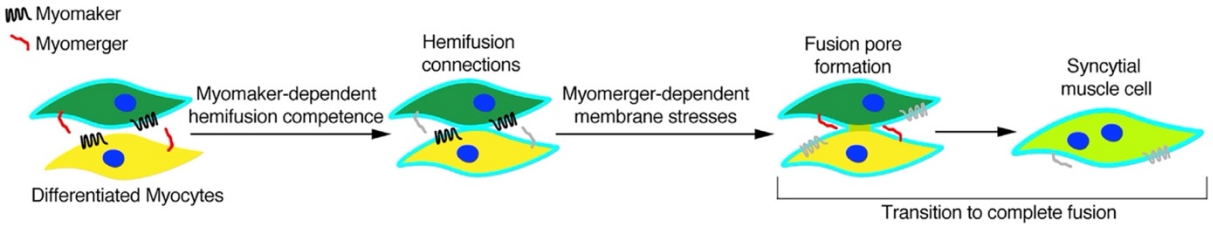

Figure 5: Schematic of step-wise mediated myoblast fusion by Myomaker and Myomerger. Myomaker and Myomerger facilitate fusion independently at different stages: 1) Myomaker initiates hemifusion competence; 2) Myomerger induces membrane stress and initiates pore formation resulting in fusion and syncytia formation. Figure taken from Leikina et al. (2018) [42].

1.4.3 Gamete fusion in invertebrates: HAP2/GSC1

In the last two decades studies on fusogens mediating gamete fusion during fertilization have mainly focused on the gamete-specific protein Hapless2 (HAP2) and its ortholog Generative Cell Specific 1 (GSC1) in flowering plants, protists and invertebrates. At first, independent studies identified *HAP2* and *GSC1* in the plants *Arabidopsis thaliana* (*A. thaliana*) and *Lilium longiflorum* (*L. longiflorum*) respecitively [43, 44]. Later, gene orthologous of *HAP2*/*GCS1* were also found in the unicellular protist such as *Plasmodium falciparum (P. falciparum*), in the algae *Chlamydomonas reinhardtii* (*C. reinhardtii*) or invertebrate animals such as honeybees. Indeed, one has found both *HAP2*/*GSC1* in almost all common eukaryotic organisms except for fungi or chordata [45, 46]. Both genes encode for a conserved type I TM protein with an extracellular domain of ~ 600 aa and a short intracellular cytoplasmic tail [8, 44, 45, 47]. The ectodomain of *HAP2* was found to insert into the membrane when transitioning from the monomer state into a stable homotrimer state. Furthermore, crystallographic studies revealed that the trimeric post-fusion form was similar to those found in viral class II fusogens and EFF-1 [48-51]. Fusogenic activity was confirmed by ectopic overexpression of *A. thaliana HAP2* in heterologous mammalian cells which resulted in multinucleation and cytoplasmic content mixing via a hemifusion intermediate. In addition, VSV virus expressing *A. thaliana HAP2* instead of the viral glycoprotein (VSVΔG-*HAP2*) resulted in homotypic virus-cell fusion [50].

1.4.3.1 HAP2 and EFF-1 follow a similar fusion mechanism

Interestingly, cells expressing VSVΔG-*HAP2* fuse with cells expressing *EFF-1* implying a similar fusion mechanism between both. In addition, it suggests a bilateral fusion mechanism of HAP2

[8, 50]. Surprisingly, *C. reinhartii HAP2* expression was found to be only required on the minus gamete (male gamete) to induce fusion suggesting a unilateral fusion mechanism [43, 47, 49, 52]. The discrepancy between a bilateral requirement in heterologous systems and an unilateral requirement in its native physiological context implies that *HAP2* might need the presence of other proteins on the apposing membrane for correct positioning and / or assembly [8, 49, 52].

1.4.3.2 HAP2 requires MAR1-FUS1 formation to mediate PM fusion

A recent study on *C. reinhartii HAP2* identified a membrane protein, Minus Adhesion Receptor 1 (*MAR1*) located on minus gametes, to functionally associate with *HAP2* and to be essential for its expression and localization. Furthermore, *MAR1* also interacts with *FUS1*, which encodes a plus gamete-specific membrane protein important for adhesion; thus, *MAR1* connects both processes. The formation of a *FUS1-MAR1* pair was found to be critical for the induction of *HAP2* mediated membrane fusion [46]. A model was proposed in which the binding of MAR1 to FUS1 induces fusogenic conformational changes within HAP2 into its trimer configuration which is required for membrane merger. Therefore, HAP2 likely mediates fusion by itself when certain pre-requisites are given [46, 51, 53].

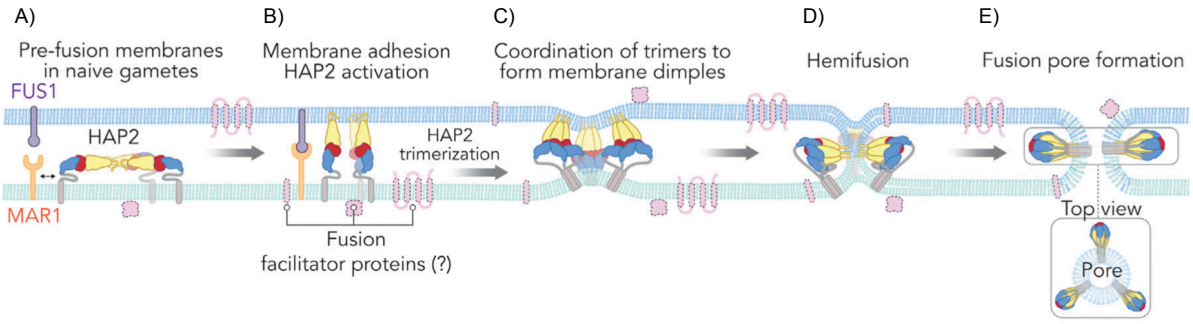

Figure 6: Schematic of HAP2 mediated gamete fusion in *C. reinhardtii*. A) Pre-fusion state with *MAR1* and *HAP2* expressed on the minus gamete and *FUS1* expressed on the plus gamete. B) Formation of Mar1-Fus1 receptor pairs initiates Hap2-trimer formation and fusion loop interactions with apposing membrane. C) Conformational changes anchor TMDs and fusion loops of HAP2 in both membranes and brings the two membranes in close proximity. D) Formation of a hemifusion intermediate is driven by a foldback of HAP2 trimers that pulls the membranes together. E) Fusion pore formation. Figure taken from Pinello & Clark, 2022 [53].

1.4.4 Superfamily of fusion proteins: Fusexins

The shared structural and functional characteristics of HAP2, EFF-1 and viral class II fusogens indicate a common ancestry. Together they form one superfamily of proteins called fusexins. Fusexins are fusion proteins essential for sexual reproduction and exoplasmic merger of PMs [50]. Two scenarios are discussed to explain the origin of fusogens: i) cell hypothesis and ii) virus hypothesis. According to the cell hypothesis, viral fusexins are thought to have emerged through the acquisition of cellular genes encoding eukaryotic fusogens from various lineages [8, 49]. The virus hypothesis proposes that sexual fusexins originate from viruses which appeared before modern eukaryotic sexual reproduction [8]. Due to the lack of sequence conservation, it is challenging to solve this evolutionary enigma [54]. Recently, a new family of fusexin in Archae, called Fusexin1 (Fsx1), was discovered. This expanse the already existing "virus or the egg" dilemma by a third scenario in which gamete fusogens may origin from prokaryotes. Further research is needed to unravel the mechanisms of various fusogens [54].

1.4.5 Sperm-oocyte fusion in vertebrates: IZUMO1 and known effector proteins

Fertilization in mammals is tightly regulated and characterized by a series of following steps: i) sperm first undergo capacitation, a maturation process that enables ii) sperm binding and penetration through the envelope surrounding the oocyte, named zona pellucida (ZP), iii) following species specific gamete adhesion between the sperm and the oolemma (space between the ZP and the egg PM) allows iv) sperm-egg fusion to generate a zygote. v) Post-fusion events block further sperm binding to prevent polyploidy and ensure monospermic fertilization (**Figure 7**) [55, 56].

While *HAP2* is widely distributed in almost all eukaryotic organisms, *HAP2* orthologs in vertebrates are lacking suggesting the presence of undiscovered fusogen families with differently designed principles [8]. Thus far, a few proteins were identified that are essential in the last stages of fertilization such as the egg-specific proteins CD9, or the sperm-specific proteins Spaca6, Tmem95, Fimp, Sof1 and Dcst1/2 (section 1.4.5.4). However, at what step

these proteins promote fusion remains unclear. Interestingly, a recent study has revealed that the sperm-specific membrane protein IZUMO1 induces cell fusion in addition to its function in facilitating species specific gamete binding together with the egg-specific membrane protein Juno [56].

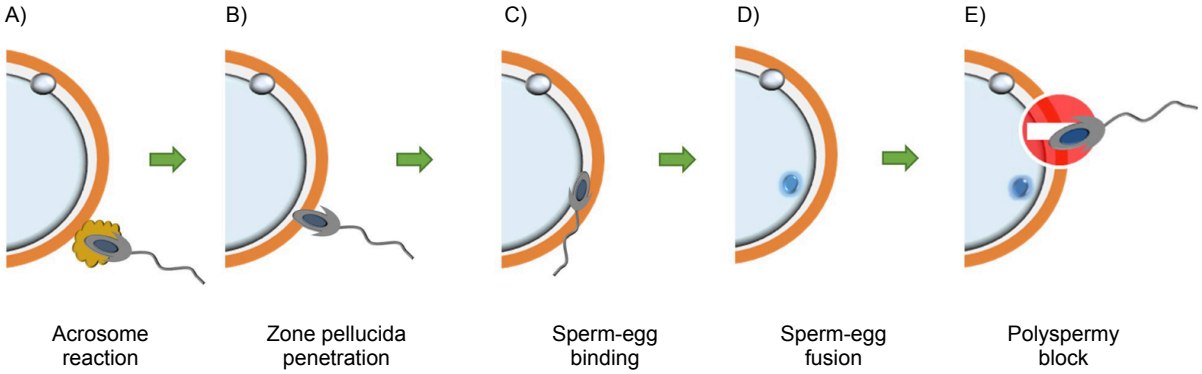

Figure 7: Schematic of sperm-egg fusion during mammalian fertilization. A) Fusion of the acrosomal membrane with the sperm PM leads to release of enzymes and exposure of previously sequestered sperm ligands. B) Acrosome-reacted sperm penetrates the ZP. C) Gamete-specific adhesion between sperm and oolemma. D) Gamete fusion and generation of a diploid zygote. E) Block of sperm-binding to prevent polyspermy. Figure adapted from Bianchi & Wright, 2020 [57].

1.4.5.1 IZUMO1-JUNO complex mediates gamete adhesion

Via a loss-of-function screen IZUMO1 was identified to be essential for sperm egg fusion in mice [58]. IZUMO1 is an immunoglobulin-(Ig-) like type I membrane protein that lacks a hydrophobic fusion loop or peptide and shows no homology to classical fusogens [56, 59]. It relocates to the fusion site of the PM in capacitated sperm and causes male infertility in its absence because sperm lacking IZUMO1 are capable to penetrate the ZP and adhere, but fail to fuse with the egg membrane [58, 60, 61].

Utilizing an Avidity-based Extracellular Interaction Screen (AVEXIS) a pairwise interaction with the glycosyl-phosphatidylinositol (GPI)-anchored membrane protein Juno was identified, the oocyte-expressed receptor of IZUMO1. This ligand-receptor interaction was found to be conserved across mammals [62]. It is hypothesized that the initial binding of IZUMO1 to JUNO induces conformational changes which in turn leads to its oligomerization enabling a possible interaction with a second receptor that brings the membranes closer together [56, 63, 64]. Upon membrane merger, JUNO sheds from the surface to prevent polyspermy [57, 65, 66].

1.4.5.2 IZUMO1 mediates gamete fusion in mice

Initially, heterologous expression of mouse *IZUMO1* in cultured HEK293T and COS-7 cells resulted in binding but not in fusion between sperm and egg which implied that the *IZUMO1*-*JUNO* interaction by itself was not sufficient to mediate fusion [58, 61, 67]. However, an additional role of *IZUMO1* beside promoting gamete adhesion was suggested because: i) the deletion of *IZUMO1* did not affect the binding of spermatozoa to the oolemma of ZP-free eggs, ii) the blocking of the N-terminal region with an antibody led to impaired fusion but did not affect the efficacy of the sperm to adhere to the egg and iii) differently to JUNO IZUMO1 remains enriched at the contact zone upon sperm-egg binding [56, 58, 68].

Recently, Benjamin Podbilewicz's group uncovered that mouse *IZUMO1* heterologously expressed in normally non-fusogenic baby hamster kidney (BHK) cells and human HEK293T cells results in syncytia formation and content mixing [52]. They identified that the fusogenic activity is partially provided by three exposed aromatic residues (F28, W88, W113) located on the four-helix bundle of the Izumo domain (**Figure 8**). A mutation of these three residues on the other hand does not affect the binding to Juno because BHK cells were still able to bind to the egg membrane. This indicates that the function of IZUMO1 in fusion is independent of its function in gamete adhesion together with Juno. This model is supported by the observation that the mutation of a residue on the hinge region (W148 residue), known to be required for Juno binding, does not affect fusion of BHK cells. These findings suggest the presence of two functional domains in Izumo1, one needed to mediate binding to Juno, and the other needed for efficient fusion. However, in a semi-heterologous system with *IZUMO1* expressed in BHK cells and *CD9* (tetraspanin effector protein in sperm egg-fusion) in mouse eggs induces only binding but no fusion. Thus, even though IZUMO1 is proposed as a unilateral fusogen it cannot exclude the possibility that additional co-factors are required to mediate the fusion process.

In summary, a model was proposed in which first, IZUMO1 transiently binds to Juno to establish membrane docking and secondly, mediates membrane fusion independently of JUNO but presumably via interaction with other proteins [56, 63].

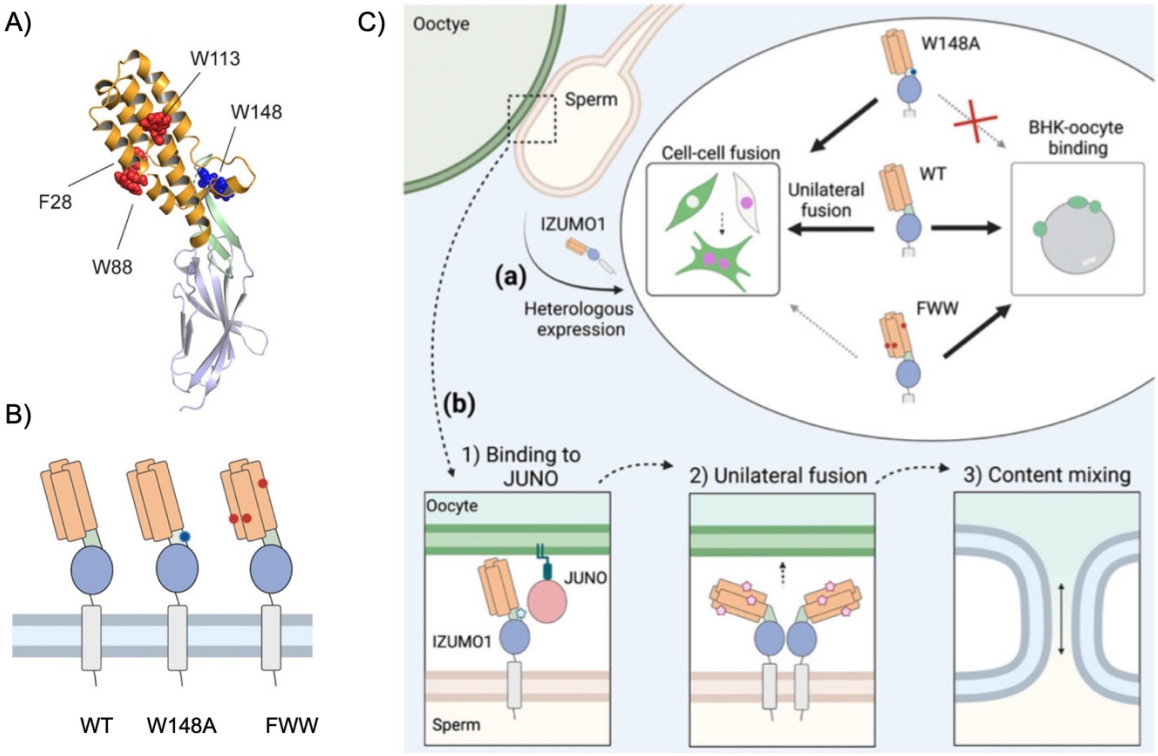

Figure 8: Schematic of IZUMO1 mediated gamete binding and fusion. A) IZUMO1 structure with the four-helix bundle (denoted orange), four aromatic residues: F28, W88, W113 (denoted in red), the hinge (denoted in light green) with the Ig-like domain (denoted in teal) and the JUNO-interacting W148 residue (denoted in blue). B) Schematic structures of WT IZUMO1, point-mutated W148A IZUMO1 (on the hinge) and triple mutated FWW IZUMO1 (on the four-helix bundle). C) (a) Different outcomes of heterologous expression of WT *IZUMO1*, W148A *IZUMO1* and FWW *IZUMO*. WT IZUMO1 unilaterally facilitates membrane fusion. W148A point mutation affects binding but not fusion of BHK cells to oocytes. Triple FWW mutation does not affect the binding of BHK cells to oocytes, but significantly reduces their fusion efficiency. (b) Left: Transient IZUMO1-JUNO interaction via W148 mediates gamete adhesion. Middle: Cell-cell fusion mediated by Izumo1in a unilateral manner supported by the action of the residues F28, W88 and W113. Right: Pore formation and cytoplasmic content mixing. Figure adapted from Brukman et al., 2023 [56].

1.4.5.3 Oocyte-specific protein: CD9

The oocyte-expressed membrane protein CD9 belongs to the tetraspanin family and was found to be required for gamete fusion in both mice and humans. CD9-deficient eggs are able to bind but not to fuse with the sperm membrane [69-72]. Even though the exact mechanism is unclear. The microvilli might be important since the absence of CD9 leads to microvilli of altered size, thickness and density resulting in an almost fusion block with spermatozoa [69, 70]. It also plays a role in adhesion activity of the oocyte via interaction of other proteins such as integrins. A recent study showed that CD9 is responsible for the induction of curvature in microvilli and a strict molecular organization of GPI-anchored proteins (GPI-AP), including Juno. The distinct

surface compartmentalization is proposed to restrict GPI-AP to the appropriate fusion zone of the oocyte [73].

1.4.5.4 Sperm-specific proteins: TMEM95, SPACA6, FIMP, SOF1

TMEM95

TMEM95 encodes a sperm acrosomal type I single pass transmembrane protein 95 which was identified through a CRISPR-KO screening in vivo for male fertility genes [74, 75]. Sperm lacking *TMEM95* have a normal motility and are able to penetrate the ZP and bind to the oolemma but then fail to fuse with the egg membrane and penetrate into the ooplasm. Fertilization is only achieved by mechanical injection of the sperm when bypassing membrane fusion showing that *TMEM95* is essential for the fusion process [74]. Even though the predicted secondary structure of TMEM95 showed α-helix and β-hairpin similar as found in the IZUMO1 domain, no interaction between TMEM95 and IZUMO1 or JUNO was detected. To be noted, residues on the β-hairpin TMEM95 differ to the one found in IZUMO1. In addition, HEK293T cells expressing *TMEM95* fail to fuse with HEK293T cells expressing either *IZUMO1* or *JUNO* [74].

Similar to IZUMO1, it was hypothesized that TMEM95 binds to eggs via a specific membrane-bound receptor. Solving the X-ray crystal structure at 1.5 Å resolution revealed an evolutionary conserved region with a positively charged surface. This region is proposed to serve as a putative egg-receptor binding site for TMEM95 since amino acid substitutions significantly reduced the egg-binding capability. Via a sperm penetration assay two monoclonal antibodies against different epitopes of TMEM95 were identified to decrease the number of fusion events between human sperm and hamster eggs without the egg-binding activity being affected. This indicates that TMEM95 has a potential role in membrane fusion. It was proposed that like IZUMO1, TMEM95 might undergoes conformational changes after binding to its hitherto unknown egg-receptor. Consequently, binding of the antibody may trap TMEM95 in a monomeric pre-fusion state. Alternatively, it is possible that the antibody inhibits the assembly of TMEM95 into a complex with other proteins or sterically hinders TMEM95 [76].

SPACA6

The sperm acrosome membrane-associated protein 6 (SPACA6) is a TM protein that causes in its absence male infertility. Similarly to *TMEM95*, *SPACA6*-deficient sperm are able to penetrate the ZP but show impaired fusion ability with the oocyte. Although no sequence homology exists, X-ray crystal structures revealed that the SPACA6 ectodomain shares structural similarities to the human Izumo1: a four-helix bundle and an Ig-like β-sandwich. Due to their structural relationship, it was therefore proposed that IZUMO1 and SPACA6 define a larger superfamily of gamete fusion-associated proteins. Since the depletion of both results in male infertility it implied that their functions are not redundant [72]. Interestingly, expression of *IZUMO1* can compensate for the loss of *SPACA6*, indicating that both act cooperatively [77]. Moreover, co-immunoprecipitation studies in HEK293T cells detected an interaction between full-length IZUMO1 and SPACA6. However, in-vitro studies with a recombinant ectodomain failed to reproduce this result, perhaps because of lacking either the C-terminal ectodomain linker or a TM helix, or alternative physiological requirements such as missing fusion facilitating proteins [72, 75].

FIMP

Similar to SPACA6 and IZUMO1, the fertilization influencing membrane protein (FIMP) is a type I TM protein that localizes to the sperm head. Sperm lacking *FIMP* can penetrate the ZP but rarely fuse with the oocyte [78]. Co-immunoprecipitation studies identified an interaction between FIMP and IZUMO1, however neither the localization nor the translocation of IZUMO1 was affected in *FIMP*-deficient sperm [75, 78, 79]. Moreover, *FIMP*-expressing HEK293T cells were unable to mediate binding or fusion to the oolemma. The exact function of FIMP remains to be uncovered [75].

SOF1

The testis enriched gene sperm-oocyte fusion required 1 (*SOF1*) encodes a TM protein that is conserved in almost all mammals providing male fertility. *SOF1*-deficient sperm show no altered morphology or motility, but are incapable to fertilize the oocyte and therefore accumulate in the perivitelline space after penetrating the ZP. This failure is however not

caused by mis-localization of IZUMO1 either before or after acrosome reaction. Moreover, SOF1 was found to presumably undergo post-translational modification because of the detection of two protein bands of different molecular weights. While during sperm maturation the upper band remains, the lower band is presumably released during the acrosome reaction [75].

Similar to *TMEM95*, *FIMP* and *SPACA6*, the overexpression of *SOF1* does not induce fusion in *IZUMO1*-deficient cells. Interestingly, HEK293T cells expressing all four genes in addition to *IZUMO1* do not improve the binding or fusion ability to ZP-free oocytes compared to HEK293T cells expressing only *IZUMO1*. This observation emphasizes that sperm-egg fusion is a tightly regulated process that requires strict timing and proper interplay of several factors involved [75].

DCST1 and DCST2

Mouse and zebrafish DSCT1 and its homolog DSCT2 belong to the class of DC-STAMP-like domain containing proteins predicted to have five or six TM helices with an intracellular C-terminus containing a RING finger domain [77, 80]. Like their homologs in invertebrates, Sneaky in Drosophila and SPE-42 and SPE-49 in *C. elegans*, both *DCST1* and *DCST2* are required in sperm for fertilization of the egg [77, 81, 82]. Sperm lacking *DCST1*/*2* show normal sperm morphology and motility, however they are unable to fertilize the egg and accumulate in the perivitelline space after passing through the ZP [77, 80]. The deletion of *DSCT1* causes an almost complete male sterility, whereby the deletion of *DCST2* and the simultaneous deletion of *DCTST1*/*2* causes full sterility. Since their overexpression in a heterologous system, even when co-expressed with *IZUMO1,* does not result in fusion indicates that these proteins are not sufficient to mediate fusion. Together with the finding that SPACA6 is absent in a *DSCT1*/*2* KO sperm, it was suggested that DSCT1/2 is important for the presentation and organization of other fusion-relevant proteins [80].

Summary

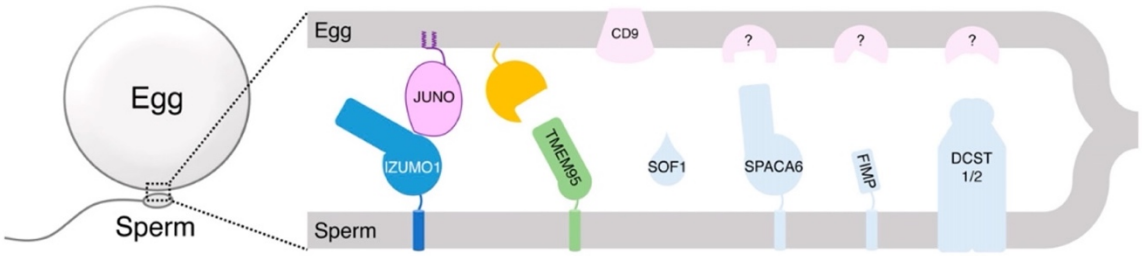

Figure 9: Schematic model of effector proteins mediating gamete binding and fusion during mammalian fertilization. The tetraspanin CD9 and the IZUMO1-receptor JUNO are located on the egg membrane. IZUMO1 facilitates gamete binding in conjunction with Juno, before it facilitates sperm-egg fusion in the absence of JUNO. All other sperm-specific proteins are proposed to act downstream of sperm-egg binding and be essential, however not sufficient to mediate gamete fusion. Figure taken from Tang et al., 2022 [76]

1.5 Cell fusion during the mating of budding yeast: *S. cerevisiae* as a model organism

Similar to other eukaryotic organisms *S. cerevisiae* possesses a sexual life cycle. Cells of distinct mating-types conjugate and form a diploid zygote. These diploid cells can reproduce asexually, but when facing nutrient starvation, undergo meiosis to produce four haploid spores contained within an ascus. Each ascus in turn contains two spores of mating type **a** (*MAT***a**) and two spores of mating type *MAT*α [83]. The mating type is determined by the *MAT* locus that harbors either the *MAT***a** or *MAT*α specific allele [84]. Under favorable nutrient conditions, the haploid spores germinate and re-enter the mitotic cycle resulting in the formation of buds which eventually mature into daughter cells. The mother cell is able to perform mating type switching and fuse with its daughter or an adjacent cell of opposite mating type to regain the diploid state [83, 85]. Laboratory yeast strains however contain a mutation in the *HO* endonuclease gene which is required for the homothallic switching. These heterothallic yeast strains therefore have one defined mating type, *MAT***a** or *MAT*α, allowing a greater control, stability and simplicity in studying various aspects of yeast genetics such as sexual reproduction during mating [83, 86].

During yeast mating, the two cells of distinct mating types fuse their plasma membranes (PM) in order to generate a diploid zygote (**a**/α) (**Figure 10**) (reviewed in [87-89]). This process encounters different challenges: first, yeast cells are typically immotile; therefore, instead of

actively moving, they grow towards each other until they find a mating partner. To signal their position yeast cells secrete mating type specific pheromones: *MAT***a** cells secrete **a**-factor which is detected by the **a**-factor specific receptor Ste3 located on *MAT*α cells whereas *MAT*α cells secrete α-factor which is detected by the α-factor specific receptor Ste2 located on *MAT***a** cells. Second, once the cells have established initial contact, the cell wall (CW) is locally degraded in a tightly regulated manner to avoid loss of cell integrity and consequently cell lysis in a hypo-osmotic environment. Finally, after CW degradation the apposing membranes have to overcome energetic barriers to initiate PM fusion. The formation of a fusion pore results in pore expansion allowing cytoplasmic content mixing, which is followed by fusion of the two nuclei and the formation of a diploid zygote. The diploid cells can then re-enter the mitotic cell cycle.

Thus far, many aspects of the underlying molecular mechanisms in the pre-fusion stages such as pheromone signaling and polarized growth are known, but how yeast exactly mediates fusion of the two PMs remains poorly understood. A mystery is still what the yeast fusogen is and whether it acts by itself or needs to assemble in a complex with other proteins to facilitate membrane merger.

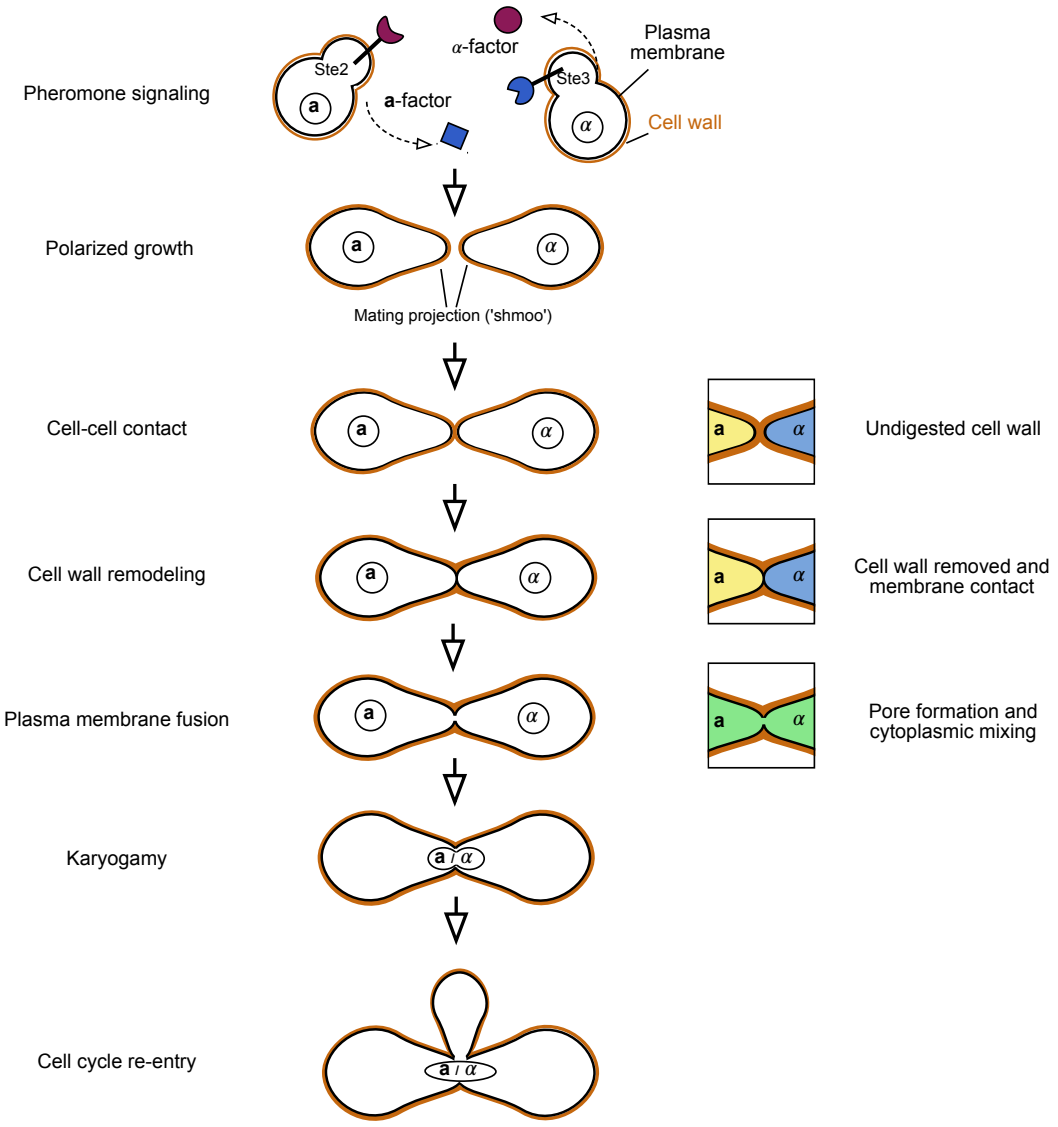

Figure 10: Yeast mating progression in *S. cerevisiae*. Haploid cells of opposite mating type, called *MAT***a** and *MAT*α, fuse to generate a diploid zygote. Mating is initiated by the exchange of pheromones causing polarized growth towards the mating partner. Upon cell-cell contact, the cell wall is locally remodeled and digested allowing the underlying membranes to merge. Cytoplasmic contents can mix and the two nuclei fuse which gives rise to a diploid zygote that re-enters the mitotic cell cycle.

1.5.1 Pheromone signaling and polarized growth

1.5.1.1 Pheromone release and sensing

Pheromone release and sensing is a prerequisite for cell-cell fusion, triggering a series of events through the activation of the MAPK kinase signaling pathway. These events include: i) arrest of the cell cycle in the G1-phase, which is permissive for pheromone signaling, ii) induction of

mating-specific gene expression, and iii) directional growth towards the mating partner along the highest pheromone gradient [87, 89] (**Figure 11**).

Haploid yeast cells of opposite mating types, *MAT***a** and *MAT*α, produce two distinct peptide hormones and possess two unique receptors on their cell surface. *MAT***a** cells secrete the prenylated peptide **a**-factor through the transporter Ste6, while *MAT*α cells release the unmodified α-factor via secretory vesicles. These peptide pheromones specifically bind to their respective cognate G protein-coupled receptors (GPCRs) which are located on cells of the opposite mating type [84, 90-94]. The excess between both secretion systems differs greatly with ~1,700 molecules of α-factor compared to presumably one **a**-factor molecule at a time. It is suggested that by controlling the secretion rate of pheromones and their ability to diffuse a consistent ratio between the two factors can be maintained. Another possibility is that the pheromone receptor Ste2 and Ste3 have distinct affinities to compensate for gradient differences [94]. Moreover, *MAT***a** cells secrete the protease Bar1, which prevents excessive accumulation of α-factor and thus receptor saturation. Despite their physical differences and modes of secretion **a**- and α-factor pheromones are thought to convey a similar spatial information for guiding polarity site movement in partner cells [94].

Binding of pheromones to their corresponding GPCR receptors induces a conformational change within the G-protein which consist of a Gα, Gβ and Gγ subunit encoded by *GPA1*, *STE4* and *STE18* genes, respectively. The conformational change leads to an exchange of a GDP with a GTP within the Gα-subunit resulting in a dissociation of the Gβ and Gγ subunits, a process that is regulated by a GTPase activating protein (GAP) [95, 96]. Freed G$\beta\gamma$, which remains anchored to the PM, is a crucial activator of a cascade of downstream events. It recruits Ste5, a scaffold protein for the Mitogen activated protein kinase (MAPK) signaling pathway, to the PM and binds to Cdc24, a guanine nucleotide exchange factor (GEF) that in turn activates the Cdc42 GTPase. Active Cdc42 induces cell polarization and triggers activation of the p21-activated kinase (PAK) Ste20, a stimulator of the subsequent MAPK signaling cascade. In addition, released G$\beta\gamma$ also binds Far1, an inhibitor of the cyclin-dependent kinase (CDK), needed to induce a cell cycle arrest in G1-phase [87, 89, 96]. Ste20 phosphorylates the MAPKKK Ste11, which is bound to its scaffold Ste50, and leads to its activation. Activated Ste11

phosphorylates the MAPKK Ste7, and Ste7 in turn the MAPK Fus3. All three kinases are bound to the Ste5 scaffold. Phosphorylated Fus3 MAPK then activates Ste12, the master transcriptional regulator of mating-specific genes. Its activation is facilitated by phosphorylation of the two bound Ste12-repressors Dig1 and Dig2, which then release Ste12 from its complex. In addition, Bni1 and Spa2 are direct targets of Fus3 that regulate actin assembly and are therefore important for polarized growth [89, 97].

Termination of signaling is regulated via a negative feedback loop, ensuring that polarized growth, referred to as shmooing, is only initiated when cells are in close proximity to its mating partner. In particular, Fus3 acts upstream of Ste5 and reduces its association to the membrane. Additionally, Fus3 activates the pheromone induced GTPase Sst2 which inactivates the Gα-subunit by hydrolyzing GTP [87, 95].

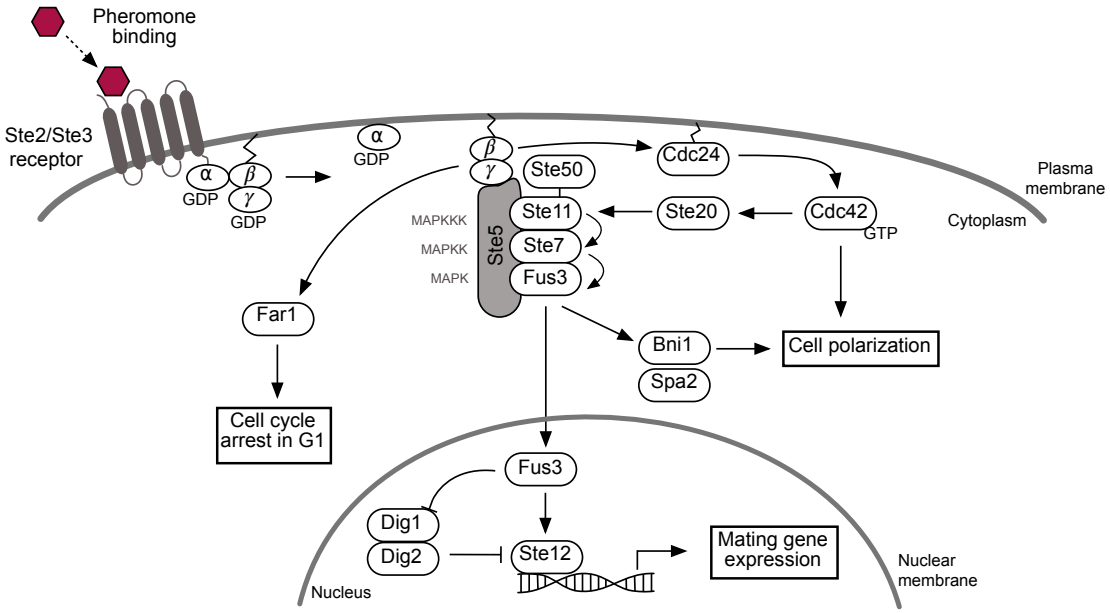

Figure 11: Pheromone signaling pathway in *S. cerevisiae*. Pheromone binding induces the release of Gβγ subunits. Following, Gβγ recruits i) Far1 which induces a cell-cycle arrest in G1, ii) Cdc24, the GEF for Cdc42 important for inducing cell polarization, and iii) the scaffold protein Ste5 required for initiating the MAPK signaling pathway. MAPK activation results in activation of Fus3, which in turn initiates cell polarization and expression of mating genes via activation of Bni1 and the transcriptional regulator Ste12, respectively.

1.5.1.2 Polarized growth towards the mating partner

In response to mating pheromones, polarized growth between two distinct mating types is observed as cellular growth towards the mating partner along the pheromone gradient,

resulting in the formation of a pear-shaped mating projection called a 'shmoo' [95]. Cell polarity is mainly mediated by Cdc42 activity which orients and stabilizes the formation of a polarity patch in close proximity to its mating partner in the presence of high local pheromone levels. Cdc42 and Fus3 activate the formin Bni1 which is important for the assembly and reorganization of the actin cables, whereby actin cables in turn are required for facilitating the myosin-dependent transportation of secretory vesicles to the contact site [98-100]. Agglutinin, Fus1 and other proteins involved in mating are recruited to the shmoo tip. Accordingly, Fus1 and components of the so-called polarisome (Spa2 and Pea2) regulate the trafficking and clustering of secretory vesicles to the fusion contact site carrying enzymes such as synthases and hydrolases need for CW digestion [100, 101]. This initiates CW remodeling, the last pre-requisite for PM fusion.

1.5.2 Cell-cell contact and cell wall remodeling

The formation of a mating projection brings the mating cells in direct contact [102]. In response to pheromones from the opposite sex, mating type-specific glycoproteins (**a**- and α-agglutinins) are upregulated on the surface of *MAT***a** and *MAT*α cells which facilitates adhesion between the two cells. The initial contact presumably causes a conformational change in both agglutinins resulting in an increase at the contact area, followed by multipoint attachments which then leads to tight binding of the cells to each other [103-105]. Subsequently, the CW is locally degraded at the fusion contact zone and the surrounding CW remodeled to form one continuous structure (**Figure 12**). Timing and position of this step is highly regulated because the cells would otherwise risk to lyse in a hypo-osmotic environment [89, 106].

CW removal involves the clustering and release of secretory vesicles that are found to contain CW hydrolytic enzymes such as the glucanases Scw4 and Scw10 [107]. While CW-synthesizing enzymes are bound to the PM, CW-degrading enzymes are free. A model has been proposed in which degradative enzymes simply diffuse through the CW and escape into the medium. However, when polarized mating partner have attached to each other diffusion through the CW is restricted leading to an increase of time and concentration of the enzyme at the contact zone [106]. The clustering and positioning of secretory vesicles involves two gene products:

Fus1, a pheromone-regulated one-pass O-glycosylated TM protein and Spa2, a formin-binding factor and component of the polarisome [108]. The localization of Fus1 at the shmoo tip depends on activated Cdc42, its GEF Cdc24 and the late Golgi trafficking protein Chs5. Together with the polarisome and the type-V myosin Myo2, Fus1 mediates localization and anchoring of other fusion proteins such as Fus2 to the fusion contact zone [109-112]. Fus2, a cytoplasmic pheromone-induced fusion protein, is transported along actin-cables and forms an amphiphysin-like complex with the BAR protein Rvs161. This complex is proposed to undergo conformational changes upon cell-cell contact and flattening of the negatively curved PM which induces the recruitment of a Cdc42 GTPase cluster. The Cdc42 cluster was found to promote late fusion steps by signaling the local release of secretory vesicles. Beside its function in CW remnant removal, Fus2 localizes as a ring at the contact zone and assists in pore expansion [89, 113-115].

The main regulators of CW removal are Fus1 and Fus2 which govern different steps as described above. In their absence, mating cells show a characteristic fusion defect phenotype with remnant CW material at the mating junction, a phenotype that is referred as early pre-zygotes. Even though Fus1 is partially necessary for Fus2 localization, both occupy additive roles as a complete fusion arrest is only achieved in a Δ*fus1*Δ*fus2* double mutant [108, 116].

In order to avoid cell lysis, yeast cells can induce a cell wall integrity (CWI) pathway which activates a repair mechanism in case of CW damage. During mating conditions, the CWI pathway prevents lysis by attenuating cell polarity and focused secretion via negative regulation of Fus2 and Cdc42 localization. Notwithstanding, to enable fusion of the mating partners it is presumed that cell-cell contact initiates a transient down-regulation of the CWI pathway [88, 117].

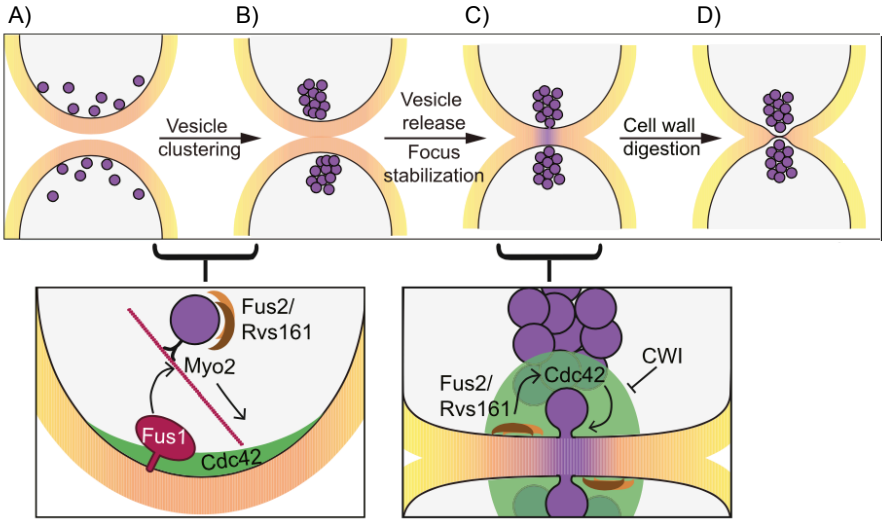

Figure 12: Schematic of vesicle clustering and local cell wall removal at the cell fusion contact zone in *S. cerevisiae.* A) Pheromone-induced directional growth towards the mating partner leads to formation of a mating-projection (shmoo). B) Clustering of secretory vesicles and fusion proteins at the shmoo-tip. C) Cdc42-complex induced release of vesicles and inhibition of the cell wall integrity (CWI) pathway. D) Local CW removal. Figure adapted from Sieber et al., 2022 [89].

1.5.3 Plasma membrane fusion

Shortly after the CW removal the underlying PMs make contact and subsequently fuse. This fusion process involves the formation of one or several fusion pores that gradually expand, ultimately leading to the mixing of cellular contents. Similarly, as described for pheromone signaling and CW degradation, PM fusion depends on continuous secretion of vesicles. One possibility is that polarized secretion is important for maintaining a concentrated cluster of fusion proteins at the contact site. Another possibility is that a continuous delivery of fusion proteins to the cell surface is necessary to replace proteins that are removed through endocytosis [118]. Moreover, an ergosterol-rich lipid composition at the mating projection was found to have an effect on efficient PM fusion [119]. Hitherto identified regulators of the PM fusion process are described in the following sections.

1.5.3.1 Prm1 presumably recruits the fusion machinery

PM fusion partially requires the tetraspan protein Prm1, a pheromone-regulated membrane (PRM) glycoprotein, which was identified through a bioinformatic-based screening for pheromone-induced TMD proteins [120]. Prm1 contains four transmembrane domains (TMDs) with 14 N-glycosylation sites and assembles in the ER into a homodimer that is covalently linked

via intermolecular disulfide bonds. Its extracellular loop contains four cysteine (Cys) residues, whereby Cys120 in loop 1 and Cys545 in loop2 are strictly necessary for the formation of disulfide cross-links and thus required for the fusion activity [121]. Upon pheromone response, Prm1 is transported through the secretory pathway and localizes at the shmoo tip and fusion contact site in mating pairs after which it is removed from the PM and delivered to vacuoles for degradation once the fusion process is completed [120, 122].

Crosses of *MAT***a** and *MAT*α lacking the *PRM1* gene exhibit a ~50% defect in PM fusion while crosses of a Δ*prm1* mutant to a mating partner expressing the wild-type (WT) gene results in almost WT fusion efficiency. Therefore, Prm1 is only required in one of the fusing membranes to facilitate fusion. Moreover, Δ*prm1* non-fused mating pairs are able to either exit G1 phase or to initiate mating with a new partner implying that these mutants have reached a dead-end state [120]. Arrested Δ*prm1* mating cells display a fusion defect phenotype which is characterized by a digested intervening CW and unfused PMs or cell lysis. Typically, cytoplasmic bubbles are present in which the PM of one mating partner pushes into the other following the direction of the osmotic gradient. These mutants are referred as late pre-zygotes (**Figure 13**) [120, 123]. About 20% of Δ*prm1* mating pairs result in membrane contact-dependent cell lysis, which was shown to occur with the same kinetics as PM fusion [123, 124]. In addition, the deletion of the CW remodeling gene *FUS1* acting upstream of *PRM1* was able to suppress cell lysis of mating pairs, implying that lysis indeed occurs after CW removal. An increase in extracellular calcium (Ca^{2+}) suppresses cell lysis and promotes fusion, whereas depletion of Ca^{2+} or deletion of *TCB3*, a gene encoding a synaptotagmin homolog, results in more frequent cell lysis events [124]. Similar to its homologs, Tcb3 was suggested to act as a Ca^{2+}-dependent regulator preventing cell lysis. However, since an effect of Ca^{2+} was not observed in WT mating cells, a Ca^{2+}-dependent repair mechanism was proposed which is only activated in mutants defective at the PM fusion stage [123, 124].

Even though *PRM1* homologs are absent in mammalian cells, *PRM1* is strongly conserved among the fungal kingdom. Similar to the defect observed in *S. cerevisiae*, the deletion of *PRM1* in *Neurospora crassa* (*N. crassa*) results in a fusion arrest in half of the mating cell population which can be suppressed in the presence of high extracellular Ca^{2+}. In *N. crassa*, *PRM1* plays an

additional role in asexual hyphal fusion [125, 126]. In *Schizosaccharomyces pombe* (*S. pombe*), *PRM1* deletion causes an almost fusion block that cannot be suppressed with the supplementation of extracellular Ca^{2+}. Moreover, Δ*prm1* mating cells in *S. pombe* exhibit CW abnormalities which is probably a result of a rapid repair response [89, 127].

The exact molecular mechanism underlying the action of Prm1 remains unknown, however two different hypotheses are proposed. In budding yeast, it is suggested that Prm1 functions through the formation of homodimers and the reduction of a disulfide bridge which exposes an extracellular loop that might interact with the adjacent PM [121, 128]. In fission yeast, it is proposed that Prm1 promotes the formation of lipid microdomains, particularly enriched in phosphatidylserine and sterol, to facilitate cell fusion [89, 127].

In summary, these findings show that *PRM1* plays an important role in promoting PM fusion. Nonetheless, ~50% of Δ*prm1* mating cells succeed with cell fusion which suggests that Prm1 is not a *bona fide* fusogen. Rather, it has been suggested that Prm1 coordinates the activation of the fusion machinery which in some cases can be rescued via a redundant fusion pathway that operates independently of Prm1 leading to the formation of fused mating pairs [119, 123].

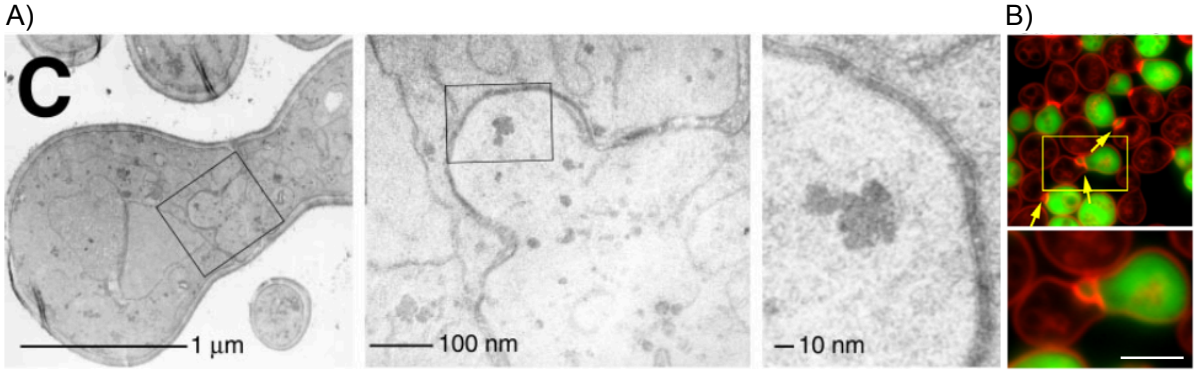

Figure 13: Δ*prm1* mating cells exhibit a defect at the stage of PM fusion. A) Representative electron microscopy images at different magnifications showing a PM fusion failure upon CW removal characterized by the presence of cytoplasmic bubbles protruding from one mating cell into the other. Figure taken from Heiman & Walter, 2000 [120]. B) Representative fluorescence microscopy images of non-fluorescent Δ*prm1 MAT*α x cytoplasmic GFP-expressing Δ*prm1 MAT***a** cells. PM is stained with FM4-64. Arrows indicate PM bubbles. Scale bar = 5 µm. Figure taken from Grote, 2010 [118].

1.5.3.2 Fig1 regulates Ca^{2+} influx during mating

The factor-induced gene 1 (*FIG1*) encodes a membrane protein that similar to Prm1, localizes to the shmoo tip and mating junction upon pheromone response [100, 124]. Fig1 belongs to

the Claudin superfamily of tetra-spanners and shows sequence similarity to the claudins Dni1 and Dni2 which promote fusion in *S. pombe* [129]. Whereas Dni1/2 mainly regulate the CW remodeling step, Fig1 was found to facilitate PM fusion by regulating the low affinity Ca^{2+} influx system (LACS) which is activated during mating and required to induce rapid cell death when exposed to high pheromone concentrations [124, 130-132].

Deletion of *FIG1* in both mating partners results in a mild fusion defect with up to ~25% reduction, whereas when crossed to the WT no significant defect is detected. As observed in Δ*prm1* mating cells, i) Δ*fig1* mutants exhibit PM bubbles, ii) ~20% of fusion arrested mating pairs lysed and iii) removal of extracellular Ca^{2+} leads to an enhanced fusion defect [124]. In contrast to Δ*prm1* matings, a Ca^{2+}-depletion in Δ*fig1* matings leads to both increased cell lysis and accumulation of late pre-zygotes. As Ca^{2+}-depletion does not affect fusion in WT cells an additional role of Fig1 in PM fusion has been put forward. [124, 131]. It is proposed that Prm1 and Fig1 form a fence-like structure corralling the fusion zone facilitating the organization of the fusion machinery. However, since a simultaneous deletion of *PRM1* and *FIG1* results in an enhanced fusion defect, they are thought to operate on independent pathways [124].

1.5.3.3 Kex2 protease likely processes substrates required for PM fusion

Kex2, also known as killer expression defective 2, is a Ca^{2+}-dependent serine protease located in the Golgi apparatus that processes secreted proteins including the α-factor pheromone. Kex2 cleaves protein sequences at dibasic sites containing Lys-Arg or Arg-Arg motifs [133-135]. Nonetheless, for full maturation the α-factor needs to be processed further by the two exopeptidases Kex1 and Ste13 which cleave the newly exposed motifs from either the C-terminus or from the N-terminus, respectively. The involvement of Kex2 in processing the α-factor precursor explains why its deletion in *MAT*α cells causes sterility during mating [135-137].

Since Kex2 is not involved in **a**-factor processing, it allowed to study its role in cell fusion. Crosses between a *MAT***a** Δ*kex2* x *MAT*α WT strain resulted in a mild fusion defect with ~15% compared to WT cells, suggesting an additional role in cell fusion distinct from impaired pheromone signaling. Further investigations revealed that *KEX2* synergizes in *trans* with *PRM1*,

as crosses between *MAT***a** Δ*kex2* x *MAT*α Δ*prm1* leads to a 2-fold fusion reduction compared to crosses with a WT strain. In contrast, crosses when Δ*kex2* mutation are placed in *cis* (*MAT***a** Δ*kex2Δprm1* x *MAT*α WT) do not enhance the defect. When *PRM1* is deleted in both mating partners, as in crosses between *MAT***a** Δ*kex2Δprm1* x *MAT*α Δ*prm1,* fusion is reduced further by 4-fold. Furthermore, differently from the observed defect phenotype in Δ*prm1* cells, electron micrographs of a *MAT***a** Δ*kex2* x *MAT*α WT mating pair showed that ~75% of arrested cells exhibited membrane-bound CW-embedded blebs which are separated from exposed PMs by a ~8 nm gap (**Figure 14**). Taken together, these finding imply that *KEX2* (or a yet to be identified Kex2 processed substrate) and *PRM1* operate on the same fusion pathway. However, since distinct morphological phenotypes were detected, it is suggested that they act at different stages in PM fusion [135].

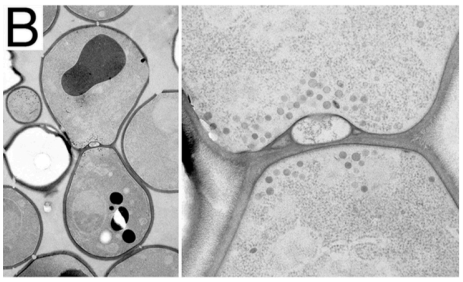

Figure 14: Fusion arrested Δ*kex2* x WT mating cells display cell wall-embedded blebs. Representative electron microscopy images at two different magnifications. Figure taken from Heiman et al., 2007 [135].

1.5.3.4 Erg6 requirement for lipid raft formation and fusion protein clustering at the shmoo tip

The yeast PM is mainly composed of the following lipids: phospholipids, sphingolipids and sterols. Phospholipids such as phosphatidylcholine, phosphatidylethanolamine, and phosphatidyl-inositol, constitute the major lipid species and contribute to the structural integrity of the membrane [138]. Compared to lipid compositions of intracellular membranes, the yeast PM is enriched in ergosterol which is important for modifying the thickness, permeability, as well as fluidity and curvature of the membrane. Via interacting with long acyl chains of sphingolipids, ergosterol forms liquid-ordered phase membrane microdomains, also referred as lipid rafts [102]. In response to pheromones, polarized yeast cells reorganize their PMs resulting in higher ergosterol content while maintaining the sphingolipid content. This

enables the retention of proteins at the shmoo tip found to be involved in cell-cell fusion such as Fus1 [102].

Ergosterol biosynthesis is a process involving the participation of several enzymes. Except for the last five enzymes encoded by *ERG2*-*ERG6*, a deletion of upstream operating *ERG*-genes is lethal [139]. In particular, the deletions of *ERG2*, *ERG3*, *ERG4* and *ERG6* have been associated with PM fusion defects [119, 140]. But rather than the absence of ergosterol, it is suggested that the accumulation of precursors leads to a fusion defect, a phenomenon that is also observed in *N. crassa* [141]. Interestingly, Δ*erg3* and Δ*erg6* mating pairs exhibit a Δ*prm1*-like fusion defect characterized by the presence of PM-bubbles (**Figure 13**). In contrast, Δ*erg*-mutants are not predisposed for contact-dependent cell lysis and moreover, the PM fusion arrest seems not to be a dead-end because over time some cytoplasmic bubbles disappear and fusion proceeds. Therefore, fusion is rather indefinitely delayed presumably due to altered sterol composition. In addition, Δ*erg*-mutants display a higher number of cells arrested as early pre-zygotes as well as haploid cells that are unable to pair. This implies an additional role in early mating stages at the level of pheromone signaling and CW remodeling. Indeed, ergosterol was found to facilitate recruitment of the MAPK scaffold protein Ste5 to the PM [119]. Consequently, the induction of cell polarization, signaling transmission and expression of mating genes might be affected. This raised the question of whether impaired pheromone signaling might be a cause of the PM fusion defect. However, when determining cell fusion in a temperature-sensitive Δ*ste5* mutant only an increase of early pre-zygotes, reflecting a CW remodeling defect, was observed. This suggests that the PM fusion defect is likely independent of impaired signaling in Δ*erg* mutants [119]. Interestingly, depletion of ergosterol was found to not affect the localization of Prm1 to site of cell fusion. In addition, the simultaneous deletion of *PRM1* and either *ERG6*/*ERG2*/*ERG3* results in an almost fusion arrest, suggesting that *PRM1* and *ERG*-genes promote cell fusion on separate pathways independently [119].

1.6 Motivation of the study

Understanding the mechanisms underlying sexual reproduction is of substantial importance, as it is a fundamental process that drives the preservation of life in eukaryotic organisms. One key aspect of sexual reproduction is PM fusion, which enables the fusion of gametes during fertilization. The complexity and potential redundancy of involved regulatory factors makes this process challenging to study. The budding yeast *S. cerevisiae* represents a suitable eukaryotic model organism as it is ease to manipulate, has a short generation time and its genome is well characterized. In contrast to human, *S. cerevisiae* reproduces through a distinct mechanism called isogamous mating which is characterized by the absence of morphological differences between the mating partners and a symmetrical nature of the mating process [89, 94]. Nevertheless, yeast and humans were found to share key aspects of functional pathways such as cell cycle, meiosis, protein folding, quality control and degradation or programmed cell death [142]. Therefore, studying PM fusion in yeast can provide insights into common underlying principles and the molecular machinery governing this process in higher eukaryotes. Uncovering conserved mechanisms can elucidate the importance and functional significance across species. Differences on the other hand can indicate evolutionary divergence providing information where species have developed unique strategies based on their specific needs and environmental constraints. Overall, this will contribute to a better understanding of phylogenetic relationships among different species [30, 54, 143].

1.7 Aim of the study

This work utilizes the budding yeast *S. cerevisiae* to study membrane merger of cells of opposite mating type during mating. Hitherto, *PRM1* has been reported as a major regulator of PM fusion. However, the absence of *PRM1* in both mating cells leads only to a partial fusion arrest, suggesting the presence of other yet unidentified players in this process. The first goal of this study therefore was to identify novel regulators of cell-cell fusion via a systematic loss-of-function screen using a customized yeast knockout (YKO) sub-library composed of mutants predicted to encode transmembrane domains (TMDs). By utilizing a multicolor flow cytometry assay based on the complementation of split-GFP cell fusion of 10,000 events of each mating reaction was quantified within a few seconds. A subsequent microscopic inspection confirmed the defect and morphological phenotype in 91 out of 125 fusion mutants from the primary screen.

The second aim of the study was to conduct an in-depth analysis of gene of interest (GOI) mutants that were as defective as Δ*prm1*. At first, the mating symmetry of fusion was analyzed which was consistent with findings from existing literature showing that the majority acts bilaterally. The next question to addressed was how novel fusion mutants are associated with known fusion mutants. For this reason, synergistic interactions were analyzed in *trans* and overexpression analysis carried out to reveal the sequential order of genes found to synergize. The subsequent analysis of double mutants provided additional knowledge of whether GOI mutants are operating on the same or distinct pathways. Throughout the screen, two major protein complexes, the V-ATPase complex and RNA polymerase II mediator complex, were identified to facilitate fusion likely indirectly via their function in endomembrane acidification and transcriptional regulation, respectively. To better understand the mechanistic basis, this study focused on determining the localization and / or expression profile in mating conditions.

Finally, this study aimed to generate a synergistic interaction network operating at PM fusion during yeast mating to provide novel insights into the underlying mechanisms on how eukaryotic organisms fuse their membranes during sexual reproduction.

2. Materials and Methods

2.1 Devices and Instrumentation

Table 2: Instruments and devices used in this study.

Device	Supplier	Use
96-pin replicator VP 408FH	V&P Scientific, Inc.	SGA procedure; generation and maintenance of 96-well yeast libraries
BD Accuri™ C6 Plus flow cytometer	BD Bioscience	BiFC fusion analysis
Benchtop centrifuge 5424	Eppendorf SE	Centrifugation of 1.5-2 ml volumes
Benchtop centrifuge 5810R	Eppendorf SE	Harvesting cells (2-50 ml cultures)
Cell density meter CO800	Eppendorf SE	OD_{600} measurements in cuvettes
ChemiDoc MP Imaging System	BioRad Laboratories	Visualization of in-gel fluorescence and chemiluminescence
Dissector microscope MSM400	Singer Instruments	Tetrad dissection of yeast spores
FastGene blue LED transilluminator	Nippon Genetics Europe GmbH	Visualization of DNA bands in agarose gels
Incubator IPP55	Memmert GmbH + Co. KG	Incubation of yeast cultures
Laminar flow cabinet BDK-S 1000	BDK Luft- und Reinraumtechnik GmbH	Generation of YKO libraries, pouring agar plates
Laser scanning microscope 800 (LSM800)	Carl Zeiss Microscopy GmbH	Confocal microscopy
Library Copier™ VP 381	V&P Scientific, Inc.	SGA procedure; generation and maintenance of 96-well yeast libraries
Light Microscope	Kolleg SHB45	Visualization of yeast cells
Magnetic stirrer RCT basic	IKA®-Werke GmbH & CO. KG	Mixing of buffers and solutions
Microplate Reader POLARstar Omega	BMG LABTECH GmbH	Determination of OD_{600} in 96-well microplates

Microwave Continent MW 800 G	IKA Labortechnik	Preparation of yeast media
Millipore Synergy	Millipore	Collecting filtered ddH_2O
New BrunswickTM Excella® E24 orbital shaker	Eppendorf SE	Incubation and shaking of yeast cultures
pH Meter 761	Knick	Determination oh pH in buffers and solutions
UV/Vis- spectrophotometer ND-1000 NanoDrop	Thermo Fisher Scientific Inc.	Determination of DNA concentration in solution
Vacuum manifold, 12 manifold	Merck KGaA	Vacuum filtration for standard yeast mating reactions
Vacuum manifold, 96-well VP408FH	Enzo Life Sciences GmbH	Vacuum filtration for yeast mating reactions in 96-well format
Vacuum pump MPC 052 Z	ILMVAC GmbH	Vacuum filtration for yeast mating reactions
Vortexer MS2	IKA®-Werke GmbH & CO. KG	Mixing of cell cultures

2.2 Chemicals and reagents

Table 3: List of used chemicals and reagents

Chemical	Supplier
Acetic acis	AppliChem
Acetone	Sigma-Aldrich GmbH
Acrylamide 4K-Soulution (30%)	PanReac AppliChem
Adenine	Formedium™
Agar	Millipore Corp
A-factor pheromone	Synthesized in-house
Alanine	Formedium™
Ampicillin	Gerbu
Asparagine	Formedium™
Aspartic acid	Formedium™

Bacto agar	Sigma-Aldrich GmbH
Beta Mercapto-ethanol	SERVA Electrophoresis GmbH
Canavanine	Sigma-Aldrich GmbH
Cononcanavalin A-Alexafluor 647	Thermo Fisher Scientific Inc.
Cononcanavalin A-Tetramethylrhodamine	Thermo Fisher Scientific Inc.
Cysteine	Formedium™
D-Glucose	Formedium™
Dimethyl sulfoxide (DMSO)	SERVA Electrophoresis GmbH
dNTPs	Thermo Fisher Scientific Inc.
Dried skimmed milk powder	Sigma-Aldrich GmbH
Ethanol	VWR International GmbH
Geneticin (G418)	Sigma-Aldrich GmbH
Glutamic acid	Formedium™
Glutamine	Formedium™
Glycerin	GERBU Biotechnik GmbH
Glycine	Formedium™
Histidine	Sigma-Aldrich GmbH
HCl	VWR International GmbH
Hydrogen peroxide	Carl Roth GmbH + Co. KG
Hygromycin	Formedium™
KCl	Sigma-Aldrich GmbH
Inositol	Formedium™
Isoleucine	Formedium™
Leucine	Formedium™
L-glutamic acid sodium salt hydrate	Formedium™
Methanol	Sigma-Aldrich GmbH
Methionine	Sigma-Aldrich GmbH
NaCl	Sigma-Aldrich GmbH
Na2HPO4	Sigma-Aldrich GmbH
NaF	Sigma-Aldrich GmbH
NaN3	AppliChem

NaOH	J.T. Baker
Nourseothricin (clonNAT)	Jena Bioscience GmbH
Para-aminobenzoic acid	Formedium™
PEG 2250	Sigma-Aldrich GmbH
Peptone	Formedium™
Phenylalanine	Formedium™
Phenylmethylsulfonyl fluoride (PMSF)	Sigma-Aldrich GmbH
PIC	Sigma-Aldrich GmbH
Ponceau stain	Sigma-Aldrich GmbH
Potassium acetate	Carl Roth GmbH + Co. KG
2-Propanol	VWR International GmbH
Proline	Formedium™
Serine	Formedium™
Sodium hypochlorite solution	Sigma-Aldrich GmbH
Sodium dodecyl sulfate (SDS)	Sigma-Aldrich GmbH
TEMED	Carl Roth GmbH + Co. KG
Thialysine	Sigma-Aldrich GmbH
Threonine	Formedium™
Trichloroacetic acid (TCA)	Sigma-Aldrich GmbH
Tris	Carl Roth GmbH + Co. KG
Triton X-100	Carl Roth GmbH + Co. KG
Tween-20	Bio Rad
Tryptophan	Formedium™
Tyrosine	Formedium™
Uracil	Formedium™
Valine	Formedium™
Yeast extract	Formedium™
YeastMaker™ Carrier DNA	Takara
Yeast nitrogen base without amino acids or ammonium sulfate	Formedium™

2.3 Enzymes, dyes and antibodies

Table 4: List of used enzymes, dyes and antibodies.

Names	Supplier
1 kb DNA Ladder	Thermo Fisher Scientific Inc.
1 kb plus DNA Ladder	Thermo Fisher Scientific Inc.
6x Loading dye	Thermo Fisher Scientific Inc.
Anti-mouse IgG2-HRP conjugate (goat)	BioRad
Anti-mouse IgM-HRP conjugate (rabbit)	BioRad
Anti-V5 antibody (mouse)	Invitrogen; Thermo Fisher Scientific Inc.
Concanavalin A Tetramethylrhodamine	Thermo Fisher Scientific Inc.
Concanavalin A Alexa Fluor 647 conjugate	Thermo Fisher Scientific Inc.
DreamTaq DNA Polymerase	Thermo Fisher Scientific Inc.
FM4-64	Invitrogen; Thermo Fisher Scientific Inc.
Gibson Assembly Master Mix	New England BioLabs
Kpn1	New England BioLabs
PageRuler Prestained ladder	Thermo Fisher Scientific Inc.
Phusion Hot start flex DNA polymerase	New England BioLabs
Phusion High Fidelity 2x Master Mix	New England BioLabs
Sac1	New England BioLabs
Zymolase 100T	US Biological Life Science

2.4 Stock solutions and buffers

Table 5: List of used stock solutions and buffers.

Name	Composition	
Glucose solution	Glucose	40% (w/v)
ConA-Alexafluor 647	ConA-647 in 1x PBS	1 mg/ml
ConA-Tetramethylrhodamine	ConA-Tet in 1x PBS	5 mg/ml
Blocking solution	Milk powder Filled up with TBS	5 % (w/v)

Lysis buffer	Tris, pH8.0 NaCl EDTA	50 mM 150 mM 2 mM
10x MES buffer (pH5.5; 0.5M)	MES Filled up with ddH_2O Adjusted to pH5.5	97.62 g 1 l
10x MES buffer (pH6.8; 0.5M)	MES Filled up with ddH_2O Adjusted to pH6.8	97.62 g 1 l
1x Phosphate buffered saline (PBS) (pH 7.4)	Sodium chloride Potassium chloride Sodium phosphate dibasic Potassium dihydrogen phosphate	137 mM 2.7 mM 8 mM 2 mM
PEG solution	LiOAc Tris-Hcl, pH 8.0 EDTA/ NaOH PEG3350	100 mM 10 mM 1 mM 40 %
Ponceau S solution	Ponceau S Acetic acid Filled up with ddH_2O	0.2% 1% 200 ml
4x SDS-PAGE sample buffer	Tris DTT SDS Glycerol Bromphenol blue	250 mM 100 mM 6% 40% 0.02%
SDS Running buffer	Tris Glycine SDS	25 mM 192 mM 0.28%
SORB	LiOAC Tris-HCl, pH 8.0 EDTA/NaOH, pH8.0	100 mM 10 mM 1 mM

	Sorbitol	1 M
TAE buffer (pH8.6)	Tris Acetate EDTA	40 mM 20 mM 1 mM
TAF buffer (pH 7.4)	Tris-Hcl (pH 7.4) Sodium azide (NaN_3) Sodium fluoride (NaF)	20 mM 20 mM 20 mM
TBS (pH 7.5)	NaCl Tris	150 mM 10 mM
TBST (pH 7.5)	NaCl Tris Tween-20	150 mM 10 mM 0.025% (v/v)
Transfer buffer	Glycine Tris SDS Methanol Filled up with ddH_2O	192 mM 25 mM 0.04% 20% 1 l

2.5 Media

Table 6: List of used amino-acids supplements for the SGA procedure.

Amino-acids (Aa) supplements	Composition	
Aa supplement for sporulation medium	Histidine Leucine Lysine Uracil	2.0 g 10.0 g 2.0 g 2.0 g
Aa supplement powder mixture (DO – Leu/Arg/Lys)	Adenine Uracil Inositol Para-aminobenzoic acid Alanine	3.0 g 2.0 g 2.0 g 0.2 g 2.0 g

	Asparagine	2.0 g
	Aspartic acid	2.0 g
	Cysteine	2.0 g
	Glutamic acid	2.0 g
	Glutamine	2.0 g
	Glycine	2.0 g
	Histidine	2.0 g
	Isoleucine	2.0 g
	Methionine	2.0 g
	Phenylalanine	2.0 g
	Proline	2.0 g
	Serine	2.0 g
	Threonine	2.0 g
	Tryptophan	2.0 g
	Tyrosine	2.0 g
	Valine	2.0 g
Aa supplement powder mixture (DO – His/Arg/Lys)	Adenine	3.0 g
	Uracil	2.0 g
	Inositol	2.0 g
	Para-aminobenzoic acid	0.2 g
	Alanine	2.0 g
	Asparagine	2.0 g
	Aspartic acid	2.0 g
	Cysteine	2.0 g
	Glutamic acid	2.0 g
	Glutamine	2.0 g
	Glycine	2.0 g
	Isoleucine	2.0 g
	Leucine	10.0 g
	Methionine	2.0 g
	Phenylalanine	2.0 g

	Proline	2.0 g
	Serine	2.0 g
	Threonine	2.0 g
	Tryptophan	2.0 g
	Tyrosine	2.0 g
	Valine	2.0 g

Table 7: Media used in this study.

Media	Composition	
YPD medium	Yeast extract	1%
	Peptone	2%
	D-Glucose	2%
	Filled up with MES buffer (pH5.5)	1 l
YPD medium buffered with MES to pH5.5	Yeast extract	1%
	Peptone	2%
	D-Glucose	2%
	Filled up with MES buffer (pH6.8)	1 l
YPD medium buffered with MES to pH6.8	Yeast extract	1%
	Peptone	2%
	D-Glucose	2%
	Filled up with ddH_2O to	1 l
YPD agar	YPD medium	
	Agar	2%
Sporulation medium	Potassium acetate	10.0 g
	Yeast extract	1.0 g
	Glucose	0.5 g
	Amino-acids powder mixture for sporulation	0.1 g
	Bacto agar	20.0 g
	G418 (150 mg/mL)	250 µl
	Filled up with ddH_2O to	1 l

SD/MSG medium used for SGA	Yeast nitrogen base without amino acids or ammonium sulfate	1.7 g
	L-glutamic acid sodium salt hydrate	1.0 g
	Amino-acids powder mixture	2.0 g
	Bacto agar	20.0 g
	40% glucose	50 ml
	Filled up with ddH_2O to	1 l
SC medium	Yeast nitrogen base without amino acids or ammonium sulfate	6.7 g
	Amino-acids supplement powder mixture	590 mg
	40% glucose	50 ml
	Filled up with ddH_2O to	1 l
SD medium	Yeast nitrogen base without amino acids or ammonium sulfate	6.7 g
	Defined amino-acids supplement powder mixture	590 mg
	40% glucose Filled up with ddH_2O to	50 ml 1 l
LB medium	NaCl	20 mM
	Bacto-tryptone	10.0 g
	Yeast extract	5.0 g
	Distilled water	1 l

Liquid media were autoclaved for 20 min at 122 °C. Canavanine, thialysine, nourseothricin and geneticin were added after autoclaving once the solution cooled down to approximately 65 °C.

2.6 Commercial kits and disposables

Table 8: Commercial kits used in this study.

Commercial Kits	Source
Qiagen Gel extraction Kit	Qiagen GmbH
Qiagen Plasmid Mini Prep Kit	Qiagen GmbH
Chemiluminescence Kit	GE Healthcare

Table 9: Disposals used in this study.

Disposables	Source
Glass beads	Carl Roth GmbH
Graduated pipettes (5, 10, 25, 50 ml)	Sarstedt AG & Co
MF Millipore Membrane Filter, 0.45 µM	Sigma-Aldrich
Micropipette tips (10, 200, 1250 µl)	Sarstedt AG & Co
Microscope glass slides	Knittel Glass and Diagonal
MultiScreen$_{HTS}$-HA filter plates 96-well (0.45 µm)	Merck KGaA, Darmstadt, Germany
Nitrocellulose membrane	GVS North America
Nunc™ OmniTray™ (242811)	Thermo Fisher Scientific Inc.
Nunc™ Sealing Tapes (236366)	Thermo Fisher Scientific Inc.
Parafilm	Pechiney Plastic Packaging
Reaction tubes (0.5, 1.5, 3.0 ml)	Eppendorf SE
Reaction tubes (15, 50 ml)	Sigma-Aldrich
TC-plate 96 -well (83.3924.005)	Sarstedt AG & Co,
Whatman Filter paper No. 4	GE Healthcare

2.7 Plasmids

From the Saccharomyces Genome Database (SGD), the respective DNA sequences of all yeast genes were received (https://www.yeastgenome.org/). The plasmids were designed in this work using the SnapGene Viewer software unless otherwise indicated.

Table 10: Plasmids used in this study.

Plasmid	Parent	Genotype	Reference
pAH02	pAS01	pFA6-kanMX6	Knop et al., 1999
pAH03	pAS01	*ADH1pr* -YGL024W 2µ ampR	This work
pAH04	pAS01	*ADH1pr* -PGD1 2µ ampR	This work
pAH06a	pAS01	*ADH1pr* -FIG1 2µ ampR	This work
pAH07a	pAS01	*ADH1pr* -VMA2 2µ ampR	This work

pAH08a	pAS01	*ADH1pr* -KEX2 2µ ampR	This work
pAH09a	pAS01	*ADH1pr* -CAX4 2µ ampR	This work
pAS01	pRS426	*ADH1pr* -URA3 2µ ampR	Anson Shek
pAS06	pAS01	*ADH1pr* -PRM1 2µ ampR	Anson Shek
pAS15	pAS01	*ADH1pr* -ERG6 2µ ampR	Anson Shek
pAS16	pAS01	*ADH1pr* -ERG3 2µ ampR	Anson Shek
pFA6		pFA6-hphNT1	Longtine et al., 1998
pMS131		pFA6a-mNeonGreen-kanMX4	Michael Skruzny

2.8 *Escherichia coli* strains

Table 11: *E. coli* strains used in this study for cloning procedures.

Strain	Genotype	Reference
XL10-Gold	TetrD(*mcrA*)*183* D(*mcrCB-hsdSMR-mrr*)*173 endA1 supE44 thi-1 recA1 gyrA96 relA1 lac* Hte [F´ proAB lacIqZDM15 Tn10 (Tetr) Amy Camr]	Stratagene

2.9 Yeast strains

Overview of used query strains used for the systematic integration of markers into the commercially obtained *MAT***a** YKO collection from EUROSCRAF. The strains derived from the genetic background S288C.

Table 12: Yeast query strains used for the SGA procedure.

Strain	Genotype	Use	Reference
*MAT***a** YKO collection (96-well array)	BY4741 *his3Δ1*, *leu2Δ0*, *met15Δ0*, *ura3Δ0*, *Δgene*::KanMX	Generation of the YKO TMD *MAT***a** sub-library	Scientific Research and Development GmbH, Oberursel
*MAT*α N-GFP query strain, clone 5B	*ura3Δ0*, *his3Δ1*, *leu2Δ0*, met15Δ0, LYS2+, eGFP(aa1-158)-TRP1-NatMX4, *can1*::STE2pr-SpHIS5, *Δlyp1*::STE3pr-LEU2	Integration of the N-GFP into the YKO TMD *MAT***a** sub-library by SGA	Max Planck Institute for Biophysical Chemistry, Göttingen, Germany

		WT control in BiFC fluorescence fusion assay	
*MAT*α C-GFP query strain, clone 4D	*ura3Δ0*, *his3Δ1*, *leu2Δ0*, met15Δ0, LYS2+, eGFP(aa159-240)-NatMX4, *can1*::STE2pr-SpHIS5, *Δlyp1*::STE3pr-LEU2	Integration of the C-GFP into the YKO TMD *MAT***a** sub-library by SGA	Max Planck Institute for Biophysical Chemistry, Göttingen, Germany
*MAT***a** C-GFP query strain, clone 18 C	*ura3Δ0*, *his3Δ1*, *leu2Δ0*, met15Δ0, LYS2+, eGFP(aa159-240)-NatMX4, *can1*::STE2pr-SpHIS5, *Δlyp1*::STE3pr-LEU2	WT control in BiFC fluorescence fusion assay	Max Planck Institute for Biophysical Chemistry, Göttingen, Germany
*MAT*α N-GFP WT	PSAY981 *ura3Δ0*, *his3Δ1*, *leu2Δ0*, *lys2Δ0*, NeGFP-TRP1-NatMX4 (p1371)	Verification of TMD sub-libraries	Pablo Aguilar (Universidad de San Martin, Argentina)
*MAT*α N-GFP *Δprm1*	PSAY981 *Δprm1 ura3Δ0, his3Δ1, leu2Δ0, lys2Δ0,* NeGFP-TRP1-NatMX4 (p1371), *Δprm1*::hphNT1	Verification of TMD sub-libraries	Max Planck Institute of Molecular Physiology, Dortmund, Germany
*MAT***a** C-GFP WT	PSAY983 *ura3Δ0, his3Δ1, leu2Δ0, lys2Δ0,* CeGFP-LEU2-NatMX4 (p1370), Δ*lys1*::KanMX-pTEF2-mCherry	Verification of TMD sub-libraries	Pablo Aguilar (Universidad de San Martin, Argentina)
*MAT***a** C-GFP *Δprm1*	PSAY983 *Δprm1 ura3Δ0, his3Δ1, leu2Δ0, lys2Δ0,* CeGFP-LEU2-NatMX4 (p1370), Δ*lys1*::KanMX-pTEF2-mCherry, *Δprm1*::hphNT1	Verification of TMD sub-libraries	Max Planck Institute of Molecular Physiology, Dortmund, Germany

Overview of yeast strains used in this study. The strains derived from the genetic background S288C and were generated in this study unless otherwise indicated.

Table 13: Yeast strains used in this study.

Strain code	Description	Genotype	Reference
BY4741	WT S288C derivative	*MAT***a** *his3Δ1 leu2Δ0 met15Δ0 ura3Δ0*	Brachmann et al., 1998
PSAY981	WT N-GFP-NATMX4 *MAT*α	*NeGFP(aa1-158)-TRP1-NatMX4 ura3Δ0 his3Δ1 leu2Δ0 lys2Δ0,*	Pablo Aguilar

PSAY983	WT C-GFP-Leu2 *MAT***a**	*CeGFP(aa159-240)-LEU2 Δlys1::KanMX-pTEF2-mCherry ura3Δ0 his3Δ1 leu2Δ0 lys2Δ0*	Pablo Aguilar
SKM001	WT C-GFP-Leu2 *MAT***a**	*CeGFP(aa159-240)-LEU2 ura3Δ0 his3Δ1 leu2Δ0 lys2Δ0*	Sheila Mainye
AH008	Δ*kex2* C-GFP MAT**a**	*Δkex2::hphNT1 CeGFP(aa159-240)-LEU2*	
AS12	Δ*erg3* C-GFP *MAT***a**	*Δerg3::kanMX4 CeGFP(aa159-240)-LEU2*	Anson Shek
AS11	Δ*erg3* N-GFP *MAT*α	*Δerg3::kanMX4 NeGFP(aa1-158)-TRP1-NatMX4*	Anson Shek
AS03A	Δ*erg6* C-GFP *MAT***a**	*erg6::kanMX4 CeGFP(aa159-240)-LEU2*	Anson Shek
AS14	Δ*erg6* N-GFP *MAT*α	*Δerg6::kanMX4 NeGFP(aa1-158)-TRP1-NatMX4*	Anson Shek
-	Δ*prm1* C-GFP *MAT***a**	*Δprm1::hphNT1 CeGFP(aa159-240)-LEU2 Δlys1::KanMX-pTEF2-mCherry*	Mara Marques
-	Δ*prm1* N-GFP *MAT*α	*Δprm1::hphNT1 NeGFP(aa1-158)-TRP1-NatMX4*	Mara Marques
AS13	Δ*prm1* C-GFP *MAT***a**	*Δprm1::hphNT1 CeGFP(aa159-240)-NatMX4*	Anson Shek
AH055a	Δ*cax4* C-GFP *MAT***a**	*Δcax4::hphNT1 CeGFP(aa159-240)-LEU2*	
AH056a	Δ*cax4* N-GFP *MAT*α	*Δcax4::hphNT1 NeGFP(aa1-158)-TRP1-NatMX4*	
AH072	Δ*fus1* C-GFP *MAT***a**	*Δfus1::hphNT1 CeGFP(aa159-240)-LEU2*	
AH073	Δ*fus1* N-GFP *MAT*α	*Δfus1::hphNT1 NeGFP(aa1-158)-TRP1-NatMX4*	
-	Δ*fus2* C-GFP *MAT***a**	*Δfus2::kanMX4 CeGFP(aa159-240)-LEU2*	Sheila Mainye
AH003	Δ*fus2* N-GFP *MAT*α	*Δfus2::kanMX4 NeGFP(aa1-158)-TRP1-NatMX4*	
AH051a	Δ*sst2* C-GFP *MAT***a**	*Δsst2::kanMX6 CeGFP(aa159-240)-LEU2*	
	Δ*vma* mutants		
AH001A	Δ*vma3* C-GFP *MAT***a**	*Δvma3::hphNT1 CeGFP(aa159-240)-LEU2 Δlys1::KanMX-pTEF2-mCherry*	
DL026A	Δ*vma3* N-GFP *MAT*α	*Δvma3::hphNT1 NeGFP(aa1-158)-TRP1-NatMX4*	Diana Ludwig

DL014A	Δ*vma16* C-GFP *MAT***a**	*Δvma16::hphNT1 CeGFP(aa159-240)-LEU2 Δlys1::KanMX-pTEF2-mCherry*	Diana Ludwig
DL013A	Δ*vma16* N-GFP *MAT*α	*Δvma16::hphNT1 NeGFP(aa1-158)-TRP1-NatMX4*	Diana Ludwig
DL030A	Δ*pkr1* N-GFP *MAT*α	*Δpkr1::hphNT1 NeGFP(aa1-158)-TRP1-NatMX4*	Diana Ludwig
DL031A	Δ*pkr1* C-GFP *MAT***a**	*Δpkr1::hphNT1 CeGFP(aa159-240)-LEU2 Δlys1::KanMX-pTEF2-mCherry*	Diana Ludwig
AH074	Δ*stv1* C-GFP *MAT***a**	*Δstv1::hphNT1 CeGFP(aa159-240)-LEU2*	
DL032	Δ*stv1* N-GFP *MAT*α	*Δstv1::hphNT1 NeGFP(aa1-158)-TRP1-NatMX4*	Diana Ludwig
DL033	Δ*stv1* C-GFP *MAT***a**	*Δstv1::hphNT1 CeGFP(aa159-240)-LEU2 Δlys1::KanMX-pTEF2-mCherry*	Diana Ludwig
DL004A	Δ*vma1* N-GFP *MAT*α	*vma1::hphNT1 NeGFP(aa1-158)-TRP1-NatMX4*	Diana Ludwig
DL005	Δ*vma1* C-GFP *MAT***a**	*Δvma1::hphNT1 CeGFP(aa159-240)-LEU2 Δlys1::KanMX-pTEF2-mCherry*	Diana Ludwig
DL006A	Δ*vma10* N-GFP *MAT*α	*Δvma10::hphNT1 NeGFP(aa1-158)-TRP1-NatMX4*	Diana Ludwig
DL007A	Δ*vma10* C-GFP *MAT***a**	*Δvma10::hphNT1 CeGFP(aa159-240)-LEU2 Δlys1::KanMX-pTEF2-mCherry*	Diana Ludwig
DL008A	Δ*vma11* N-GFP *MAT*α	*Δvma11::hphNT1 NeGFP(aa1-158)-TRP1-NatMX4*	Diana Ludwig
DL009A	Δ*vma11* C-GFP *MAT***a**	*Δvma11::hphNT1 CeGFP(aa159-240)-LEU2 Δlys1::KanMX-pTEF2-mCherry*	Diana Ludwig
DL010	Δ*vma13* N-GFP *MAT*α	*Δvma13::hphNT1 NeGFP(aa1-158)-TRP1-NatMX4*	Diana Ludwig
DL011A	Δ*vma13* C-GFP *MAT***a**	*Δvma13::hphNT1 CeGFP(aa159-240)-LEU2 Δlys1::KanMX-pTEF2-mCherry*	Diana Ludwig
AH020a	Δ*vma2* C-GFP *MAT***a**	*Δvma2::hphNT1 CeGFP(aa159-240)-LEU2*	
DL002A	Δ*vma2* C-GFP *MAT***a**	*Δvma2::hphNT1 CeGFP(aa159-240)-LEU2 Δlys1::KanMX-pTEF2-mCherry*	Diana Ludwig
DL003A	Δ*vma2* N-GFP *MAT*α	*Δvma2::hphNT1 NeGFP(aa1-158)-TRP1-NatMX4*	Diana Ludwig
DL019A	Δ*vma21* C-GFP *MAT***a**	*Δvma21::hphNT1 CeGFP(aa159-240)-LEU2 Δlys1::KanMX-pTEF2-mCherry*	Diana Ludwig

DL029A	Δ*vma21* N-GFP *MAT*α	*Δvma21::hphNT1 NeGFP(aa1-158)-TRP1-NatMX4*	Diana Ludwig
DL022A	Δ*vma5* N-GFP *MAT*α	*Δvma5::hphNT1 NeGFP(aa1-158)-TRP1-NatMX4*	Diana Ludwig
DL023A	Δ*vma5* C-GFP *MAT***a**	*Δvma5::hphNT1 CeGFP(aa159-240)-LEU2 Δlys1::KanMX-pTEF2-mCherry*	Diana Ludwig
DL012A	Δ*vma7* N-GFP *MAT*α	*Δvma7::hphNT1 NeGFP(aa1-158)-TRP1-NatMX4*	Diana Ludwig
DL012B	Δ*vma7* C-GFP *MAT***a**	*Δvma7::hphNT1 CeGFP(aa159-240)-LEU2 Δlys1::KanMX-pTEF2-mCherry*	Diana Ludwig
DL015A	Δ*vma8* C-GFP *MAT***a**	*Δvma8::hphNT1 CeGFP(aa159-240)-LEU2 Δlys1::KanMX-pTEF2-mCherry*	Diana Ludwig
DL018A	Δ*vma8* N-GFP *MAT*α	*Δvma8::hphNT1 NeGFP(aa1-158)-TRP1-NatMX4*	Diana Ludwig
DL027A	Δ*vma9* N-GFP *MAT*α	*Δvma9::hphNT1 NeGFP(aa1-158)-TRP1-NatMX4*	Diana Ludwig
DL028A	Δ*vma9* C-GFP *MAT***a**	*Δvma9::hphNT1 CeGFP(aa159-240)-LEU2 Δlys1::KanMX-pTEF2-mCherry*	Diana Ludwig
DL038A	Δ*voa1* N-GFP *MAT*α	*Δvoa1::hphNT1 NeGFP(aa1-158)-TRP1-NatMX4*	Diana Ludwig
DL039A	Δ*voa1* C-GFP *MAT***a**	*Δvoa1::hphNT1 CeGFP(aa159-240)-LEU2 Δlys1::KanMX-pTEF2-mCherry*	Diana Ludwig
AH075	Δ*vph1* C-GFP *MAT***a**	*Δvph1::hphNT1 CeGFP(aa159-240)-LEU2*	
DL020	Δ*vph1* N-GFP *MAT*α	*Δvph1::hphNT1 NeGFP(aa1-158)-TRP1-NatMX4*	Diana Ludwig
DL021A	Δ*vph1* C-GFP *MAT***a**	*Δvph1::hphNT1 CeGFP(aa159-240)-LEU2 Δlys1::KanMX-pTEF2-mCherry*	Diana Ludwig
DL016A	Δ*vph2* N-GFP *MAT*α	*Δvph2::hphNT1 NeGFP(aa1-158)-TRP1-NatMX4*	Diana Ludwig
DL017A	Δ*vph2* C-GFP *MAT***a**	*Δvph2::hphNT1 CeGFP(aa159-240)-LEU2 Δlys1::KanMX-pTEF2-mCherry*	Diana Ludwig
	Δ*med* mutants		
DL049	Δ*gal11* C-GFP *MAT***a**	*Δgal11::hphNT1 CeGFP(aa159-240)-LEU2*	Diana Ludwig
DL050	Δ*gal11* N-GFP *MAT*α	*Δgal11::hphNT1 NeGFP(aa1-158)-TRP1-NatMX4*	Diana Ludwig
AH015a	Δ*med2* C-GFP *MAT***a**	*Δmed2::hphNT1 CeGFP(aa159-240)-LEU2*	

AH016a	Δ*med2* N-GFP *MAT*α	*Δmed2::hphNT1 NeGFP(aa1-158)-TRP1-NatMX4*	
AH050a	Δ*pgd1* C-GFP *MAT***a**	*Δpgd1::hphNT1 CeGFP(aa159-240)-LEU2*	
DL089	Δ*pgd1* N-GFP *MAT*α	*Δpgd1::hphNT1 NeGFP(aa1-158)-TRP1-NatMX4*	Diana Ludwig
AH021a	Δ*sin4* C-GFP *MAT***a**	*Δsin4::hphNT1 CeGFP(aa159-240)-LEU2*	
DL052a	Δ*sin4* N-GFP *MAT*α	*Δsin4::hphNT1 NeGFP(aa1-158)-TRP1-NatMX4*	Diana Ludwig
AH022a	Δ*soh1* C-GFP *MAT***a**	*Δsoh1::hphNT1 CeGFP(aa159-240)-LEU2*	
AH023a	Δ*soh1* N-GFP *MAT*α	*Δsoh1::hphNT1 NeGFP(aa1-158)-TRP1-NatMX4*	
AH017a	Δ*srb2* C-GFP *MAT***a**	*Δsrb2::hphNT1 CeGFP(aa159-240)-LEU2*	
AH018	Δ*srb2* N-GFP *MAT*α	*Δsrb2::hphNT1 NeGFP(aa1-158)-TRP1-NatMX4*	
DL088	Δ*ssn3* N-GFP *MAT*α	*Δssn3::hphNT1 NeGFP(aa1-158)-TRP1-NatMX4*	Diana Ludwig
AH019a	Δ*ssn3* C-GFP *MAT***a**	*Δssn3::hphNT1 CeGFP(aa159-240)-LEU2*	
	double mutants		
AH024a	Δ*prm1*Δ*cax4* C-GFP *MAT***a**	*Δprm1::hphNT1 Δcax4::kanMX6 CeGFP(aa159-240)-NatMX4*	
AH025a	Δ*prm1*Δ*cax4* N-GFP *MAT*α	*Δprm1::hphNT1 Δcax4::kanMX6 NeGFP(aa1-158)-TRP1-NatMX4*	
AH009	Δ*prm1*Δ*vma2* C-GFP *MAT***a**	*Δprm1::hphNT1 Δvma2::kanMX4 CeGFP(aa159-240)-NatMX4*	
AH010	Δ*prm1*Δ*vma2* N-GFP *MAT*α	*Δprm1::hphNT1 Δvma2::kanMX4NeGFP(aa1-158)-TRP1-NatMX4*	
AH026a	Δ*vma2*Δ*erg6* C-GFP *MAT***a**	*Δvma2::hphNT1 Δerg6::kanMX6 CeGFP(aa159-240)-LEU2*	
AH027a	Δ*vma2*Δ*erg6* N-GFP *MAT*α	*Δvma2::hphNT1 Δerg6::kanMX6 NeGFP(aa1-158)-TRP1-NatMX4*	
AH013	Δ*vma2*Δ*erg3* C-GFP *MAT***a**	*Δvma2::hphNT1 Δerg3::kanMX4 CeGFP(aa159-240)-NatMX4*	
AH014	Δ*vma2*Δ*erg3* N-GFP *MAT*α	*Δvma2::hphNT1 Δerg3::kanMX4 NeGFP(aa1-158)-TRP1-NatMX4*	
AH028a	Δ*vma2*Δ*cax4* C-GFP *MAT***a**	*Δvma2::hphNT1 Δcax4::kanMX6 CeGFP(aa159-240)-LEU2*	

AH029a	Δ*vma2*Δ*cax4* N-GFP *MAT*α	*Δvma2::hphNT1 Δcax4::kanMX6 NeGFP(aa1-158)-TRP1-NatMX4*	
AH064a	Δ*prm1*Δ*erg6* C-GFP *MAT***a**	*Δprm1::hphNT1 Δerg6::kanMX6 CeGFP(aa159-240)-NatMX4*	
AH064b	Δ*prm1*Δ*erg6* N-GFP *MAT*α	*Δprm1::hphNT1 Δerg6::kanMX6 NeGFP(aa1-158)-TRP1-NatMX4*	
AH067a	Δ*cax4*Δ*erg6* C-GFP *MAT***a**	*Δcax4::hphNT1 Δerg6::kanMX6 CeGFP(aa159-240)-LEU2*	
AH068a	Δ*cax4*Δ*erg6* N-GFP *MAT*α	*Δcax4::hphNT1 Δerg6::kanMX6 NeGFP(aa1-158)-TRP1-NatMX4*	
AH076	Δ*vph1*Δ*stv1* C-GFP *MAT***a**	*Δvph1::hphNT1 Δstv1::kanMX4 CeGFP(aa159-240)-LEU2*	
AH077	Δ*vph1*Δ*stv1* N-GFP *MAT*α	*Δvph1::hphNT1 Δstv1::kanMX4 NeGFP(aa1-158)-TRP1-NatMX4*	
AH004	Δ*fus1*Δ*fus2* C-GFP *MAT***a**	*Δfus1::hphNT1 Δfus2::kanMX4 CeGFP(aa159-240)-LEU2*	
AH005	Δ*fus1*Δ*fus2* N-GFP *MAT*α	*Δfus1::hphNT1 Δfus2::kanMX4 NeGFP(aa1-158)-TRP1-NatMX4*	

2.10 Primers

From the Saccharomyces Genome Database (SGD), the respective DNA sequences of all yeast genes were received (https://www.yeastgenome.org/). The majority of gene specific primers were obtained from the Primers4Yeast platform provided by the Weizmann Institute of Science (https://www.weizmann.ac.il/Primers-4-Yeast/). The sequencing primers were designed using the SnapGene Viewer software.

Table 14: List of used primers.

Primer	Sequence (5'-3')
CAX4 5'UTR CHK F	ACGCCAAACTAGTGGTACAG
CAX4 C'-Tag CHK F	TTCATGGGGTTTTGTTTTAC
CAX4 C'-Tag pYM F	AATAAATCAGCGATCTTTCAATGATAAATCCAAAAGGGATcgtacgctgcaggtcgac
CAX4 C'-Tag pYM R	AAATAGATGAAAAAAAATAAGAAAAAATGAAATGTTCAACCTAatcgatgaattcgagctcg

CAX4 KO pYM F	TATCTACATCAAAATTTGTTTTGAATCGGATCATATCATGcgtacgctgcaggtcgac
CAX4 KO pYM R	AAATAGATGAAAAAAAATAAGAAAAAATGAAATGTTCAACCTAatcgatgaattcgagctcg
CAX4 WT CHK F	TTCATGGGGTTTTGTTTTAC
CAX4 WT CHK R	CAATACGCCTCGTAATTCTC
ERG3 5'UTR CHK F	TATTTCGGTCGTTTAGTTGC
ERG3 C'-Tag CHK F	CATCTACCCATTGATTCTGC
ERG3 C'-Tag pYM F	TAGAATCTATGAAAACGACCCAAATACCAAGAAGAACAACCgtacgctgcaggtcgac
ERG3 C'-Tag pYM R	AGAAAGAAAAAAGATGAGACAAACAAGGCAACCGTATTCAatcgatgaattcgagctcg
ERG3 KO pYM F	AAAGATAATAAGAAAAATATTCGTCTAGATTTGAGATATGcgtacgctgcaggtcgac
ERG3 KO pYM R	AGAAAGAAAAAAGATGAGACAAACAAGGCAACCGTATTCAatcgatgaattcgagctcg
ERG3 WT CHK F	CAGCTACGTGTTTGTGTTTG
ERG3 WT CHK R	GAAAGAATGAGATGCGAAAG
ERG6 5'UTR CHK F	ATGCAACAGGGTAAGATCAG
ERG6 C'-Tag CHK F	ACCTTTGCTGTTTACGAATG
ERG6 C'-Tag pYM F	CGCCGAAACCCCCTCCCAAACTTCCCAAGAAGCAACTCAAcgtacgctgcaggtcgac
ERG6 C'-Tag pYM R	TCGTGCGCTTTATTTGAATCTTATTGATCTAGTGAATTTAatcgatgaattcgagctcg
ERG6 KO pYM F	AACAAGAATAAAATAATAATATAGTAGGCAGCATAAGATGcgtacgctgcaggtcgac
ERG6 KO pYM R	TCGTGCGCTTTATTTGAATCTTATTGATCTAGTGAATTTAatcgatgaattcgagctcg
ERG6 WT CHK F	TCGAAGAAAACACTTTCGAC
ERG6 WT CHK R	AACGTACTTCCACTCACCAG
KEX2 5'UTR CHK F	TCAATGAGGGTCATTTTCTG
KEX2 C'-Tag CHK F	CCTGATTCTGATCCAAACAC
KEX2 C'-Tag pYM F	AGAATTACAGCCTGATGTTCCTCCATCTTCCGGACGATCGcgtacgctgcaggtcgac
KEX2 C'-Tag pYM R	GCTATTTTGTAATTTGAAGCTTTCTGTACATATCGAATCAatcgatgaattcgagctcg

KEX2 KO pYM F	CTCGTCACATAATTATAAACTACTAACCCATTATCAGATGcgtacgctgcaggtcgac
KEX2 KO pYM R	GCTATTTTGTAATTTGAAGCTTTCTGTACATATCGAATCAatcgatgaattcgagctcg
KEX2 WT CHK F	TCTATTTCCATCACGCGCTAC
KEX2 WT CHK R	TCAAAATCGAAGTCCTCAAC
PRM1 5'UTR CHK F	TTCCGATGATGCCTACATAC
PRM1 C'-Tag CHK F	ATGTGCCATTGAAAATAAGC
PRM1 C'-Tag pYM F	GGTAATTCTCCGATTACGTCTTCGCAAAGCCACCTTTGACcgtacgctgcaggtcgac
PRM1 C'-Tag pYM R	ATAGAGTTATGACGGAAAAAGTCTATCAACTAATTAATCAatcgatgaattcgagctcg
PRM1 KO pYM F	AGGATGATTCCCTTTCGAATTTGTGAACGTTGATGATATGcgtacgctgcaggtcgac
PRM1 KO pYM R	ATAGAGTTATGACGGAAAAAGTCTATCAACTAATTAATCAatcgatgaattcgagctcg
PRM1 WT CHK F	TTCCTCAATCAACGATAAGC
PRM1 WT CHK R	TCCAGAGCTTGATTTCATTC
VMA2 5'UTR CHK F	ATATCCCATGGCTACTGGAC
VMA2 C'-Tag CHK F	GTCTTGCCTTCGTTGAGTAG
VMA2 C'-Tag pYM F	CGGTAAGAAGAAGGACGCCAGCCAAGAAGAATCTCTAATCcgtacgctgcaggtcgac
VMA2 C'-Tag pYM R	AAAATAAAAAAAGCCTTTTTCTTCAGCAACCGTCCTCTTAatcgatgaattcgagctcg
VMA2 KO pYM F	GTAGACAGTACATCAAGCGAAAATAAATATTGCAGGAATGcgtacgctgcaggtcgac
VMA2 KO pYM R	AAAATAAAAAAAGCCTTTTTCTTCAGCAACCGTCCTCTTAatcgatgaattcgagctcg
VMA2 WT CHK F	CTGGTAGACCCATTGACAAC
VMA2 WT-CHK-R	TTTCTTCGAAATCCTGTTG
FUS1 5'UTR CHK F	AACAGAACAATAACGGCAAC
FUS1 KO pYM F	GAGCAGGATATAAGCCATCAAGTTTCTGAAAATCAAAATGcgtacgctgcaggtcgac
FUS1 KO pYM R	AGGTATAGATTAAATGCGAACGTCAATATTATTTTCATCAatcgatgaattcgagctcg
FUS1 WT CHK F	GATATAATGCCTGACGAACG

FUS1 WT CHK R	GCAATGGTTTAGAACGTGAC
FUS2 5'UTR CHK F	TGCTTGGTGGACTTAGAAAC
FUS2 KO pYM F	GTAAGTTCTTAAGAAAAAAGACAAGAAAACCCCTTGCGATGcgtacgctgcaggtcgac
FUS2 KO pYM R	AACATTCTAAAAACTATAAGCTAAATATACTCTTTTGTTAatcgatgaattcgagctcg
FUS2 WT CHK F	TCAGGGCTAGAAATTGTCAC
FUS2 WT CHK R	TTTCGAGCTCTGTGAGTTTC
GAL11 5'UTR CHK F	AGGCATTACCCTACATTGTG
GAL11 KO pYM F	GATCAAGGATTAAAACGCTATTTCTTTTAAATCTGCTATGcgtacgctgcaggtcgac
GAL11 KO pYM R	ACTTCAAAAGTATCAAAAGTATGAAACTTCAAATGTTCAatcgatgaattcgagctcg
GAL11 WT CHK F	GATCAACGGTAAGGTGAATG
GAL11 WT CHK R	GCGATGTTTAAAACGAGAAG
MED2 5'UTR CHK F	TTTTATTGCAAGGCCAGAG
MED2 KO pYM F	GGCGGATCCTCCCAAATAAACTGCCCGTCTGAAAGTAATGcgtacgctgcaggtcgac
MED2 KO pYM R	GGTTTACAAGTCAATAGTTAACAATAGGAAGACCAAGCTAatcgatgaattcgagctcg
MED2 WT CHK F	AAGTTGGAGCAGAAATGATG
MED2 WT-CHK R	TTTTCCTTTGAATTTTGCTG
PGD1 5'UTR CHK F	CGACGAAGAAGCAGATAATG
PGD1 KO pYM F	GCGCAAAACGGACACAACAGCAGTAAAGACAACCGGAATGcgtacgctgcaggtcgac
PGD1 KO pYM R	ACAGATAATTACTATCTTGGATACATAGATGCACCAGTCAatcgatgaattcgagctcg
PGD1 WT CHK F	CCAGGGACAAAAGTGTGTAAG
PGD1 WT CHK R	TTACAACAGTTGCTGTCGAG
PKR1 5'UTR CHK F	TTACCGTTGTTTCTTTCGTC
PKR1 KO pYM F	AAAAATCGCAGGGATATAACTTCGAAAATTTCAAAATGcgtacgctgcaggtcgac
PKR1 KO pYM R	ATAACAGAGATAATTATGTAGTCAATTATGTATCTGTCTAatcgatgaattcgagctcg
PKR1 WT-CHK F	TGGGAAAGTGTATTTGAACC
PKR1 WT-CHK-R	CCTAGATTGTGCTTGAGTCC

SIN4 5'UTR CHK F	GAACGAAGATGTGGATGAAG
SIN4 KO pYM F	AACTAGCAGACCTGACCTTCTGTTGGTAAATATTAGTATGcgtacgctgcaggtcgac
SIN4 KO pYM R	AACAATTCTATACAAAACTATGCTATAGTACTAATAATCAatcgatgaattcgagctcg
SIN4 WT CHK F	ACTTCTGAGATGTTCGATGC
SIN4 WT CHK R	CTTTTCACGTATCCAAATGC
SOH1 5'UTR CHK F	TAGCATTTACCAGACCATCC
SOH1 KO pYM F	TCATAAGACGGCAAAGTCCCCAAGCTCCACCCAGGATGcgtacgctgcaggtcgac
SOH1 KO pYM R	TATGAATGCGTGCGAATGTAGTTATAATTAGGTGTGTTCAatcgatgaattcgagctcg
SOH1 WT CHK F	ACTAATGGAAACGCACCAG
SOH1 WT CHK R	ACCATTTCATTCATCCATTG
SRB2 5'UTR CHK F	CGTTATCTACTGGGAGCAAG
SRB2 KO pYM F	TGTAAGTCGGCGCTCGAAAGCACAGTAGCAATCCATCATGcgtacgctgcaggtcgac
SRB2 KO pYM R	ACAGAAAAAAAAAAAAAGAAAAAGCATTCGTAAGAACTCAatcgatgaattcgagctcg
SRB2 WT CHK F	ACTAACGGAACTGAAGGATG
SRB2 WT-CHK-R	GTCCAAGATCAACGTCTCAC
SSN3 5'UTR CHK F	CATATTTTGGGAAATGGTTG
SSN3 KO pYM F	AATTAAGGCCGCCTAGTTTTGACGGGAGGAGAGAGAAATGcgtacgctgcaggtcgac
SSN3 KO pYM R	GGAATGAAAAATTCCAAATATATATAAAAATAGAAGCCTAatcgatgaattcgagctcg
SSN3 WT-CHK F	ATTGGACCTTATAGGGCAAG
SSN3 WT CHK R	TAATGAGGGTTTGTTTTTGG
STV1 5'UTR CHK F	GGGGCTTATTTTTGTTTCTC
STV1 KO pYM F	CTTATTCTCTAAAATTCCTCGAGTTATATGAATAATTATGcgtacgctgcaggtcgac
STV1 KO pYM R	GGGGGTAGATGAGAAAATTTACAGTAATTTAAGGTTATTAatcgatgaattcgagctcg
STV1 WT CHK F	GGATTACATTGAAACGTTGG
STV1 WT CHK R	GCACCCATCAACAATAAAC
VMA10 5'UTR CHK F	CTCTGGACATAAGCATTTCG

VMA10 KO pYM F	CTGCAATCTCCAAAGTTGGCAAGGTATACAAAGCAGAATGcgtacgctgcaggtcgac
VMA10 KO pYM R	AAGATATATGATTAGAAAACTAGAATGTAATGCAATATTAatcgatgaattcgagctcg
VMA10 WT CHK F	ACCTCGTGACAAAGGTATTG
VMA10 WT CHK R	AAATTTTGACAACGTCATCC
VMA11 5'UTR CHK F	AGAAACCTGTCAAAATGGTG
VMA11 KO pYM F	GAGGAGGAAAGGGTCCATTCTATTATTCTCTGTAAACATGcgtacgctgcaggtcgac
VMA11KO pYM R	TTTTATTGTAATTATTTTTTTTTTTTAAACTTTTGACTCAatcgatgaattcgagctcg
VMA11 WT CHK F	CATATATGCTCCATTGTACGC
VMA11 WT-CHK-R	TTTCTAACACCAACGTCACC
VMA13 5'UTR CHK F	ATCTCACGATCAAAAACAGG
VMA13 KO pYM F	CAAGAGATATAAAAGTGCACTGGCGATTTCAGGAACAATGcgtacgctgcaggtcgac
VMA13KO pYM R	CTTCAAAACCCACTACTACTTTACGGTCTTCTATATCTTTAatcgatgaattcgagctcg
VMA13 WT CHK F	GGTGAAGAAGAACATTGGTG
VMA13 WT-CHK-R	TGTTTTTCAACAGCTTTTCC
VMA16 5'UTR CHK F	CAAGTGCTCCTGAAACTAC
VMA16 KO pYM F	AGGCGAATAAAATACAGGGAGCTAGAGCGTGTAAGATAATGcgtacgctgcaggtcgac
VMA16KO pYM R	CTCGTAAAACGGAAAAGAAAAGCCTGGTTTGAGCGCTTAatcgatgaattcgagctcg
VMA16 WT CHK F	AGTTTTCCTTCTCCCACTTC
VMA16 WT-CHK-R	AGTAGCCACAGTCAATTTCG
VMA21 5'UTR CHK F	GATTTGGTTTCCAGACAGTG
VMA21 KO pYM F	TAGTAGAAAACTAACCAAGACTTCAAAAGAATCAAATAATGcgtacgctgcaggtcgac
VMA21KO pYM R	TCTTGTATATTCTCTTCTAGCAACATATACTACTCAATCAatcgatgaattcgagctcg
VMA21 WT CHK F	GCTGTAGATGTTCCTCGTG
VMA21 WT CHK R	ACCATCAACTTTGTGATCTTC
VMA3 5'UTR CHK F	CAATGAAATAGGCCGTCTAC

VMA3 KO pYM F	TAATCAATTAGAATAACAAAAGAAACATATACATATAATGcgtacg ctgcaggtcgac
VMA3 KO pYM R	TATACTCTATTCCTGCTTTAGTGATTCAGAAGCTGCCTTAatcgatga attcgagctcg
VMA3 WT CHK F	ACTGCTAAGTCTGGTTGG
VMA3 WT CHK R	AACAAAGCAACAATCAAACC
VMA5 5'UTR CHK F	TGATTACCCCATACTTACGC
VMA5 KO pYM F	CTAATTCTAGATCAATTCTTTTTTCTGAAAAAAAAATGcgtacgctgc aggtcgac
VMA5KO pYM R	GAAATATATTAATCTAAGTTAGTATTATAAATCGATTAatcgatgaat tcgagctcg
VMA5 WT CHK F	CTGCTGAGAGAAAGAAGACG
VMA5 WT CHK R	GTTCTAAACTGGCAGCAGAG
VMA7 5'UTR CHK F	GGTTGACCATTTGTTGTGAC
VMA7 KO pYM F	TTCATAGCTAGTCTCACTGACGCATAGTAACTAAATCATGcgtacgc tgcaggtcgac
VMA7 KO pYM R	ACCAGTAATTGTGTTTGTTTTGGGAAAGATCGTCGCTTAatcgatga attcgagctcg
VMA7 WT CHK F	AGCTGTGATAGCTGACGAAG
VMA7 WT CHK R	ACTCACCGAACAACTTTCTG
VMA8 5'UTR CHK F	CCACCGATTGGGTTACTAAG
VMA8 KO pYM F	CATAGGTTCCTAACAGCATTGTGAAAAAGGTTCAAAAATGcgtacg ctgcaggtcgac
VMA8 KO pYM R	ACATATTTTTGAAAAGGGTCTTGTTCTGCCTGAAACTTCAatcgatg aattcgagctcg
VMA8 WT CHK F	GGCTATCAAGTGCAAGAAAG
VMA8 WT CHK R	CTGTCCAACTCATCCAACTC
VMA9 5'UTR CHK F	TTTTACCGGGTACATACTGG
VMA9 KO pYM F	AAACAAAGGTCCAACGAATAATAAAGAACAAAGAGTAATGcgtac gctgcaggtcgac
VMA9 KO pYM R	CTCAGGAAACGTCACTTGGCTTGATATACTCGACGCTTTAatcgatg aattcgagctcg
VMA9 WT CHK F	TTCCCTTTTCTTCCTTCTTC
VMA9 WT CHK R	GCAAATTCAGGTCTCAAATC
VOA1 5'UTR CHK F	GTCTGAGATACGCTTCGTTG

VOA1 KO pYM F	CTATATATAATAAGAATCGAACTGTAAAGTTAAAGCAATGcgtacg ctgcaggtcgac
VOA1 KO pYM R	KATATGTTTCTTTCAAATATATGAGTATATATAACGATTAatcgatga attcgagctcg
VOA1 WT CHK F	TACCTGAAAGTGCCTCTGAC
VOA1 WT CHK R	AACAATAGCAACGCAGAAAC
VPH1 5'UTR CHK F	CAGATTGAAATGTCATCACG
VPH1 KO pYM F	CAAAAAAAAAACATTTAAAGGTTACACAAGGAAAATAATGcgtac gctgcaggtcgac
VPH1 KO pYM R	ACTTAAATGTTTCGCTTTTTTTAAAAGTCCTCAAAATTTAatcgatga attcgagctcg
VPH1 WT CHK F	CATTGGATGCCAATCTTTAC
VPH1 WT CHK R	CAGGACTTGGATAATGGATG
VPH2 5'UTR CHK F	TAGGGTAATGAATGGCAAAG
VPH2 KO pYM F	GGATAATTGACGATTGGCATCACATAAAAGAACTCTAATGcgtacg ctgcaggtcgac
VPH2 KO pYM R	TCTCGGATCTCGGAGTTCTTATTTATAAAATGATCAGTTAatcgatg aattcgagctcg
VPH2 WT CHK F	GACAGTGATCTCCAATGCTC
VPH2 WT CHK R	AAGCACAACAAAAGACGAAC
AFG3 5'UTR CHK F	AAGAGTGTGTCCAATTACGC
AFG3 WT CHK F	CACAATACACCGTTCTACCC
AFG3 WT-CHK-R	ACGACGTAAATCTTGGACAC
ALG5 5'UTR CHK F	TGTGGTGTTTGGGTTTATTC
ALG5 WT CHK F	CGTTGAGATTCCTGATTGAG
ALG5 WT CHK R	TATCTGTGGAACCATCATCC
ANP1 5'UTR CHK F	CATCTGGTCTAGTTGCCTTC
ANP1 WT-CHK F	AACTCTCGTTCAACCCTACC
ANP1 WT-CHK R	AGAGTCACTCACCAAAAAACG
BUD9 5'UTR CHK F	TGCCACATACGTACATTGAC
BUD9 WT CHK F	TCTTGTTTCTCCTGTGGAAG
BUD9 WT CHK R	TTTCGTTGGTATTCTTCTGC
BUR2 5'UTR CHK F	ATCTCATTCCCCTGTTATGG
BUR2 WT CHK F	AGCCAGTTTCTTTTATTGTGC
BUR2 WT CHK R	AACTCTTCCTTCACCTCACC
CAX4 5'UTR CHK F	ACGCCAAACTAGTGGTACAG

CAX4 WT CHK F	TTCATGGGGTTTTGTTTTAC
CAX4 WT CHK R	CAATACGCCTCGTAATTCTC
CHS3 5'UTR CHK F	ATATTCAATAGCGTCGATGG
CHS3 WT CHK F	TACTTCCGTTGGACTGTAGC
CHS3 WT CHK R	TTCATTCGAGAGTTTCCAAG
CHS7 5'UTR CHK F	AGACTTCTTCCAATGTCAG
CHS7 WT CHK F	TGGGTCATATCCATACTTCG
CHS7 WT CHK R	TAGCTCCTGTGACCCATAAG
COX8 5'UTR CHK F	TGTAACAATGGGTGAAATAGC
COX8 WT CHK F	GCCAACAGATGATTAGAACG
COX8 WT CHK R	AATTGAACATAGCAGGCAAC
CTR1 5'UTR CHK F	AACTGCACCTCAACTATTCG
CTR1 WT CHK F	CTTCAGCAACTCCAAAGAC
CTR1 WT CHK R	CTACCACATTGGCAGTTACC
CTS1 5'UTR CHK F	AATATGGACGGAAGTATTTGG
CTS1 WT CHK F	TTTACCTGGTTCTGCTTCTG
CTS1 WT-CHK R	GCTTGCAGTTGGAGATAAAG
CYB5 5'UTR CHK F	GATTCAACGACCAAAATCAC
CYB5 WT-CHK F	TACCAAGAAGTTGCCGAAC
CYB5 WT-CHK-R	AAAATGGCCAATGACAAC
DFG16 5'UTR CHK F	CGGTGATTGCCATATATACAC
DFG16 WT CHK F	AAACACATCGACAACATTCC
DFG16 WT CHK R	ACACAGATACACCCAGAAGC
ECM33 5'UTR CHK F	ACGTGCAGTAAACAACCATC
ECM33 WT CHK F	TCTCGAGTAGATTCGTGGTC
ECM33 WT-CHK-R	ATTTTGTCCAAATCAGCTTG
EMP70 5'UTR CHK F	ACCAATACTGCCTGAGAATG
EMP70 WT CHK F	CAACCTTGGTTTGTACAGG
EMP70 WT CHK R	AAGAAGTCGCTGATTCATTG
ERG3 5'UTR CHK F	TATTTCGGTCGTTTAGTTGC
ERG3 WT CHK F	CAGCTACGTGTTTGTGTTTG
ERG3 WT CHK R	GAAAGAATGAGATGCGAAAG
FIG2 5'UTR CHK F	TGTCCTTCTTTGTTTCAAGC
FIG2 WT CHK F	GCATGTAGTGGAGAAGGATG
FIG2 WT CHK R	GCAGCAACAAAAGAAGTAGC

FPS1 5'UTR CHK F	AATTAGTTCTGTTGCGCTTG
FPS1 WT CHK F	TCCTCAAAAAGCTCTAAACG
FPS1 WT CHK R	TGTATGCGCTAGGAATAACC
FYV5 5'UTR CHK F	GGCAGATTAACTTTGCTACG
FYV5 WT CHK F	ATCATTTCGATCTGCTTCAG
FYV5 WT CHK R	AATAACTCAAGGGCATTTAGC
LÜCKE1 5'UTR CHK F	TGGATGCTTTTTCTTACGTC
GAP1 WT CHK F	TACTAGCCTTGTCTGGGTTG
GAP1 WT CHK R	TACCCGTATCAATGTCCATC
GAS1 5'UTR CHK F	GTAGCTGATAAAGCGAGCTG
GAS1 WT CHK F	AATGTTATCCGTGTCTACGC
GAS1 WT CHK R	CTTCGTCATCATTGGAAGAG
GDA1 5'UTR CHK F	TCTATTTAACCCGCACAGTC
GDA1 WT CHK F	TCGCCTGGATTACTACAAAC
GDA1 WT CHK R	ATTAACTTTAGGCGGTAGGC
HOC1 5'UTR CHK F	AAGCAAGCAACAAAGAGTTG
HOC1 WT CHK F	CAAAGAGCTGACTGGAGAAC
HOC1 WT CHK R	TTGGTTTGGACAGTTAAAGG
ILM1 5'UTR CHK F	AATAGCGACGGTGAAGAAC
ILM1 WT CHK F	TCCCCTGTTAGAAAACAATG
ILM1 WT-CHK-R	TATCTTTCCCATCTTCATCG
IRA2 5'UTR CHK F	CTTCTAGAACGCTCCCTTG
IRA2 WT CHK F	AAACAACAAGGACAAACAGC
IRA2 WT CHK R	AATAAGACAAACCGCAAATG
ISC1 5'UTR CHK F	CTGCTCTCTGGTGGTATTTG
ISC1 WT CHK F	ACAGAGATGTTCACGAGAGG
ISC1 WT CHK R	AACGCTGATACGGATACTTG
KAR3 5'UTR CHK F	TCGCTTTATTCATAGCATCTG
KAR3 WT CHK F	CACTGAACTGGGTATGAAGG
KAR3 WT CHK R	CCGTATGCGAAGATACAAAC
KEX1 5'UTR CHK F	TTCAGCTTCTCTAACTTCG
KEX1 WT CHK F	CGACCAACCTACTGGTACTG
KEX1 WT CHK R	TTTCTTCTCCATAGCAAACG
MF(A)1 5'UTR CHK F	TAGACATCCGTTCTCTTTG
MF(A)1 WT CHK F	AGATTTAGAAGGGGATTTCG

MF(A)1 WT CHK R	GGTTTTAACTGCAACCAATG
MNN10 5'UTR CHK F	TTTATGTTCTCGCATCACTG
MNN10 WT CHK F	TCAAGGCCAAAATAGTAACG
MNN10 WT CHK R	ATTAGGAAACTCCCTGAACG
MSN5 5'UTR CHK F	AGGTTGTTTTCCAAAGAG
MSN5 WT CHK F	AATGATTGTTTGCCCTATTG
MSN5 WT CHK R	CTCGATCTATGGTCATTTGG
NHX1 5'UTR CHK F	AAGACGCATCACATATTTCG
NHX1 WT CHK F	KATATGTCCGGTATCGTCTC
NHX1 WT CHK R	TAGGGTATTTCACGGGAAC
NUP84 5'UTR CHK F	ATCACCCTCAGGAAGAGTTC
NUP84 WT CHK F	ATTGAAAAGCTGTGACTTGG
NUP84 WT-CHK-R	GAATAGCGCCACTCAAATAG
OST3 5'UTR CHK F	CAATTGACCCTTGAAGAAAG
OST3 WT-CHK F	TCAAAAAGCAGTCCAAACTC
OST3 WT-CHK R	TGAATAAGGCACAAAAGGAG
PAP2 5'UTR CHK F	ACCTTTATCCCAAATTAGCC
PAP2 WT CHK F	AAACAATTCCTACACGCAAG
PAP2 WT CHK R	AATGTTAAAGGACCCTCGAC
PEP12 5'UTR CHK F	TCAGATTTTTGCCTTAGCTG
PEP12 WT CHK F	GCGAGAGAGAAACTTGTGAG
PEP12 WT CHK R	TGAACAACACTTCCCAAATC
PET117 5'UTR CHK F	TGATTACCGGATTAGAATGG
PET117 WT CHK F	GGCTAGCAAGATAACGTTTG
PET117 WT CHK R	TAACCACCTCTCCATCTTTG
PMP2 5'UTR CHK F	TAAATTACCGCAATCCTACG
PMP2 WT CHK F	ATGTTGATGAGCACGTTACC
PMP2 WT CHK R	TTGTCTAGCTTGCCATTTTC
PMT1 5'UTR CHK F	CACCAATTGTCCTCTTTCAG
PMT1 WT CHK F	GTCTTTTCACGGTTACATGG
PMT1 WT CHK R	GAACCAGCTGGATAATTGTG
PMT2 5'UTR CHK F	AAACGCCATCATTTACAGTC
PMT2 WT CHK F	CCAACCAACAACAAGTAACC
PMT2 WT CHK R	TCTCCAAGTTCTTGATACGG
PMT4 5'UTR CHK F	TTTAGAGTTAATGCCGCTTG

PMT4 WT CHK F	ATCCTTCGTTGAAGTACACG
PMT4 WT CHK R	TATGGAGCTGGATGAGTTTC
PRM1 5'UTR CHK F	TTCCGATGATGCCTACATAC
PRM1 WT CHK F	TTCCTCAATCAACGATAAGC
PRM1 WT CHK R	TCCAGAGCTTGATTTCATTC
SAC1 5'UTR CHK F	AAAATAAGCCAAGACAGTGG
SAC1 WT CHK F	CTATGGGTATGCCAAGACAG
SAC1 WT-CHK R	TCGCCATATAACTCCTTTTG
SEC66 5'UTR CHK F	CCTAGATCCATCACTGTTCG
SEC66 WT CHK F	TCAAGCTACAGAAAGAAGCAG
SEC66 WT-CHK-R	CCATAACGAACAATTGAACC
SFP1 5'UTR CHK F	CTCCGTTAACAAGGTTTGAC
SFP1 WT-CHK F	ACAGGACATTGCCAAGTTAC
SFP1 WT-CHK R	ACCTGGTAAGGAAAGACCAC
SHS1 5'UTR CHK F	ACATTCAAGGCAAATGAAAG
SHS1 WT CHK F	AGACAGTCAAATGCTCCAAG
SHS1 WT CHK R	GACATATGGAACGGTTTCTG
SLG1 5'UTR CHK F	TTTGACGTTAGTGGAAAAGC
SLG1 WT CHK F	CGCTAACTTCGGATACTTTG
SLG1 WT CHK R	GCCTCTTGGTATTCCTTTTC
SLM6 5'UTR CHK F	GATGCAGCTCTATACCATCG
SLM6 WT CHK F	ATTACTCTTTCCCGCCATTTC
SLM6 WT CHK R	AATTTGAAAAGACGTGTTGC
SNC2 5'UTR CHK F	GCGTATCCCTTTATCAGTCC
SNC2 WT CHK F	GTCGTCATCAGTGCCATAC
SNC2 WT CHK R	AAATGGACGACGATAGGAAC
SSN3 5'UTR CHK F	CATATTTTGGGAAATGGTTG
SSN3 WT-CHK F	ATTGGACCTTATAGGGCAAG
SSN3 WT CHK R	TAATGAGGGTTTGTTTTTGG
STB5 5'UTR CHK F	CCTTGCAACCTTCTATTTTG
STB5 WT CHK F	TTCCAGTGAAAAGGAACAAG
STB5 WT CHK R	CTCCGAATGATGAAGTTGTC
STE13 5'UTR CHK F	GAGTTCTCATTTGCTTTTGG
STE13 WT CHK F	AAACATTTACCACCAAGTCG
STE13 WT CHK R	CCGTGTAAACGGAATCATAC

STE24 5'UTR CHK F	CAAGAAACTTGCAAAACCAG
STE24 WT CHK F	GGAAGACGAAATTGATGATG
STE24 WT CHK R	TATCGGTGATCCATAGTTGG
SWF1 5'UTR CHK F	AGTAATGTCCAAGGGCTTTC
SWF1 WT CHK F	AGGCTCGACAGAGGAATATC
SWF1 WT CHK R	CAATGGCCAATTGAAGATAC
SYS1 5'UTR CHK F	ATAACCCGGCTTTTAATCAG
SYS1 WT CHK F	ATCAAGGAATGGCTGTTTTC
SYS1 WT CHK R	ACCAATCCAACTTCTCCTTC
TAT1 5'UTR CHK F	CCGGGTCTTAGAGATTTTTGC
TAT1 WT CHK F	GAAGATACATCGGTGCTGAG
TAT1 WT CHK R	AAGTGAGCACAACTTTGAC
TLG2 5'UTR CHK F	CAGCTCATACAATCGAAAGC
TLG2 WT CHK F	TGGCTTTGAAGACAAGAGTC
TLG2 WT-CHK R	CCCTCTCTCTTCTCTCTTGC
UIP5 5'UTR CHK F	CGGTAGATCTGTCAAACCAG
UIP5 WT CHK F	CGATCAAATTGACTCAGGAC
UIP5 WT-CHK-R	AAGGGTACCTCCTTATGGTC
URA7 5'UTR CHK F	TCTGTACCTCTGTGAAAGG
URA7 WT CHK F	CAAATTGTCCCTCATTTGAC
URA7 WT CHK R	GCAATCTTATCGATTGTTGG
VPS64 5'UTR CHK F	GCGGTTCTACCTCTTCAATC
VPS64 WT CHK F	ACTGCAACATTCTCCCTATG
VPS64 WT CHK-R	TACGGCTTCTACAGGAATTG
YBL062W 5'UTR CHK F	GACCTGAAGCGTCAGTAATC
YBL062W WT CHK F	ATCCTTCTTGTTCTTCAAGC
YBL062W WT CHK R	CGTAGGGTCAAATTCAAGAG
YBR196C-A 5'UTR CHK F	GGGTTAGAGGCGAGTAAGAC
YBR196C-A WT CHK F	TCTATATATTCCATTGACGGTATTC
YBR196C-A WT-CHK R	AATGGGACGAAACAAATAGG
YDR149C 5'UTR CHK F	ATTCATCGTCTTTTGGTTTG
YDR149C WT CHK F	ACTCAACCAACAAATTCTCG
YDR149C WT-CHK R	GTTCGAATATGTCCCACAAC
YDR445C 5'UTR CHK F	AATACTGGCATTTCAGCTTC
YDR445C WT CHK F	GTTTTTCCAACGAAATAGCC

YDR445C WT CHK R	TCGGATCCAAGGTTTGTAG
YEL045C 5'UTR CHK F	CACGCTAAGTAAACCCAAAG
YEL045C WT CHK F	CTTCCCCTATCTGGAAAAAG
YEL045C WT CHK R	CAGCGGAAACAATGTACG
YFL013W-A 5'UTR CHK F	TGAAGCCAGACTCTCAAAAG
YFL013W-A WT CHK F	CATGAAATCCGTCTCAAATC
YFL013W-A WT-CHK R	AGCACCAACAGAAACAGAAG
YGL024W 5'UTR CHK F	GGTTTTCTTGGCTTTTTAGG
YGL024W WT CHK F	ATTGAACTGCAATCGCAAC
YGL024W WT CHK R	AACACTTTCCTGAGGATTTTC
YGL072C 5'UTR CHK F	GCGGTTTATACTTCAACCTG
YGL072C WT CHK F	ACGCTATTTAATGACCTTGC
YGL072C WT CHK R	GAGGGAAGTACAAGGGTGTC
YGR026W 5'UTR CHK F	TCAAATTGCCTTACGTATCC
YGR026W WT CHK F	TAGTTTGGAAAATCGGACAC
YGR026W WT-CHK R	AAGACTTACCACCACCAAAG
YGR045C 5'UTR CHK F	TAAACAGGCTGAAGGGTATG
YGR045C WT CHK F	TGTCACAGATTACATCAAAAGG
YGR045C WT CHK R	AACAATGTCAGTTCCAATGC
YJR018W 5'UTR CHK F	TTTTCTTTTCATGGGTTCAG
YJR018W WT CHK F	GTCTTCTTGAATCCTTGTGC
YJR018W WT CHK R	ATCATACCTTTTTCCCTTCG
YNL228W 5'UTR CHK F	GGGATCTTTATTCCTCTTCG
YNL228W WT CHK F	TCTCCTAGTGATGCCCAAAAG
YNL228W WT CHK R	CTGAGAAATTTGATTCAGC
YPL205C 5'UTR CHK F	AACCGTCTTAAAGGAGAACC
YPL205C WT CHK F	GTCGAATATGTCGTAACTTTTC
YPL205C WT CHK R	TTTCTGGAGAATTTTTGGTG
YPS7 5'UTR CHK F	ATGCACTAGTGTTTCGGTTC
YPS7 WT CHK F	CAGATATGGGTGTCTCCTTG
YPS7 WT-CHK-R	TTTGCGTAAGGAATGTAACC
YSP1 5'UTR CHK F	AATTGGGTTAAATGGGAAAC
YSP1 WT CHK F	ATGATCCGAAAAGAGTTGTG
YSP1 WT CHK R	TTTTCTCGCCAATTGATAAC
kanMX CHK rev	GAATTTAATCGCGGCCTCGAA

HYGR CHK rev	CAGCTATTTACCCGCAGGAC
mNG CHK rev	TCAATTCTTCGTAACCGTCG
	Primers used for cloning and sequencing
M13-40 F	GTTTTCCCAGTCACGAC
AS027	CTCGTCATTGTTCTCGTTC
M13 rev	TAATTCCAGATTGTTCGGGTCTAGAGAATCCA
PGD1 GA F in paS01	CAAGCATACAATCAACTgaattgggtaccATGGACTCGATTATACCGGC
PGD1 SEQ primer 1 F	GAAGCACGCGATGAAATTCTG
PGD1 GA R in paS01	TAAGAAATTCGCccaagctggagctcTCACAAGAAATCCATGTTCAGAC
YGL024w GA F in pAS01	CAAGCATACAATCAACTgaattgggtaccATGTTTGCCATTATCTGTATGAATTC
YGL024w GA R in pAS01	TAAGAAATTCGCccaagctggagctcTTAATATAATATGATATAATATAATATAATATATAACACTAACACTTTC
KEX2 GA F in pAS01	CAAGCATACAATCAACTgaattgggtaccATGAAAGTGAGGAAATATATTACTTTATGC
KEX2 GA R in pAS01	TAAGAAATTCGCccaagctggagctcTCACGATCGTCCGGAAGATG
CAX4 GA F in pAS01	CAAGCATACAATCAACTgaattgggtaccATGAATAGTACCGCCGCTGC
CAX4 GA R pAS01	TAAGAAATTCGCccaagctggagctcCTAATCCCTTTTGGATTTATCATTGAAAG
VMA2 GA F in pAS01	CAAGCATACAATCAACTgaattgggtaccATGGTTTTGTCTGATAAGGAGTTG
VMA2 GA R in pAS01	TAAGAAATTCGCccaagctggagctcTTAGATTAGAGATTCTTCTTGGCTGG

2.11 Cloning

2.11.1 DNA restriction, digestion and ligation

Plasmids were generated via Gibson assembly (GA) and are listed in **Table 10**. Designed primers with a 20 bp homology upstream and downstream of the vector restriction sites are listed in Table 14. Firstly, the desired DNA fragment (GA insert) was amplified by PCR using the high fidelity Phusion polymerase (**Table 15**). After isolating the fragment via agarose gel electrophoresis, the DNA was extracted using the Qiagen Gel Extraction Kit according to the

manufacturer's protocol, and eluted in 25 µl water. For restriction digestion of the vector commercially available restriction enzymes from NEB were used, according manufacturer's instructions. After running an agarose gel and extraction, the linearized vector DNA was eluted in 20 µl water. Finally, the GA reaction was performed in a total volume of 10µl with 5 µl 2x Gibson assembly mix, according manufacturer's instructions. The GA insert and linearized vector containing 20-40 ng DNA were mixed in a 3:1 ratio and incubated for about 30-40 min at 50˚C. Typically, 1 µl of the reaction mix was then transformed into competent *E. coli* cells.

Table 15: General PCR reaction using Phusion polymerase.

Reagent	[Stock]	[Final]	Unit	Volume per reaction (µl)
Phusion HF Buffer (5x)	5	1	x	10
Forward Primer	100	0,5	µM	0,25
Reverse Primer	100	0,5	µM	0,25
dNTPs	12,5	0,2	mM	0,8
Phusion Polymerase			µl	0,3
Plasmid DNA template or		10-20	ng	1
Genomic DNA				4
ddH_2O				filled up to 50 µl

Table 16: General Phusion PCR thermocycling protocol for amplifying the GA insert.

Step	Temperature (˚C)	Time	Cycles
1. Initial denaturation	98	1 min	1
2. Denaturation	98	15 sec	20-25
3. Annealing	55	30 sec	
4. Extension	72	30 sec/kb	
5. Final extension	72	5 min	1
6. Hold	8	infinite	1

Table 17: General protocol for restriction digestion.

Reagent	[Stock]	[Final]	Unit	Volume [µl] / reaction
Cutsmart Buffer (NEB)	10	1	x	2
DNA (EV pAS01)		0.5 – 1	µg	Y
SacI				1
KpnI				1
ddH_2O				Filled up to 20 µl

2.11.2.Transformation of *E. coli* cells

Chemical transformation was used to introduce 1 µl plasmid DNA into 60µl competent *E. coli* cells. After gentle mixing, the cells were incubated on ice for 15 min, followed by a heat shock at 42˚C for 75 sec. The cells cooled down on ice for 2 min before adding 1 ml LB media and subsequent incubation for 40-60 min at 37˚C with shaking at 300 rpm. The cells were harvested at 10,000 rpm for 1 min and resuspended in a final volume of 100 µl LB medium. The entire cell suspension was plated on LB selection agar plates containing 100 µg/ml Ampicillin (LB + Amp). Cells were incubated over night at 37˚C and examined for colony formation.

2.11.1.1 Plasmid miniprep and DNA quantification

Single colonies containing the desired plasmid DNA were picked and inoculated in 5 ml pre-warmed LB + Amp media to apply selection pressure. After incubation over night at 37˚C and shaking at 220 rpm, plasmid DNA was isolated using the QIAprep Spin Miniprep Kit (Qiagen) according to the manufacturer's protocol. DNA was eluted in 30µl H_2O and the concentration determined via absorbance at 260 nm using a NanoDrop 1000. The DNA was stored at -20˚C until use.

2.11.1.2 DNA sequencing

To confirm the correct sequence an aliquot of the obtained plasmid DNA was sent to Microsynth Seqlab, Germany. For each SANGER sequencing reaction, about 40-100 ng/µl plasmid DNA, and custom designed primers (Table 14) were used.

2.12 Yeast-specific procedures

2.12.1 gDNA extraction

To extract genomic DNA (gDNA) for PCR, a small amount of yeast cells was scraped off an agar plate using a sterile pipette tip and resuspended in 80 µl 20 mM NaOH solution. Glass beads of 0.5 mm size (Sigma) were added, and samples mixed for 10 min at 100 ˚C and shaking at 1400 rpm. After centrifugation at max. speed (13,000 rpm) for 1 min, the supernatant containing the gDNA was used for subsequent PCR reaction.

2.12.2 Competent yeast cell preparation

Competent yeast cell preparation was performed using the lithium acetate method as described by Knop et al. with some modifications [144]. Briefly, the respective yeast cells were grown over night in 5 ml YPD medium at 30˚C, and 220 rpm shaking up to saturation. The following day, the saturated culture was used to inoculate 50 ml fresh YPD medium. The cells were grown over night typically for about 15-16 h at 25˚C and 220 rpm to OD_{600} of 0.6 – 1.0. Next day, the cells were harvested by centrifugation at 1,700 x g for 5 min at RT. Subsequently, the cells were washed once with 0.4 volumes sterile water and 0.4 volumes SORB solution at RT. Finally, the supernatant was decanted and the cell pellet resuspended in 360 µl SORB solution before adding 40 µl of 8 mg/ml single stranded carrier DNA (ssDNA). 60 µl aliquots were prepared and competent yeast cells either used immediately for subsequent transformation, or stored at -80˚C until use.

2.12.3 Transformation of yeast cells

For transformation, an aliquot of 60 µl competent yeast cells was mixed with 4 ng/µl desired PCR product (amplified DNA). A 6-fold volume of PEG solution was added, cells gently mixed and incubated for 30 ˚C at RT. After adding a 1/9 volume of DMSO, the cells were heat shocked at 42 ˚C for 18 min in a thermomixer. The cells were pelleted by centrifugation at 2,500 rpm for 3 min. The supernatant was removed before resuspending the cells in YPD medium for generating knockout (KO) or tagged strains, or in SD-URA medium for plasmid transformation. To generate yeast ko or gene tagging strains, cells were resuspended in 3 ml YPD medium and cultivated for at least 4-5 h at 30˚C and 220 rpm to allow expression of the respective antibiotic resistance marker. Cells were harvested by centrifugation and resuspended in 80-100 µl YPD. The entire cell suspension was plated on YPD selection agar plates containing the respective antibiotics and plates incubated at 30˚C for 2-3 days or until colony formation. For plasmid transformation, the cells were mixed in 1 ml SD-URA, pelleted by centrifugation and resuspended in a final volume of 80-100 µl. The entire cell suspension was directly plated on SD-URA plates and incubated for 2-3 days at 30˚C until colony formation. To select for true positive transformants and reduce the number of transiently transformed colonies, single

colonies were selected and plated on a fresh selection agar plate. Afterwards, a colony PCR was performed to verify the correct gene deletion or gene tagging.

2.12.4 C-terminal gene tagging and generation of gene deletion strains by PCR

For the majority of generated yeast strains, genes were C-terminally tagged or deleted by PCR according to Janke et al. [145]. The antibiotic resistance cassettes hphNT1 or kanMX6 and the C-terminal tagging cassette mNG-kanMX4, conferring resistances hygromycin B or G418 respectively, were PCR amplified using primers that were generated with the Primers4Yeast tool. Used primers contained at their 5' end a 40 bp homology to the chromosomal locus of interest allowing the integration of the amplicon into the chromosome via homologous recombination. PCR reaction was carried out using DreamTaq or Phusion polymerase, typically in a 50 µl volume. A general PCR reaction can be viewed in Table 18, and thermocycling protocols in Table 19 and Table 20. DNA was gel extracted and 0.5 – 1 µg of PCR product transformed into 60 µl competent yeast cells as described in section 2.12.3.

Table 18: General PCR reaction for PCR-mediated gene knockout or C-tagging.

Reagent	[Stock]	[Final]	Unit	Volume / reaction
PCR Buffer (DreamTaq / Phusion)	10 / 5	1	x	5 / 10
Plasmid (pFA6 / pAH02 /pMS131)		10	ng	Y
Forward Primer	50	0,5	µM	0,5
Reverse Primer	50	0,5	µM	0,5
dNTPs	12,5	0,3	mM	1,2
DreamTaq Polymerase				0,5
dd H_2O				filled up to 50 µl

Table 19: General DreamTaq thermocycling protocol for PCR-mediated gene knockout.

Step	Temperature (˚C)	Time	Cycles
1. Initial denaturation	95	3 min	1
2. Denaturation	95	30 sec	10
3. Annealing	54	30 sec	
4. Extension	68	1min/kb	
5. Denaturation	95	30 sec	20

6. Annealing	54	30 sec	
7. Extension	68	2:40 min + 20sec / cycle	
8. Hold	8	infinite	1

Table 20: General Phusion PCR thermocycling protocol for C-tagging of genes.

Step	Temperature (˚C)	Time	Cycles
1. Initial denaturation	98	5 min	1
2. Denaturation	98	30 sec	20
3. Annealing	58	30 sec	
4. Extension	72	30 sec/kb	
5. Denaturation	98	30 sec	20
6. Annealing	58	30 sec	
7. Extension	72	30 sec/kb + 20 sec / cycle	
8. Hold	8	infinite	1

2.12.5 Generation of gene deletion strains by tetrad dissection

Tetrad dissection and sporulation was carried out according a protocol provided by Dieter Schmidt (Max Planck Institute for Biophysical Chemistry). Haploid yeast cells of opposite mating types were crossed on a YPD agar plate and incubated at 30˚C overnight. Formed diploids were grown in 5 ml sporulation media (YP + 2% Gal) overnight at 30˚C and 220 rpm. Next day, cells were pelleted by centrifugation at 3,000 rpm for 5 minutes, and resuspended in a volume of about 100 µl. The entire cell suspension was plated out on a K-acetate plate, a selective medium with reduced level of nitrogen and carbon to induce sporulation. After 5-7 days incubation at 20˚C, enough asci with four individual spores had formed. A sufficient number of cells was scraped from the plate, transferred to a 1.5 reaction tube containing 200 µl of 0.33 mg/ml zymolase, an enzyme to digest the asci, and incubated for 18 min at RT. Using a sterile inoculation loop, the cells were transferred to a YPD agar plate. The spores were selected with the help of a Singer Micro-manipulator according to the manufactures protocol. The plates incubated for 1-2 days at 30˚C until colonies have formed and were then replica-plated on pertinent selection agar plates. Grown colonies were selected and finally confirmed by colony PCR (see section 2.12.6) for the desired genotype.

2.12.6 Verification of yeast strains by colony PCR

Single colonies of transformed yeast cells were replated on respective selection agar plates to remove transient transformants. To confirm for the correct C-tagging or gene knockout, gDNA of single colonies was extracted (see section 2.12.1) for a subsequent colony PCR. Two PCR reactions were carried out using two different sets of primers. One set of primers annealed inside the ORF of interest to check for the presence of the WT gene (WT check); the other primer set annealed to the 5'UTR region and the selection resistance cassette verifying whether the gene was replaced with the respective selection marker (KO check). A general PCR reaction and thermocycling protocol is demonstrated in Table 21 and Table 22. Colonies that showed a band with the correct size for the KO check and absence of a band for the WT check in the agarose gel were counted as correctly transformed. Back-up glycerol stocks were prepared and stored at -80˚C.

Table 21: General PCR reaction for colony PCR.

Reagent	[Stock]	[Final]	Unit	Volume per reaction (µl)
PCR Buffer	10	1	x	2,5
Forward Primer	100	0,5	µM	0,125
Reverse Primer	100	0,5	µM	0,125
dNTPs	12,5	0,2	mM	0,4
Dream Taq Polymerase			µl	0,25
Genomic DNA				4
ddH_2O				filled up to 25 µl

Table 22: General thermocycling protocol for colony PCR.

Step	Temperature (˚C)	Time	Cycles
1. Initial denaturation	95	5 min	1
2. Denaturation	95	30 sec	28
3. Annealing	55	30 sec	
4. Extension	72	1min / kb	
5. Final extension	72	5 min	1
6. On hold	8	infinite	1

2.12.7 Pin replicator sterilization

Yeast cells were pin replicated by using a 96-floating pin-replicator. Before each pinning step, the pin replicator was sterilized by washing twice in ddH_2O for 30-60 sec, whereby most of the cells dropped from the pins. Followed by 30 sec incubations in sodium hypochlorite solution to eliminate the remaining cells, which was rinsed by two washing steps in ddH_2O. Finally, the replicator was disinfected for 10 sec in 70 % ethanol, followed by 5 sec incubations in 100 % isopropanol and passed through a flame before it cooled down until use.

2.12.8 Synthetic genetic array procedure

The purchasable yeast knockout (YKO) collection harbors a mutant selection of the entire open reading frame (ORF) of non-essential yeast genes (5,133 mutants), whereby each deletion is bar coded and linked to a G418 resistance cassette conferring resistance to the antibiotic Gentamycin (G418). Since the focus of this study was on membrane proteins which are likely to be involved in PM fusion, the YKO collection was condensed to include 1,696 mutants of ORFs predicted to encode transmembrane domains (TMDs). TMDs were determined by utilizing the Saccharomyces genome database (https://www.yeastgenome.org/) and the webtool TOPCONS (https://topcons.cbr.su.se/). A schematic workflow of the generation of the *MAT***a** YKO TMD sub-library is shown in **Figure 15**.

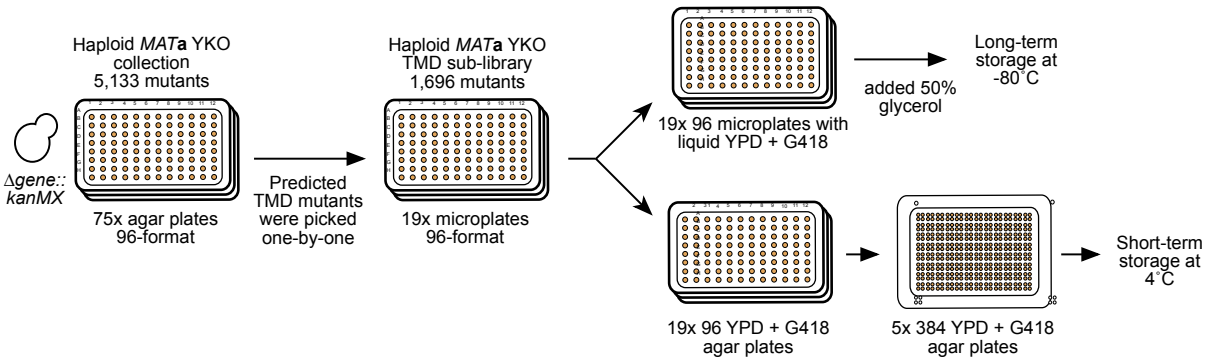

Figure 15: Schematic workflow for generating a customized *MAT*a YKO TMD sub-library. The *MAT***a** yeast knockout (YKO) collection composed of 5,133 gene deletion mutants was condensed by selecting 1,696 mutants of ORFs predicted to encode transmembrane domains (TMDs). Cells were transferred to a 96-well microplate containing 120 µl liquid YPD + G418 (200 mg/l). After two days incubation at 30˚C, 60 µl glycerol (50 % v/v) was added. The plates were sealed and stored at -80˚C until use. For short-term storage, the cells were pin-replicated on YPD + G418 selection agar and stored at 4˚C.

In this work, synthetic genetic array (SGA) methodology, according to Cohen and Schuldiner and Tong and Boone, was used to incorporate non-fluorescent split-GFP marker into each mutant of the customized *MAT***a** YKO TMD sub-library [146, 147]. This was done by crossing a *MAT*α query strain array containing the C-GFP marker (aa159-240) to the *MAT***a** YKO TMD sub-library to generate a *MAT***a** C-GFP library. This was repeated with a *MAT*α query strain array containing the N-GFP marker (aa1-158) allowing the generation of the corresponding *MAT*α N-GFP library. Both GFP marker were linked to a NatMX4 resistance cassette conferring resistance to the antibiotic nourseothricin (clonNAT). The query strains also contained two selection cassettes, Δ*lyp1* and Δ*can1*, that enabled the removal of diploid cells after the sporulation step. Δ*lyp1*::*STE3*pr-*LEU2* is only expressed in *MAT*α cells and *can1*::*STE2pr*-Sp*HIS5* only in *MAT***a** cells under the haploid mating-type specific promoter *STE3pr* or *STE2pr*, respectively. The *LYP1* gene encodes an arginine permease allowing the entry of its toxic analog thialysine. Comparably, *CAN1* encodes a lysine permease which enables the entry of the toxic analog canavanine. *LYP1* and *CAN1* are non-proteogenic amino acids (aa) whose incorporation leads to non-functional proteins. Since the mutants of the YKO collection are *LYP*+ and *CAN*+, formed heterozygous diploids are sensitive to thialysine and canavanine. Consequently, haploid spores that carry both deletions, Δ*lyp1* and Δ*can1*, are able to survive and grow on media containing both toxic analogs. Because the *MAT***a** specific Ste2pr is conjugated to HIS, and the *MAT*α specific Ste3pr to LEU, a selection of a single mating type after the sporulation step was conceivable by depleting either HIS or LEU in the media.

Experimental procedure:

An overview of the experimental outline is given in (**Figure 16**)**.**

Day 1 and 2: Overnight cultures (ON). To increase the mating efficiency, a fresh copy of the *MAT***a** C-GFP YKO TMD sub-library and the *MAT*α N-GFP query strain was prepared. On day 1, the glycerol stock of the *MAT***a** C-GFP array was thawed and transferred to a new YPD +G418 (150 mg/l) selection agar plate, followed by 2 days incubation at RT. On day 2, 20 ml liquid YPD + clonNAT (100 mg/l) medium were inoculated with a single colony of the *MAT*α N-GFP query strain and incubated for 1 day at 30˚C and 220 rpm.

Day 3: Arraying the *MAT*a C-GFP library and *MAT*α N-GFP query strain. The *MAT*α query strain was poured into a sterile container and 120 µl transferred into each well of a 96-well microplate. Following, the cells were pin-replicated four times on a new YPD + clonNAT (100 mg/l) agar plate to create a 384 array. Similarly, the *MAT***a** C-GFP YKO TMD sub-library was replicated on a YPD + G418 (150 mg/l) agar plate. Both 384 arrays were incubated for one day at 30˚C.

Day 4: Mating the *MAT*a C-GFP with the *MAT*α query strain array. The *MAT***a** C-GFP array was crossed to the *MAT*α query strain array to produce heterozygous diploids containing both genotypes (**a**/α). This was done by firstly pin-replicating the *MAT*α query strain array on a YPD agar plate, followed by pin-replicating the *MAT***a** C-GFP array on top of the query cells. The cells incubated for 1 day at RT.

Day 5 and 7: Diploid selection. To select for diploid cells harbouring the selectable markers (KanMX, NatMX) of both genotypes (**a**/α), the cells were replicated from the mating plate on YPD agar plates containing clonNAT (100 mg/l) and G418 (300 mg/l). The cells were allowed to mate for 2 days at 30˚C, before repeating the diploid selection step to eliminate all haploid cells.

Day 9: Sporulation. The cells were replicated from the diploid selection plate on medium with reduced levels of nitrogen and carbon to induce sporulation and generate haploid meiotic progeny. To increase the sporulation efficiency, a larger number of diploid cells was transferred by replicating twice. Subsequently, the cells incubated for 5 days at 22˚C.

Day 14: Haploid selection. To select for haploid spores of single mating types and eliminate diploid cells that did not undergo sporulation, cells were transferred from the sporulation plate to selection agar containing canavanine (50 mg/l) and thialysine (50 mg/l). To select for haploid spores of *MAT*α mating type, the synthetic defined (SD) medium lacked leucin, arginine and lysine (DO – Leu/Arg/Lys). To select for haploid spores of *MAT***a** mating type, the SD medium lacked histidine, arginine and lysine (DO – His/Arg/Lys). Additionally, G418 was added to avoid contamination. Monosodium glutamic (MSG) was added to alleviate the acidity of the medium and maintain the efficacy of G418. To transfer a large number of cells, the replication step was performed twice, followed by 2 days incubation at 30˚C.

Day 16 and 18: Final mutant selection. To finally select for haploid cells of one mating type that harbor all selectable markers, the cells were replicated on SD/MSG agar containing clonNAT, G418, canavanine and thialysine. For generating the *MAT*α YKO TMD sub-library, the media lacked Leu/Arg/Lys, for generating the *MAT***a** YKO TMD sub-library, the medium lacked His/Arg/Lys. After incubation for 2 days at 30˚C, the final selection step was repeated.

Library maintenance and storage: For long-term storage, a back-up glycerol stock of the *MAT***a** C-GFP and *MAT*α N-GFP YKO TMD sub-library was prepared and stored at -80˚C. Briefly, cells were transferred to a 96-well microplate filled with 120 µl YPD + G418 + clonNAT and incubated for 2 days at RT. 60 µl glycerol (50 % v/v) was added as a cryoprotectant. Each plate was sealed and subsequently stored at -80˚C. For short-term storage, the libraries were stored at 4 ˚C and replicated every 4 weeks on fresh YPD + G418 + clonNAT agar plates.

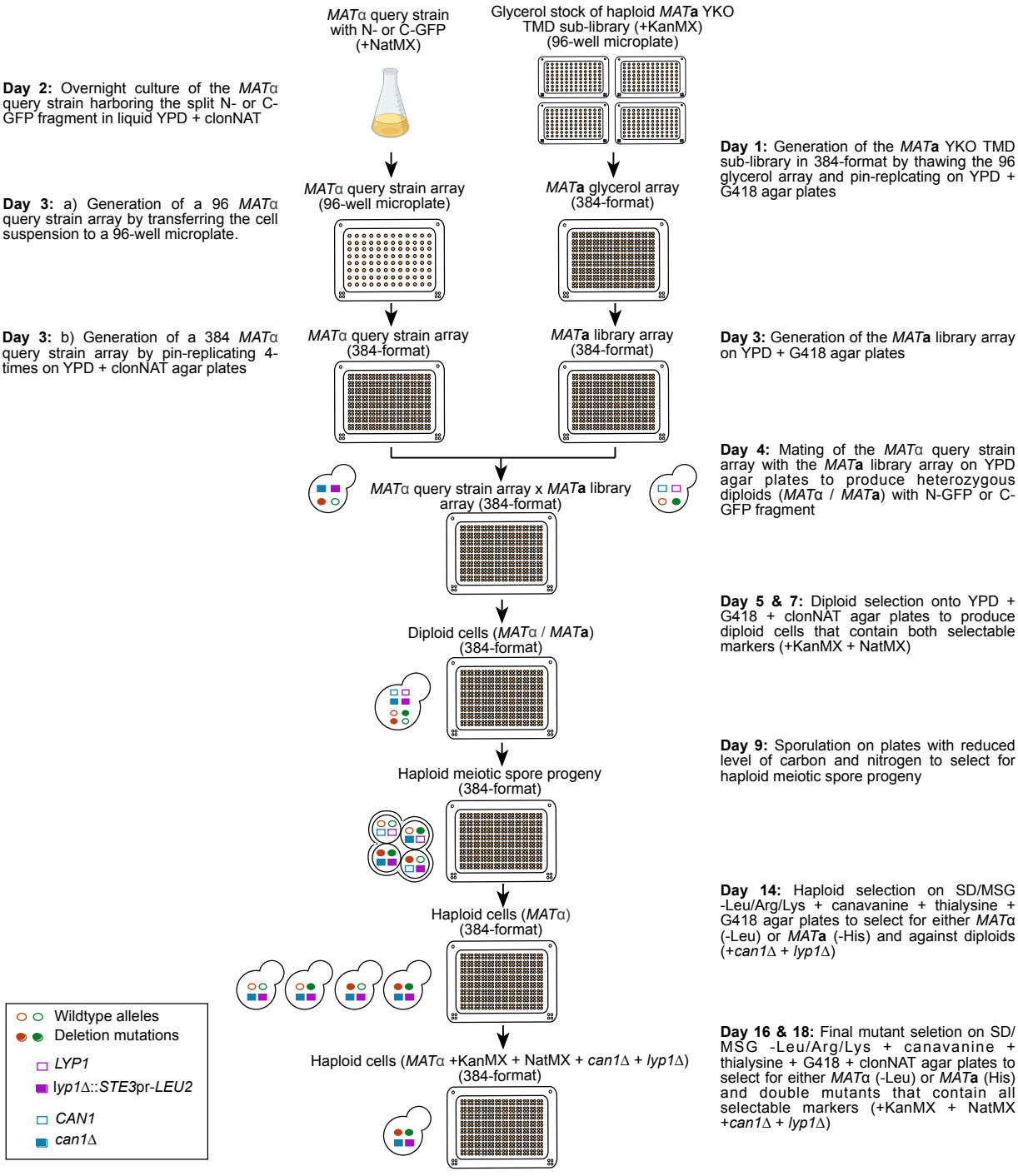

Figure 16: Schematic for generating a haploid *MAT*a C-GFP and a *MAT*α N-GFP YKO TMD sub-library using SGA methodology. Synthetic Genetic Array (SGA) methodology, according to Cohen & Schuldiner and Tong & Boone, was used to integrate a non-fluorescent split-GFP fragments into each mutant of the *MAT***a** TMD sub-library. Each gene deletion is bar coded and linked to a kanamycin resistance cassette conferring resistance to the antibiotic kanamycin (G418). For this, a *MAT*α query strain, harboring either a C- or N-GFP marker, linked to a nourseothricin resistance cassette natMX conferring resistance to the antibiotic nourseothricin (clonNAT), was mated to an ordered array of the 1,696 mutants from the *MAT***a** TMD sub-library. In 384-well format, a series of replica-pinning steps was used to first produce heterozygous diploids. After inducing sporulation upon nutrient starvation, haploid *MAT***a** or *MAT*α progeny was selected bearing the selectable markers of the array and the query strain mutations.

2.12.9 Pheromone response assay

*MAT***a** cells expressing mNeonGreen (mNG) tagged proteins were grown in YPD at 30˚C up to saturation. Following day, saturated overnight cultures were used to inoculate 5 ml fresh YPD medium. Cells were grown over night for about 15-16 h at 25˚C and 220 rpm to OD_{600} of 0.6 – 0.8. Cells were pelleted by centrifugation at 3,000 rpm for 4 min, washed three times with water, and resuspended in fresh synthetic complete (SC) or YPD medium. Cell suspension was split into half, whereby one half was treated with synthetic α-factor pheromone (20 µM final concentration) and the other half with DMSO. After incubation at 30˚C and 220 rpm for 60 min, another 10 µM were added and shaking continued at 30˚C for 60-90 min. The presence of shmoos was microscopically confirmed before washing twice with water. Cells were resuspended in 1 ml ice-cold TAF buffer, concentrated by centrifugation, resuspended in a final volume of 50 µl TAF buffer and stored at 4˚C until imaging.

2.12.10 Qualitative growth inhibition assay

In this assay, a *Δsst2 MAT***a** tester strain was used whose gene disruption causes super sensitivity to pheromone leading to cell death when exposed to the opposite mating pheromone. *MAT*α cells were patched on a thin lawn of *Δsst2 MAT***a** cells and their ability to produce pheromone determined by visual inspection of a zone of growth inhibition, referred to as halo. The size of the halo corresponds to the extent of produced pheromone.

In detail, *Δsst2 MAT***a** cells were grown to saturation in 5 ml YPD at 30˚C and 220 rpm overnight. The saturated culture was used to inoculate 5 ml fresh YPD medium and cells were grown overnight at 25˚C and 220 rpm to OD_{600} of 0.6 – 0.8. Next morning, fresh YPD medium was prepared and cooled down before an equivalent of OD_{600} = 1.0 was added, gently mixed and poured into sterile OmniTrays. Meanwhile, small amounts of single colonies of *MAT*α cells were scraped from the plate and resuspended in 100 µl sterile water, after which 7.5 µl were patched twice on the *Δsst2 MAT***a** tester plate. The plate incubated for 24-48 h until a halo around the region of patched cells was visible. The halo size of tested mutants was compared to the halo size produced by wildtype cells.

2.12.11 BiFC-based cell fusion assay

Based on bimolecular fluorescence complementation (BiFC) of split GFP originally developed by Aguilar and coworkers, cell fusion between *MAT***a** and *MAT*α cells was determined [148]. Typically, *MAT***a** and *MAT*α cells expressing non-fluorescent GFP fragment, NeGFP and CeGFP respectively, which due to membrane merger and subsequent cytoplasm mixing assemble into a fluorescent GFP protein whose fluorescence was detected by flow cytometry. Prior to mating, *MAT***a** and *MAT*α cells were differentially stained with cell wall binding Concanavalin A (ConA)-fluorophore conjugates, named Tetramethylrhodamine (ConA-Tet) and Alexa Fluor 647 (ConA-647). ConA are carbohydrate-binding proteins, referred to as lectins, that bind to mannopyranosyl and α-glucopyranosyl residues located on the cell surface. After mating, the cell suspension containing unpaired haploids and mating pairs was analyzed. Due to the double labeling of the CW mating pairs were rapidly identified and the percentage of cells that have successfully fused their membranes, following referred to as fusion efficiency, discriminated by BiFC of GFP.

2.12.11.1 Small scale BiFC assay

Haploid *MAT***a** and *MAT*α cells were grown in YPD at 30˚C up to saturation. Diluted cell cultures were grown at 25˚C or 30˚C for 15-18 h to OD_{600nm} of 0.2-0.8 in YPD. Cells were pelleted by centrifugation, washed once with 1x PBS and subsequently stained with ConA-Tet (final concentration: 100 µg/ml) or ConA-647 (final concentration: 5 µg/ml) for 45-60 min in the dark. Cells were resuspended in YPD and equal amounts of 2 x 10^6 *MAT***a** and *MAT*α cells mixed in fresh 5 ml YPD and uniformly vacuumed on 0.45 µm nitrocellulose filters using a 12-position vacuum manifold. After incubation on YPD agar for 3 h at 30˚C, the mating reaction was stopped by washing of the cells from the filters in 1ml ice cold TAF buffer, briefly mixed and stored on ice. The homogenous cell suspensions were then analyzed in a BD Accuri C6 Plus flow cytometer as described in Salzman et al. 2015 and demonstrated in (**Figure 17**).

2.12.11.2 96-well microplate BiFC assay

The BiFC assay was adapted to the 96-well format as described in section 3.1.4 allowing the systematic fusion screening of the entire YKO TMD sub-library. Using a stainless-steel floating

pin-replicator, mutants of the *MAT***a** C-GFP and *MAT*α N-GFP YKO TMD sub-libraries were transferred from YPD + clonNAT + G418 OmniTray agar plates to 96-well microplates filled with 180 µl YPD per well. Microplates were incubated typically for about 24-30 h at 30˚C until saturation. Following day, cells were pin-replicated from the saturated overnight culture to a new 96-well microplate containing 180 µl liquid YPD, from which a series of three additional dilutions with different cell densities was prepared. The four microplates of each mating type were incubated overnight at 25˚C for 14-15 h to early-mid log phase with an OD_{600nm} of 0.01-0.2 measured with a microplate reader, corresponding to OD_{600nm} 0.2-0.8 measured in a cuvette.

Using a multichannel pipette, *MAT***a** and *MAT*α cells were transferred to 96-well filter plates and vacuumed to remove the media. Cells were washed twice with 180 µl 1x PBS, vacuumed and resuspended in 180 µl 1x PBS before staining with ConA-Tet (final concentration: 100 µg/ml) or ConA-647 (final concentration: 5 µg/ml) for 45 min in the dark. Cells were washed twice with 180 ml YPD and then resuspended in 90µl YPD. *MAT*α cells were transferred to the 96-well filter plate containing the *MAT***a** cells, mixed with the multichannel pipette and vacuumed on the filter. Before placing the filter plate on YPD agar the filter guard was carefully removed. Cells were allowed to mate for 4 h at 30˚C before stopping the mating reaction by resuspension in 180 µl ice-cold TAF buffer. Mating mixtures were then transferred to a new 96-well microplate and fusion of homogenous cell suspensions analyzed by flow cytometry.

2.12.11.3 Flow cytometry analysis

Cell fusion analysis was performed using a BD Accuri C6 Plus Flow Cytometer (BD Bioscience) equipped with two lasers (blue laser: 488 nm; red laser: 640 nm). GFP and ConA-Tet were excited at 488nm, ConA-647 at 640nm. The band pass filters 510/15, 585/40 and 675/25 were used for detection of GFP, ConA-Tet and ConA-647 signals, respectively. Data acquisition and analysis were conducted using the BD CSampler Plus 1.0.23.1 software.

At first, samples were gated in a forward scatter (FSC) versus side scatter (SSC) plot to excluded cell debris from the analysis (Gate 1) (**Figure 17A**). The gated population was then applied in a logarithmic (log) ConA-Tet versus ConA-647 plot (**Figure 17B**), allowing the distinction between

four sub-populations in the mating mixtures: unstained cells (bottom left), ConA-Tet stained *MAT***a** C-GFP cells (top left), ConA-647 stained *MAT*α N-GFP cells (bottom right) and double stained ConA-Tet and ConA-647 cells (Gate 2) (top right). The double stained population represents mating pairs which have irreversible attached their cell walls. In a SSC versus log (GFP) plot, the double stained cell population (Gate 2) was scored for GFP fluorescence (Gate 3). (**Figure 17C**), which was only detectable in mating pairs that had successfully fused their plasma membranes enabling cytoplasmic mixing and thus complementation of C- and N-GFP fragments. The percentage of fused mating pairs was then calculated from the number fused mating pairs out of the total number of mating pairs in the SSC versus GFP plot multiplied with 100. Additionally, the flow cytometry data provided insights into the pairing efficiency, a parameter that elucidates how many haploid cells were able to obtain a partner of opposite mating type and proceed with cell adhesion and downstream mating events. The percentage of paired cells was calculated as the number of paired cells over total number of cells, including paired and unpaired cells, multiplied with 100. The unpaired **a** or α population with the lower number of counted events was considered as the rate limiting factor.

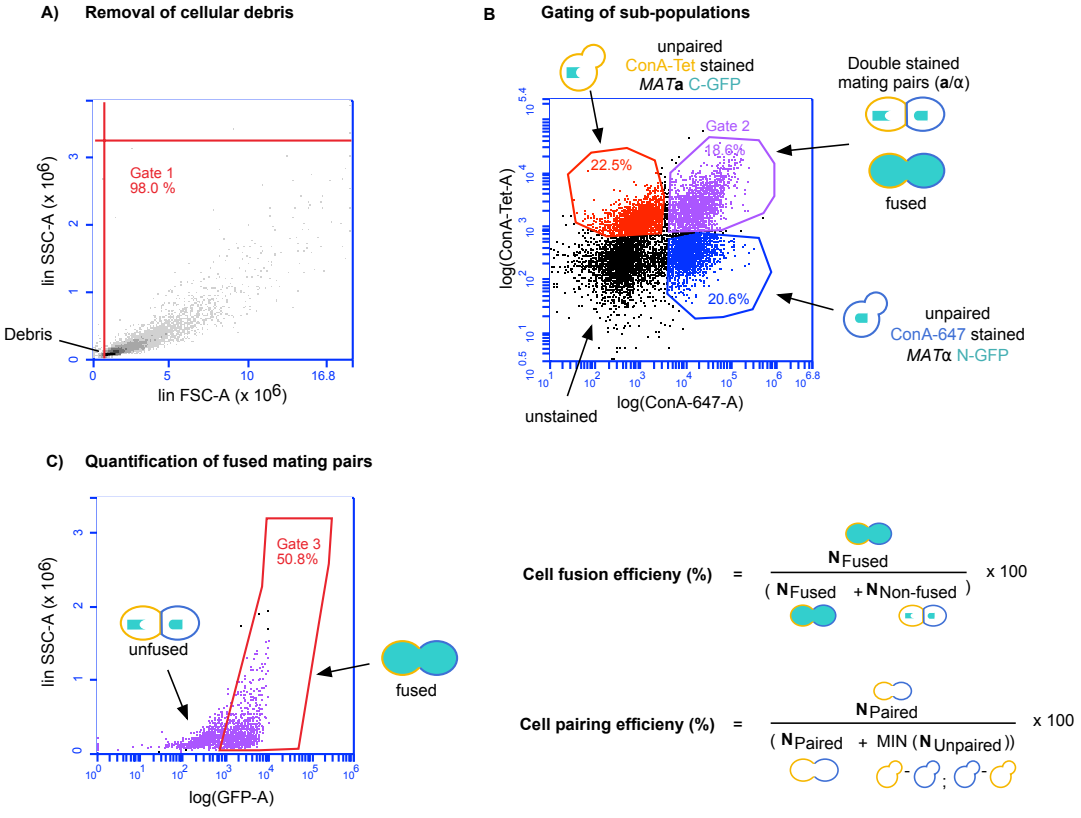

Figure 17: Schematic of gating strategy for cell fusion quantification by BiFC flow cytometry. A) Cellular debris removal in a SSC versus FSC plot. Gate 1 contains 10,000 events of each mating reaction. Subsequent plots refer to this region. B) The logarithmic ConA-Tet versus ConA-647 plot allows the distinction of all sub-populations in the mating mixture. C) Events of Gate 2 are plotted as SSC versus log(GFP), containing unfused (GFP-) and fused (GFP+) mating cells (Gate 3). The percentage of fusion efficiency is calculated as: ($N_{Fused\ pairs}$) / ($N_{Fused\ pairs}$ + $N_{Non\text{-}fused\ pairs}$) x 100. The percentage of pairing efficiency is calculated as: ($N_{Paired\ cells}$) /(MIN ($N_{paired\ pairs}$ + $N_{Non\text{-}paired\ cells}$)) x 100. (N = number).

2.12.12 Confocal microscopy

For acquiring microscopic images, a confocal laser scanning microscope (CLSM) LSM800 (Zeiss) was utilized with either a 40x plan-apochromat water-immersion objective (NA=1.0) or a 63x plan-apochromat oil-immersion objective (NA = 1.4). For quantitative mating assays, the 40x objective was used and fitted with Airyscan. With transmitted light random image fields were determined and images collected automatically using laser channels for GFP and FM4-64. After data acquisition, the 'Airyscan processing' function was applied to generate images with deconvolution and pixel reassignment. Final processing was carried out with the software ImageJ. For manual counting, the plugin function 'Cell Counter' was used.

2.12.12.1 Plasma membrane staining with FM4-64 for phenotype classification

Haploid *MAT***a** and *MAT*α cells were grown in YPD at 30˚C until saturation. Diluted cell cultures were grown at 25˚C or 30˚C overnight to OD_{600nm} of 0.2-0.8 in YPD. Cells were pelleted by centrifugation, washed once with 1x PBS and resuspended in YPD. Equal amounts of 4 x 10^6 *MAT***a** and *MAT*α cells were mixed in fresh 5 ml YPD and vacuumed on 0.45 µm nitrocellulose filters using a 12-position vacuum manifold. After incubation on YPD agar for 3 h at 30˚C, the mating reaction was stopped with 1ml ice cold TAF buffer. Cells were mixed, concentrated in 50 µl TAF buffer by centrifugation and placed on ice until imaging. Before imaging, arrested cells were stained with FM4-64 as described in Grote, 2008 [83]. FM4-64 is a lipophilic dye that is used to monitor endocytic membrane trafficking in live yeast cells but is retained in the plasma membrane when cells are maintained at 4˚C. Here, 2µl of cells were mixed with 2 µl FM4-64 with a final concentration of 4 mM. Generally, a volume of 2 µl stained cells was transferred to a microscope slide and imaged. In this work, FM4-64 was used to classify mating pair phenotypes as described in section 3.1.6.

2.12.12.2 Localization of C-terminally tagged proteins

To observe localization of proteins in mitotic or mating cells, corresponding genes of interest were chromosomally tagged at the C-terminus with mNeonGreen (mNG). mNG is a monomeric green fluorescent protein with an excitation maximum at 506 nm and an emission maximum at 517 nm, and was excited by a 488 nm laser. Cells were grown to early log phase, pelleted by centrifugation, washed once with 1x PBS and resuspended in 50 µl TAF buffer. 2 µl of cells were loaded on a microscope slide and imaged.

2.13 Protein procedures

2.13.1 Cell lysis of yeast cells and protein extraction

Δprm1 and *Δprm1Δcax4 MAT***a** cells expressing *PRM1*-V5 were grown in 5 ml SD-URA at 30℃ until saturation. 40 ml of diluted cell cultures were grown at 30˚C to OD_{600nm} of 0.8-1.0 in SD-URA and divided into two equal halves. Cell cultures were pelleted by centrifugation, washed once with water and resuspended in 10 ml SD-URA containing either DMSO or 20 µM α-factor as described in section 2.12.9. After 90 min incubation at 30˚C, cell cultures were concentrated by centrifugation and washed once with 2 ml TAF buffer to block endocytosis. For lysis, the cells were resuspended in 500 µl Roedel Mix containing 2 M NaOH, 1.25% β-mercaptoethanol, 1 mM PMSF and 2x protease inhibitor cocktail (PIC), and incubated ice for 10 min. First, 250 µl Lysis buffer and about half the final volume of 0.5 mm glass beads was added, followed by intense mixing at high-speed for 10 min with 30 sec pause on ice after each minute. After centrifugation, 600 µl of the cell lysate was transferred to a new tube and proteins were precipitated with 100% TCA (final concentration: ~33 %), pelleted by centrifugation, washed once with 100% acetone and dried at room temperature for 10 min. The protein extracts were then solubilized in 150 µl water and ready for subsequent sodium dodecyl sulfate-polyacrylamide gel electrophoresis (SDS-PAGE).

2.13.2 SDS-PAGE

50 µl of 4X SDS sample buffer was added to a volume of 150 µl in water resuspended protein extract. Proteins were denatured at 95˚C for 5 minutes, pelleted at max speed for 90 sec and

stored at -20℃ before use. 5-10 µl protein lysates and 5 µl PageRuler Prestained protein ladder were loaded onto a 10 % SDS-polyacrylamide gel in SDS running buffer. Initially, the gels were electrophoresed at 100 V for about 10 min or until the samples reached the stacking line. The voltage was then increased to 120-140 V for approximately 80-90 min. Samples were separated until the dye reached the bottom and transferred to a nitrocellulose membrane for Western blot analysis.

Table 23: Recipe for SDS-PAGE gel. Volumes listed are enough for two gels.

Reagents	Volume for 10 % separating gel	Volume for 5 % stacking gel
Water	3.5 ml	3.6 ml
30 % Acrylamide	3 ml	0.9 ml
1.5 M Tris-HCl pH 8.8	2.2 ml	0.7 ml
10 % SDS	90 µl	53.3 µl
10 % APS	90 µl	53.3 µl
TEMED	4 µl	5.3 µl

2.13.3 Western blot

Following the SDS-PAGE, proteins were transferred to a nitrocellulose membrane for Western Blot analysis using the wet transfer method in a Mini-Trans Blot apparatus (BioRad) together with a magnetic stirrer at constant 0.35 A for 1h or 0.09 A for 16 h at 4 ˚C. Membranes were then stained with Ponceau S solution to visualize the protein bands and verify completed transfer. Membranes were then blocked with blocking solution containing 5% milk in TBS-T for 1h at RT and gentle agitation. Membranes were incubated with a mouse monoclonal anti-V5 primary antibody (Invitrogen) at 1:5,000 dilution in blocking solution for 1h at RT. After a series of washing steps with blocking solution, membranes were incubated with a goat anti-mouse secondary antibody conjugated with Horse Reddish Peroxidase (HRP) at 1:5,000 dilution in blocking solution for 1h at RT. Membranes were washed again in TBS blocking solution before chemiluminescence detection using a ChemiDoc MP Imaging System (BioRad).

3. Results

3.1 A systematic BiFC-based loss-of-function screen identifies 56 mutants exhibiting a defect in cell fusion

Mating of haploid *S. cerevisiae* cells of the opposite sex is an ideal system to study cell-cell fusion in eukaryotic organisms. The merger of the opposite mating types *MAT***a** and *MAT*α haploid cells results in the formation of a diploid zygote, a process that is analogous to sperm-oocyte fusion during fertilization. Despite its importance, the molecular mechanisms of how the two apposing yeast cells merge their plasma membranes (PM) to enable cytoplasmic content mixing and diploid formation, remains poorly understood. The critical steps after cell-cell contact are local cell wall (CW) digestion followed by PM fusion, for which a few proteins have been identified. For instance, the two proteins Fus1 and Fus2 are important for CW remodeling and cause an almost complete fusion block when simultaneously deleted [108, 149]. The pheromone-regulated protein 1 (Prm1) was identified via a reverse screen to directly regulate PM fusion [150]. Other genes, such as the ergosterol (*ERG*) biosynthesis genes *ERG2*, *ERG3*, *ERG4* as well as *KEX2* and *FIG1* have also been reported to be involved in this process [119, 124, 131]. However, none of their null mutants led to a complete membrane fusion arrest, indicating the existence of additional unknown players. To tackle this challenge and to overcome certain limitations such as the bilateral fusion nature of proteins involved, functional redundancy or technical limits like restriction of quantified cells via microscopy, a multicolor flow cytometry assay was adapted to a 96-well format and a customized yeast knockout (YKO) library screened for fusion defects.

3.1.1 Generation of a *MAT*a C-GFP and *MAT*α N-GFP YKO sub-library via SGA methodology

To enable the screening for fusion mutants by determining BiFC of GFP, synthetic genetic array (SGA) methodology was utilized to incorporate non-fluorescent split-GFP marker into each

mutant of the *MAT***a** YKO TMD sub-library to generate a *MAT***a** C-GFP and a complementary *MAT*α N-GFP YKO TMD sub-library.

The original *MAT***a** (BY4741) yeast knockout (YKO) collection consisting of an ordered array of 5,133 gene deletion mutants provides an almost complete library of non-essential open reading frames (ORFs). Since membrane proteins are likely to be involved during cell fusion, first a customized *MAT***a** YKO TMD sub-library was generated containing 1,696 mutants of ORFs predicted to encode transmembrane domains (TMDs) (section 2.12.8). This sub-library was arrayed in 19x 96-well microplates and used to then incorporate non-fluorescent split GFP fragments (**Figure 18**). In brief, the *MAT***a** YKO TMD sub-library was mated once to an array of a *MAT*α query strain containing C-GFP, and once to an array of a *MAT*α query strain containing N-GFP marker. After a series of replica-pinning steps to produce heterozygous diploid and subsequent sporulation, haploid *MAT***a** or *MAT*α progeny bearing the selectable markers of both arrays was then selected. In total, 45 of 1,696 deletion strains failed to survive the SGA procedure (**Table 24**)**.** Therefore, the subsequent cell fusion screen covers >98% of TMD mutants.

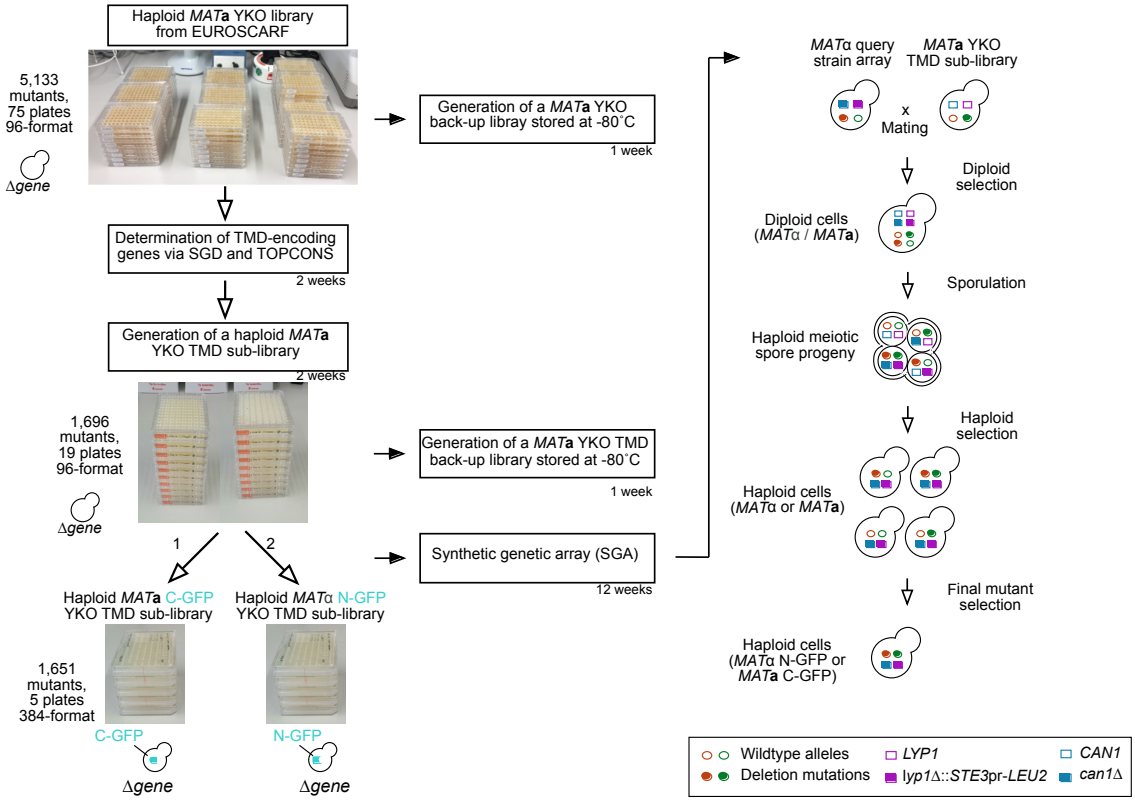

Figure 18: Schematic workflow for generating the MATa C-GFP and MATα N-GFP TMD sub-library by synthetic genetic array (SGA) methodology. Generation of a customized *MAT***a** YKO TMD sub-library generated containing 1,696 mutants of ORFs encoding transmembrane domains (TMD). SGA methodology was used to integrate non-fluorescent complementary C-or N-GFP fragments. After multiple replica-pinning steps, a *MAT***a** C-GFP and *MAT*α N-GFP YKO TMD sub-library was generated.

Table 24: Overview of deletion strains that failed to survive the SGA procedure. Mutants highlighted with an asterisk failed to produce heterozygous diploids during the selection step.

No.	Systematic name	Gene name	Mating type	No.	Systematic name	Gene name	Mating type
1	*YFL026W*	*STE2*	**a** / α	**24**	*YDR506C*	*GMC1*	**a**
2	*YBL095W*	*MRX3*	**a** / α	**25**	*YDR508C*	*GNP1*	**a**
3	*YPL050C*	*MNN9*	**a** / α	**26**	*YGL038C*	*OCH1*	**a**
4	*YEL060C*	*PRB1*	**a** / α	**27**	*YHR183W*	*GND1*	**a**
5	*YEL063C*	*CAN1*	**a** / α	**28**	*YDR506C*	*GMC1*	**a**
6	*YEL064C*	*AVT2*	**a** / α	**29**	*YCR028C*	*FEN2*	**a**
7	*YER068C-A*	*YER068C-A*	**a** / α	**30**	*YNL268W*	*LYP1*	α
8	*YBR085W*	*AAC3*	**a** / α	**31**	*YNR050C*	*LYS9*	**a** / α
9	*YBR106W*	*SND3*	**a** / α	**32**	*YLR322W*	*VPS65*	**a** / α
10	*YCL005W*	*LDB16*	**a** / α	**33**	*YLR396C*	*VPS33*	**a**
11	*YDL041W*	*YDL041W**	**a** / α	**34**	*YPR087W*	*VPS69*	**a** / α
12	*YDL072C*	*YET3**	**a** / α	**35**	*YPR139C*	*LOA1*	**a** / α
13	*YDL012C*	*YDL012C*	α	**36**	*YPR159W*	*KRE6*	**a** / α
14	*YNL270C*	*ALP1*	**a** / α	**37**	*YDR034W-B*	*YDR034W-B*	**a**
15	*YOR130C*	*ORT1*	**a** / α	**38**	*YKL096C-B*	*YKL096C-B*	α
16	*YNL268W*	*LYP1*	α	**39**	*YNL280C*	*ERG24*	α
17	*YDL198C*	*GGC1*	**a** / α	**40**	*YGR062C*	*COX18*	**a**
18	*YDR003W*	*RCR2*	α	**41**	*YER044C*	*YER044C*	**a** / α
19	*YDR008C*	*YDR008C*	α	**42**	*YDL067C*	*YDL067C*	**a** / α
20	*YDR011W*	*SNQ2*	α	**43**	*YIL134W*	*FLX1*	**a**
21	*YDR264C*	*AKR1*	**a** / α	**44**	*YDR521W*	*YDR521W**	**a** / α
22	*YDR410C*	*STE14*	**a** / α	**45**	*YDL067C*	*COX9**	**a** / α
23	*YDR504C*	*SPG3*	**a**				

3.1.2 Four mutants failed to produce heterozygous diploids during the SGA procedure

During the SGA procedure (section 2.12.8), the *MAT*α query strain array was crossed to the *MAT***a** YKO TMD sub-library to produce diploid zygotes carrying both selectable markers (KanMX, NatMX) of both genotypes (**a** and α). The mutant strains Δ*cox9*, Δ*ydr521w*, Δ*ydl041w* and Δ*yet3* failed to grow on YPD agar containing the antibiotics G418 and clonNat indicating that the mating process was not completed and diploid cells were not formed. To clarify whether this was caused by a mating defect, microscopic examinations were carried out. For this, equal amounts of early-log phase grown *MAT***a** and *MAT*α cells were mixed, vacuum filtered and mated for 3 h on YPD agar. The mating reaction was arrested in TAF buffer and imaged by confocal microscopy as described in section 2.12.12.1. Δ*cox9*, Δ*ydr521w* and Δ*ydl041w* failed to produce diploid cells suggesting an early mating defect e.g. in pheromone signaling. However, matings of Δ*yet3* resulted in the formation of diploid zygotes. Thus, it was possible that the defect occurred after membrane fusion such as karyogamy, the fusion of the two nuclei. To test whether Δ*yet3* was defective in karyogamy, the mating cells were stained with the fluorescent dye DAPI before microscopic inspection. DAPI binds to adenine (A) thymine (T) regions of double-stranded DNA (dsDNA) and stains the nucleus. Δ*yet3* mating cells showed only one single DAPI stained nucleus, indicating that the karyogamy process was completed (**Figure 19**). Consequently, the inability to produce diploids during the SGA procedure was probably not caused by a karyogamy defect, but rather due to a technical issue during the replica-pinning step.

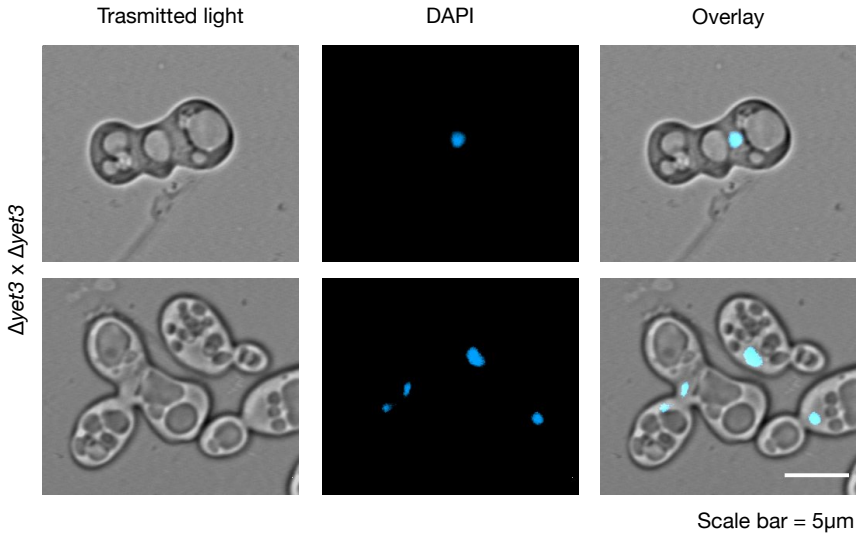

Figure 19: Δ*yet3* mating cells complete karyogamy. Δ*yet3* mating cells expressed only one DAPI-stained nucleus indicating that the nuclei of both mating cells successfully fused. Scale bar = 5 µm.

3.1.3 Verification of the *MAT***a** C-GFP and *MAT*α N-GFP YKO TMD sub-libraries by flow cytometry

To verify the successful incorporation of split-GFP into the *MAT***a** C-GFP and *MAT*α N-GFP YKO TMD sub-libraries, cell fusion was quantified by flow cytometry. This analysis included three previously reported fusion mutants (Δ*prm1*, Δ*fig1* and Δ*fus1*) and three randomly picked mutants (Δ*toh1*, Δ*kap114* and Δ*dsc2*) (**Figure 20A**). The mutant strains were crossed to the corresponding mating partner containing the same mutant allele, or to a wild-type (WT) partner. Matings of all SGA-generated mutants to the WT showed fusion efficiencies between 81-86%. Fusion efficiencies of *TOH1*, *KAP114* and *DSC2* when deleted in both mating cells were comparable to the fusion levels when crossed to WT. As expected, Δ*prm1* x Δ*prm1* matings showed 25% fusion efficiency which is consistent to a reported 40-60% fusion defect in previous studies [120, 135]. The fusion data of the Δ*prm1* strain generated via SGA as well as the Δ*prm1* tester strain generated by PCR displayed similar fusion defects confirming the robustness of the constructed libraries. Furthermore, Δ*fig1* x Δ*fig1* matings exhibited a fusion defect of about 10% compared to Δ*fig1* x WT, which was consistent with ~3-25% in previous reported studies [131, 151]. By contrast, the CW remodeling mutant Δ*fus1* did not display the expected fusion defect of ~ 50% [152], even though the deletion of the *FUS1* gene was

confirmed by colony PCR in both mating types, as it was also shown for Δ*fig1* and Δ*prm1* (**Figure 20B**).

In summary, the quantification of cell fusion by flow cytometry and thus, the incorporation of the complementary non-fluorescent C- and N-GFP fragments into the *MAT***a** YKO TMD sub-libraries via SGA methodology was successful. Furthermore, the correct positioning of the mutants Δ*prm1*, Δ*fus1* and Δ*fig1* in the array was demonstrated first, by confirming the gene deletion by colony PCR and secondly, by exhibiting the expected fusion scores, except for Δ*fus1*. Because most fusion mutants, like Δ*prm1,* exhibit only a pronounced fusion defect when the gene is absent in both mating cells, it was indispensable to create a mutant library in which the corresponding genes were deleted in both mating types. Therefore, this customized YKO TMD library represents a unique and powerful tool to identify novel regulators in cell fusion during the mating of *S. cerevisiae*.

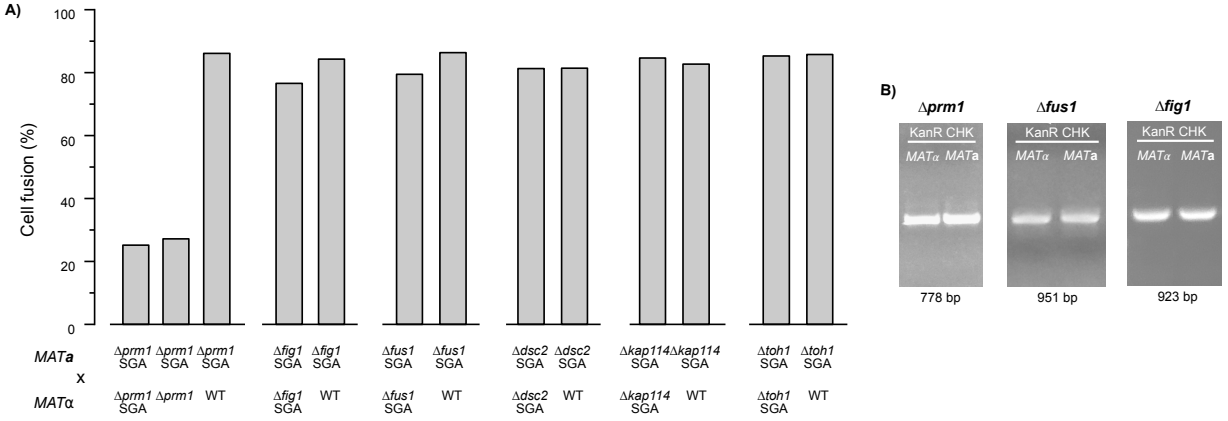

Figure 20: Verification of the YKO TMD *MAT*a C-GFP and *MAT*α N-GFP sub-libraries. A) Cell fusion analysis of three known fusion mutants (Δ*prm1*, Δ*fig1* and Δ*fus1*) in addition to three random mutants (Δ*dsc2*, Δ*kap114*, Δ*dsc2*). B) Confirmation of gene deletion by colony PCR in *MAT***a** and *MAT*α mating type using gene-specific 5'UTR forward and KanR reverse primers.

3.1.4 Adaptation of the multicolor BiFC flow cytometry assay to the 96-well microplate format

Following the verification of the *MAT***a** C-GFP and *MAT*α N-GFP TMD sub-libraries, the bimolecular fluorescence complementation (BiFC)-based cell fusion assay, originally developed by Pablo Aguilar and his team in 2015 [148], was adapted to a 96-well format to allow a high-throughput fusion screening of the entire YKO TMD sub-library (**Figure 21**). BiFC allows

determining fusion between *MAT***a** and *MAT*α mating cells, in which due to cytoplasm mixing between both cells, the non-fluorescent GFP fragments are assembled into a fluorescent molecule. To detect mating pairs, haploid *MAT***a** and *MAT*α cells are stained with two distinct CW dyes. With flow cytometry, cell fusion of the double stained population is then analyzed within seconds. Since this approach allows the detection of mating pairs that have established cell-cell contact, it faithfully reflects fusion efficiency of late mating stages during CW remodeling and PM fusion. The assay was adapted to the 96-well array as follows:

(1+2) Determination of optimal cell growth conditions

Typically, *MAT***a** and *MAT*α cells are grown to saturation at 30℃, followed by a secondary culture incubated over night at 25˚C to early log-phase, which corresponds to an OD_{600} of 0.1-0.8 in YPD media [83]. Cell growth was acquired by measuring the optical density at 600 nm (OD_{600}). To define the OD_{600} equivalent in a 96-well microplate, a series of five different cell densities was measured with a cuvette and microplate reader. As a result, it was established that the OD_{600} reading via the cuvette ranging from 0.1 to 1.2 corresponded to an OD_{600} between 0.02 – 0.35 in the microplate. After linear fitting, the early log-phase in a microplate reader was defined to range from 0.02 to 0.2. However, via successive trial and error, the optimal OD_{600} in a microplate was finally determined to OD_{600}= 0.01 – 0.1.

(3) Differential cell wall staining with Concanavalin A

To later detect different cell populations, prior to mixing *MAT***a** and *MAT*α cells were stained with two distinct Concanavalin A (ConA) fluorophore conjugates, Tetramethylrhodamine (ConA-Tet) and Alexa Fluor 647 (ConA-647). To minimize the reagent costs, the recommended working concentrations of ConA-Tet = 250 µg/ml and ConA-647 = 20 µg/ml were reduced to ConA-Tet = 100 µg/ml and ConA-647 = 5µg/ml. Additionally, the staining time was increased from 30 min to 45 min in the dark.

(4) Yeast mating conditions

Typically, equal amounts of *MAT***a** and *MAT*α cells are mixed manually and subsequently vacuumed on a filter membrane. This approach is not suitable in 96-well format and consequently, the entire volume of ConA-647-stained *MAT*α cells was transferred to the filter

plate containing the ConA-Tet stained *MAT***a** cells. It was observed that the staining result of *MAT***a**-Tet cells was better when the cell transfer occurred in this order. To subsequently ensure proper contact between the filter membrane and the YPD agar to allow sufficient mating events to take place, the agar was tailored to a size that fit precisely below the 96-well filter plate. In addition, with the help of duct tape and gentle force, the filter plate was fixed to the agar. By testing different time points, the optimal mating time in 96-well format was increased from 2.5 to 4 h at 30˚C. Furthermore, the mating reaction was arrested with ice-cold TAF-buffer instead of 1x PBS. TAF inhibits the metabolic activity of a cell and therefore captures its state at a certain time. This in turn enabled a better comparison of measured fusion efficiencies after quantification of fusion events by flow cytometry.

(5) Cell fusion analysis by flow cytometry

To maintain a homogenous cell suspension and avoid sedimentation to the bottom of the plate, the cells were mixed before measuring, ideally after 6 samples, latest after the measurements of one row were completed. The mating strategy was performed according to Salzman et al. 2015 as described in section 2.12.11.3 [148]. Briefly, in total 10,000 events were counted excluding the debris. Via differential CW staining, single stained *MAT***a**-ConA-Tet, single stained *MAT*α-ConA-647 and double stained cell populations were detected. For cell fusion quantification, the double stained cell population that contained the mating pairs was selected. A SSC versus GFP plot was then applied to differentiate between fused and unfused mating pairs based on the complementation of split-GFP after membrane merger occurred.

(6) Comparison of standard versus 96-well cell fusion quantification by flow cytometry

To verify the accuracy of the adapted 96-well assay, fusion of WT and Δ*prm1* matings as internal controls as well as three randomly picked mutants (Δ*ygl024w*, Δ*cax4* and Δ*kex1*) were analyzed and compared to fusion efficiencies generated on a separate day via small scale BiFC assay in a final volume of 5 ml YPD. The fusion efficiencies of both were found to be similar, concluding that the method adaption was successful and produced repeatable fusion data. Hereby, an important milestone was accomplished that allowed the screening of the entire YKO TMD sub-library in a high-throughput manner.

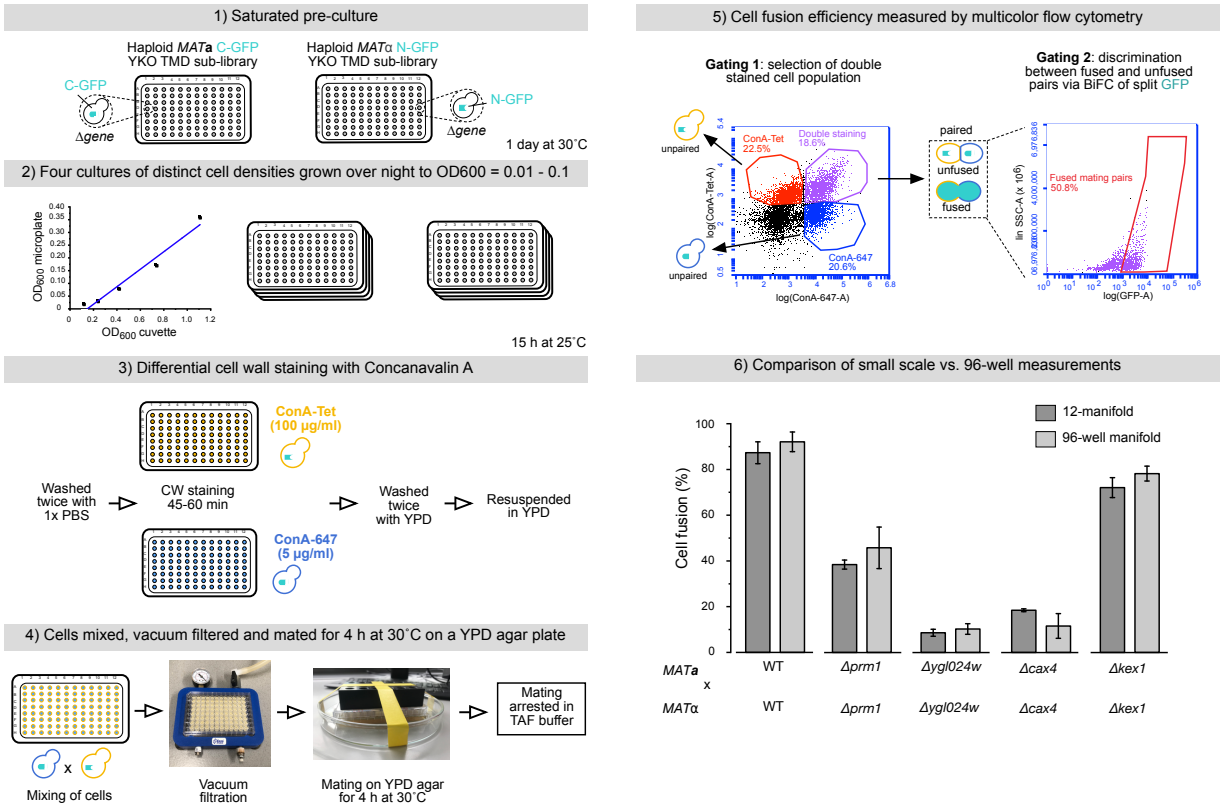

Figure 21: Schematic workflow for adapting the multicolor BiFC flow cytometry assay to the 96-well format. (1) Yeast cells are grown over night upon saturation. (2) Cultures of four distinct densities are grown over night to early log-phase. (3) CW staining of *MAT***a** and *MAT*α cells with Concanavalin A (ConA) fluorophore conjugates. (4) Cells are mixed, vacuumed on a filter membrane and allowed to mate on YPD agar. Mating is arrested in TAF buffer and fusion measured by flow cytometry. (5) Cell fusion efficiency of double stained cell population is determined by BiFC of split GFP. (6) Comparison of cell fusion measured by the small scale BiFC and 96-well microplate BiFC assay.

3.1.5 A systematic loss-of-function screen uncovers 125 putative cell fusion mutants

The adaptation of the multicolor flow cytometry assay to the 96-well format allowed a systematic high-throughput screening of the entire YKO TMD sub-library to identify mutants exhibiting a fusion defect. Cell fusion of 19x 96-well microplates harboring 1,655 gene deletion mutants was determined as described in section 2.12.11.2 and illustrated in **Figure 22** (top). In total, 125 mutants displayed less than 75% fusion efficiency after normalization to the median of each plate, as shown in **Figure 22** (middle). Fusion efficiencies were sorted from lowest to highest fusion efficiencies. A cut-off of 75% was chosen to narrow down the mutants of interest exhibiting the most dominant fusion defect. A summary of results is illustrated in **Figure 22**

(bottom). In total, 72 mutants displayed fusion efficiencies between 51-75%, 28 mutants between 26-50% and 25 mutants less than 25%. Post-analysis via the yeast genome data base (SGD) gave insights into the hitherto reported roles of identified fusion mutants, including mutants with established roles in yeast mating. For instance, Δ*kex2*, Δ*ste3* and Δ*ste13* which are well known to cause defects in pheromone processing and maturation, as well as Δ*erg2* and Δ*erg3* which have been reported to lead to cell polarization defects [91, 119, 136, 153]. As expected, genes involved in cell fusion such as Δ*prm1*, Δ*fig2* and Δ*erg3*, Δ*fus1* and Δ*fig1* were identified [100, 116, 119, 120, 124, 154]. However, fusion efficiencies of Δ*fus1* and Δ*fig1* matings were above the cut-off of 75%.

An intriguing observation was that 15 mutants related to the vacuolar membrane ATPase (V-ATPase) were identified. The V-ATPase is a multiunit enzyme complex responsible for acidification of intracellular organelles such as the vacuole, Golgi complex and endosomes [155]. In total, nine mutants of genes which encode for one of the V-ATPase subunits *VMA3*, *VMA5*, *VMA7*, *VMA8*, *VMA9*, *VMA11, VMA13*, *VMA16 and VPH1* were uncovered. Three others were found to encode for V-ATPase associated assembly factors: *VMA21*, *VPH2* and *PKR1*. Another three mutants were identified whereby the gene deleted overlapped to ORFs of an adjacent V-ATPase related gene: *YOR331C* (*VMA4*), *YCL007* (*VMA9*) and *YKL188W* (*VPH2*).

Finally, several novel mutants with as of yet unreported roles in cell fusion were uncovered, with genes involved in mannosylation and glycosylation such as Δ*pmt1*, Δ*pmt2*, Δ*pmt4*, Δ*cax4* and Δ*gas1* being highly represented [156-158]. Other mutants play roles in protein sorting, trafficking and degradation, like Δ*sec66*, Δ*vps64* and Δ*pep12*, or transport activity such as Δ*nhx1*, Δ*trk1* and Δ*tat1* [132, 159, 160].

To summarize, a loss-of-function high-throughput screen of the entire set of TMD-encoding genes was carried out in which mutants defective in cell fusion were detected. Moreover, this established screening method allowed the detection of 10,000 events within a few seconds for accurate quantification. In addition, the limitation of the bilateral fusion nature of genes involved have been circumvented since the corresponding genes were deleted in both mating partners. Next, I focused on validating the 125 defective mutants by employing a secondary screen using microscopy.

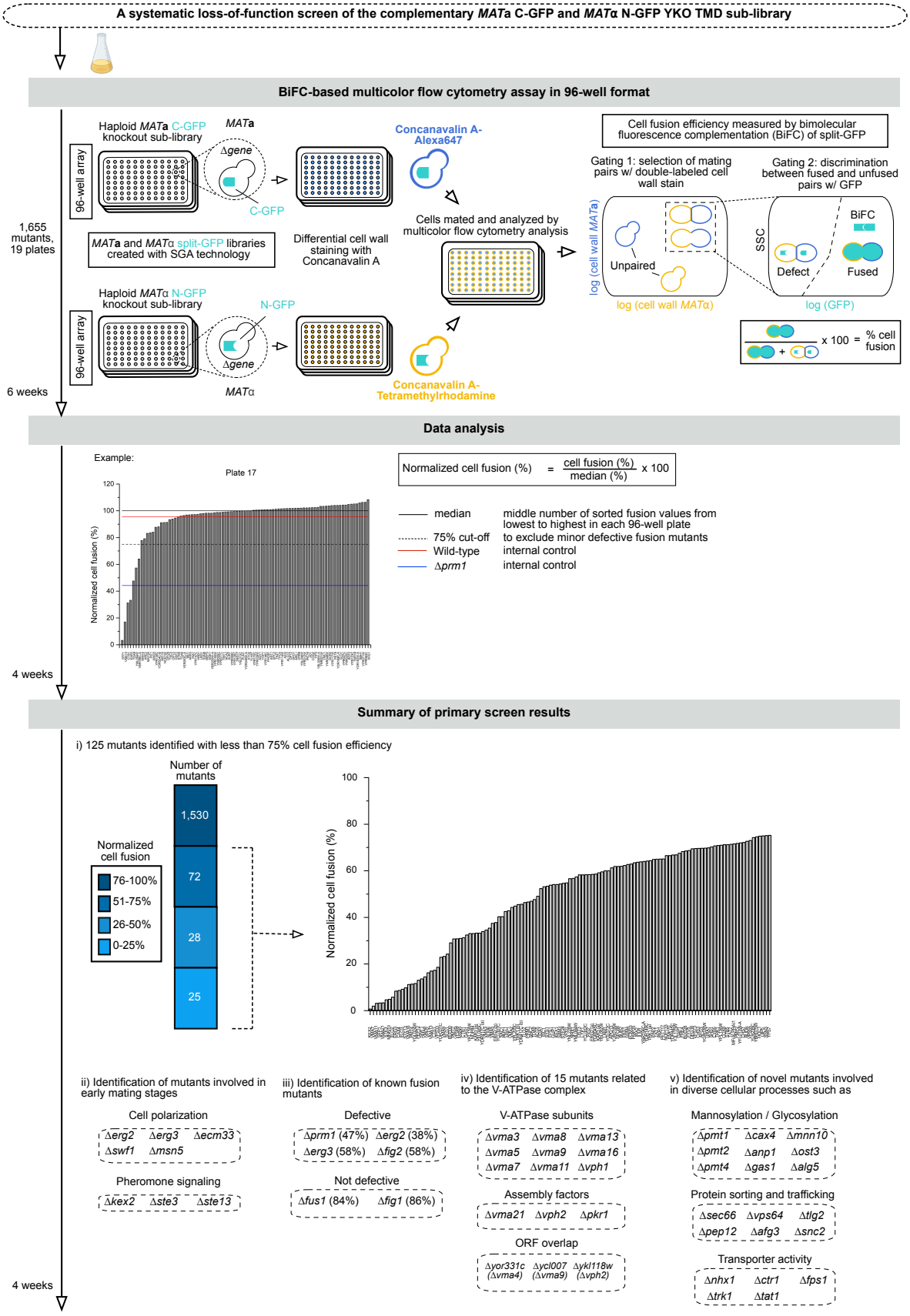
A systematic loss-of-function screen of the complementary MATa C-GFP and MATα N-GFP YKO TMD sub-library
BiFC-based multicolor flow cytometry assay in 96-well format
1,655 mutants, 19 plates
Haploid MATa C-GFP knockout sub-library
96-well array
MATa
Δgene
C-GFP
MATa and MATα split-GFP libraries created with SGA technology
Differential cell wall staining with Concanavalin A
Concanavalin A-Alexa647
Cells mated and analyzed by multicolor flow cytometry analysis
Cell fusion efficiency measured by bimolecular fluorescence complementation (BiFC) of split-GFP
Gating 1: selection of mating pairs w/ double-labeled cell wall stain
Gating 2: discrimination between fused and unfused pairs w/ GFP
log (cell wall MATa)
log (cell wall MATα)
Unpaired
SSC
BiFC
Defect
Fused
log (GFP)
x 100 = % cell fusion
Haploid MATα N-GFP knockout sub-library
N-GFP
MATα
Concanavalin A-Tetramethylrhodamine
6 weeks
Data analysis
Example:
Plate 17
Normalized cell fusion (%)
Normalized cell fusion (%) = cell fusion (%) / median (%) x 100
median
middle number of sorted fusion values from lowest to highest in each 96-well plate
75% cut-off
to exclude minor defective fusion mutants
Wild-type
internal control
Δprm1
internal control
4 weeks
Summary of primary screen results
i) 125 mutants identified with less than 75% cell fusion efficiency
Number of mutants
Normalized cell fusion
76-100%
51-75%
26-50%
0-25%
1,530
72
28
25
Normalized cell fusion (%)
ii) Identification of mutants involved in early mating stages
Cell polarization
Δerg2 Δerg3 Δecm33 Δswf1 Δmsn5
Pheromone signaling
Δkex2 Δste3 Δste13
iii) Identification of known fusion mutants
Defective
Δprm1 (47%) Δerg2 (38%) Δerg3 (58%) Δfig2 (58%)
Not defective
Δfus1 (84%) Δfig1 (86%)
iv) Identification of 15 mutants related to the V-ATPase complex
V-ATPase subunits
Δvma3 Δvma8 Δvma13 Δvma5 Δvma9 Δvma16 Δvma7 Δvma11 Δvph1
Assembly factors
Δvma21 Δvph2 Δpkr1
ORF overlap
Δyor331c (Δvma4) Δycl007 (Δvma9) Δykl118w (Δvph2)
v) Identification of novel mutants involved in diverse cellular processes such as
Mannosylation / Glycosylation
Δpmt1 Δcax4 Δmnn10 Δpmt2 Δanp1 Δost3 Δpmt4 Δgas1 Δalg5
Protein sorting and trafficking
Δsec66 Δvps64 Δtfg2 Δpep12 Δafg3 Δsnc2
Transporter activity
Δnhx1 Δctr1 Δfps1 Δtrk1 Δtat1
4 weeks

Figure 22: A systematic screen to identify novel regulators facilitating cell fusion. Top: A customized YKO sub-library harboring 1,655 mutants of ORFs encoding TMDs was screened for fusion defects by BiFC of split GFP with flow cytometry. Middle: Cell fusion was normalized to the median of each 96-well plate and sorted from the lowest to highest value. WT and Δ*prm1* served as an internal control. Bottom: The screen identified 125 known and novel mutants exhibiting less than 75% normalized fusion efficiency.

3.1.6 Microscopic confirmation of 91 fusion mutants

As shown in section 3.1.5, the primary screen revealed 125 mutants with fusion efficiencies lower than 75%. As part of a secondary screen, microscopic inspection was performed to confirm the defect. Advantageously, confocal fluorescence microscopy combined the GFP BiFC assay with PM staining with the lipophilic dye FM4-64. The complementation of split-GFP allowed the differentiation between fused and unfused mating pairs, while FM4-64 served as an independent tracer to visualize and characterize the phenotypic fusion defect phenotypes since it exclusively stains lipid bilayers. Matings of fusion mutants can result in four different phenotypes after cell-cell contact is established: fusion, lysis or arrest as early or late pre-zygotes (**Figure 23**). Early pre-zygotes are characterized by the presence of a CW at the mating junction providing structural support to the PM delineating a flat PM interface. Known CW remodeling mutants with these characteristics include Δ*fus1* and Δ*fus2* [108]. Late pre-zygotes on the other hand have completed CW degradation but fail to fuse their PMs. Due to the flexibility of the PM, unfused mating pairs often exhibit PM bubbles protruding from one cell into the other following the direction of the osmotic gradient. This phenotype is often displayed by mutants defective in membrane fusion such as Δ*prm1* and Δ*erg6* [119, 150].

The microscopic examination of FM4-64- stained mating mixtures was performed as described in section 2.12.12.1 according to Grote, 2008 [83]. In brief, equal amounts of early log-phase grown *MAT***a** and *MAT*α cells (approximately $4x10^6$ cells/ml) were mixed and allowed to mate for 3 h at 30˚C. Cells were arrested in 1 ml ice cold TAF buffer and imaged by confocal microscopy. With transmitted light random image fields were determined and at least two 9-tile images were collected automatically using excitation channels for GFP and FM4-64. For each mutant, a minimum of 100 mating cells was counted. Mating pairs that expressed cytoplasmic GFP fluorescence were counted as fused, while mating pairs that lysed or exhibited

no GFP and PM staining at the mating junction were considered unfused or defective. Representative microscopic images are depicted in **Figure 23**.

In total, 20 mutants were incapable of forming mating pairs which was indicative for a defect in early stages of yeast mating, presumably occurring at the level of cell polarization or pheromone signaling (Table 26) 10 mutants exhibited fusion efficiencies over 99% similar to wild-type fusion efficiency. These mutants were excluded from further analysis (Table 25). Interestingly, 94 mutants exhibited fusion defects appearing at the stage of CW remodeling or PM fusion. Their fusion efficiencies ranged from 24 % to 98% and are listed in Table 25. Mutants that expressed almost WT fusion levels with 90-98% were also considered as defective because microscopic counting includes only a limited number of mating cells and can be user biased. Therefore, the cut-off was higher to avoid premature removal of true fusion mutants. The fusion defect of the 15 previously identified V-ATPase related mutants was confirmed, although Δ*vma2* matings cells were categorized initially into early defective mutants, but retroactively grouped into confirmed fusion mutants (highlighted with an asterisk). This result corroborated the importance of the V-ATPase complex in cell fusion. In total, 3 out of 94 mutants were present as duplicates in the original YKO library, or in case of Δ*trk1* as triplicates, for which reason only one was picked and further analyzed. In the end, 76 putative fusion mutants, excluding the vacuolar membrane ATPase (VMA)-mutants, were selected and further re-analyzed via flow cytometry in 96-well format for a more accurate quantification of the defect.

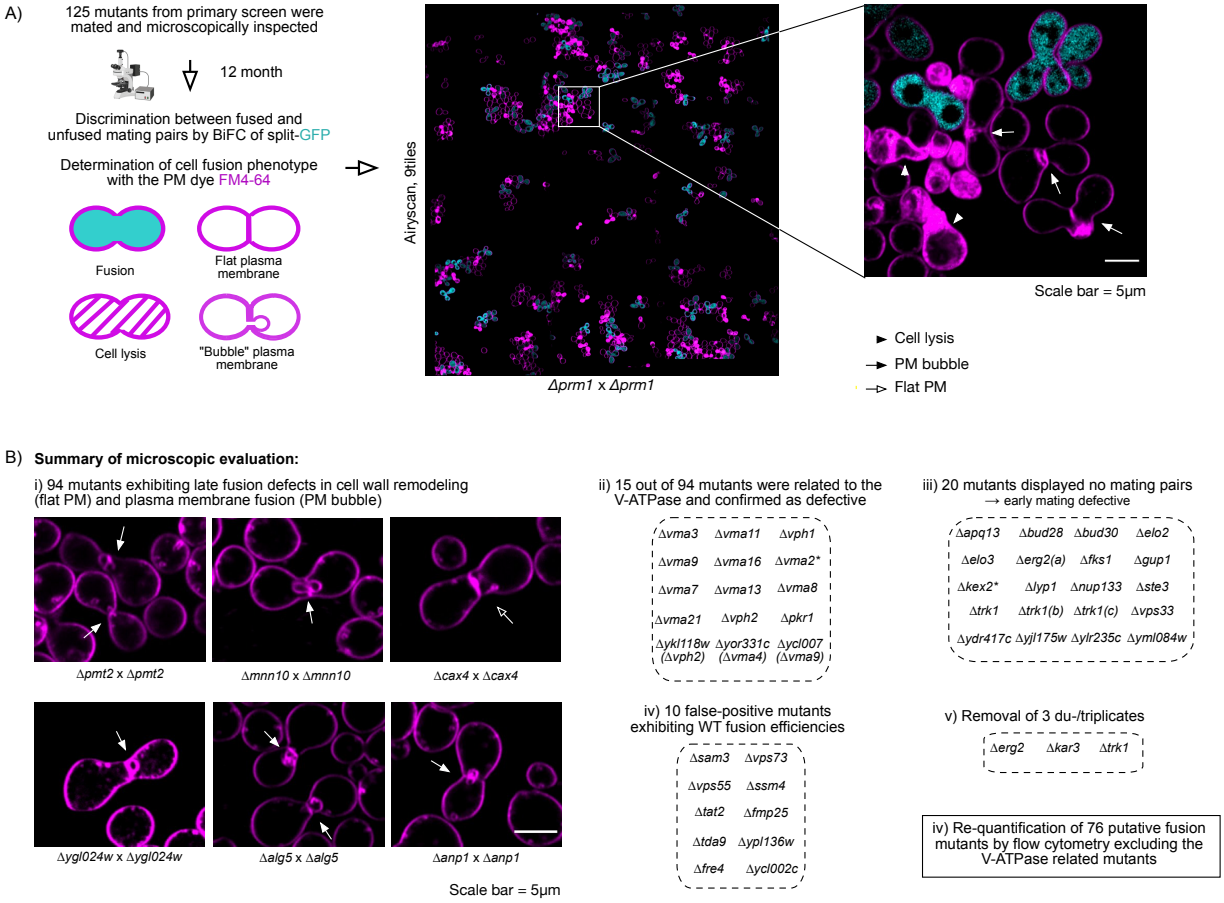

Figure 23: Microscopic confirmation of 91 fusion mutants from primary screen. A) Workflow of secondary screen. Microscopic inspection of 125 mutants to confirm the fusion defect in yeast mating pairs by employing PM staining with FM4-64. Mating cells expressing GFP fluorescence were counted as fused. Fusion defect phenotypes are denoted as: lysed (white arrow head), PM bubble (white filled arrow), flat PM (unfilled arrow). B) Summary of microscopic evaluation. Representative images of selected mutants showing late fusion defects at the level of PM fusion (PM bubble) and CW remodeling (flat PM).

Table 25: Fusion efficiencies of 125 mutants from primary and secondary screen.

		Primary Screen - flow cytometry	Secondary Screen - microscopy with FM4-64 staining			
Gene ID	**ORF name**	**Fused (% - normalized to median)**	**Fused pairs**	**Defective pairs**	**Fused (%)**	**Notes**
YPR124W	*CTR1*	31	29	91	24	
YNL279W	*PRM1*	47	106	215	33	
YGL024W	*YGL024W*	12	16	25	39	
YKL118W	*YKL118W*	33	40	53	43	Partially overlapping V-

						ATPase subunit VPH2
YPL234C	*VMA11*	3	52	58	47	V0 subunit of the V-ATPase
YDR245W	*MNN10*	5	57	58	50	
YMR307W	*GAS1*	32	69	66	51	
YJR143C	*PMT4*	11	42	39	52	
YKL080W	*VMA5*	37	74	67	53	V1 subunit of the V-ATPase
YGR020C	*VMA7*	2	100	89	53	V1 subunit of the V-ATPase
YCL007C	*YCL007C*	40	46	29	61	Overlapping with V-ATPase subunit VMA9
YDR200C	*VPS64*	31	80	48	63	
YEL027W	*VMA3*	35	92	54	63	V0 subunit of the V-ATPase
YCL005W-A	*VMA9*	23	52	28	65	V0 subunit of the V-ATPase
YMR202W (b)	*ERG2 (b)*	38	61	31	66	Duplicate mutant (YMR202W(a)) contained no mating pairs; discarded for further analysis
YGR105W	*VMA21*	3	92	43	68	V-ATPase assembly factor
YKL212W	*SAC1*	40	109	49	69	
YKL119C	*VPH2*	16	72	32	69	V-ATPase assembly factor
YOR008C	*SLG1*	24	107	43	71	
YBR171W	*SEC66*	62	183	71	72	
YOR219C	*STE13*	10	45	17	73	
YOR085W	*OST3*	58	94	35	73	
YDL095W	*PMT1*	43	94	34	73	
YEL036C	*ANP1*	43	83	29	74	
YGR036C	*CAX4*	9	46	14	77	

YLR056W	*ERG3*	8	18	5	78	
YBR078W	*ECM33*	63	100	26	79	
YGL072C	*YGL072C*	60	104	27	79	
YEL051W	*VMA8*	14	193	48	80	V1 subunit of the V-ATPase
YDR349C	*YPS7*	75	275	63	81	
YHR178W	*STB5*	71	261	59	82	
YGR041W	*BUD9*	73	134	30	82	
YLL043W	*FPS1*	54	85	19	82	
YGL203C	*KEX1*	54	92	20	82	
YOR331C	*YOR331C*	23	37	8	82	Overlapping with V-ATPase subunit VMA4
YJR018W	*YJR018W*	62	126	25	83	
YBR196C-A	*YBR196C-A*	64	71	14	84	
YDR335W	*MSN5*	31	43	8	84	
YCR089W	*FIG2*	58	147	27	85	
YKR044W	*UIP5*	75	112	19	86	
YPL227C	*ALG5*	49	131	22	86	
YPR141C (b)	*KAR3 (b)*	33	49	8	86	Duplicate mutant (YPR141C(a)); discarded for futher analysis
YHR142W	*CHS7*	72	208	33	86	
YOR030W	*DFG16*	69	204	30	87	
YHR026W	*VMA16*	11	197	29	87	V0 subunit of the V-ATPase
YOR270C	*VPH1*	55	179	26	87	V0 subunit of the V-ATPase
YGR026W	*YGR026W*	70	160	21	88	
YDR417C (a)	*YDR417C (a)*	34	200	26	89	Duplicate (YDR417C(b)) mutant contained no mating pairs; mutant not analyzed further
YLR226W	*BUR2*	62	144	18	89	

YDL116W	*NUP84*	33	159	19	89	
YCL058C	*FYV5*	69	123	14	90	
YNL228W	*YNL228W*	57	119	13	90	
YLR403W	*SFP1*	3	125	13	91	
YMR123W	*PKR1*	65	141	14	91	V-ATPase assembly factor
YPR036W	*VMA13*	17	91	9	91	V1 subunit of the V-ATPase
YJR117W	*STE24*	55	164	16	91	
YOR327C	*SNC2*	47	103	10	91	
YEL042W	*GDA1*	52	143	13	92	
YDL225W	*SHS1*	70	157	14	92	
YBR023C	*CHS3*	70	176	14	93	
YBR075W	*YBR075W*	75	263	21	93	
YOL018C	*TLG2*	46	229	18	93	
YPL205C	*YPL205C*	45	203	16	93	
YPR141C (a)	*KAR3 (a)*	59	124	9	93	
YOL115W	*PAP2*	65	97	7	93	
YPL042C	*SSN3*	75	111	8	93	
YLR286C	*CTS1*	17	225	15	94	
YDR149C	*YDR149C*	64	169	11	94	
YER019W	*ISC1*	53	265	17	94	
YDR126W	*SWF1*	14	176	11	94	
YPL187W	*MF(A)1*	72	250	14	95	
YGR045C	*YGR045C*	59	235	13	95	
YBR069C	*TAT1*	65	129	7	95	
YLR395C	*COX8*	71	114	6	95	
YNL111C	*CYB5*	71	347	16	96	
YKR039W	*GAP1*	68	466	21	96	
YJR118C	*ILM1*	64	356	16	96	
YDR456W	*NHX1*	57	155	7	96	
YJR075W	*HOC1*	75	117	5	96	
YBL039C	*URA7*	70	94	4	96	

YER058W	*PET117*	65	119	5	96	
YBR266C	*SLM6*	35	248	10	96	
YAL023C	*PMT2*	31	381	15	96	
YLR083C	*EMP70*	67	147	5	97	
YDR445C	*YDR445C*	67	211	7	97	
YHR155W	*LAM1*	60	267	8	97	
YOR036W	*PEP12*	13	139	4	97	
YFL013W-A	*YFL013W-A*	72	345	9	98	
YOL081W	*IRA2*	64	371	9	98	
YBL062W	*YBL062W*	60	279	7	98	
YEL017C-A	*PMP2*	72	135	3	98	
YER017C	*AFG3*	70	162	3	98	
YEL045C	*YEL045C*	33	374	7	98	
YJL004C	*SYS1*	53	459	8	98	
YPL274W	*SAM3*	54	256	4	99	False positive
YJR044C	*VPS55*	73	322	5	99	False positive
YOL020W	*TAT2*	71	288	4	99	False positive
YML081W	*TDA9*	48	211	3	99	False positive
YNR060W	*FRE4*	68	337	4	99	False positive
YGL104C	*VPS73*	70	408	5	99	False positive
YIL030C	*SSM4*	63	398	4	99	False positive
YPL136W	*YPL136W*	71	269	2	99	False positive
YCL002C	*YCL002C*	58	126	0	100	False positive
YLR077W	*FMP25*	63	83	0	100	False positive
-	Wild-type	100	407	3	99	

Table 26: Early defective mutants displaying no mating pairs.

Gene ID	ORF name	Gene description	Comment	ORF classified as early mating defective?
YJL075C	*APQ13*			Y
YLR062C	*BUD28*	BUD site selection		Y
YDL151C	*BUD30*	BUD site selection		Y
YCR034W	*ELO2*	fatty acid ELOngation		Y
YLR372W	*ELO3*	fatty acid ELOngation		Y
YMR202W (a)	*ERG2*	ERGosterol biosynthesis	2 mutants of same ORF in YKO; 2nd mutant exhibited defective mating pairs; gene was therefore not classified as early mating defective	N
YLR342W	*FKS1*	FK506 Sensitivity		Y
YGL084C	*GUP1*	Glycerol UPtake		Y
YNL238W	*KEX2*	Killer EXpression defective		Y
YNL268W	*LYP1*	LYsine-specific Permease		Y
YKR082W	*NUP133*	NUclear Pore		Y
YKL178C	*STE3*	STErile		Y
YJL129C	*TRK1*	TRansport of potassium (K)	No cells found in wells; 3 mutants of same ORF in YKO	Y
YJL129C (a)	*TRK1*	TRansport of potassium (K)	3 mutants of same ORF in YKO	
YJL129C (b)	*TRK1*	TRansport of potassium (K)	3 mutants of same ORF in YKO	
YLR396C	*VPS33*	Vacuolar Protein Sorting		Y
YDR417C (b)	*YDR417C*			Y
YJL175W	*YJL175W*			Y
YLR235C	*YLR235C*			Y
YML084W	*YML084W*			Y
VMA2	*VMA2*	Vacuolar ATPase subunit	14 additional V-ATPase ORFs identified in screen; gene was therefore not classified as early mating defective	N

3.1.7 Cell fusion quantification of 76 putative fusion mutants by flow cytometry

To more accurately quantify cell fusion efficiency, 76 fusion mutants confirmed in the secondary screen (section 3.1.6) were re-analyzed by the BiFC flow cytometry assay as quadruplicates. Due to their abundance, the fifteen V-ATPase related genes were excluded from this analysis and investigated separately in section 3.3. Beforehand, the deletion of the corresponding genes in both mating types was confirmed by colony PCR, or, in case of non-confirmation, individually generated in a new genetic background as described in section 2.12.4.

Initially, a new customized *MAT***a** C-GFP and *MAT*α N-GFP HIT library was generated, which harbored the 76 mutants in quadruplicates, as well as the WT and Δ*prm1* (independently generated by knockout PCR) as an internal control. A schematic workflow is illustrated in (**Figure 24A)**. Subsequently, cell fusion of the four 96-well plates was determined via flow cytometry by employing differential CW staining and BiFC of GFP (section 2.12.11.2). Cell fusion was then normalized to the WT fusion efficiency of the respective plate and plotted from lowest to highest fusion efficiencies (**Table 27**). The extent of the fusion defect of Δ*prm1* mutants present in the HIT library was equal to the fusion defect of Δ*prm1* mutants generated by PCR, demonstrating the robustness of the SGA procedure (**Figure 24B**).

Since Δ*prm1* is the current reference strain for PM fusion, a heat map was generated using Z-efficiencies standardized to Δ*prm1* (**Figure 24C**). The Z-score extended from +6 (blue) to -6 (orange) and was defined as less or more defective than Δ*prm1*. The columns correspond to one single measurement and the rows represent individual cell fusion mutants. The analysis revealed the existence of three major cluster groups: (A) 21 mutants were identified to be more defective than Δ*prm1*, typically displaying fusion efficiencies lower than 40%, (B) 13 mutants exhibited similar defects like Δ*prm1* with fusion levels between 40-70%, (C1) 21 mutants were weakly defective with fusion values between 70-90%, and lastly, (C2) 20 mutants were not found to be significantly distinct from WT fusion levels, even though arrested mating cells were observed by microscopy in the secondary screen. The remaining part of my thesis will be

focusing on the mutants from group A and B, containing those mutants exhibiting fusion levels at least as defective as Δ*prm1*.

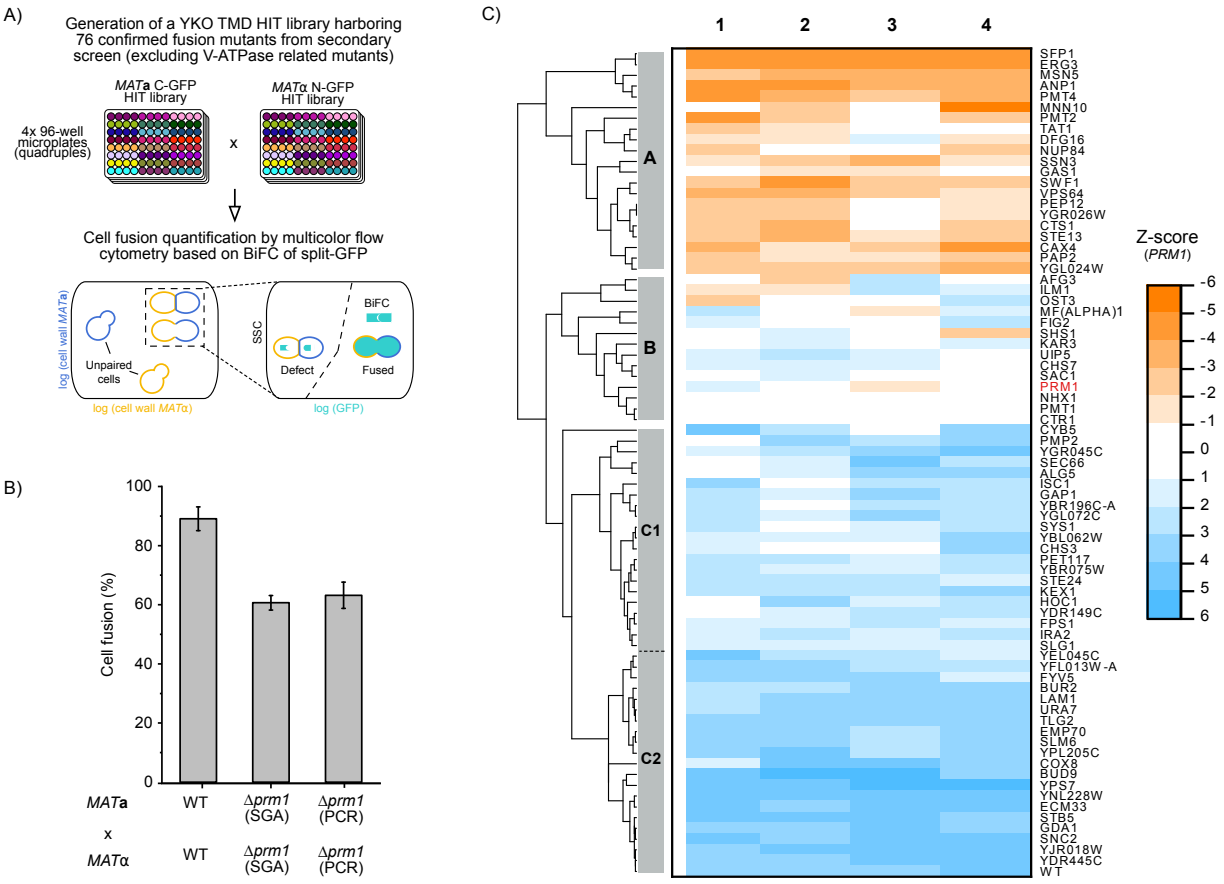

Figure 24: Quantification of TMD HIT library containing 76 putative fusion mutants. A) Workflow showing the generation of a new TMD HIT library and subsequent cell fusion quantification by BiFC of GFP with flow cytometry. B) Δ*prm1* x Δ*prm1* matings in different genetic backgrounds exhibit equal fusion levels. C) Heat map analysis of quantified fusion mutants standardized to Δ*prm1*. The Z-score extends from +6 (blue) to -6 (orange) as fusion efficiencies less or more defective than Δ*prm1*, respectively. The columns represent single measurements and the rows the individual mutants.

Table 27: Fusion efficiencies of 76 mutants determined by flow cytometry (96-well).

No	*MAT*a	*MAT*α	Cell fusion (%)	STD EV (%)	No	*MAT*a	*MAT*α	Cell fusion (%)	STD EV (%)
1	*Δsfp1*	*Δsfp1*	2,3	1,0	**39**	*Δydr149c*	*Δydr149c*	75,3	8,6
2	*Δerg3*	*Δerg3*	4,9	1,5	**40**	*Δybl062w*	*Δybl062w*	75,3	10,4
3	*Δanp1*	*Δanp1*	11,8	4,4	**41**	*Δira2*	*Δira2*	75,4	6,7
4	*Δpmt4*	*Δpmt4*	15,1	8,3	**42**	*Δfps1*	*Δfps1*	75,6	4,0

5	*Δmsn5*	*Δmsn5*	19,0	4,0	**43**	*Δybr075w*	*Δybr075w*	77,7	6,6
6	*Δcax4*	*Δcax4*	22,6	10,4	**44**	*Δisc1*	*Δisc1*	78,2	16,0
7	*Δswf1*	*Δswf1*	23,9	10,4	**45**	*Δsec66*	*Δsec66*	78,3	20,1
8	*Δvps64*	*Δvps64*	26,2	9,9	**46**	*Δhoc1*	*Δhoc1*	78,8	9,6
9	*Δygl024w*	*Δygl024w*	26,4	4,3	**47**	*Δste24*	*Δste24*	79,2	3,2
10	*Δste13*	*Δste13*	28,0	10,7	**48**	*Δybr196c-a*	*Δybr196c-a*	79,5	11,2
11	*Δcts1*	*Δcts1*	30,1	15,5	**49**	*Δalg5*	*Δalg5*	79,5	15,9
12	*Δssn3*	*Δssn3*	31,7	13,3	**50**	*Δpet117*	*Δpet117*	80,2	7,1
13	*Δpap2*	*Δpap2*	32,3	4,2	**51**	*Δygl072c*	*Δygl072c*	80,5	9,5
14	*Δpmt2*	*Δpmt2*	33,1	22,3	**52**	*Δpmp2*	*Δpmp2*	82,0	18,1
15	*Δpep12*	*Δpep12*	33,7	9,9	**53**	*Δcyb5*	*Δcyb5*	82,9	22,8
16	*Δygr026w*	*Δygr026w*	34,2	10,8	**54**	*Δkex1*	*Δkex1*	84,8	4,0
17	*Δnup84*	*Δnup84*	41,2	11,9	**55**	*Δgap1*	*Δgap1*	85,1	11,6
18	*Δgas1*	*Δgas1*	41,8	7,4	**56**	*Δfyv5*	*Δfyv5*	86,4	9,0
19	*Δmnn10*	*Δmnn10*	44,0	8,9	**57**	*Δyel045c*	*Δyel045c*	86,7	10,2
20	*Δtat1*	*Δtat1*	44,6	13,3	**58**	*Δyfl013w-a*	*Δyfl013w-a*	86,9	6,1
21	*Δdfg16*	*Δdfg16*	48,6	12,8	**59**	*Δygr045c*	*Δygr045c*	87,6	16,5
22	*Δshs1*	*Δshs1*	53,5	18,5	**60**	*Δbur2*	*Δbur2*	89,0	5,4
23	*Δafg3*	*Δafg3*	55,1	21,7	**61**	*Δura7*	*Δura7*	90,2	2,0
24	*Δnhx1*	*Δnhx1*	55,2	6,0	**62**	*Δslm6*	*Δslm6*	91,7	5,0
25	*Δost3*	*Δost3*	55,4	21,5	**63**	*Δemp70*	*Δemp70*	92,8	4,5
26	*Δctr1*	*Δctr1*	55,5	6,8	**64**	*Δtlg2*	*Δtlg2*	92,9	2,3
27	*Δilm1*	*Δilm1*	56,6	21,8	**65**	*Δypl205c*	*Δypl205c*	93,7	8,9
28	*Δpmt1*	*Δpmt1*	58,8	4,8	**66**	*Δlam1*	*Δlam1*	94,2	4,9
29	*Δprm1*	*Δprm1*	59,9	12,0	**67**	*Δcox8*	*Δcox8*	96,6	14,3
30	*Δmf(α)1*	*Δmf(α)1*	60,9	20,6	**68**	*Δgda1*	*Δgda1*	97,9	3,0
31	*Δsac1*	*Δsac1*	62,8	7,2	**69**	*Δydr445c*	*Δydr445c*	99,5	3,1
32	*Δfig2*	*Δfig2*	64,7	15,4	**70**	*Δstb5*	*Δstb5*	100,3	3,1
33	*Δkar3(a)*	*Δkar3(a)*	64,8	9,5	**71**	*Δsnc2*	*Δsnc2*	100,5	4,4
34	*Δchs7*	*Δchs7*	65,9	11,4	**72**	*Δyjr018w*	*Δyjr018w*	102,1	2,7
35	*Δslg1*	*Δslg1*	72,0	1,0	**73**	*Δecm33*	*Δecm33*	104,4	4,9

36	*Δchs3*	*Δchs3*	72,3	12,4	**74**	*Δynl228w*	*Δynl228w*	106,2	3,4
37	*Δsys1*	*Δsys1*	74,1	9,7	**75**	*Δbud9*	*Δbud9*	106,9	7,2
38	*Δuip5*	*Δuip5*	74,4	10,2	**76**	*Δyps7*	*Δyps7*	111,7	3,3

3.2 Cell fusion symmetry analysis of 37 gene of interest (GOI) mutants

For a more in-depth analysis of fusion mutants a new GOI TMD sub-library was constructed containing mutants that were at least as defective as Δ*prm1*. Based on the results of the heat map analysis (section 3.1.7), 28 mutants of group A and B were selected, whereby mutants that e.g., exhibited a strong growth defect were excluded (**Table 28**). Two representative subunits of the V-ATPase complex and one associated assembly factor (Δ*vma11*, Δ*vma2*, Δ*vma21*) as well as known fusion mutants (Δ*fig1*, Δ*erg6* Δ*fus1*, Δ*fus2*, Δ*chs3*), which the primary screen failed to identify, were supplemented to the list. Additionally, a null mutant of *KEX2* was supplemented, which is known to encode a serine-type endopeptidase which causes defects in the maturation of α-factor pheromone when deleted and presumably proteolytically processes other substrates important for cell fusion [135]. The subsequent fusion assessment of the GOI TMD sub-library was switched from the 96-well format to the small-scale yeast mating procedure carried out in 5ml YPD medium and a 12-manifold because growth conditions of each deletion strain could be conveniently adjusted to its individual growth rate. In order to determine the symmetry of the fusion defect, bilateral and unilateral matings were carried out and fusion efficiency quantified by BiFC-based flow cytometry as described in section 2.12.11.1.

A fusion mutant is considered to act bilaterally when the presence of the gene in only one of the mating partners is sufficient to sustain cell fusion levels close to WT levels. Consequently, the corresponding gene must be absent in both mating cells to lead to a fusion defect as shown for Δ*prm1* matings in (**Figure 25A**) (left). By contrast, mutants displaying a unilateral defect give rise to a pronounced fusion defect when the gene is absent in one mating partner, as demonstrated for Δ*kex2* matings in (**Figure 25A**) (right). (**Figure 25B**) depicts only unilateral cell

fusion data of each mutant, whereby the fusion of *MAT***a** mutant crossed to WT *MAT*α (Δ*mut* a x WT α) was plotted on the y-axis, and fusion of *MAT*α mutant crossed to WT *MAT***a** (WT a x Δ*mut* α) on the x-axis. As can be seen, most of the mutants displayed fusion efficiencies over 75% fusion close to WT level (denote in black dashed lines). This means, that the majority exposed a bilateral mating symmetry. However, some exceptions were noticeable. For instance, Δ*kex2* and Δ*ste13* exhibited reduced fusion efficiency when absent in *MAT*α mating type. Their unilateral mating symmetry was expected because of their known role in α-factor pheromone processing. Surprisingly, the deletion of *YGL024W* resulted in a mating-type independent unilateral defect with about 50% fusion efficiency in both mating types. **Figure 25C**, includes both, the unilateral as well as bilateral fusion data. The bilateral fusion efficiencies of the 20 most defective mutants are highlighted in pink circles and sorted from lowest to highest. The unilateral data of the respective fusion mutants are depicted in grey, when the gene was deleted in *MAT***a** and crossed to the WT gene expressed in *MAT*α (Δ*mut* **a** x WT α), or in white when vice versa (WT **a** x Δ*mut* α). WT fusion efficiencies are illustrated in black. The bilateral fusion efficiencies of the remaining 17 mutants are depicted in pink brackets. Error bars indicate the standard error of the mean of three independent measurements. In the statistical analysis of the top 20 mutants, the known fusion mutants Δ*prm1*, Δ*erg3*, Δ*erg6* and Δ*fus1* were included.

Altogether, this in-depth analysis provides a broad overview of the mating symmetry of known and novel fusion mutants identified in this screen. As expected, most of them operated bilaterally. Exceptionally, the Δ*ygl024w* mutant displayed a unique mating-type independent unilateral fusion mechanism. Moreover, all three selected Δ*vma* mutants were highly defective implying a yet undescribed role for the V-ATPase in cell fusion during yeast mating.

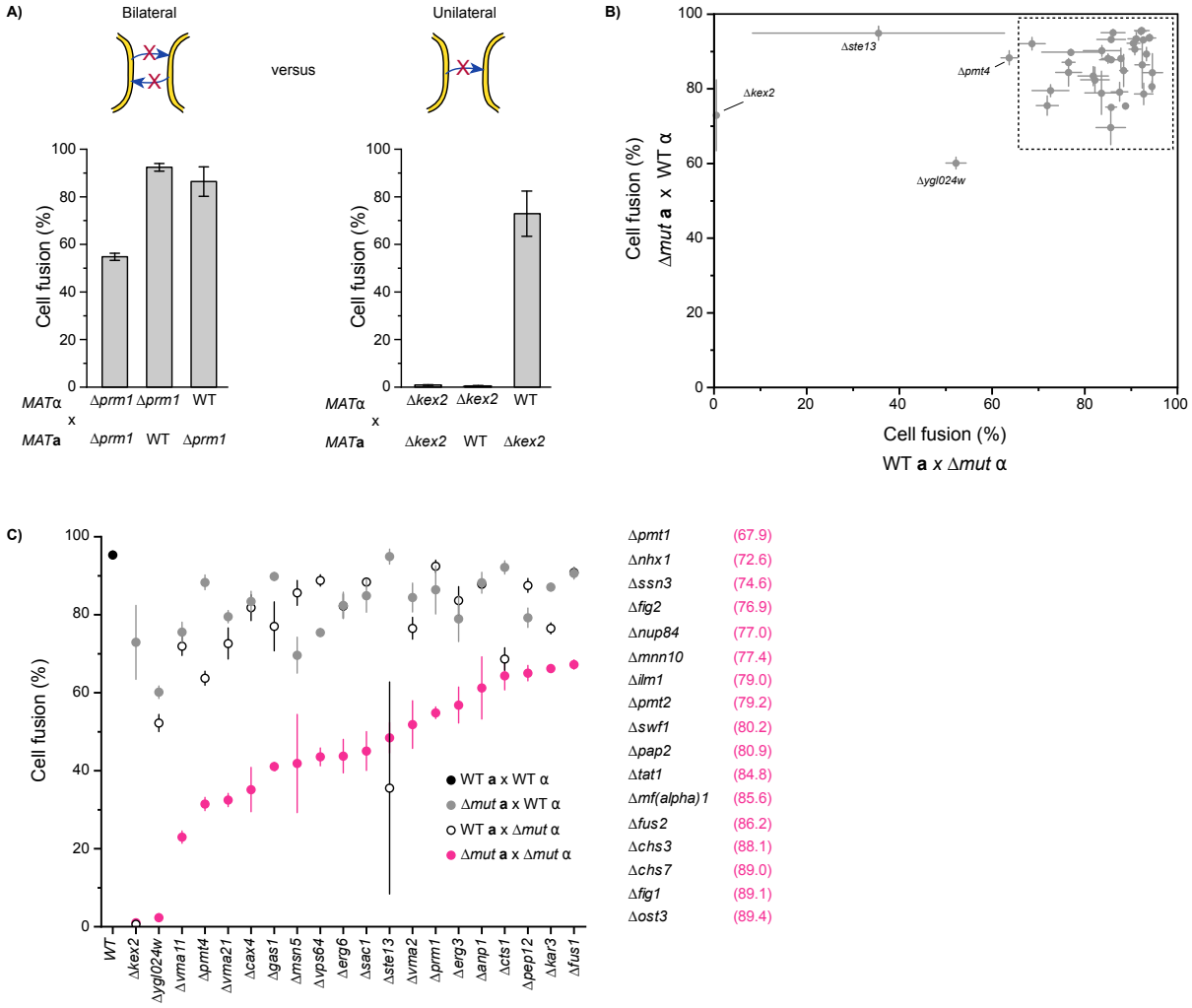

Figure 25: Determination of cell fusion symmetry of 37 GOI mutants. A) Bilateral versus unilateral fusion symmetry. Δ*prm1* displaying a bilateral defect (left); Δkex2 displaying a mating-type dependent unilateral defect when deleted in *MAT*α. B) Majority of fusion mutants displays a bilateral fusion defect. Unilateral fusion efficiencies are mostly higher than 75% (denoted in black dashed lines). C) Bilateral fusion efficiencies of the 20 most defective mutants are sorted from the lowest to the highest and denoted in pink circles. Unilateral efficiencies are denoted in grey (Δ*mut* **a** x WT α) or white (WT **a** x Δ*mut* α), WT fusion efficiencies in black. Bilateral fusion efficiencies of the remaining 17 mutants are shown in pink brackets. Error bars indicate the standard error of the mean of three independent measurements.

Table 28: Overview of genes excluded from gene of interest (GOI) collection.

Gene deletion strain	Reason for exclusion from GOI collection
Δafg3	Strong defect could not be replicated in mutants generated by PCR
Δctr1	Strong growth defect observed on one mating-type
Δdfg16	Indistinguishable from wild-type
Δsfp1	Pronounced growth defect, cells appeared sick
Δuip5	Mutant not measured
Δygr026w	Indistinguishable from wild-type

3.3 A functional role of the V-ATPase activity in cell fusion

The primary screen (section 3.1.5) revealed that the absence of 15 V-ATPase related genes led to impaired fusion activity which implies a hitherto undescribed role of the complex in this process in yeast. The V-ATPase is a multi-subunit enzyme complex (**Figure 26**) that is important for intracellular acidification and pH regulation [161]. In previous studies, it has been shown, that the disruption of almost any *VMA*-gene results in a characteristic conditional lethal phenotype, called *VMA*$^{-}$phenotype. This phenotype is characterized by the capability of cells to grow on acidic media buffered to pH 5.0 and a failure to grow on neutral media buffered to pH 7.5, and was key for the identification of the subunit composition [162-164]. The present work provides the evidence for the importance of the V-ATPase in promoting cell fusion in the context of yeast mating.

A)

Domain	Subunit	Gene
V1	A	*VMA1*
	B	*VMA2*
	E	*VMA4*
	C	*VMA5*
	F	*VMA7*
	D	*VMA8*
	G	*VMA10*
	H	*VMA13*
V0	c	*VMA3*
	d	*VMA6*
	e	*VMA9*
	c'	*VMA11*
	c''	*VMA16*
	a	*VPH1*
	a	*STV1*
		Gene
Assembly factors		*VPH2*
		VMA21
		VMA22
		PKR1
		VOA1

B)

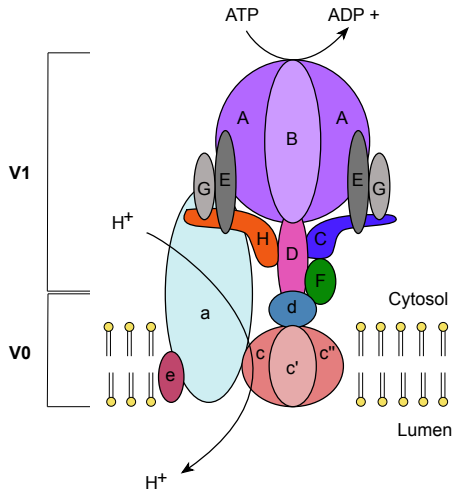

Figure 26: Schematic of the yeast vacuolar membrane ATPase (V-ATPase) A) List of genes encoding for V-ATPase subunits and its associated assembly factors. B) The V-ATPase consists of several subunits structured into two domains, a membrane-located V0-domain facilitating proton translocation, and a soluble V1-domain containing the ATP-binding site and is important for intracellular acidification and pH regulation.

3.3.1 Disruption of V-ATPase-associated genes leads to a defect in cell fusion

To confirm whether the impaired fusion activity in yeast mating is caused by the lack of the enzyme activity induced by the absence of any V-ATPase subunit or specific to some individuals, cell fusion of all Δ*vma*-mutants was determined by BiFC flow cytometry (section 2.12.11.2). For this, a new *VMA* sub-library in 96-well format was constructed containing mutants of all V-

ATPase encoding subunits and associated assembly factors in quadruplicates (**Figure 27A**). Δ*vma* null mutants were generated in a new genetic background (*MAT***a** PSAY983 and *MAT*α PSAY981) and confirmed by PCR as described in section 2.12.6. Since subunit 'a' is encoded by one of the two isoforms *VPH1* or *STV1* which can compensate for each other when only one is depleted, a Δ*vph1*Δ*stv1* double mutant was generated and included in the analysis.

After cell fusion assessment, the fusion efficiencies were normalized to WT fusion efficiency and sorted numerically within their position and / or function as assembly factors (**Figure 27B**). The analysis revealed that the deletion of almost all *VMA*-genes resulted in a strong fusion defect exhibiting fusion levels between ~5-30%. A less pronounced or no defect was observed in the mutants encoding for either the non-essential assembly factors Pkr1 and Voa1 or the subunit a isoforms Vph1 and Stv1. However, the simultaneous disruption of both isoforms led to a strong decrease in fusion. These results strongly suggests that the complex integrity, and thus the enzyme activity, is needed for efficient cell fusion rather than any specific subunit.

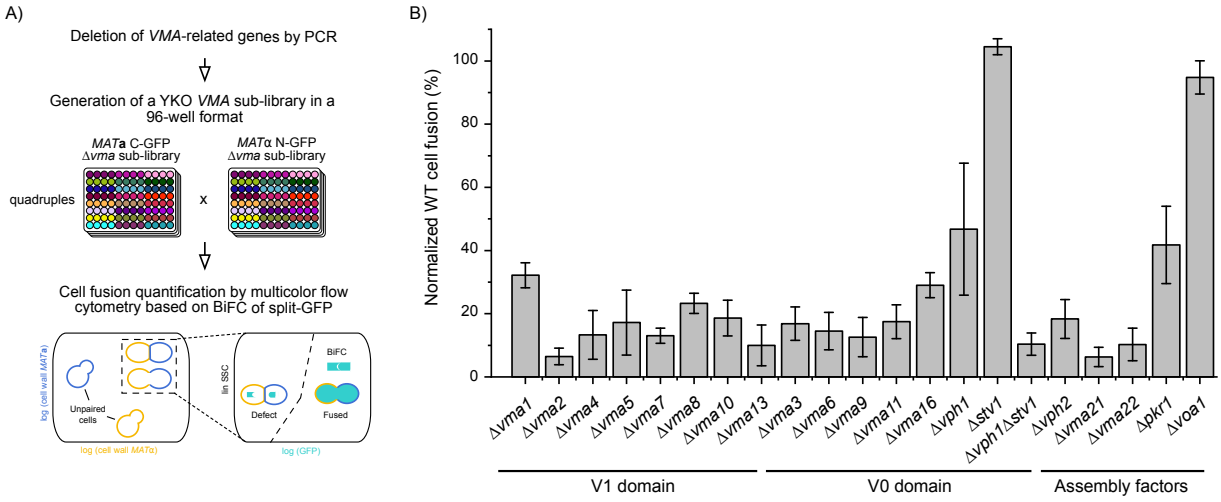

Figure 27: Cells lacking the V-ATPase activity exhibit a defect in cell fusion. A) Workflow for generating a new *VMA* sub-library containing null mutants of V-ATPase subunits and associated assembly factors and subsequent cell fusion assessment by BiFC-based flow cytometry in 96-well format. B) Normalized cell fusion efficiencies are numerically sorted within the respective subunits or function as assembly factors.

3.3.2 V-ATPase activity facilitates cell fusion by acidifying endomembrane organelles

In the previous section it was shown, that the absence of almost any *VMA*-genes led to impaired fusion activity during yeast mating (**Figure 27B**). To determine whether the V-ATPase localizes at the shmoo tip or mating junction, *VMA2*, a gene encoding for subunit B of the V1 domain, was chromosomally tagged at the C-terminus with mNeonGreen (mNG) as described in section 2.12.4. Afterwards, the localization profiles of Vma2 in vegetative and pheromone-treated conditions were determined. Specifically, haploid *MAT***a** cells expressing the *VMA2*-mNG construct were grown to OD_{600} = 0.6-0.8, treated with DMSO or 20µM α-factor for ~2h and fixed in TAF buffer. Additionally, *VMA2*-mNG *MAT***a** cells were mated for 3h at 30˚C on YPD to *MAT*α cells expressing the cytoplasmic marker *PGK1*-mCherry and arrested in TAF buffer. Thereafter, all conditions were imaged by confocal microscopy. Indeed, *VMA2*-mNG was constitutively expressed in vegetative, pheromone-treated and mating conditions (**Figure 28A**) and excluded from the shmoo tip and mating junction. Therefore, these results suggest that the V-ATPase probably promotes cell fusion indirectly by acting in proxy via acidification of the vacuole and other endomembrane organelles.

To support this hypothesis, a cell fusion rescue experiment was designed in which the matings of Δ*vma2* were carried out at acidic (pH5.5) and neutral pH (pH6.8). Cell fusion was then measured by flow cytometry to test whether at low pH the fusion defect can be partially rescued due to external uptake of protons. To maintain a stable pH the used media and washing solutions were buffered with 50 mM MES (2-(N-morpholino)ethanesulfonic acid) to the desired pHs. Because the fluorophore conjugate ConA-Tet was quenched at low pH, the CF770 conjugate with an excitation maximum at 770 nm and an emission maximum at 797 nm was used instead. *MAT*α cells were stained with ConA-647 as usual. Error bars indicate the standard error of the mean of three measurements. As shown in **Figure 28B**, WT fusion remained the same at both pH conditions displaying about 70-75% fusion. In contrast, fusion was partially rescued in Δ*vma2* mating cells at acidic pH 5.5 when compared to fusion at pH 6.8.

Taken together, the defect could only partially be restored implying the existence of additional factors in this process. However, acidification seemed to be the most important contributing

factor of the V-ATPase complex in promoting cell fusion. Further investigations were conducted to better understand the mechanistic basis of the V-ATPase in cell fusion.

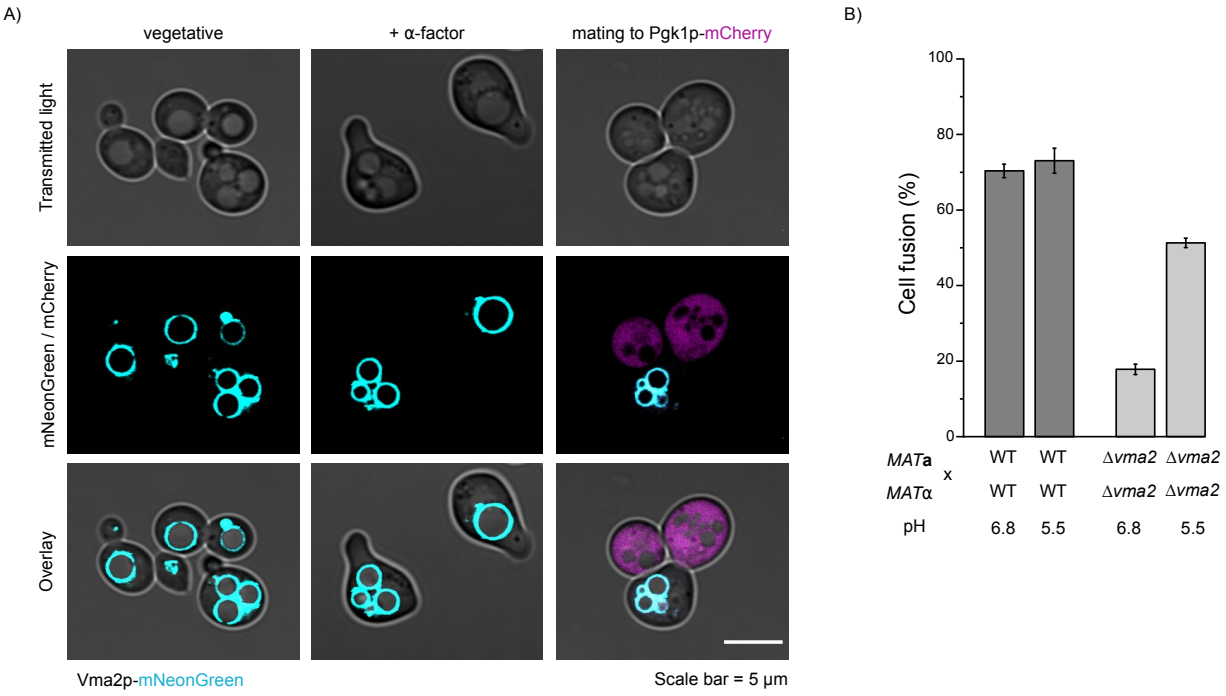

Figure 28: V-ATPase activity facilitates cell fusion indirectly by acidifying the vacuole and other endomembrane organelles. A) *MAT***a** cells expressing Vma2-mNeonGreen (mNG). In vegetative, pheromone treated and mated cells Vma2 localizes exclusively at the vacuole and is excluded from the shmoo tip and mating junction. B) Cell fusion analysis of WT and Δ*vma2* mating cells at acidic pH 5.5 and neutral pH 6.8. Error bars indicate the standard error of the mean of three measurements.

3.3.3 V-ATPase activity operates late at the stage of both CW remodeling and PM fusion

So far, deletion of almost all *VMA*-genes resulted in decreased fusion efficiency suggesting a functional role of the proton pump activity of the V-ATPase complex (section 3.3.1). Furthermore, fusion was partially restored by lowering the extracellular pH (section 3.3.2) likely by partial acidification of vacuoles via passive proton transport [165], and further, that V-ATPases were excluded from the shmoo tip and mating junction (section 3.3.2). The latter observation implies an indirect role via acidification of the vacuole and other endomembrane organelles. Previous analyses as shown in section 3.2 identified a bilateral cell fusion mechanism, in which only the disruption of *VMA*-genes in both mating cells leads to impaired fusion efficiency. Within the secondary screen (section 3.1.6) microscopic inspection in

conjunction with PM staining revealed that bilateral matings of *VMA*-mutants arrested fusion at the stage of CW remodeling, indicated by a flat PM interface, and PM fusion, characterized by cytoplasmic bubbles. Representative images of Δ*vma11* (subunit c' of V0-domain), Δ*vma2* (subunit B of V1-domain) and Δ*vma21* (assembly factor) matings are shown in (**Figure 29A**).

To determine to what extent the lack of the V-ATPase affects CW remodeling and PM fusion, the next section will be focusing on synergistic interaction analyses between a Δ*vma2* mutant and mutants that are implicated in CW remodeling and PM fusion. A synergistic interaction is considered proven when crosses between two different mutants across the two mating types *MAT***a** and *MAT*α produce a fusion defect. It may also indicate that these genes are operating within the same or overlapping pathways.

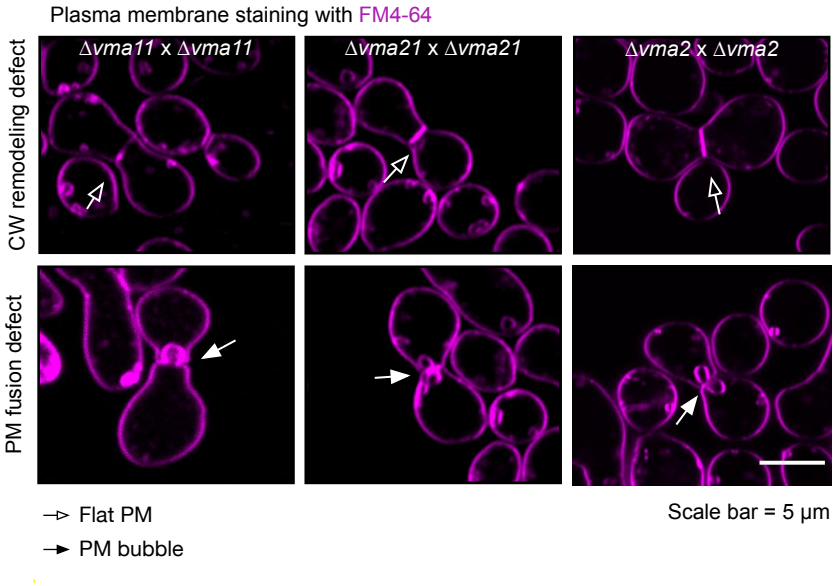

Figure 29: Disruption of *VMA*-genes leads to defects in CW remodeling and PM fusion. Shown are representative images of three V-ATPase-associated mutants displaying CW remodeling (flat PM interface) and PM fusion (cytoplasmic PM bubbles) defects. Scale bar = 5µm.

3.3.3.1 The V-ATPase affects CW remodeling and PM fusion approximately equally

At first, a Δ*vma2* mutant was crossed to a Δ*fus1*Δ*fus2* double mutant to determine to what extent the V-ATPase affects CW remodeling in mating. *FUS1* and *FUS2* are two key regulators of this process and their absence results in a fusion defect phenotype that is characterized by remnant CW material at the mating junction. These mutants are referred to as early-pre-zygotes [108, 116]. Due to their functional redundancy, the presence of only one protein can

compensate for the other, albeit with less efficiency. Simultaneous deletion of *FUS1* and *FUS2* results in an almost complete fusion arrest with an undigested CW and unfused PM [116, 149]. Representative images are shown in (**Figure 30A**).

Cell fusion analysis by flow cytometry was carried out in which bilateral matings of Δ*fus1* and Δ*fus2*, as well as Δ*fus1* crossed to Δ*fus2*, all exhibited fusion defect of ~ 50% (**Figure 30B**). This demonstrated firstly, that matings of Δ*fus1* x Δ*fus1* and Δ*fus2* x Δ*fus2* exhibited an equal defect and secondly, that *FUS1* and *FUS2* synergize because of the defect presented in Δ*fus1* x Δ*fus2* matings. Unilateral matings of Δ*fus1* x WT (data not shown) and Δ*fus2* x WT (**Figure 25**) resulted in fusion efficiencies between 80-85% suggesting that both are bilateral fusion mutants. As expected, bilateral matings of the double mutant Δ*fus1*Δ*fus2* resulted in a complete fusion arrest. Taken that *FUS1* and *FUS2* synergize in *trans* this implies that the two genes operate on partially overlapping yet separate pathways. When a Δ*fus1*Δ*fus2* mutant is instead crossed to a WT partner, about 50% of pairs are arrested as depicted in (**Figure 30C**). This indicates that the strong Δ*fus1*Δ*fus2* phenotype can be partially suppressed by WT genes expressed on the apposing cell. Analogously, a Δ*fus1*Δ*fus2* mutant that is crossed to a mutant that encodes for a gene that does not synergize with *FUS1FUS2* would express similar fusion scores. By contrast, an apposing mutant that encodes for a gene that synergizes with *FUS1FUS2*, it would present a similar fusion defect as seen in Δ*fus1*Δ*fus2* x Δ*fus1*Δ*fus2* crosses.

To assess the reliability of this analysis, first the Δ*fus1*Δ*fus2* double mutant was crossed to a Δ*prm1* single mutant (**Figure 30D**). *PRM1* is not expected to synergize because it acts downstream of *FUS1FUS2* [123]. As expected, bilateral matings of Δ*prm1* showed a 50% efficiency, whereas unilateral matings exhibited fusion close to WT fusion levels. Matings of Δ*fus1*Δ*fus2* also displayed expected fusion efficiencies with about 50% fusion in unilateral matings and an almost fusion block in bilateral matings. Crosses between Δ*fus1*Δ*fus2* and Δ*prm1* resulted in similar fusion efficiencies as when Δ*fus1*Δ*fus2* was crossed to WT verifying that *FUS1FUS2* and *PRM1* do not synergize in *trans*.

Following the same rationale, a Δ*vma2* mutant was crossed to a Δ*fus1*Δ*fus2* mutant. About 20% of mating cells fused in bilateral crosses of Δ*vma2*, whereas when crossed to WT, about 65% fused. Interestingly, an intermediate fusion level between a complete and partial fusion

arrest was observed in crosses between Δ*fus1*Δ*fus2* and Δ*vma2* which was lower than the expected additive unilateral defects (pink box) (**Figure 30E**). The fusion reduction suggests that *VMA2* operates at CW remodeling. However, since fusion is not completely blocked as seen in a *Δfus1Δfus2* x *Δfus1Δfus2* mating pair it implies that *VMA2* operates approximately equally at CW remodeling and PM fusion stages.

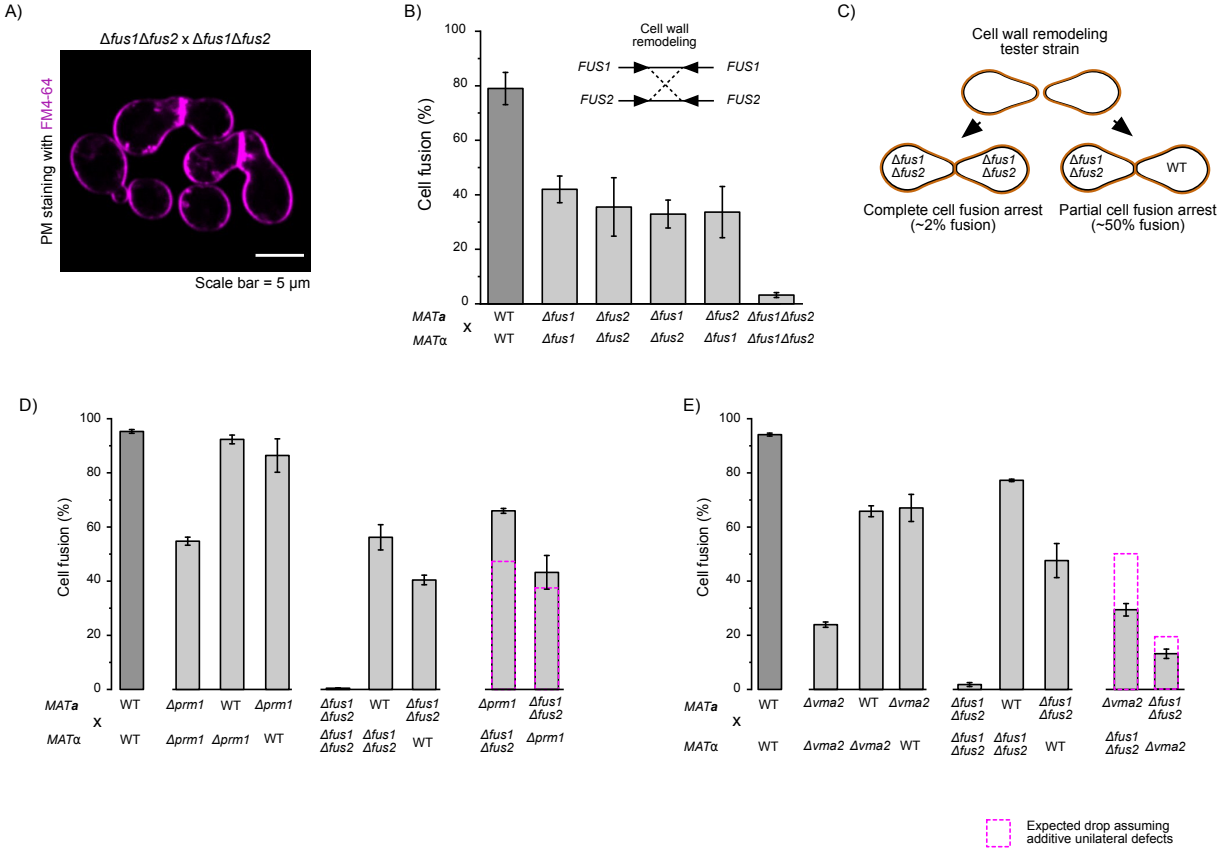

Figure 30: V-ATPase affects CW remodeling and PM fusion approximately equally. Cell fusion was measured by BiFC of split-GFP with flow cytometry. Error bars indicate SD of triplicate reactions. The pink box in dashed line depicts the expected drop assuming additive unilateral defects. A) Representative images of a Δ*fus1*Δ*fus2* double mutant arrested as early pre-zygotes displaying a CW remodeling defect (flat PM). Scalebar = 5 µm. B) *FUS1* and *FUS2* operate on two separate but partially overlapping pathways. C) Schematic showing expected fusion efficiencies of the Δ*fus1*Δ*fus2* double mutant in bilateral and unilateral matings. D) *FUS1FUS2* and *PRM1* do not synergize in *trans*. E) *FUS1FUS2* and *VMA2* synergize in *trans*. Crosses between the two mutants result in an intermediate fusion phenotype.

3.3.3.2 *VMA2* operates on a distinct but partially overlapping fusion pathway with *ERG6*

As shown in the previous section, the V-ATPase affects both CW remodeling and PM fusion approximately equally. To assess whether a deletion of V-ATPase affects PM fusion via a synergistic interaction with *PRM1*, crosses between Δ*vma2* and Δ*prm1* were carried out. *PRM1*

is a known key regulator of PM fusion and causes typically a ~50% fusion defect when absent in both mating cells [150]. Defective Δ*prm1* mating pairs arrest as late pre-zygotes exhibiting cytoplasmic bubbles projecting from one cell into the other. Representative images of Δ*prm1* mating cells with FM4-64-stained PMs are depicted in (**Figure 31A**). As seen in previous studies, crosses between Δ*prm1* and a WT partner result in fusion efficiencies close to WT fusion levels, as schematically illustrated in **Figure 31B**) and shown in **Figure 25A** [135]. Likewise, a Δ*prm1* mutant that is mated to a mutant of a gene that is not synergizing with *PRM1* would result in comparable fusion efficiencies. Whereas matings to mutants of genes that synergizes with *PRM1* would lead to a fusion defect close to Δ*prm1* x Δ*prm1* fusion levels.

As a proof of concept, initially a Δ*prm1* mutant was crossed to a Δ*erg6* mutant. Erg6 is involved in ergosterol biosynthesis and like Prm1 has been implicated in PM fusion. For instance, Erg6 is important for the formation of lipid rafts to facilitate the clustering of fusion proteins at the mating junction [119]. In its absence, mating cells also accumulate as late pre-zygotes. Notably, it has been shown that Erg6 promotes fusion independently of Prm1 [119]. In this work, bilateral matings of Δ*prm1* and Δ*erg6* exhibited a fusion defect of 55% and 44%, respectively (**Figure 31C**). Crosses between Δ*erg6* and WT resulted in fusion efficiencies close to WT fusion efficiency, a phenotype that was also detected in crosses between Δ*prm1* and Δ*erg6*, confirming that *ERG6* and *PRM1* do not synergize in *trans*.

Thereafter, synergistic interactions between Δ*prm1* and Δ*vma2* were investigated. Both displayed bilateral fusion defects of about 50% (**Figure 31D**). Unilateral fusion efficiency of Δ*vma2* matings was moderately reduced compared to the WT fusion level. However, considering the additive unilateral defect (pink box), crosses between Δ*prm1* and Δ*vma2* did not result in a stronger defect. Consequently, *VMA2* and *PRM1* do not synergistically interact. To further investigate whether *VMA2* synergized with other genes implicated in PM fusion, a Δ*vma2* mutant was crossed to a Δ*erg6* mutant strain. Interestingly, crosses between Δ*vma2* and Δ*erg6* indeed resulted in impeded fusion efficiency, similar to bilateral fusion efficiencies of Δ*vma2* and Δ*erg6*. This suggested, that *VMA2* and *ERG6* synergize in *trans* across both mating types (**Figure 31E**).

To verify whether genes are operating on the same or separate fusion pathway, double gene deletion mutants were generated. An enhanced fusion defect would indicate that the genes are operating on separate pathways, while an unchanged defect would indicate that both genes operate on the same pathway. Double mutants were generated as described in section 2.12.4 / 2.12.5.

In the case of the Δ*erg6*Δ*prm1* double mutant bilateral matings resulted in an enhanced fusion defect phenotype showing only little to no fusion (**Figure 31F**), as has been shown in a previous study [119]. To further analyze whether V*MA2* (partially) overlaps pathways in which *PRM1* and *ERG6* are operating, fusion of a Δ*prm1*Δ*vma2* and Δ*erg6*Δ*vma2* double mutant was determined. The Δ*prm1*Δ*vma2* double mutant resulted in an enhanced fusion defect exhibiting lower fusion efficiency than the Δ*prm1* and Δ*vma2* single mutants (**Figure 31G**). Given that *PRM1* and *VMA2* do not synergize in *trans*, this result indicates they operate on completely distinct fusion pathways. The Δ*erg6*Δ*vma2* mutant exhibited an enhanced fusion defect as well (**Figure 31H**). Given that *ERG6* and *VMA2* synergize in *trans* indicate that they operate on distinct but partially overlapping pathways, similarly as it was demonstrated for the CW remodeling mutants *FUS1* and *FUS2* (**Figure 30A**).

Together, these findings suggest that the V-ATPase operates in a novel fusion pathway in yeast mating independent of *PRM1* and independent yet partially overlapping of *ERG6*. The next question that was addressed was whether *VMA2* may also synergize with other genes identified in this work which will be further elaborated in the next section.

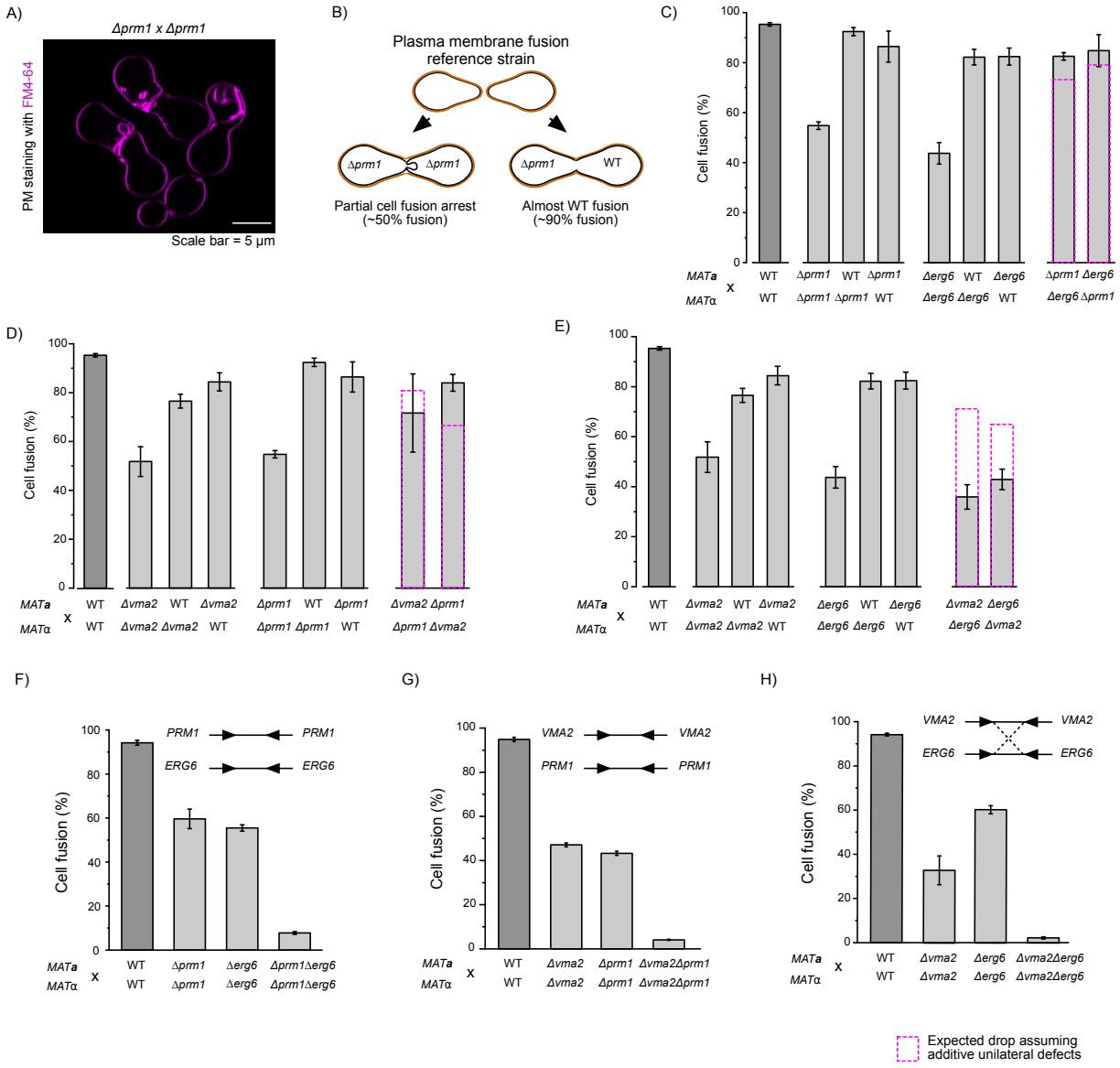

Figure 31: *VMA2* acts on a partially overlapping yet distinct pathway with *ERG6*. Matings and cell fusion analysis was quantified by flow cytometry. Error bars indicate SD of triplicate reactions. The pink box in dashed line depicts the expected drop assuming additive unilateral defects. A) Representative images of Δ*prm1* crosses with FM4-64-stained PMs. Cells arrest as late pre-zygotes exhibiting PM bubbles. Scalebar = 5 µm. B) Schematic showing bilateral and unilateral fusion efficiencies of Δ*prm1*. C) *PRM1* and *ERG6* do not synergize in *trans*. D) *VMA2* and *PRM1* do not synergize in *trans*. E) *VMA2* and *ERG6* synergize in *trans*. F) Simultaneous deletion of *PRM1* and *ERG6* leads to an enhanced fusion defect. Since they do not synergize in *trans* it indicates that they operate on completely separate pathways. G) Simultaneous deletion of *VMA2* and *PRM1* leads to an enhanced fusion defect. Since they do not interact in *trans* it indicates that they operate on complete separate pathways. H) Simultaneous deletion of *VMA2* and *ERG6* results in an enhanced fusion defect. Because of their interaction in *trans,* it suggests that they operate on partially overlapping pathways.

3.3.3.3 *VMA2* promotes cell fusion likely by proxy via interaction with at least 12 genes

To further investigate whether *VMA2* synergized with other genes identified in this work besides *ERG6*, a newly generated Δ*vma2* mutant array in 96-well format was crossed to the same GOI TMD sub-library from section 3.2. WT and Δ*prm1* strains were included and served as internal controls. Synergistic interactions in *trans* were then determined by quantifying cell fusion via the BiFC flow cytometry assay as described in section 2.12.11. Mutants that exhibited a fusion reduction of at least 50% compared to Δ*vma2* x WT fusion were selected and re-analyzed by flow cytometry via small scale yeast mating procedure. A schematic of the workflow is shown in (**Figure 32A**).

As explained in previous sections, a *trans* interaction was considered as such when the fusion defect between Δ*vma2* and the analyzed fusion mutant was comparable to the respective bilateral mating defect, or stronger than the additive unilateral defects. In total, 12 mutants including *ERG6* were identified to synergize with *VMA2* in *trans* (**Figure 32B**). According to the yeast genome database (SGD), the genes have reported roles in ergosterol biosynthesis (*ERG3*), protein glycosylation (*CAX4*, *ANP1*, *PMT2* and *PMT4*), CW synthesis and integrity (*CHS3*, *GAS1*), protein nuclear export and import (*MSN5*, *NUP84*), proteolytic processing (*KEX2)* and one with thus far unknown function (*YGL024w*).

Taken together with the findings from the previous sections it suggests that *VMA2* represent a third independent fusion pathway with *PRM1*, *ERG6* as illustrated in (**Figure 32B**) (black arrow), and synergizes with at least 12 genes (grey dashed lines). These widely diversified synergistic interactions provide an explanation for the mixed phenotype observed in Δ*vma2* mating cells as shown in (**Figure 29A**). The next section will evaluate whether these interactions are mediated directly by interfering with the localization of proteins or more indirectly via its function in acidifying endomembrane organelles.

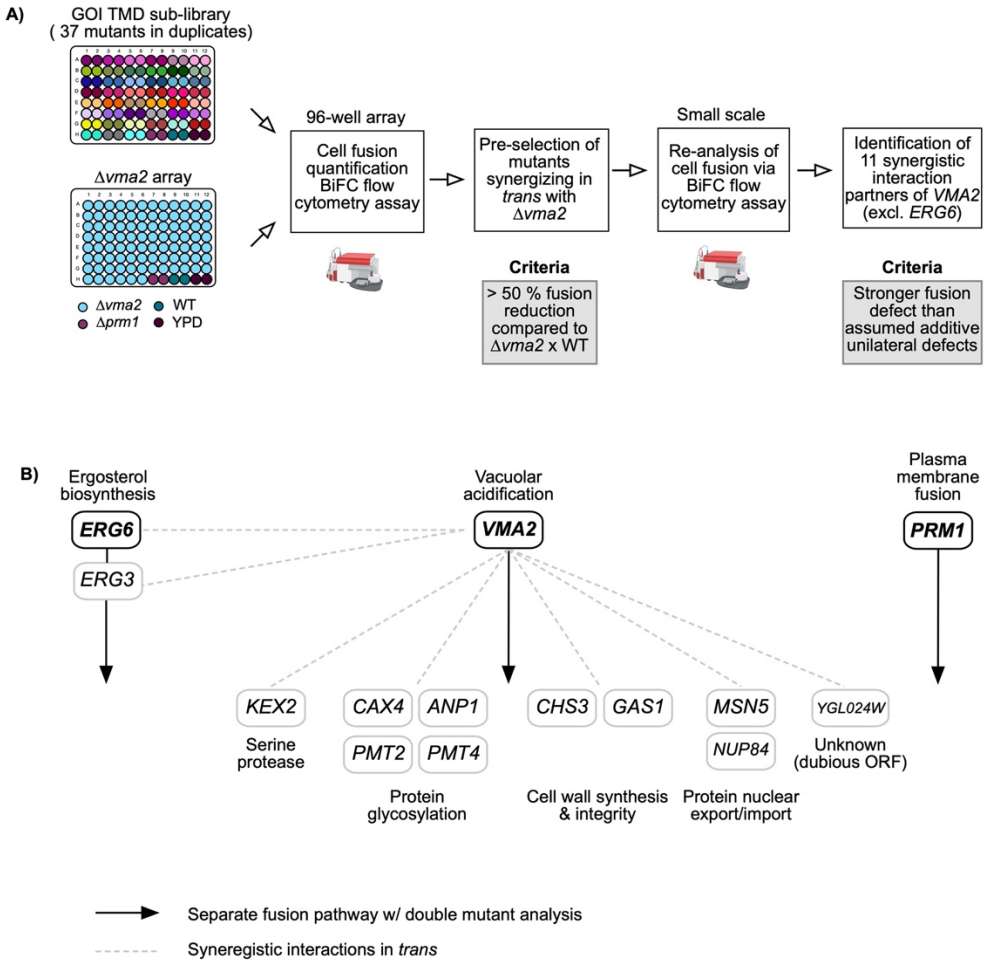

Figure 32: V-ATPase synergizes with 12 genes promoting cell fusion during yeast mating but operates on distinct pathways to *ERG6* and *PRM1*. A) Schematic showing workflow for identification of synergistic interactions between Δ*vma2* and mutants from the GOI TMD sub-library. B) Overview of three fusion pathways in which *VMA2* operates on distinct pathways to *PRM1* and *ERG6* (black arrows). *VMA2* synergizes in *trans* with at least 12 genes (grey dashed line), including *ERG6* suggesting a partial overlap between both pathways.

3.3.4 Deletion of *VMA2* does not affect the localization of Kex2, Cax4 and Erg6

As shown in the previous section, the V-ATPase was identified to promote cell fusion likely by proxy via interaction with at least 12 genes with roles in diverse cellular activities such as protein glycosylation or CW integrity. To assess whether these synergistic interactions are mediated more directly by interfering with the localization of proteins, next the localization of three representative genes was investigated.

The genes *KEX2*, *CAX4* and *ERG6* were selected as examples and chromosomally tagged at the C-terminus with mNG in Δ*vma2* and, as a control, in WT *MAT***a** cells. Afterwards, the localization profiles of the proteins in vegetative and pheromone treated cells were determined by confocal microscopy as described in section 2.12.12.2. All were constitutively expressed in vegetative and pheromone-treated cells (**Figure 33**). Based on the YeastRGB database (https://shmoo.weizmann.ac.il/elevy/YeastRGB/HTML/YeastRGB.html) and previous studies, the proteins retained at their expected cellular localizations in WT as well as Δ*vma2 MAT***a** cells: Kex2 localized mainly at the *trans*-Golgi network (left), Cax4 at the endoplasmic reticulum (ER) (middle), and Erg6 mainly at lipid droplets (right) [166, 167].

Taken together, these findings show that the lack of the V-ATPase in Δ*vma2* cells does not affect the protein localization of Kex2, Cax4 or Erg6. Moreover, it supports the hypothesis that the V-ATPase affects fusion via acidification rather than directly regulating a specific protein.

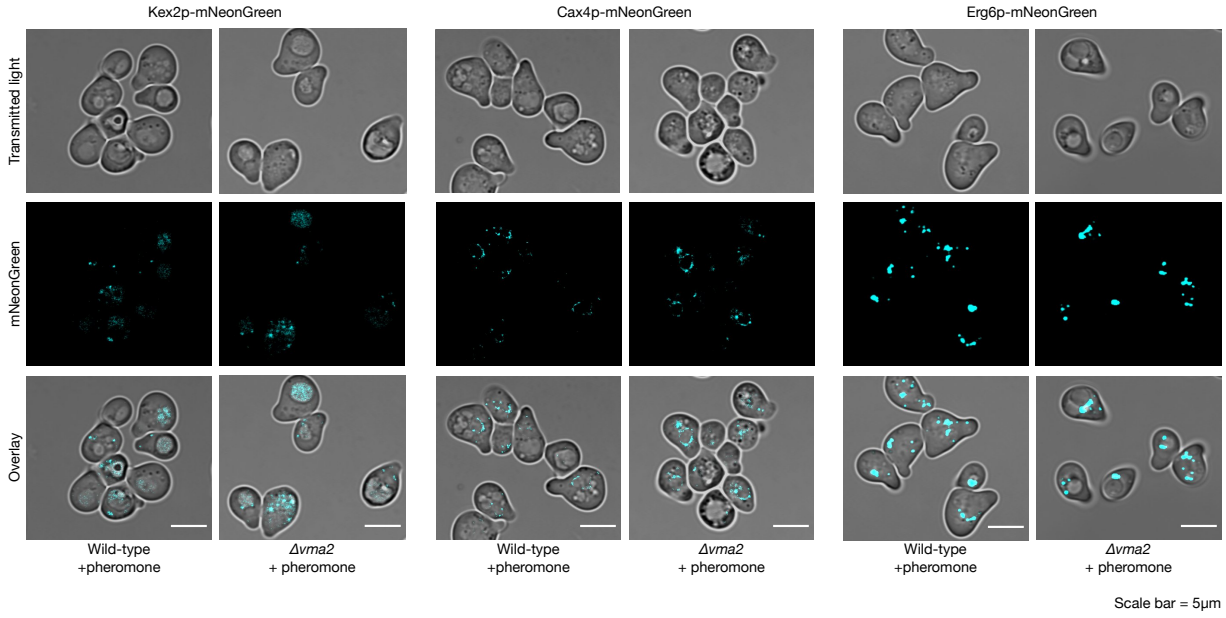

Figure 33: Absence of V-ATPase does not affect the localization of Kex2, Cax4 or Erg6. Representative images of *MAT***a** cells expressing either *KEX2*, *CAX4* or *ERG6* chromosomally tagged at the C-terminus with mNG. Kex2p, Cax4 and Erg6 exhibited similar localization patterns in vegetative and pheromone-treated cells. Left: Kex2-mNG localizes at the vacuole and *trans*-Golgi network. Middle: Cax4-mNG localizes to the endoplasmic reticulum (ER). Right: Erg6-mNG mainly localizes at lipid droplets. Scale bar = 5µm.

3.4 *CAX4* operates on partially overlapping yet distinct pathways to *PRM1*, *VMA2* and *ERG6*

Prm1 is thus far the only membrane protein known to be directly involved in PM fusion. It is only expressed upon pheromone exposure, localizes at the mating contact site prior to fusion and is subsequently transported to the vacuole after the process is completed [121, 122]. To gain further insights on the interaction landscape of *PRM1*, a 96-well Δ*prm1* array was crossed to the same GOI TMD sub-library used for the *VMA2* analysis (section 3.3.3.3). After re-analysis via small scale yeast mating procedure, *PRM1* synergistic interaction with two genes *KEX2* and *CAX4* was identified (**Figure 34A**). A synergistic defect between Δ*kex2* on the *MAT***a** and Δ*prm1* on the *MAT*α mating-type was previously reported by Heiman and colleagues [135]. It has been proposed, that Kex2 likely acts by proxy through a substrate at the same step in cell fusion as Prm1. However, the synergism between *PRM1* and *CAX4* is thus far novel. Cax4 is a dolichyl pyrophosphate (Dol-P-P) phosphatase required for N-linked glycosylation that leads to cell wall defects when absent [157, 168]. A fusion defect phenotype at CW remodeling was microscopically confirmed in the secondary screen by the presence of early pre-zygotes displaying a flat FM4-64-stained PM interface (section 3.1.6).

To test whether *PRM1* and *CAX4* operate on the same pathway, cell fusion analysis of a Δ*prm1*Δ*cax4* double gene deletion mutant via BiFC fusion assay was carried out which resulted in an almost complete fusion block (**Figure 34B**). This suggested that *PRM1* and *CAX4* operate on partially overlapping yet distinct pathways. Interestingly, as shown in section 3.3.3.3, *CAX4* was also found to synergize in *trans* with *VMA2* (**Figure 34C**). Simultaneous deletion of *VMA2* and *CAX4* also led to a stronger defect than the Δ*vma2* and Δ*cax4* single deletions (**Figure 34D),** indicating a partial overlap of both fusion pathways.

To further clarify whether *CAX4* operates on the same fusion pathway as *ERG6*, cell fusion of crosses between Δ*cax4* and Δ*erg6* was analyzed. Interestingly, considering the additive unilateral defects as highlighted in pink, *CAX4* also synergized with *ERG6* in *trans* (**Figure 34E**). Subsequent Δ*erg6*Δ*cax4* double mutant analysis further revealed that simultaneous deletion of both genes leads to an almost complete arrest (**Figure 34F**), indicating that *CAX4* and *ERG6*

also operate on distinct but partially overlapping pathways, in the same manner as with *PRM1* and *VMA2*.

To sequentially order synergizing genes acting on the same or partially overlapping pathway, overexpression studies were performed. In the context of cell fusion, the overexpression of a gene in a genetically sensitized background, such as Δ*prm1*, can reveal whether the fusion defect can be suppressed or not. A suppression of the defect would imply that the overexpressed gene operates downstream of the deleted gene.

To determine as a part of a pathway the order of *CAX4*, *VMA2* and *PRM1*, the effect of high-copy (2µ plasmid) expression from the constitutive *ADH1* promoter was investigated. *MAT***a** Δ*vma2*, Δ*cax4* and Δ*prm1* mutants were transformed with 2µ plasmids, mated to the corresponding *MAT*α mutants and cell fusion determined. The attempt to transform *ADH1pr-VMA2* in Δ*erg6* cells failed despite multiple attempts. Because all analyzed mutants were shown to act bilaterally on fusion, as shown in (**Figure 25**), overexpression of the investigated genes was sufficient to test for a suppression of fusion defects.

In Δ*prm1* cells, fusion was only restored when *PRM1* was overexpressed (**Figure 34G**). These results are consistent with the earlier finding that *VMA2* and *PRM1* are not synergizing. Likewise, in Δ*vma2* mating cells, only *VMA2* overexpression could restore fusion efficiency (**Figure 34H**). Interestingly, cells overexpressing *VMA2* in Δ*cax4* cells partially recovered fusion when compared to EV overexpression (**Figure 34I**) implying that *VMA2* operates downstream of *CAX4.* Noticeably, even though *PRM1* and *CAX4* were found to synergize in *trans*, the overexpression analysis did not provide clues about their sequential order implying a more complicated mechanism taking place.

Together with the findings from the synergistic interaction and double mutant analysis, it was proposed that *CAX4* is an important player in promoting cell fusion and moreover, might represent a fourth independent but partially overlapping fusion pathways with *PRM1*, *ERG6* and *VMA2*.

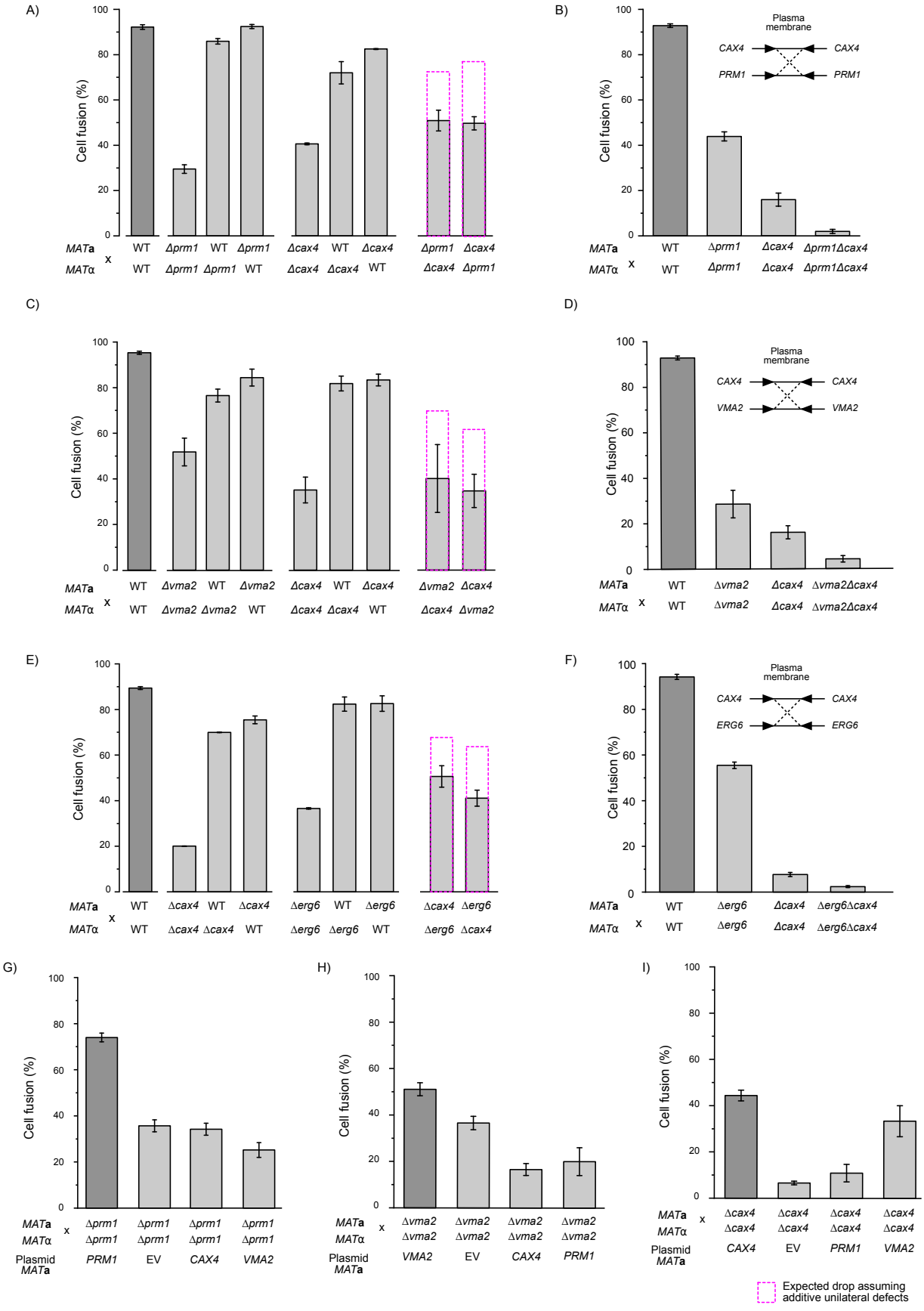
A)
Cell fusion (%)
MATa WT Δprm1 WT Δprm1 Δcax4 WT Δcax4 Δprm1 Δcax4
MATα WT Δprm1 Δprm1 WT Δcax4 Δcax4 WT Δcax4 Δcax4 Δprm1
B)
Plasma membrane
CAX4 CAX4
PRM1 PRM1
MATa WT Δprm1 Δcax4 Δprm1Δcax4
MATα WT Δprm1 Δcax4 Δprm1Δcax4
C)
MATa WT Δvma2 WT Δvma2 Δcax4 WT Δcax4 Δvma2 Δcax4
MATα WT Δvma2 Δvma2 WT Δcax4 Δcax4 WT Δcax4 Δvma2
D)
Plasma membrane
CAX4 CAX4
VMA2 VMA2
MATa WT Δvma2 Δcax4 Δvma2Δcax4
MATα WT Δvma2 Δcax4 Δvma2Δcax4
E)
MATa WT Δcax4 WT Δcax4 Δerg6 WT Δerg6 Δcax4 Δerg6
MATα WT Δcax4 Δcax4 WT Δerg6 Δerg6 WT Δerg6 Δcax4
F)
Plasma membrane
CAX4 CAX4
ERG6 ERG6
MATa WT Δerg6 Δcax4 Δerg6Δcax4
MATα WT Δerg6 Δcax4 Δerg6Δcax4
G)
MATa Δprm1 Δprm1 Δprm1 Δprm1
MATα Δprm1 Δprm1 Δprm1 Δprm1
Plasmid PRM1 EV CAX4 VMA2
MATa
H)
MATa Δvma2 Δvma2 Δvma2 Δvma2
MATα Δvma2 Δvma2 Δvma2 Δvma2
Plasmid VMA2 EV CAX4 PRM1
MATa
I)
MATa Δcax4 Δcax4 Δcax4 Δcax4
MATα Δcax4 Δcax4 Δcax4 Δcax4
Plasmid CAX4 EV PRM1 VMA2
MATa
Expected drop assuming additive unilateral defects

Figure 34: *CAX4* synergism with *PRM1*, *VMA2* and *ERG6*. Cell fusion analysis was quantified by flow cytometry. Error bars indicate SD of triplicate reactions. The pink box denotes the expected drop assuming additive unilateral defects. A) *PRM1* synergizes with *CAX4* in *trans*. B) Simultaneous deletion of *CAX4* and *PRM1* results in an almost complete arrest, suggesting that both act on distinct but partially overlapping pathways. C) *CAX4* synergizes with *VMA2* in *trans*. D) Δ*vma2*Δ*cax4* double mutant analysis result in an enhanced defect, suggesting that *VMA2* and *CAX4* operate on distinct but partially overlapping pathways. E) *CAX4* synergizes with *ERG6* in *trans*. F) The simultaneous deletion of *CAX4* and *ERG6* leads to an enhanced defect, indicating that both genes act on distinct yet partially overlapping pathways. G) Only overexpression of *ADH1pr-PRM1* in Δ*prm1 MAT***a** cells restores fusion. H) Only overexpression of *ADH1pr-VMA2* in Δ*vma2 MAT***a** cells restores fusion. I) Partial fusion rescue in Δ*cax4 MAT***a** cells expressing *ADH1pr-CAX4*.

3.5 Synergistic interaction network operating at PM fusion involving four distinct but partially overlapping fusion pathways

To provide more insights into the synergistic interaction network operating at PM fusion involving at least four independents but partially overlapping fusion pathways (section 3.3.3 and 3.4) further synergistic interaction and double mutant studies were carried out. Here, the main focus was towards interactions across the PM fusion mutant Δ*prm1*, the ergosterol mutants Δ*erg3* and Δ*erg6*, the V-ATPase mutant Δ*vma2*, the glycosylation mutant Δ*cax4* and lastly, the serine protease mutant Δ*kex2*.

All data are summarized in a fusion matrix (**Figure 35**) whereby the fusion efficiencies represent the average of three independent replicates. Standard error bars are not shown. Distinct mutants are denoted in magenta (mutant A) and light blue (mutant B). Mutants that are synergizing in *trans* across the two mating types are denoted in yellow. Mutants that are not synergizing are denoted in grey. Strong fusion arrests upon double gene deletion are denoted in blue.

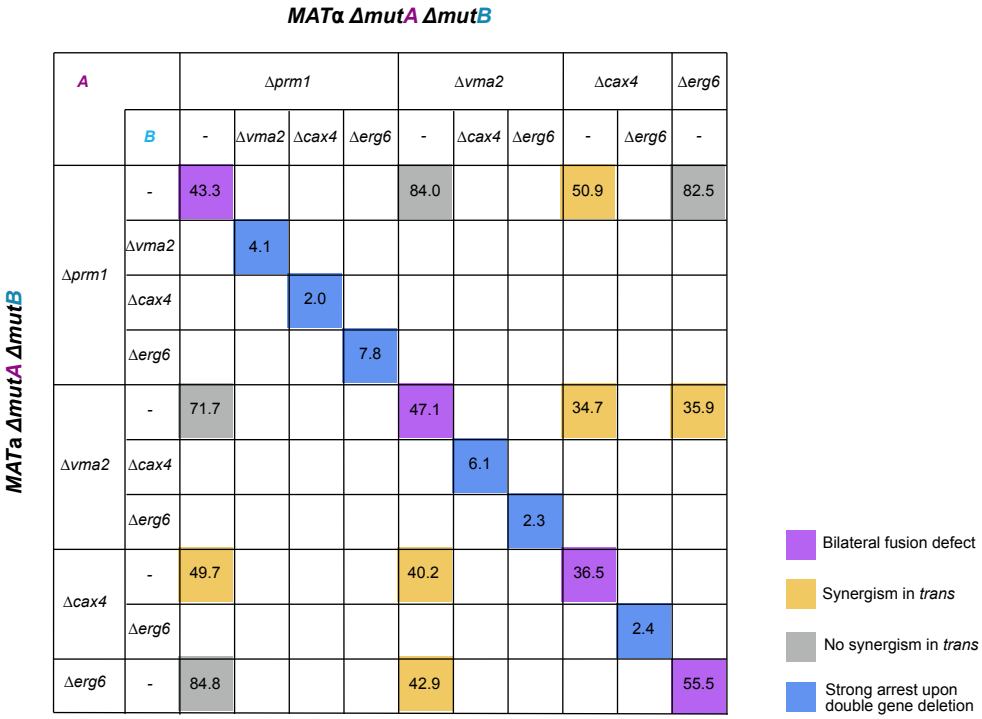

Figure 35: Overview of synergistic interactions in trans of *PRM1*, *VMA2*, *CAX4* and *ERG6*. A) Fusion matrix of *trans* interactions demonstrating a bilateral fusion defect of single mutants denoted in purple, synergism denoted in yellow, no synergism denoted in grey and a strong fusion arrest when genes are simultaneously deleted denoted in blue.

Considering all data, a synergistic interaction network was generated providing insights into functional relationships between genes required for efficient cell fusion (**Figure 36**). Synergistic interactions in *trans* that are verified by double mutant analysis are denoted in black dashed lines. Because disruptions of *KEX2* in *MAT*α mating type are known to cause defects in α-factor pheromone processing, only interactions of the Δ*kex2* mutant in *MAT***a** mating type were investigated and denoted in orange dashed lines. *VMA2* interactions that were not further studied by double mutant analysis are denoted in blue.

In summary, two novel fusion pathways with *VMA2* and *CAX4* beside the previously reported *PRM1* and *ERG6* were identified. Moreover, this work provides insights into the complex synergistic interaction network operating at PM fusion involving at least four fusion pathways. The next section will be focusing on the novel identified synergism between *PRM1* and *CAX4* on a more mechanistic level.

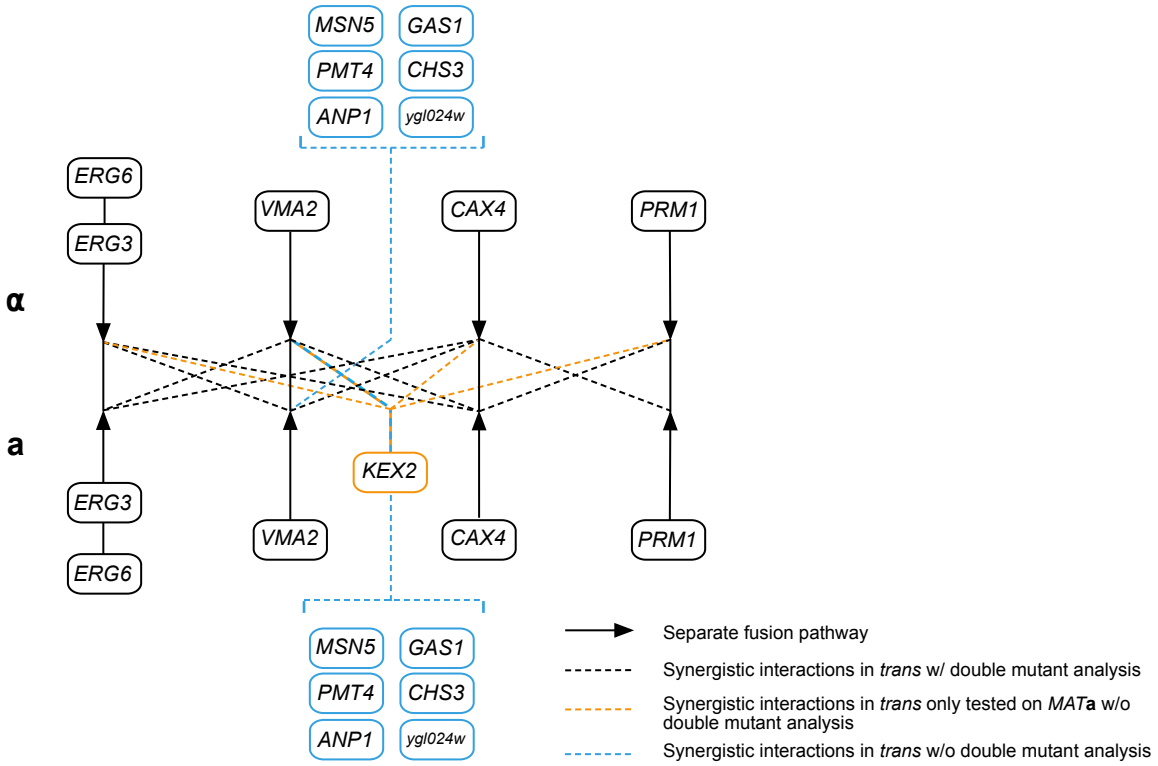

Figure 36: A synergistic interaction network operating at PM fusion during yeast mating. A) *PRM1*, *ERG6*, *VMA2* and *CAX4* represent four independent fusion pathways (black arrow). Synergism in *trans* that are confirmed by double mutant analysis are denoted in black dashed lines. *KEX2* synergism is only tested on *MAT***a** mating type and highlighted in orange dashed lines. *VMA2* synergism that is not verified by double mutant analysis is denoted in blue dashed lines.

3.6 Functional relationship between *PRM1* and *CAX4*

As shown in section 3.4, *PRM1* synergizes with *CAX4* across the two mating types *MAT***a** and *MAT*α. *CAX4*, also known as *CWH8*, is a gene that encodes a putative transmembrane protein that is required for facilitating the initial step in N-linked glycosylation, a post-transcriptional modification that serves as a protein quality control point and determines the characteristics of a protein such as stability, function or activity [168]. Cells lacking the *CAX4* gene are reported to display defects in CW biogenesis [157].

The following section will provide insights on the functional relationship between *CAX4* and *PRM1* in cell fusion by investigating the localization and expression profile of Prm1 in a sensitized Δ*cax4* background

3.6.1 Prm1 is correctly localized at the shmoo tip but in less abundance

At first, in order to investigate whether the depletion of *CAX4* affects the localization of the pheromone regulated protein Prm1, the *PRM1* gene was chromosomally tagged at the C-terminus with mNG in a Δ*cax4* background and as a control in WT *MAT***a** cells. Subsequently, the localization profiles upon pheromone treatment were determined by confocal microscopy as described in section 2.12.12.2. Consistent with previous findings, Prm1-mNG in WT cells localized at the shmoo tip of polarized cells in response to α-factor pheromone. Representative images are shown in **Figure 37A** [122]. Noticeably, a decrease in Prm1 expression was observed in cells lacking the *CAX4* gene. In addition, the total number of cells that have formed shmoos were counted and classified into two groups: i) shmoo tips with Prm1-mNG and ii) shmoos without Prm1-mNG expression (**Figure 37B**). It was observed that despite equal pheromone treatment conditions, only ~25% of Δ*cax4* cells contained Prm1-mNG at the shmoo tip whereas 70% of WT cells showed Prm1-mNG expression and localization at the tip of the shmoo. It was therefore hypothesized that Cax4 might be important for the stability or turnover of Prm1. Next, it was investigated whether Cax4 could be directly regulating Prm1 by post-transcriptionally modifying it.

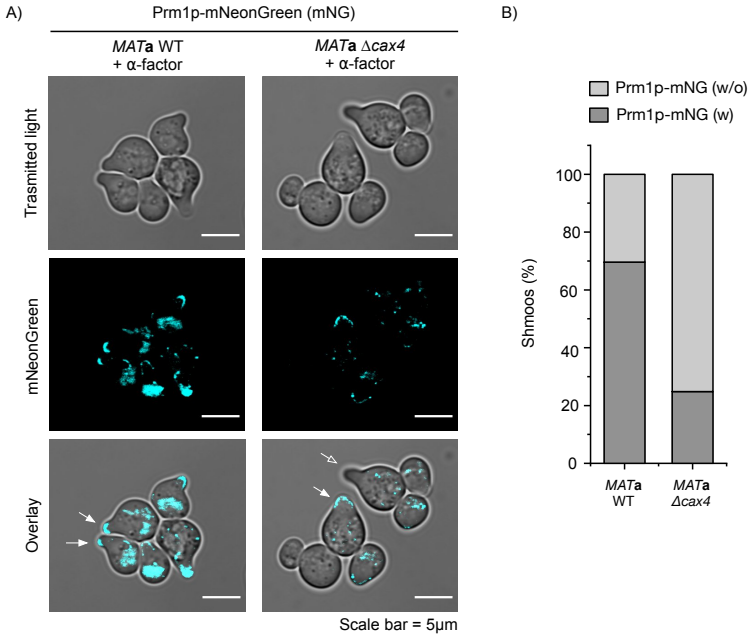

Figure 37: Less abundance of Prm1-mNG at the mating projection in Δ*cax4* cells. A) Representative images of *MAT***a** cells expressing Prm1-mNG at the shmoo tip in polarized cells upon α-factor treatment (white filled arrow). In a Δcax*4* sensitized background less abundance of Prm1-mNG was observed (white empty arrow). Scale bar = 5µm. B) In WT cells, 75% contained Prm1-mNG at the shmoo tip, in Δ*cax4* cells only ~25% of cells.

3.6.2 Cax4 does not post-transcriptionally process Prm1 but affects its cellular abundance

To test the hypothesis whether Prm1 is processed post-transcriptionally by *CAX4*, *PRM1* was C-terminally tagged with a V5 epitope tag and expressed from a plasmid under the control of an endogenous promotor. Subsequently, the expression level of *PRM1*-v5 in *MAT***a** Δ*prm1* and Δ*prm1*Δ*cax4* cells was determined in absence or presence of pheromone by SDS-PAGE and Western blot as described in section 2.13. Since *PRM1* expression is pheromone-regulated, no protein was expressed in the absence of pheromone (**Figure 38A**). In the presence of pheromone, *MAT***a** Δ*prm1* cells showed a strong molecular weight (MW) band of ~100 kDa, corresponding to the MW of monomeric glycosylated Prm1. In contrast, in Δ*prm1*Δ*cax4* cells the corresponding band appeared faint. Consistent with previous findings presented in section 3.6.1 it implies a lower abundance of Prm1 in Δ*prm1*Δ*cax4* cells. However, since the monomeric band did not shift to a lower MW indicates that Prm1 is not post-transcriptionally processed by Cax4.

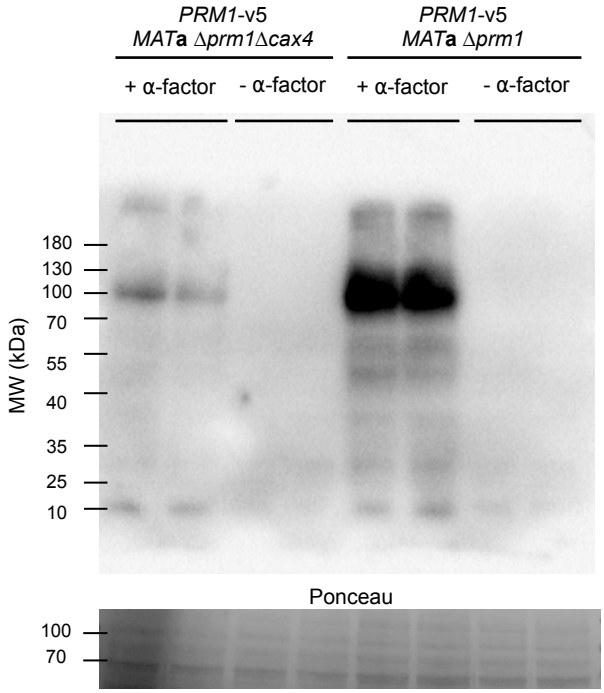

Figure 38: Prm1 is not post-transcriptionally processed by Cax4. A) Western blot analysis of *PRM1*-v5 expression in vegetative and pheromone treated Δ*prm1* and Δ*prm1*Δ*cax4 MAT***a** cells (duplicates). Ponceau staining serves as a loading control. *PRM1* was only expressed after pheromone treatment. A strong molecular weight (MW) band of about 100 kDa corresponding to the MW of monomeric and glycosylated Prm1 is present in WT *PRM1*-v5 cells as well as in Δ*cax4 PRM1*-v5 cells, albeit with less abundance.

3.7 The RNA-polymerase II mediator complex regulates cell fusion

As reported in section 3.2, the primary cell fusion screen revealed that the Δ*ygl024w* mutant displayed a unique unilateral defect which was mating-type independent, and an almost complete fusion arrest in bilateral matings. According to SGD, *YGL024w* encodes a putative TMD protein that has been associated with the yeast pheromone signaling pathway. However, it is unclear whether it is an authentic gene, and has been therefore assigned as "dubious" [169]. Interestingly, the ORF of *YGL024w* partially overlaps the promoter and 5'-coding regions of an adjacent gene, called *PGD1*. *PGD1*, also called *MED3*, encodes a subunit of the RNA-polymerase II mediator complex, referred to as mediator complex (MC), and is important for transcriptional regulation [170, 171]. As a consequence of deleting *YGL024w*, mRNA synthesis might be disrupted which in turn possibly affects the expression of proteins involved in cell fusion. In the following sections, experiments that clarify which gene is causing the fusion phenotype are described.

3.7.1 Pgd1 promotes cell fusion during yeast mating

Because of the partial gene overlap of *YGL024w* and *PGD1*, a *MAT***a** and *MAT*α Δ*pgd1* mutant was generated by PCR followed by cell fusion analysis by BiFC flow cytometry. Indeed, Δ*pgd1* mating crosses resulted in the same fusion phenotype as observed in Δ*ygl024w* matings (**Figure 39A**). In order to clarify whether the absence of *YGL024w* or *PGD1* was causing the pronounced fusion defect, overexpression rescue studies were carried out in *Δygl024w* and *Δpgd1* mutants. For this, *MAT***a** and *MAT*α cells of Δ*ygl024w* and *Δpgd1* mutants were transformed with a 2µ plasmid encoding *PGD1* and *YGL024w* under the constitutive control of the *ADH1* promoter. Cell fusion efficiency was determined via the BiFC fusion assay. As shown in (**Figure 39B**) *YGL024w* overexpression in Δ*ygl024w* and Δ*pgd1* cells resulted in no restoration of fusion, similar as when compared to cells expressing the empty vector (EV). However, *PGD1* overexpression in both sensitized backgrounds resulted in a fusion rescue of up to 80-85% fusion, suggesting that *PGD1* is the relevant gene required for cell fusion.

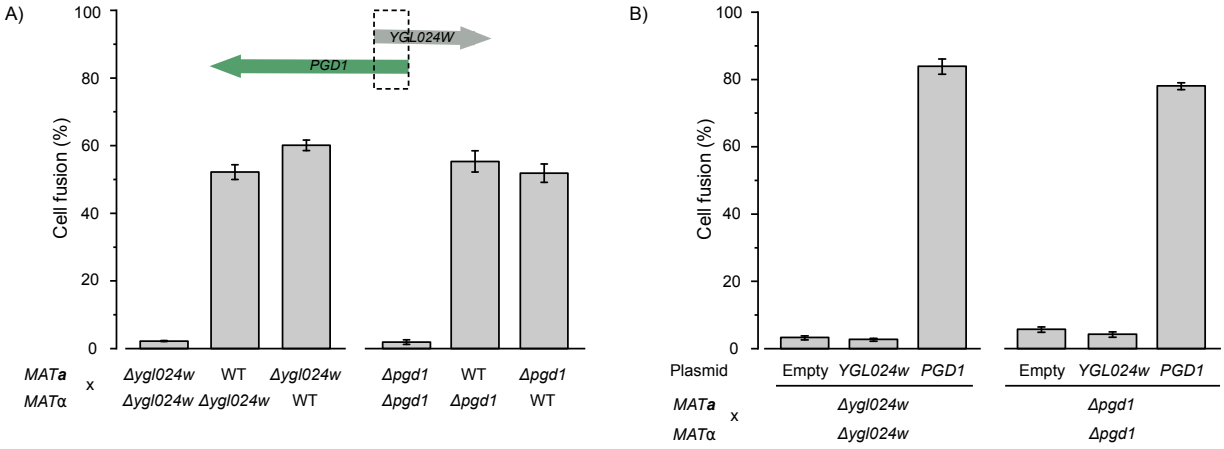

Figure 39: *PGD1* restores cell fusion of Δ*ygl024w*. A) Cell fusion analysis by BiFC flow cytometry verified, that Δ*pgd1* matings caused the same fusion phenotype as observed in Δ*ygl024w* matings. B) Cell fusion rescue analysis shows, that *YGL024w* overexpression failed to restore fusion, similar to cells expressing the EV, whereas *PGD1* overexpression restored fusion efficiency.

3.7.2 Pgd1 localized at the nucleus in vegetative and mating cells

To determine whether *PGD1* facilitates fusion indirectly in its role as a transcriptional regulator, or directly in a yet undescribed functionality, protein localization studies were performed. In *MAT***a** cells, *PGD1* was tagged with mNG and its localization profile observed in vegetative cells and during mating. In a previous study, GFP-tagged *PGD1* was shown to co-localize with a DAPI-stained nucleus [172]. Similarly, Pgd1-mNG localized solely at the nucleus and was excluded from the mating tip in pheromone-treated cells, as well as from the mating junction when crossed to *MAT*α cells. This observation suggested that *PGD1* promotes cell fusion indirectly, likely through its involvement in the mediator complex in the nucleus.

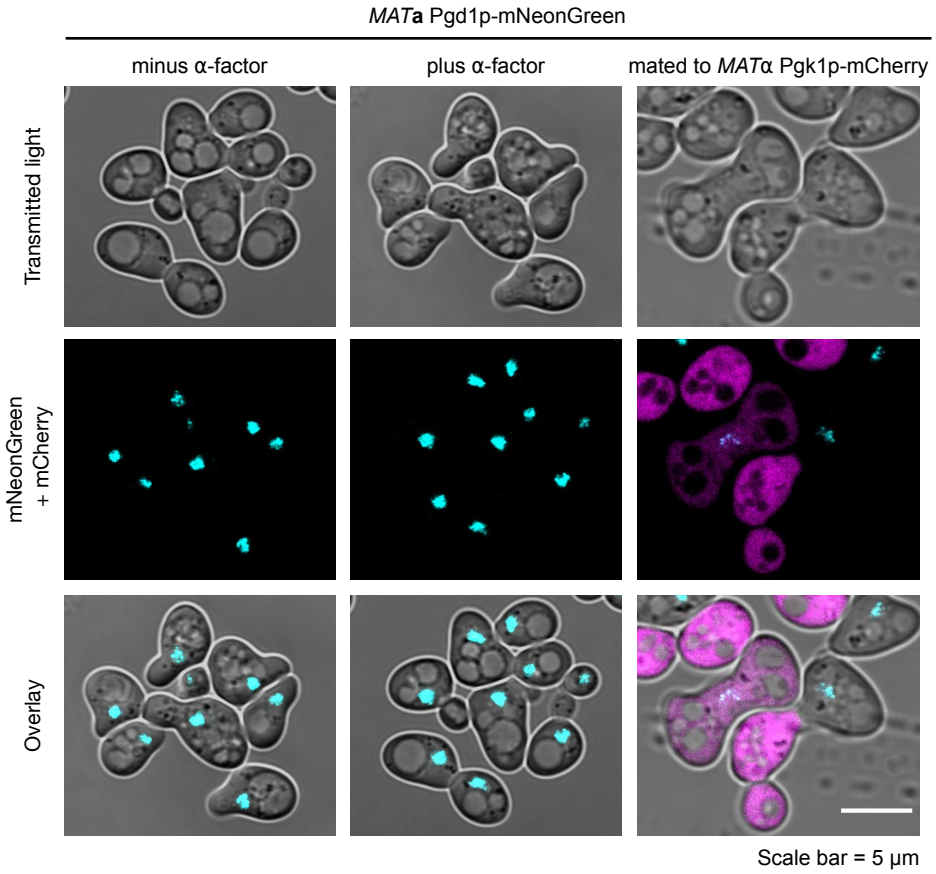

Figure 40: Pgd1-mNG localizes exclusively at the nucleus. Localization profiles of *MAT***a** cells expressing C-terminally tagged *PGD1*-mNG. Pgd1-mNG exclusively localized to the nucleus in vegetative cells (left), α-factor treated cells (middle), and mating cells (right) and was absent from the shmoo tip and mating junction.

3.7.3 Disruption of mediator complex subunits results in a strong fusion defect

To determine whether the fusion defect is exclusively for Δ*pgd1*, or whether the deletion of other subunits of the mediator complex caused a similar defect, mating crosses of a total of 11 out of 14 non-essential mediator mutants (Δ*med*) were conducted and microscopically examined. The mutant strains were selected from the YKO collection and therefore did not harbor a complementary split-GFP marker. Three mutants Δ*med2,* Δ*med18* and Δ*med20* failed to grow. As a representative subunit of the head module Δ*med20* was generated by PCR and supplemented to the library of mediator complex mutants. A schematic of the mediator complex subunit composition is illustrated in (**Figure 41B**).

Preliminary microscopic analysis served as a qualitative screening method to identify Δ*med* mutants which showed a strong fusion defect phenotype as observed in Δ*pgd1* cells. For this, cells were arrested in TAF buffer and stained with the lipophilic dye FM4-64 before imaging by microscopy. The Δ*med* mutants were categorized into non-defective, mildly defective and strongly defective for fusion. No defect was observed in Δ*med1*/*5*/*9*/*15* and Δ*cycC* and were therefore excluded from further analysis. A mild defect was observed in Δ*med12* and Δ*cdk8*. Based on SGD Δ*cycC* is also known as Δ*ssn3* which was previously identified in the primary fusion screen in section 3.1.5. Δ*med31*, Δ*med15* and Δ*med16* exhibited strong fusion defects at the level of CW remodeling (flat PM) and PM fusion (PM bubble). Representative images are shown in **Figure 41A**. As an initial result, it was demonstrated that firstly, not all Δ*med* mutants led to impaired fusion and secondly, the extent of the defect varied among the mutants.

After generating Δ*med* mutants in a new genetic background harboring the complementary C- or N-GFP fragments, cell fusion levels of Δ*med15* (tail), Δ*med16* (tail), Δ*med20* (head), Δ*med31* (middle) and Δ*ssn3* (kinase) were quantified by BiFC flow cytometry. Subsequent cell fusion analysis revealed that all Δ*med* mutants exhibited fusion defects, with fusion lower than 50% as depicted in **Figure 41C**. The deletion of the tail subunits Δ*med15*, Δ*pgd1* and Δ*med16* resulted in the strongest defect, followed by Δ*med20*, Δ*ssn3* and Δ*med31* matings. These data confirm that the degree of the defect among the mediator complex subunits and modules varied. This finding suggests that the disctinct subunits have different roles in the fusion process.

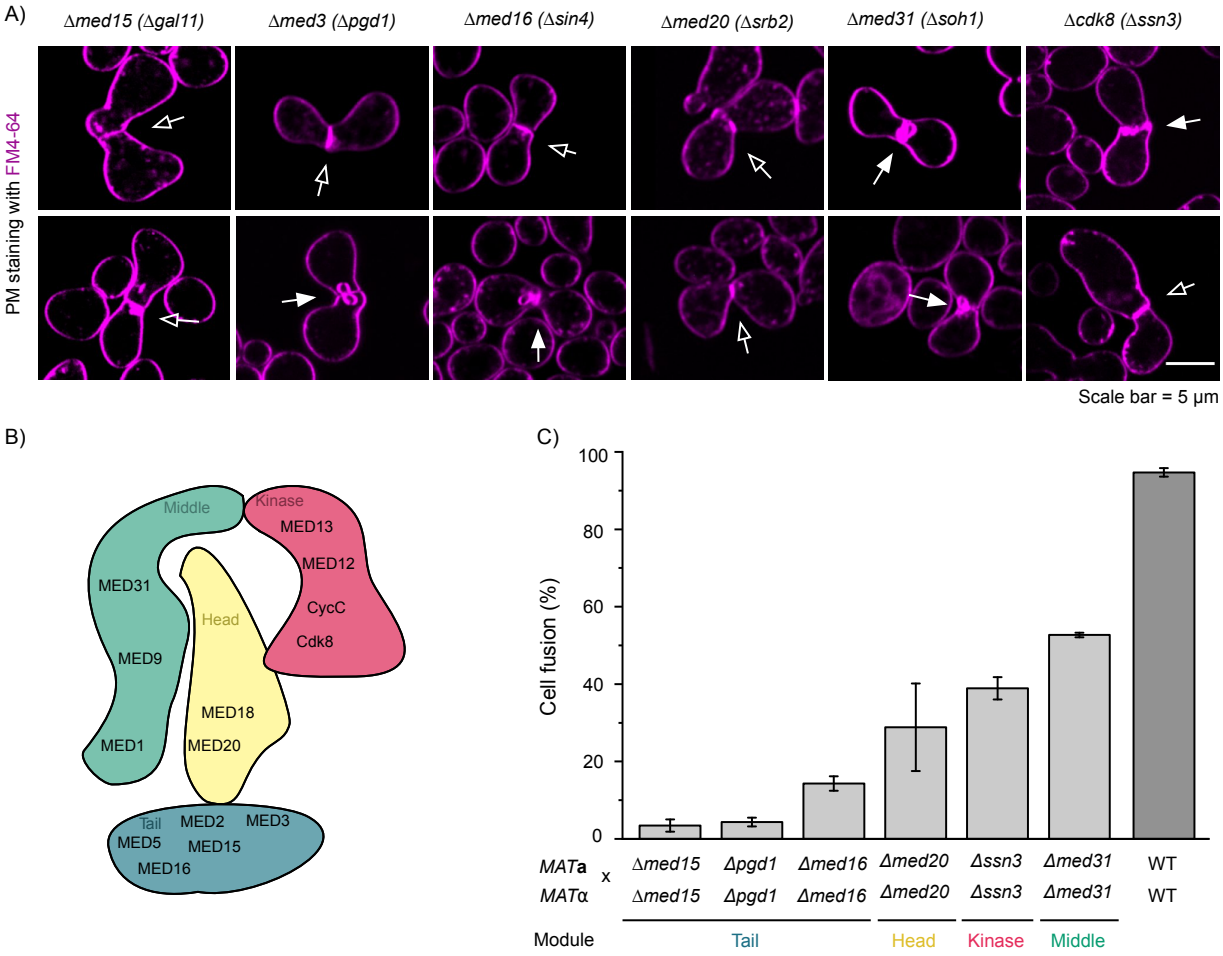

Figure 41: Absence of mediator complex subunits results in different fusion phenotypes. A) Representative images of mediator complex subunit mutants (Δ*med*) with FM4-64-stained PMs. Mutants exhibit defects at the level of CW remodeling (flat PM) and PM fusion (PM bubble). Scale bar = 5 µm. B) Schematic of the mediator complex composition. The Mediator is composed of four modules: head (yellow), middle (green), tail (blue), and a kinase (red). Each module consists of several subunits. Shown are only non-essential subunits. C) Cell fusion quantification of representative mediator subunit mutants ordered from lowest to highest fusion scores. Fusion was measured by BiFC flow cytometry. Error bars indicate the standard error of the mean of three replicates.

3.7.4 Mutants of the mediator complex exhibit a defect in cell pairing and pheromone secretion

In addition to quantifying cell fusion efficiency, the multicolor flow cytometry assay also allows the independent determination of cell pairing efficiency in the same mating reaction. The percentage of pairing indicates how many cells are able to obtain a mating partner, establish cell-cell contact and undergo downstream events of the mating pathway. Interestingly,

compared to WT cells all Δ*med* mutants exhibited a ~50% decrease in pairing (**Figure 42A**). In Δ*med15* pairing efficiency was even more strongly affected.

Since pairing defects often correlate with defects in pheromone signaling a qualitative growth inhibition (halo) assay was performed to test for the ability of the *Δmed* mutants to secrete pheromone, as described in section 2.12.10 [89, 153]. In this approach, a *Δsst2 MAT***a** tester strain was used whose deletion leads to super sensitivity to pheromone causing cell death when exposed to the mating pheromone [173]. Therefore, the halo size correlates with the ability of the opposite mating type, here *MATα*, to release pheromone. As shown in (**Figure 42B**), the Δ*med* mutants exhibited smaller halos than those compared to WT, confirming that indeed the α-factor secretion is affected in the absence of mediator complex subunits. The extent of the defect (halo size) was ordered from the biggest to the smallest halo, with the Δ*med15* mutant displaying the strongest secretion defect. These data show that the pairing defect observed in Δ*med* mutants is probably caused by a defect in pheromone secretion.

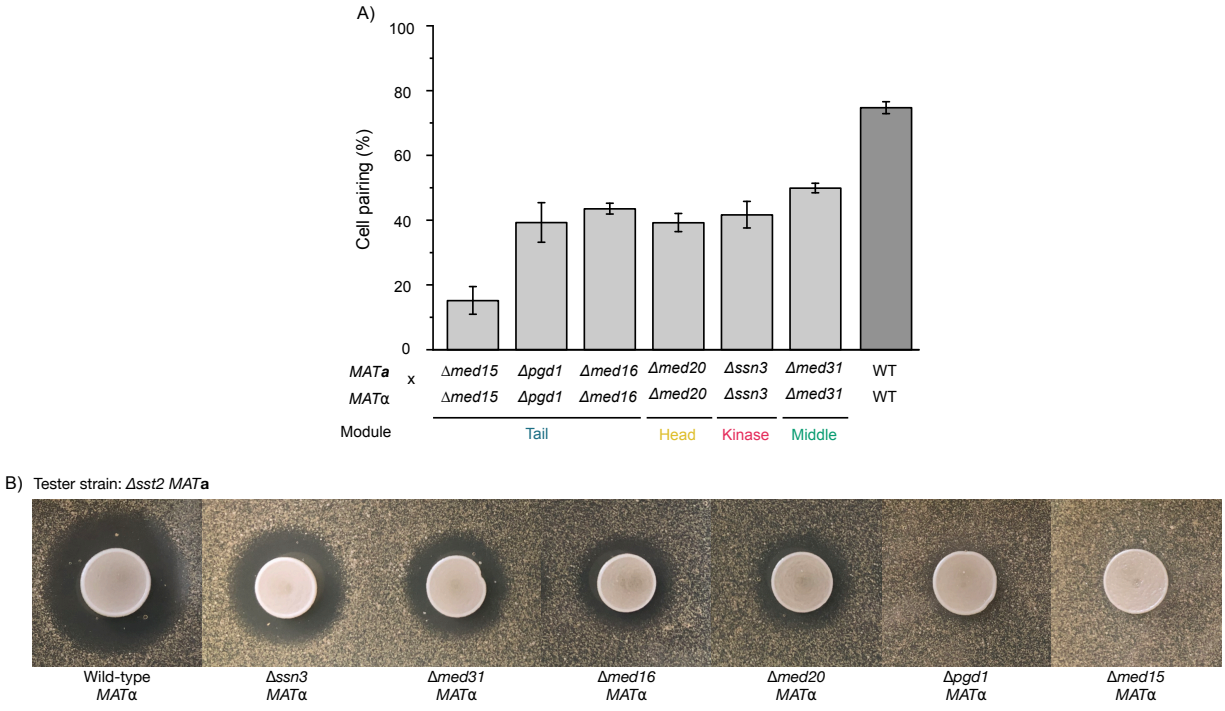

Figure 42: Deletion of mediator complex subunits leads to a defect in cell pairing and pheromone secretion. A) Reduced pairing efficiency in Δ*med* mutants with Δ*med15* exhibiting the strongest pairing defect. B) Qualitative growth inhibition (halo) assay to test for pheromone secretion.

3.7.5 Depletion of mediator subunits leads to defects in both CW remodeling and PM fusion

As shown in section 3.7.3, the deletion of subunits of the mediator complex results in a mixed fusion phenotype at the level of CW remodeling and PM fusion. To determine to what extent both stages were affected, crosses between Δ*med* mutants and mutants that are either implicated in CW remodeling (Δ*fus1*Δ*fus2*) or PM fusion (Δ*prm1*, Δ*erg6*) were carried out similarly as described in section 3.3.3 and 3.4. A synergistic interaction between gene pairs was classified as such when the fusion reduction was stronger than the additive unilateral fusion defect of the individual mutants (indicated by the pink dashed line). As shown for *PGD1*, cell fusion quantification revealed, that *PGD1* synergizes in *trans* with *FUS1FUS2* and *ERG6*, but not with *PRM1* (**Figure 43**).

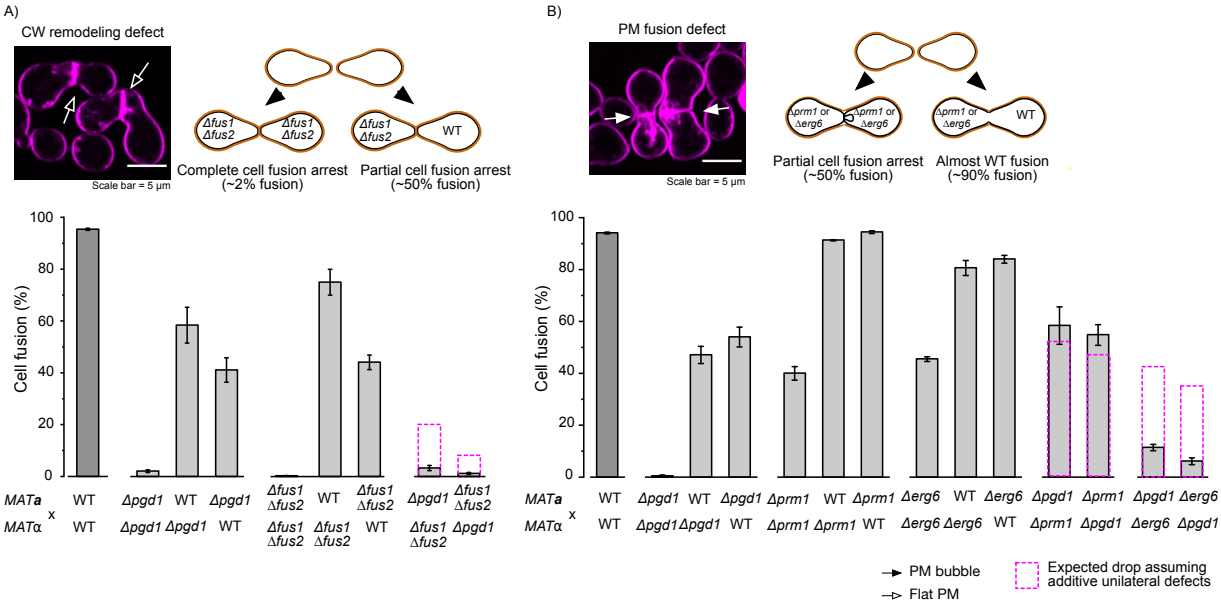

Figure 43: The mediator complex facilitates both CW remodeling and PM fusion but operates independently from Prm1. Cells fusion was measured by flow cytometry assay. Error bars indicate SD of triplicate reactions. The pink box in dashed line depicts the expected drop assuming additive unilateral defects. A) *PGD1* synergizes with *FUS1FUS2* in *trans*. B) *PGD1* synergizes with *ERG6* but not with *PRM1*.

Following the same rational, *trans* interactions of Δ*med20* (head), Δ*med31* (middle) and Δ*ssn3* (kinase) with Δ*fus1*Δ*fus2*, Δ*prm1* and Δ*erg6* were analyzed and synergistic interactions depicted in a color matrix (**Figure 44**). The different colors represent the degree of interaction which was calculated as the ratio between fusion efficiency of the synergistic interaction and

the calculated additive unilateral defects of the individual mutants. In general, a lower ratio indicates a stronger synergistic interaction than a higher ratio.

Here, a synergism with a ratio lower than 0.6 was defined as strong and identified to occur between Δ*fus1*Δ*fus2* and Δ*pgd1*, Δ*med20* and Δ*med31*, as well as between Δ*erg6* and Δ*pgd1* and Δ*med20*. A medium synergism with a ratio between 0.61 and 0.8 was observed in crosses between Δ*erg6* and Δ*ssn3*. A weak synergism with a ratio between 0.81-0.9 was detected in crosses between Δ*erg6* and Δ*med31*. No synergism with a ratio above 0.91, highlighted in grey, were identified in crosses between Δ*prm1* and any Δ*med* mutant, as well as between Δ*ssn3* and Δ*fus1*Δ*fus2*.

Together with the previous findings shown in section 3.7.4 and 3.7.5 this study revealed that certain subunits of the mediator complex are involved at early (cell pairing and pheromone secretion) and late stages (CW remodeling and PM fusion) in yeast mating to different degrees.

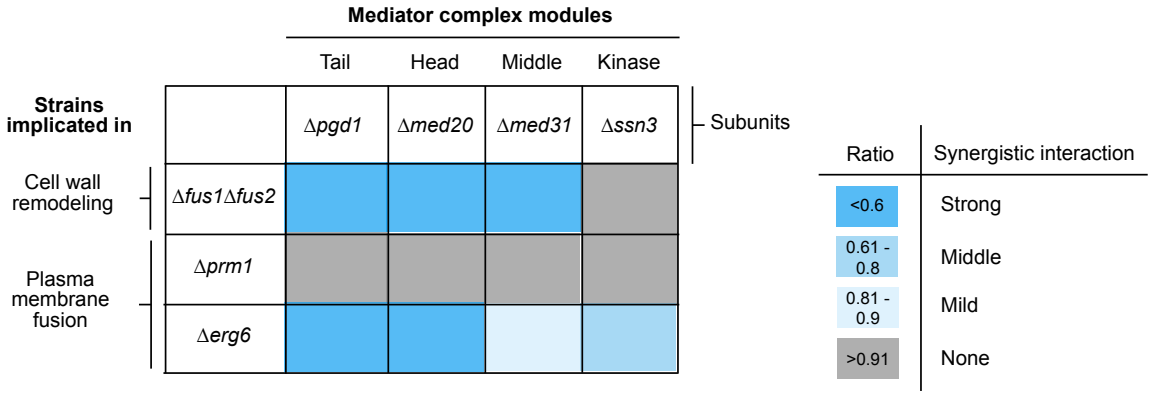

Figure 44: Subunits of the mediator complex mediate CW remodeling and PM fusion to different degrees. Color matrix showing the degree of synergistic interactions between Δ*med* mutants and mutants implicated in CW remodeling and PM fusion.

3.7.6 *PGD1* synergistically interacts with *ERG6, ERG3, VMA2, CAX4, FUS1* and *KEX2*

As demonstrated in the previous section, *PGD1* synergized in *trans* with *ERG6*, a gene with an established role in cell fusion [119]. In addition, it was shown that *PGD1* and other subunits of the mediator complex do not interact with *PRM1*. To identify whether *PGD1* synergistically interacts with other fusion mutants identified in this study, five additional GOI mutants were

selected: *Δerg3*, *Δvma2*, *Δcax4*, *Δfus1* and *Δkex2*. Subsequent cell fusion quantification by flow cytometry revealed that *PGD1* also interacts with *ERG3*, *VMA2*, *CAX4*, *FUS1* and *KEX2.* The degree of interaction is depicted in a color matrix (**Figure 45A)** similarly as explained in section 3.7.5. For completeness, *ERG6* was included. A strong synergistic interaction was observed in crosses between Δ*pgd1* and the mutants Δ*erg6* and Δ*kex2*. A medium strong interaction was observed in crosses between Δ*pgd1* and Δ*erg3*, Δ*vma2*, Δ*cax4* and Δ*fus1.* Depending on the most frequently presented fusion phenotype in microscopic examinations, the mutants were categorized into PM fusion mutants (Δ*erg6*, Δ*erg3*), mutants exhibiting an intermediate phenotype at the level of CW remodeling and PM fusion (Δ*vma2*), and mutants exhibiting a CW remodeling defect (Δ*cax4*, Δ*fus1*).

Finally, the effect of *KEX2*, *CAX4*, *PRM1*, *VMA2*, *ERG3* and *ERG6* 2µ plasmid expression from the constitutive *ADH1* promoter was investigated in Δ*pgd1* mating cells to determine whether fusion can be partially rescued. As shown in (**Figure 45B**), only *PGD1* could restore cell fusion, all other tested genes showed similar fusion efficiencies when compared to the control cells carrying the EV (**Figure 45B**).

Taken together, these findings suggest that *PGD1* is affecting multiple fusion pathways. Thus, the activation of only one pathway is unlikely to be sufficient enough to suppress the Δ*pgd1* fusion defect. This suggested that the mediator complex acts as a master regulator of at least three redundant fusion pathways leading to cell fusion during yeast mating.

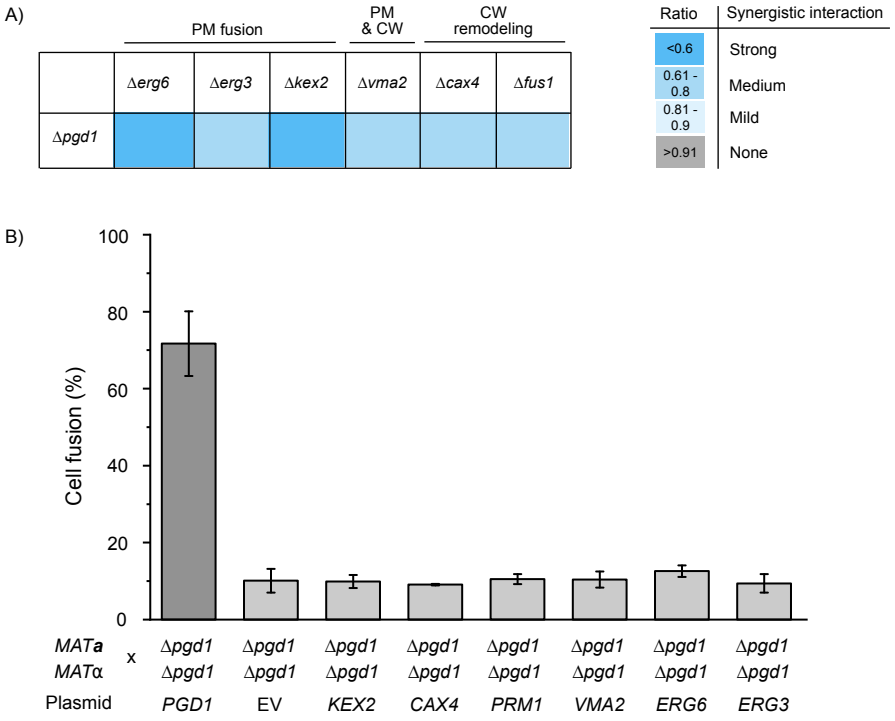

Figure 45: *PGD1* synergizes with genes involved in PM fusion and CW remodeling. A) Color matrix showing the degree of synergistic interactions between Δ*pgd1* mutants and selected GOI mutants implicated in CW remodeling and PM fusion. B) Only overexpression of *ADH1pr-PGD1* in Δ*pgd1 MAT***a** cells restores fusion. Error bars indicate the standard error of the mean of three independent measurements.

4. Discussion

4.1 Identification of novel late-stage cell fusion mutants

In this work a systematic screening for bilateral fusion mutants was accomplished by utilizing a customized yeast knockout sub-library. This stands apart from previous studies by:

i) Adapting a BiFC-based multicolor flow cytometry to allow fusion analysis in a high-throughput and quantitative manner.
ii) Simultaneous analysis of cell fusion symmetry and cell pairing efficiency which enables the distinction between late-stage fusion mutants exhibiting a bilateral defect and early-stage fusion mutants exhibiting a unilateral defect.
iii) Corroboration of corresponding gene deletions of all fusion mutants by PCR.

Together, this led to the identification of several genes affecting different late steps in mating that are required to complete cell fusion. Among them, known fusion mutants such as Δ*prm1*, Δ*erg3*, Δ*fig1* and Δ*fus1* demonstrating robustness of the conducted screen.

In addition, 28 novel mutants exhibiting similar fusion defects as Δ*prm1* were identified. The majority of identified fusion mutants have been already implicated in processes such as manno-/ glycosylation, protein trafficking/ sorting/ degradation or transporter activity. An additional role in cell fusion can be either direct, as for example by being part of the fusogen complex, or indirect. Indirectly can mean through establishment of a high pheromone gradient, down-regulation of the CWI pathway, ongoing secretion for delivery of CW digesting enzymes and presumably components of the fusion machinery, post-translational modification or organization of an actin cytoskeleton network at the mating projection.

The Δ*pmt4* mutant is one example for playing an indirect role in cell fusion. *PMT4*, a gene encoding a mannosyltransferase, is involved in the initial step of O-glycosylation. One study found that in Δ*pmt4* cells Fus1 is severely under-glycosylated. Consequently, Fus1 accumulates in the late Golgi apparatus instead of being delivered to the cell surface to mediate CW remodeling [174]. Notwithstanding, microscopic characterization of the fusion defect phenotype within the attempted secondary screen exhibited a mixed fusion defect phenotype

at the level of CW remodeling and PM fusion. This suggests that Pmt4 likely glycosylates other proteins involved in PM fusion.

Some of the other identified mutants from the primary screen have been previously reported in a microscopic screen for positive and negative regulators of yeast mating with focus on mutants exhibiting a defect at early mating stages in pheromone sensing and chemotropism. The following mutants were found to negatively affect mating efficiency when deleted in *MAT***a** mating type and crossed to a WT *MAT*α partner: Δ*msn5*, Δ*tat1*, Δ*gas1,* Δ*ste13*, Δ*ygl024w*, Δ*ost3* and Δ*mfα1, Δvma5* and *Δvma21*. In contrast to the findings of that study, *CAX4* has been identified to suppress the mating defect when deleted, thus acting as a negative regulator [175]. However, since these data were generated in different conditions in which mating efficiency was assessed microscopically and only in unilateral crosses against WT cells it is difficult to directly compare with the data of the present work. Moreover, none of the aforementioned mutants have been either manually confirmed nor have been specifically studied in a bilateral fusion context with focus on late-fusion stages during mating.

An unexpected finding was that the deletion of the dubious gene *YGL024w* resulted in a unique unilateral mating-type independent fusion defect with about 50% fusion. Moreover, an almost complete fusion block was observed when *YGL024w* was deleted in both mating types. A study that aimed to uncover novel components of the pheromone signaling pathway via a genome-scale approach identified Δ*ygl024w* to exhibit increased pheromone sensitivity and pheromone-independent signaling [169]. It was proposed, that *YGL024w* or rather the partially overlapping gene *PGD1*, might play a role in full expression of *SST2*. Sst2 is a negative regulator of the pheromone response pathway which causes super-sensitivity to pheromone when deleted. As a consequence, Δ*sst2* mutant cells are unable to discriminate a mating partner [176]. Nevertheless, due to the native of the BiFC-based flow cytometry assay, an additional role in late stages of yeast mating is proposed. A detailed discussion of this aspect will be presented in section 4.5.

Another major finding of the screen was that mutants of genes encoding subunits or associated factors of the vacuolar membrane ATPase (V-ATPase) resulted in a fusion defect. From the

existing literature, the function of the V-ATPase is mainly studied in mitotic yeast cells [162, 177-180]. When studied in context of yeast mating, the focus was on vacuolar morphology [181, 182]. One study reported that the high osmolarity glycerol (HOG) pathway in Δ*vma2* mitotic cells is constitutively activated at a low-level [181]. The HOG pathway, which shares upstream components of the pheromone pathway, is usually down-regulated in response to pheromone to slightly decrease cellular osmolarity and favor the fusion process by reducing the risk of cell lysis.[109]. In addition, down-stream targets of the mating pathway including *FIG1*, *FUS1* and *BAR1*, were found to be down-regulated in a Δ*vma2* mutant [109, 181]. However, this study is very limited because it does not address the aspect of mating directly. Therefore, in this work for the first time the effect of the V-ATPase on facilitating cell fusion during yeast mating was investigated. For more details see section 4.2.

As noticed for the Δ*pmt4* and Δ*vma*-mutants most of the other mutants also exhibited a mixed late-fusion defect phenotype at both stages, CW remodeling and PM fusion. Since *S. cerevisiae* apparently does not have such a rapid CW repair mechanism as *S. pombe*, the transition between CW digestion and fusion of the underlying PMs is likely to be tightly coupled. This is necessary to avoid cell lysis and consequently cell death. Therefore, it is plausible that some genes overtake functions at both stages. Moreover, the identification of genes impacting various biological processes emphasizes a system wide complexity of pathways involved. Presumably, the presence of several redundant pathways serves as a lifeguard mechanism to ensure successful cell fusion.

In summary, the conducted cell fusion screen revealed various novel genes providing a fundamental groundwork for future research. Furthermore, the adapted flow cytometry assay may open avenues for other fluorescence based large-scale fusion studies in other sexually reproducing organisms.

4.2 How does the V-ATPase facilitate cell fusion during yeast mating?

4.2.1 V-ATPase likely facilitates cell fusion via its role in intracellular acidification

V-ATPases are membrane embedded ATP-driven proton pumps that can be functionally divided into a proton translocation domain V0- and a soluble V1-domain driving ATP-hydrolysis. They are responsible for acidifying intracellular organelles in eukaryotes such as the yeast vacuole or mammalian lysosome, Golgi and endosomes. In higher eukaryotes, the V-ATPase is also located at the PM facilitating extracellular acidification [183]. Yeast cells lacking the V-ATPase activity show a characteristic conditional lethal phenotype at basic pH which was key for the identification of the subunit composition. Since the deletion of *VMA*-genes in *S. cerevisiae* is not lethal, it is an ideal model system to study their biological function [162-164].

The present work shows that in yeast the proton pump activity of an intact complex is the most important contributing factor in facilitating cell fusion during mating. This hypothesis is supported by the following findings:

i) Except for the non-essential assembly factor Voa1 and the subunit a isoform Stv1, deletions of all V-ATPase subunits and associated factors leads to impaired fusion efficiency. This suggests that the enzyme integrity, rather than any specific subunit, is required.

ii) The V-ATPase localizes solely at the vacuole and was absent from the shmoo tip and mating junction. Thus, a direct role in PM fusion is unlikely.

iii) The cell fusion efficiency is exclusively rescued by lowering the external pH in Δ*vma2* cells while WT cells remain unaffected. A mechanism has been proposed by which extracellular weak acids can passively diffuse the PM, followed by dissociation of protons which then cross the endosomal and vacuolar membrane and acidify the lumen [184].

iv) The absence of the V-ATPase does not affect the localization of select fusion associated proteins. Therefore, a broad effect via acidification rather than a direct effect by regulating a specific protein is likely.

A heterologous expression of an unrelated proton pump system such as the pyrophosphatase (PPi)-dependent proton pump from *A. thaliana* (Avp1) would be conceivable to additionally verify that fusion can be rescued by restoring organelle acidification activity in yeast cells lacking V-ATPase activity [185, 186].

In the context of cell fusion, V-ATPases have been reported to play a role in extracellular fusion events in *C. elegans*. In contrast to the finding of this study a disruption of the PM located V-ATPase affects the localization of the fusogen EFF-1 resulting in ectopic cell fusion [187]. It is proposed that within the endocytic pathway EFF-1 is not properly degraded [188]. Thus, it is plausible that the V-ATPase governs different functions in extracellular fusion events.

In yeast, the V-ATPase is a central player of intracellular organelle acidification and therefore affects several processes within the secretory and endocytic pathway. Beside protein degradation, sorting and maturation, also the receptor-recycling pathway can be affected. The ligand-independent degradation and ligand-dependent down-regulation of the pheromone receptor Ste2 and Ste3 takes place at the vacuole [94, 189]. However, if a deletion of the V-ATPase would affect this process severely, the Δ*vma*-mating cells would have been unable to polarize and form mating pairs, and importantly, would have displayed a unilateral defect for cell fusion.

One surprising finding in previous studies was that some processes that were thought to be absolutely dependent on vacuolar acidification, such as effective activation of zymogen forms of vacuolar proteases, were only moderately affected in a *VMA*-mutant [189]. This suggests that the dependency on sorting and maturation of hydrolytic enzymes is less critical, but are important for the efficiency of this process. In the context of yeast mating, a deletion of the V-ATPase may therefore have an effect on the efficacy of hydrolytic enzymes needed for CW thinning at the fusion contact side. However, this does not explain the observed defect at the stage of PM fusion in *VMA*-mutants.

In summary, the present work shows that the V-ATPase activity is likely the most important contributing factor in facilitating cell fusion and its deletion has a significant impact on various biological processes contributing to both CW remodeling and PM fusion.

4.2.2 V-ATPase affects CW remodeling and PM fusion approximately equally likely by proxy via interaction with at least 12 genes involved in cell fusion

Through mating crosses of a Δ*vma2* mutant to a Δ*fus1*Δ*fus2* double mutant it was discovered that the V-ATPase has a partial effect of ~50% on CW remodeling. The remaining portion of the defect is proposed to affect PM fusion. Further investigations of synergistic interactions in *trans* between Δ*vma2* mutants and select GOI mutants revealed that *VMA2* synergizes with at least 12 genes involved in cell fusion affecting different biological processes. This provides an explanation for the mixed fusion defect phenotype. Among them are genes with reported roles in ergosterol biosynthesis (*ERG3, ERG6*), protein glycosylation (*CAX4*, *ANP1*, *PMT2* and *PMT4*), CW synthesis and integrity (*CHS3*, *GAS1*), protein nuclear export and import (*MSN5*, *NUP84*), proteolytic processing (*KEX2)* and one dubious gene with a potential role in pheromone signaling (*YGL024w*). As described in previous sections *ERG3*, *ERG6*, *PMT4* and *KEX2* are additionally implicated in facilitating PM fusion. Exceptionally, *VMA2* does not synergize with the major PM fusion regulator *PRM1*, strongly suggesting its involvement in a completely distinct and independent pathway. The upcoming paragraph aims to elucidate interconnections and shared functionalities between the V-ATPase and its synergizing genes in cell fusion, even though one has to consider that the following findings were generated in vegetative and not mating yeast cells.

In a genomic screen for yeast V-ATPase mutants displaying a pH-conditional phenotype the mutants Δ*kex2* and Δ*anp1* have been previously identified [160]. One study reported that even though the V-ATPase was fully assembled in a Δ*kex2* mutant, the proton pump activity was not functional. A model was proposed in which the late Golgi resident endopeptidase Kex2 acts as

an activator by proteolytically processing a negative regulator of the V-ATPase, which however has not been identified yet [178].

Furthermore, combined cryogenic electron microscopy (Cryo-EM) structure and mass spectrometry analysis of human V-ATPase revealed that isoforms of the subunits a and e of the V0-domain are glycosylated at their luminal sites. Mutations of these glycosylation sites leads to increased proteasomal degradation, retention in the ER and an inability to integrate into the V-ATPase complex affecting assembly, stability, and localization. It was also suggested that glycans act as a shield to protect the V-ATPase from lysosomal proteolysis [180]. In yeast however, only the non-essential assembly factor Voa1 was found to contain three possible N-glycosylation sites, which is not an integral component of the V-ATPase complex itself [190]. In addition, as exemplified in this work, the Δ*voa1* mutant does not show impaired fusion efficiency during mating. Therefore, it seems unlikely that a defect in glycosylation affects V-ATPase activity.

On its way to the vacuole to overtake proteolytic function the carboxypeptidase Y (CPY) undergoes several stages of post-translational processing, including N-linked glycosylation [191, 192]. Determining the level of secreted CPY into the medium suggests that CPY is not properly sorted to the vacuole. One study identified that Δ*vma*-mutants, Δ*anp1*, Δ*cax4*, Δ*pmt2* and Δ*nup84* exhibited increased levels of CPY, thus representing a defect in sorting of proteins to the vacuole which may provide an explanation for the observed synergism between *VMA2* and *ANP1*/*CAX4*/*PMT4* and *NUP84*. [160]. In the regard of *CAX4*, a deletion of the *CAX4*-encoded dolichyl pyrophosphate phosphatase (Dol-PP) was reported to result in N-glycosylation defects of the vacuolar CPY. This N-glycosylation defect in-turn leads to accumulation of unfolded or mis-folded proteins in the ER which induces ER-stress and causes abnormal ER and vacuolar membrane morphology. Moreover, a compensatory mechanism was proposed in which cytotoxicity due to accumulation of un-/misfolded proteins in the cytosol is compensated by an increase in phospholipid levels to expand the ER membrane. Therefore, it is thought that *CAX4* connects protein glycosylation and lipid metabolism [192].

Interestingly, a requirement for ergosterol in the function of the V-ATPase was reported. Through a genome-wide screen the PM fusion implicated *ERG*-mutants Δ*erg2*, Δ*erg3*, Δ*erg6*

were identified to exhibit the pH-conditional phenotype which represents a failure in vacuole acidification [193]. The strongest phenotype was observed in the most upstream acting mutant Δ*erg24* showing ~40% impaired proton-pump activity compared to WT cells. A restoration of vacuolar acidity was gained by ergosterol supplementation. A deletion of *Δerg24* however did not result in i) dissociation of enzyme complex into separate V1- and V0-domains, ii) unaltered V1/V0 ratio, iii) reduced V-ATPase abundance, or iv) mis-localization of the V-ATPase. Even though the exact mechanism remains to be determined, two hypotheses were suggested: first, alteration in the composition of sterols affect membrane packing and rigidity which in turn might restrict the structural flexibility and thus the function of the V-ATPase. Second, depleting ergosterol affects lipid requirements of other membrane proteins with regulatory effects on the V-ATPase. The first hypothesis finds support by another study which investigated the structure of the V-ATPase by cryo-EM. One has found densities around the c-ring of the membrane embedded V0-domain of V-ATPase which may correspond to ergosterol [194].

Lastly, a recent study reported that V-ATPases are present in the nuclear membrane regulating a nucleo-cytosolic proton gradient facilitating the coupled transport of substrates to regulate nuclear functions [195]. This may link the synergism between *VMA2* with *MSN5* and *NUP84* which are both known to be involved in nucleo-cytoplasmic transport of proteins and other macromolecules [196]. In the case of *MSN5* a connection between mating and the nucleocytoplasmic transport was reported. *MSN5* encodes the receptor for pheromone-stimulated nuclear export of Ste5, the scaffold protein for the pheromone response MAPK cascade [197]. Furthermore, in response to mating pheromones, Msn5 exports the Far1-Cdc24 complex from the nucleus to the cytoplasm which is crucial for polarization of the actin cytoskeleton which contributes to efficient mating [198]. A role of *MSN5* distinctively in PM fusion was however not reported.

Beside *MSN5* and *NUP84*, all other *VMA2*-synergizing genes encode enzymes which indicates that in particular these group of proteins depends on optimal pH-ranges for proper functionality. In addition, the identified synergistic interaction partners govern physiological processes in intracellular membranes, the residence of yeast V-ATPases. Because Prm1 localizes at the PM, this may explain why *PRM1* does not synergize with *VMA2*. It may also suggest, that

even though both govern roles in PM fusion, they operate on different pathways to ensure proper fusion in case one path is disrupted.

In summary, the findings of the present work highlight the importance of the V-ATPase at late stages of cell fusion. The complexity of the V-ATPase in diverse biological processes highlights the challenge in pinpointing a specific role in PM fusion during the mating of yeast. Nevertheless, by identifying genes that operate with *VMA2* in *trans* one can assign genes that cooperate functionally in late stages of cell fusion, uncovering a new branch of the fusion pathway.

4.3 *CAX4* acts in conjunction with *PRM1*, *KEX2, VMA2 and ERG6* to facilitate cell fusion

Thus far, *CAX4*-encoded Dol-PP-phosphatase has been mainly implicated in cell wall integrity in mitotic cells [191]. Therefore, it was not surprising that the majority of Δ*cax4* mating cells arrested as early pre-zygotes with remnant CW material at the mating junction. Interestingly, this work uncovered a novel synergistic interaction in *trans* between *PRM1* and *CAX4* which emphasizes the requirement of tight coupling between CW remodeling by Cax4 and PM fusion by Prm1. Microscopic localization and Western Blot expression analysis of Prm1 in a Δ*cax4*-sensitized background revealed a lower abundance of Prm1 in pheromone treated cells compared to WT cells. This led to the hypothesis that Cax4 is important for the stability or turnover of Prm1. The hypothesis that Prm1 might be post-transcriptionally processed by Cax4 through glycosylation was however not supported.

Since Cax4 is involved in actin cytoskeleton organization in budding cells, one can assume that it is also involved in its organization in mating cells [199]. As a consequence, a deletion of *CAX4* could affect actin cable polarization and thus the delivery of Prm1 to the fusion contact site [122]. This may explain the reduced abundance of Prm1 in Δ*cax4* cells and the synergistic interaction between the two genes. To test this hypothesis, one could perform co-localization experiments of Δ*cax4* cells expressing C-terminally tagged *PRM1*-mNG and another gene encoding an actin polarization protein such as *CDC42*, *BNI1* or *SPA2* distinctively tagged with

mCherry. A reduced abundance of these proteins compared to WT cells would imply that Cax4 affects the delivery of Prm1 and possibly other fusion proteins that might be part of a potential fusion machinery complex. Even though the exact mechanisms that may explain the synergism between *CAX4* and *PRM1* could not be determined, the present work is the first in the last 16 years that has identified a novel synergistic interaction partner of Prm1, the major regulator of PM fusion.

Furthermore, this work detected a synergism between *CAX4* and *KEX2*, the hitherto only known synergistic interaction partner of *PRM1*. Among other substrates, Kex2 processes α-factor pheromone [136]. Cax4 has been implicated in actin cytoskeleton organization. Since a defect in mature α-factor secretion and accumulation of α-factor-processing intermediates in Δ*cax4* and other actin mutants was detected, it is proposed that the actin cytoskeleton recycles Kex2 from the pre-vacuolar compartment to the Golgi [160]. However, if an α-factor secretion defect would be the most contributing factor for the observed fusion defect, then one would have already detected a unilateral defect in Δ*cax4* mating cells. One possible scenario that may explain the synergism between *CAX4* and *KEX2* might be that Kex2 also proteolytically processes Cax4. This assumption is supported by the fact that Cax4 contains a potential cleavage site sequence of Kex2. Future Western Blot analysis may clarify whether Cax4 depends on Kex2-dependent proteolysis.

The dolichol and ergosterol biosynthesis pathway share the pre-cursor molecule farnesyl pyrophosphate (FPP) which serves as a branching point for the biosynthesis of either dolichol or sterol [200]. Early thermo-sensitive ergosterol deficient mutants (*erg8*, *erg9*, *erg12*) showed a 4-fold reduction of dolichol-phosphate (Dol-P) production compared to WT cells [201]. This connection however is unlikely to provide an explanation for the observed synergism between *CAX4* and *ERG6* (or *ERG3*), because both Erg6 and Erg3 act at the very late stages in the ergosterol biosynthesis pathway where both pathways have already diverged [139].

Another explanation for the synergism between *CAX4* and *ERG*-genes might be the role of Cax4 in lipid droplet (LD) formation which is important for the storage of sterols [192, 202]. *CAX4* is suggested to be required for the expression and activity of the O-acyltransferase (ASAT), an enzyme that initiates sterol esterification [202]. LDs in turn serve as energy reservoirs storing

biologically inert forms of fatty acids and sterols such as triacylglycerol (TAG) and sterol ester (SE) [192, 203]. Interestingly, 80% cellular Erg6 was found to mainly locate at LDs from where ergosterol is delivered to its final membranous destinations [139, 204]. In Δ*cax4* deletion strains a significant reduction in the number of LDs was observed which may have an effect on the abundance of Erg6 which might explain the impaired fusion efficiency observed in Δ*erg6* x Δ*cax4* mating cells [202]. To test this hypothesis, one could consider performing localization experiments of Δ*cax4* cells expressing C-terminally tagged *ERG6*-mNG or protein expression analysis of *ERG6*-v5 by Western Blot analysis in future studies.

4.3.1 *VMA2* overexpression suppresses fusion defect in Δ*cax4* cells

One interesting finding was that the overexpression of *VMA2* partially rescues the fusion defect of Δ*cax4* cells which suggests a subunit-specific role of Vma2 independently of the function of the V-ATPase complex in intracellular acidification. This putative additional role may provide an explanation why the Δ*vma2* fusion defect at acidic pH could only partially be restored. One study supports the hypothesis that V-ATPase subunits might govern additional roles beside vacuolar acidification [202]. It has been reported that solely the subunit Vma9 (subunit e of V0-domain) and Vma21 (V-ATPase-associated assembly factor) act as negative regulator of ASAT. With this, the function of *VMA9* and *VMA21* is in direct contrast to *CAX4* in which a deletion of both *VMA9* and *VMA21* results in increased ASAT activity and elevated number of LDs. Since no effect of *VMA2* on ASAT activity was detected, this linkage seems to be an unlikely scenario that would explain why cell fusion could be restored in Δ*cax4* cells expressing *VMA2*. Moreover, a simultaneous deletion of *CAX4* and expression *VMA2* would likely result in an excess of free sterols and free fatty acids in the cytosol which would lead to lipotoxicity [192].

One other possible explanation for the fusion rescue might be that *VMA2* can compensate for the Δ*cax4* fusion defect by surmounting *CAX4* via upregulation of an upstream gene of the dolichol pathway such as *SEC59.* Both *CAX4* and *SEC59* are implicated in the formation of Dol-P. Dol-P serves as a lipid carrier which is important for the assembly of oligosaccharide Dol-P which is further processed to oligosaccharide Dol-PP. After transferring the oligosaccharide from Dol-PP to a nascent polypeptide chain, the *CAX4*-encoded Dol-PP phosphatase catalyzes

dephosphorylation of Dol-PP to form Dol-P. Dol-P can then be recycled for further glycosylation processes [192]. Cells lacking *CAX4* showed an accumulation of Dol-PP which resulted in relative lack of Dol-P and consequently a N-glycosylation defect of proteins [191, 205]. The *SEC59*-encoded dolichol kinase on the other hand catalyzes the terminal step of de novo Dol-P synthesis and thus synthesizes Dol-P through a distinct pathway than *CAX4*. Consequently, cells expressing *SEC59* can complement Dol-P and rescue the Δ*cax4* phenotype [192].

For further confirmation, it is necessary to examine whether low-copy expression of *VMA2* as well as expression from the endogenous promoter in a Δ*cax4* sensitized background would result in a similar outcome. Moreover, it is important to test whether this effect is specific for *VMA2* or whether the expression of other V-ATPase subunits would show a similar effect. The confirmation of whether *SEC59* is the gene up-regulated by *VMA2* and the cause of the fusion rescue is not straightforward due to its essential gene status. Nevertheless, one could attempt to study the effect of temperature-sensitive *SEC59* (*sec59*^{ts}) mutants to investigate its role in cell fusion and even try to over-express *VMA2* in this strain. To determine if the lack of Dol-P in Δ*cax4* cells is the primary cause of the fusion defect, one could explore whether exogenous supplementation with Dol-P could restore fusion efficiency [206, 207].

4.4 Evidence for two novel cell fusion pathways with *VMA2* and *CAX4* operating independently of *PRM1* and *ERG6*

The identified late fusion mutants exhibited a partial defect which suggests either genetic redundancy between the fusion pathways or yet unidentified key components of the fusion machinery. Previous analysis of synergistic interactions of a set of select GOI fusion mutants provided insights into the complexity of the fusion process and cellular processes involved. The subsequent double mutant analysis verified whether genes are operating on the same or a distinct fusion pathway. Hereby, a focus was on the known fusion regulator *PRM1* and *ERG6* as well as the novel candidates *VMA2* and *CAX4*. *VMA2*, because of its novel role in affecting several genes involved in cell fusion via acidification, and *CAX4* mainly because of its new role in PM fusion via synergizing with *PRM1*.

The main results of this analysis are:

i) All possible combinations of corresponding double mutants resulted in an enhanced fusion defect compared to the respective single mutants. This suggests that *PRM1*, *ERG6*, *VMA2* and *CAX4* all operate on distinct fusion pathways.

ii) Considering the data from the synergistic interaction analysis, *CAX4* partially overlaps all fusion pathways. Intriguingly, *CAX4* was the only gene found to synergize with all three genes, including *PRM1*.

iii) *PRM1* acts independently of *VMA2* and *ERG6*.

iv) *CAX4*, *VMA2* and *ERG6* operate on distinct, yet partially overlapping pathways.

In addition, the present work attempted to sequentially order synergizing genes by overexpression analysis in a genetically sensitized background. This analysis revealed that *VMA2*-overexpression in a Δ*cax4* mutant partially restored cell fusion suggesting that *VMA2* operates downstream of *CAX4* (section. 4.3.1). The exact mechanism however remains to be uncovered. Additionally, pre-liminary data (not shown in this study) indicated that *ERG3* and *ERG6* act downstream of *VMA2* since a restoration of fusion was achieved when both were individually over-expressed in a Δ*vma2* mutant. However, these data are limited because they could not be reproduced in this work. Actually, in most of the studied cases no restoration of fusion was obtained. One explanation for the lack of the fusion rescue through over-expression is that genetic synergism can occur through complex interactions and dependencies that might not be fully compensated by over-expression alone.

Nevertheless, these findings provide evidence for the existence of two novel pathways involving *VMA2* and *CAX4,* which in addition to *ERG6* and *PRM1*, all ensure robustness of the fusion process. Future research may aim to identify all synergistic interactions of the four proposed fusion pathways to gain a complete picture of the genetic interaction network facilitating cell fusion during yeast mating. Note, that *FIG1* operates on another separate fusion pathway, which however was not a primary focus of this work because of the requirement to deplete extracellular Ca^{2+} to fully obtain the Δ*fig1* fusion defect phenotype [131]. Therefore, future research may additionally aim for analyzing fusion efficiency in different environmental conditions such as low Ca^{2+} or pH.

4.5 The RNA polymerase II mediator complex acts as a putative master regulator of cell fusion

Initially, *YGL024w* was identified to exhibit a mating type independent unilateral fusion defect of about 50% and an almost fusion block when deleted in both mating types. Subsequent overexpression analysis revealed that *PGD1* to which *YGL024w* partially overlaps is the underlying cause of the defect. *PGD1* encodes a subunit of the RNA polymerase II mediator complex (continuously referred to as mediator complex) which plays a role in transcription initiation and regulation [208, 209]. Because Pgd1 exclusively localizes to the nucleus and was absent from the shmoo tip and mating junction supports the assumption that *PGD1* facilitates cell fusion indirectly, likely through its involvement in the mediator complex rather than occupying a direct role in fusion.

The mediator complex is conserved across eukaryotes and is composed of 21 subunits in yeast and 26 subunits in human which are organized into three distinct modules (head, middle and tail) and a four-subunit dissociable kinase-module [210]. One major function is facilitating the regulation of gene expression by serving as a mediator between transcription factors (TFs) and the basal transcriptional machinery including the RNA polymerase II (pol II) and general transcription factors (GTFs). The mediator complex starts the transcription initiation via interaction with TFs bound to specific DNA sequences and recruitment of the pol II to gene promotors supporting the establishment of a stable pre-initiation complex. Pol II phosphorylation promoted by the mediator complex enables the escape from the promoter followed by the transition from the initiation to the elongation step with the final goal to transcribe protein-coding genes [171, 210]. It is suggested that due to its intrinsic disorder and conformational flexibility the mediator is able to interact with a myriad of regulatory factors simultaneously [211]. Binding of specific TF to the tail is proposed to induce conformational changes within the complex which is followed by a transfer of regulatory signals to the core mediator and finally to the pre-initiation complex. Therefore, different TFs and thus, the corresponding signaling pathways that activate them, depend on distinct mediator subunits to coordinate their transcriptional responses [171, 210, 212, 213].

Interestingly, the present work revealed that deletions of different mediator subunits from different modules exhibit fusion defects to different degrees at both early- and late-fusion stages. These include defects in cell pairing and pheromone secretion as well as CW remodeling and PM fusion, respectively. The identification of certain mediator subunits and their involvement in distinct stages of cell fusion makes these findings exceptional from previous studies in the context of yeast mating.

Thus far, studies from the 1990s and early 2000s reported that a deletion of *PGD1* and *MED15* leads to defects in the production of mating-pheromones, which was confirmed in this study. For Δ*pgd1* a decreased expression of *SST2*, the negative regulator of the pheromone response pathway, and in the case of Δ*med15* a decreased expression of *MFα1*, the gene encoding the pheromone α-factor, is proposed as the cause [169, 214]. In addition, Δ*med15* and Δ*med16* mating cells have been reported to show reduced mating efficiency. However, this study only determined the general efficiency of two haploid cells to mate and form diploid colonies on plate [208, 215]. Another study reported that a deletion of the kinase subunit *SSN3* affects the transcription factor Ste12. Ste12 can be activated by the MAPK signaling cascade leading to either activation of mating genes or genes involved in pseudohyphal growth. However, only upon nitrogen starvation a Ssn3-depended phosphorylation was reported to cause increased pseudohyphal growth, whereas an effect on pheromone response and mating efficiency was not detected [216]. These results contradict the findings of this study in which Δ*ssn3* cells show a defect in pheromone secretion, as well as cell pairing and cell fusion.

Future studies may focus on the role of Ste12 as a target of other mediator subunits in the context of cell fusion during mating. Mating-defective amino acid variants of Ste12 resulted in significantly down-regulated expressed mating genes. Among them, genes that act at every step of the mating process including pheromone signaling (e.g. *GPA1*, *SST2*, *MFα1/2*), cell cycle arrest and polarized growth (e.g. *FAR1*), cell agglutination (e.g. *FIG2*), cell fusion (e.g. *FUS1*, *FUS2*, *FIG1*, *PRM1*) and karyogamy (e.g. *KAR4*) [217]. In regard to Δ*pgd1* and Δ*med15*, an over-expression of *STE12* may clarify if and to what extend the defect in pheromone secretion, and thus cell pairing, can be suppressed by rescuing the defect presumably caused by decreased expression of *SST2* and *MFα1*, respectively. Moreover, it might be interesting to determine how

the overexpression of *STE12* in the different mediator mutants (Δ*pgd1*, Δ*med15*, Δ*med16*, Δ*med20*, Δ*med31* and Δ*ssn3*) may also restore cell fusion efficiency.

Surprisingly, when analyzing synergistic interactions between select mediator subunits from each module, none of them were found to synergize with *PRM1* in *trans*. If one of the tested mediator subunits would target Ste12, one would expect a synergistic interaction, because *STE12* regulates the expression of *PRM1* [217]. In contrast, *PGD1* (tail), *MED20* (head), *MED31* (middle) and *SSN3* (kinase) synergize all with *ERG6* in *trans*. In addition, *PGD1* synergizes with all other genes which were focus of this study, including *ERG3*, *KEX2*, *VMA2*, *CAX4* and *FUS1*. This suggests that *PGD1* affects at least three out of four fusion pathways discussed in this work. The attempt to suppress the Δ*pgd1* fusion defect by overexpressing the above-mentioned genes failed. This suggests that the activation of only one pathway is probably insufficient to restore fusion efficiency. Moreover, it led to the hypothesis that the mediator complex acts as a master regulator of cell fusion. In the future, utilizing RNA-Seq or microarray analysis on pheromone-treated mediator mutants compared to WT cells could provide valuable insights into the regulation of mating-specific genes in the absence of particular mediator subunits.

4.6 A model of the synergistic interaction network facilitating cell fusion during the mating of *S. cerevisiae*

By conducting an unprecedent loss-of-function screening of the entire YKO TMD sub-library, the present work significantly contributes to a better understanding of the intricate gene network facilitating cell fusion during the mating of *S. cerevisiae*. The findings of this work have led to the development of the current fusion model, as depicted in (**Figure 46**). For brevity, only genes that were the main focus of this study are shown.

In summary, the majority of identified mutants showed a partial fusion defect when deleted in both mating partners as well as a fusion arrest as early and late pre-zygotes. This implies, that some genes likely cover several functions in order to ensure a tight coupling of CW remodeling and PM fusion to prevent dead-end lysis. This assumption for instance is supported by the

novel identified synergism between *CAX4* and *PRM1*. Previously, both have been exclusively linked to either CW integrity or PM fusion processes. As demonstrated for *CAX4* and *PRM1,* this study uncovered even more functional relationships between a set of known (*FUS1*, *FUS2*, *PRM1*, *ERG6*, *KEX2*) and novel (*CAX4*, *VMA2, PGD1*) fusion related genes. Interestingly, the *PGD1*-encoded mediator complex subunit was found to interact with all prior mentioned genes, except for *PRM1*. Together, these data provide novel insights into the complexity of diverse cellular processes involved facilitating the process of PM merger.

Excitingly, this study provides evidence for the existence of two novel independent fusion pathways with *VMA2* and *CAX4* beside the known paths with *ERG6* and *PRM1*. Such a presence of redundant fusion pathways supports the assumption that the process of CW removal and PM fusion must be tightly coupled. Therefore, it is likely that *S. cerevisiae* has evolved a mechanism based on redundancy that serves as a lifeguard mechanism. In this scenario, the disruption of one path can be compensated by another ensuring successful fusion and thus, genetic diversity and survival of the cell. Apart from Prm1 however, none of the four investigated genes were found to encode proteins that localize at the fusion site. Therefore, future research is necessary to identify the gene responsible for the expression of the fusion protein likely to be directly involved in PM fusion.

The top panel of the developed model (**Figure 46A**) provides a general scheme that includes pre-fusion and late fusion stages. Many aspects of the pre-fusion stages including polarized growth upon pheromone response have been extensively studied and can be reviewed in [87, 89, 95, 218]. The main focus of this study was on late-fusion stages including CW remodeling, PM fusion and finally fusion pore opening and expansion. The CW is colored in brown, the PM in black. Synergistic interactions that are verified by double mutant analysis, are denoted in black lines. Interactions that are not confirmed are denoted in black dashed lines. *KEX2*-interactions were only investigated in *MAT***a** mating type because of its sterility in *MAT*α mating type. The letters depicted in (**Figure 46A**) refer to (**Figure 46B**) which represent possible scenarios for the underlying cause of the synergism. These scenarios are based on the results of the current study and prior research, as discussed previously.

Following, a concise overview outlining possible scenarios for underlying causes:

A. Different subunits from distinct modules of the mediator complex affect fusion to different degrees at early and late fusion stages. Due to its conformational flexibility and intrinsic disorder, the mediator can interact with a myriad of TFs such as Gal4, Sip4 or Ste12 [170]. It is hypothesized that the mediator acts as a master regulator of synchronizing different stages of fusion at the appropriate time.
B. Cax4 contains a putative cleavage site sequence for Kex2, indicating that Kex2 may process Cax4. Due to its role in N-glycosylation and actin cytoskeleton organization, Cax4 might have a broad effect on proteins involved in CW remodeling and PM fusion [199, 219].
C. 1) It is proposed that *KEX2* or a yet to be identified Kex2 processed substrate, and *PRM1* operate at different stages of the same fusion pathway [135]. 2) Cax4 might play a role in actin cable polarization in mating cells, and thus affect the delivery of Prm1 to the fusion contact site.
D. A model has been proposed suggesting that Kex2 activates V-ATPases by cleaving a negative regulator of the enzyme [178]. The V-ATPase is proposed to indirectly facilitate cell fusion by its function in acidification of intracellular organelles and pH regulation. The V-ATPase affects both CW remodeling and PM fusion likely via interaction with at least 12 other genes involved in fusion (see **Figure 32**).
E. Cryo-EM studies detected densities around the c-ring of the membrane embedded V0-domain of the V-ATPase which may correspond to ergosterol [194].
F. Erg6 is mainly located at lipid droplets (LDs). Since a deletion of *CAX4* leads to a reduced number of LDs, it may affect the abundance of Erg6 [139, 204].
G. Dol-P serves as a lipid carrier during N-glycosylation [192]. Left: Dol-P derives from de novo synthesis, catalyzed by Sec59, and from recycling of Dol-PP after each N-glycosylation cycle. Cax4 dephosphorylates Dol-PP to form Dol-P. Middle: The lack of *CAX4* leads to accumulation of Dol-PP and a relative reduction of Dol-P resulting in N-glycosylation defects. Right: It is hypothesized that Δ*cax4* cells overexpressing *VMA2* might upregulate *SEC59*, or another upstream acting gene, which can compensate for the Δ*cax4* phenotype.

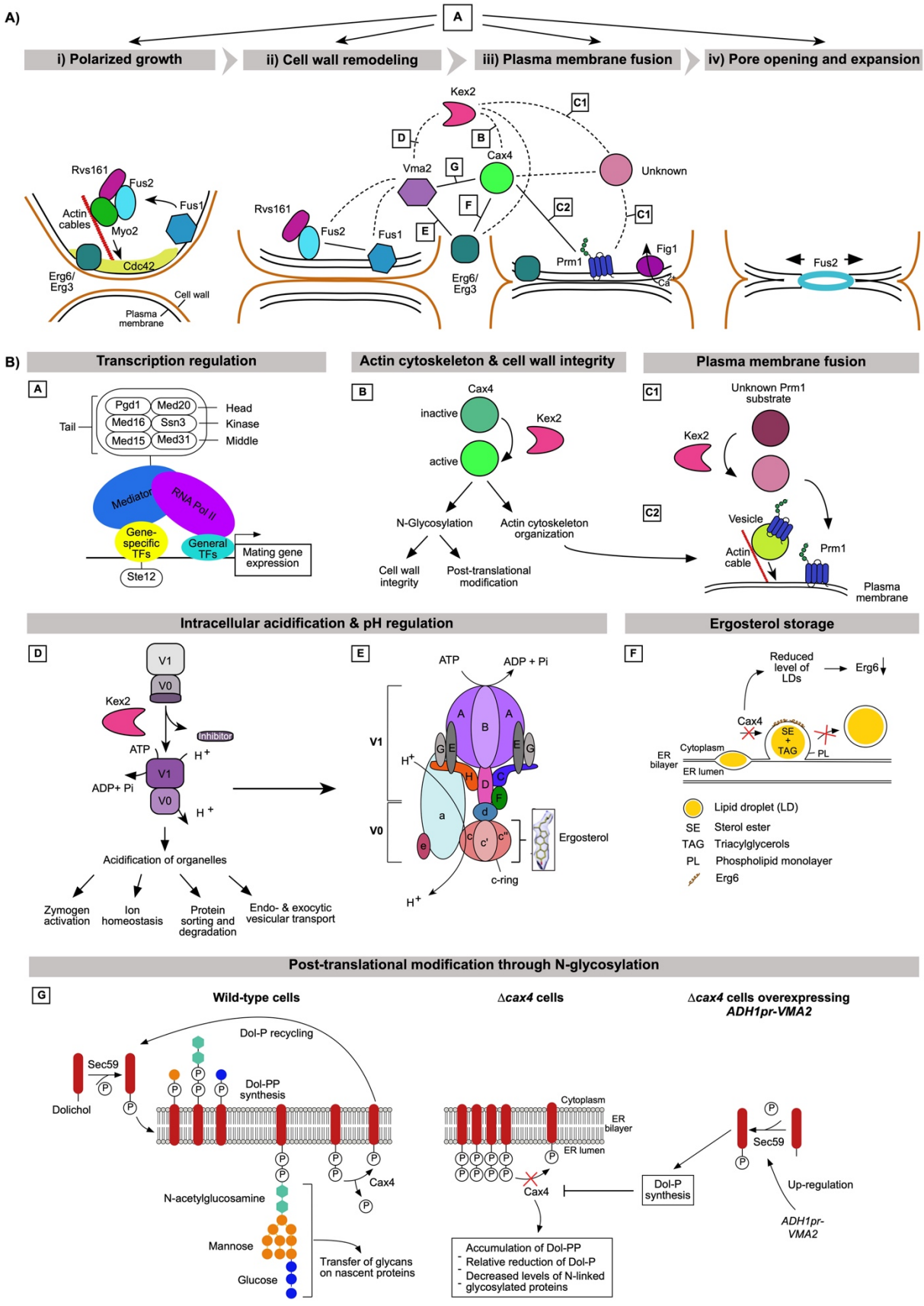
A)
A
i) Polarized growth
ii) Cell wall remodeling
iii) Plasma membrane fusion
iv) Pore opening and expansion
Rvs161
Fus2
Fus1
Actin cables
Myo2
Cdc42
Erg6/ Erg3
Cell wall
Plasma membrane
Kex2
C1
D
B
Cax4
Vma2
G
Unknown
F
C2
E
Prm1
Fig1
Ca2+
B)
Transcription regulation
Actin cytoskeleton & cell wall integrity
Plasma membrane fusion
Pgd1
Med20
Head
Tail
Med16
Ssn3
Kinase
Med15
Med31
Middle
Mediator
RNA Pol II
Gene-specific TFs
General TFs
Mating gene expression
Ste12
inactive
active
N-Glycosylation
Actin cytoskeleton organization
Cell wall integrity
Post-translational modification
Unknown Prm1 substrate
Vesicle
Actin cable
Intracellular acidification & pH regulation
Ergosterol storage
V1
V0
Inhibitor
ATP
ADP+ Pi
H+
Acidification of organelles
Zymogen activation
Ion homeostasis
Protein sorting and degradation
Endo- & exocytic vesicular transport
ADP + Pi
Ergosterol
c-ring
Reduced level of LDs
Erg6
SE + TAG
PL
Cytoplasm
ER bilayer
ER lumen
Lipid droplet (LD)
SE Sterol ester
TAG Triacylglycerols
PL Phospholipid monolayer
Erg6
Post-translational modification through N-glycosylation
Wild-type cells
Δcax4 cells
Δcax4 cells overexpressing ADH1pr-VMA2
Dol-P recycling
Sec59
Dolichol
Dol-PP synthesis
Cax4
N-acetylglucosamine
Mannose
Glucose
Transfer of glycans on nascent proteins
Dol-P synthesis
Accumulation of Dol-PP
Relative reduction of Dol-P
Decreased levels of N-linked glycosylated proteins
Up-regulation
ADH1pr-VMA2

Figure 46: Proposed model of the synergistic interaction network operating during PM fusion in the mating of *S. cerevisiae*. A) Cell fusion progression. i) Polarized growth towards the opposite mating partner initiates cell contact. ii) The CW is locally remodeled and digested, iii) allowing the underlying PMs to fuse. iv) The fusion pore expands and cytoplasmic contents can mix. Depicted are known (*FUS1*, *FUS2*, *PRM1*, *ERG6*, *KEX2*) and novel (*CAX4*, *VMA2*) regulator of the fusion process. Synergistic interactions that are confirmed by double mutant analysis, are denoted in black lines, non-confirmed interactions in black dashed lines. *KEX2*-synergism is only tested on *MAT***a**. The letters refer to B) Possible scenarios for the underlying cause of the identified synergism. A: Different subunits of the mediator complex affect fusion at early and late fusion stages, likely indirectly via its function in transcriptional regulation. B) Kex2 might proteolytically process Cax4. C) 1) *KEX2,* or a yet to be identified Kex2 processed substrate, operates with *PRM1* on the same fusion pathway. 2) Delivery of Prm1 to the fusion contact site might depend on Cax4 induced actin cable polarization. D) Kex2 activates the V-ATPase complex by cleavage of an inhibitor. E) Ergosterol might be present at the c-ring of the V0-domain of the V-ATPase. Structure of ergosterol is taken from [194]. F) Deletion of *CAX4* leads to decreased level of lipid droplets. This might affect abundance of Erg6. G) Dol-P synthesis via Sec59, and recycling via Cax4. The absence of *CAX4* causes accumulation of Dol-PP and lack of Dol-P. Hypothesis: *VMA2* upregulates *SEC59*, resulting in Cax4-independent synthesis of Dol-P which suppresses the Δ*cax4*-phenotype.

5. Concluding remarks and future perspectives

Cell-cell fusion during sexual reproduction is a fundamental process observed in various eukaryotic organisms. Investigating the mechanisms and components involved in this process can shed light on its evolutionary origin and conservation. By understanding both the similarities and differences in fusion mechanisms, valuable insights into the general principles governing this process can be obtained. Despite decades of research, the mechanism underlying plasma membrane fusion during sexual reproduction in yeast cells remains poorly understood, leaving many questions unanswered.

Investigating cell fusion in yeast is a challenging task due to the requirement for studying bilateral fusion of mutants, genetic redundancy within and between mating partners, and the need for rapid and precise high-throughput quantification. By addressing all these challenges, this work identified more than 20 novel positive regulators of cell fusion during the mating of *S. cerevisiae*, and uncovered a synergistic interaction operating at late fusion stages. Moreover, two novel fusion pathways with *VMA2* and *CAX4* have been identified leading to the hypothesis that together with *PRM1* and *ERG6* at least four independent pathways exist. The presence of such redundant pathways ensures cell integrity and survival during the delicate process of CW removal and subsequent PM fusion preventing cell lysis. This provides also an explanation why redundancy can be found in other fungi such as *N. crassa* and *S. pombe* [89, 220, 221]. In contrast, higher eukaryotes, including mammals, have probably evolved different mechanisms to ensure successful cell fusion during sexual reproduction which rely less on genetic redundancy but rather on specialized regulatory mechanisms and precise protein interactions. That mechanism is exemplified by the absence of redundancy in sperm proteins such as SPACA6 and IZUMO1 and the protein interaction between IZUMO1 and its receptor JUNO mediating sperm-egg adhesion [72, 79, 222].

Another interesting finding was the discovery of the V-ATPase and the RNA polymerase II mediator complex. Both complexes likely facilitate cell fusion indirectly via intracellular acidification and transcriptional regulation, respectively. Interestingly, both complexes and other regulators identified in this study, such as *CAX4*, have homologues either in other yeast

such as *S. pombe* or in mammals [180, 211, 223]. Therefore, this work provides a large entry-point into fusion processes for further studies which may contribute to valuable insights into conserved biological processes and pathways beyond the scope of the current study.

It is worthwhile to mention that the discovery of *PGD1* and thereafter the involvement of the mediator complex in fusion was serendipitous. It emerged during the investigation of the dubious gene *YGL024w*. *YGL024w* was part of the primary screen due to the presence of its predicted TMD [169]. Thus, by excluding non-TMD encoding genes from the analysis, there is a possibility that potential genes involved in this process might have been overlooked. In addition, to cover the entire set of TMD-encoding genes, one should consider investigating all deletions of small ORFs with less than 100 aa, which were missing from the original YKO collection used in this work. A possible relevance of small ORFs has been demonstrated by the identification of the fusion proteins FAST and Myomerger [38, 40]. Therefore, it is suggested to expand the adapted fusion screen and encompass the entire YKO collection including deletions of small ORFs to comprehensively elucidate the synergistic interaction network operating at PM fusion.

6. References

1. Chernomordik, L.V. and M.M. Kozlov, *Mechanics of membrane fusion.* Nat Struct Mol Biol, 2008. **15**(7): p. 675-83.
2. Jahn, R., T. Lang, and T.C. Südhof, *Membrane Fusion.* Cell, 2003. **112**: p. 519-533.
3. Marsden, H.R., I. Tomatsu, and A. Kros, *Model systems for membrane fusion.* Chem Soc Rev, 2011. **40**(3): p. 1572-85.
4. Albanesi, V.S.M.a.J.P., *Membrane Fusion: Stalk Model Revisited.* Biophys J, 2002. **82**: p. 693-712.
5. Markin, V.S., M.M. Kozlov, and V.L. Borovjagin, *On the Theory of Membrane Fusion. The Stalk Mechanism.* Gen. Physiol. Biophys., 1984. **5**: p. 361-377.
6. Chernomordik, L.V. and M.M. Kozlov, *Membrane hemifusion: crossing a chasm in two leaps.* Cell, 2005. **123**(3): p. 375-82.
7. Segev, N., O. Avinoam, and B. Podbilewicz, *Fusogens.* Curr Biol, 2018. **28**(8): p. R378-R380.
8. Hernandez, J.M. and B. Podbilewicz, *The hallmarks of cell-cell fusion.* Development, 2017. **144**(24): p. 4481-4495.
9. Oren-Suissa, M. and B. Podbilewicz, *Cell fusion during development.* Trends Cell Biol, 2007. **17**(11): p. 537-46.
10. Podbilewicz, B., et al., *The C. elegans developmental fusogen EFF-1 mediates homotypic fusion in heterologous cells and in vivo.* Dev Cell, 2006. **11**(4): p. 471-81.
11. Aguilar, P.S., et al., *Genetic basis of cell-cell fusion mechanisms.* Trends Genet, 2013. **29**(7): p. 427-37.
12. Sapir, A., et al., *Viral and developmental cell fusion mechanisms: conservation and divergence.* Dev Cell, 2008. **14**(1): p. 11-21.
13. Harrison, S.C., *Viral membrane fusion.* Nat Struct Mol Biol, 2008. **15**(7): p. 690-8.
14. Podbilewicz, B., *Virus and cell fusion mechanisms.* Annu Rev Cell Dev Biol, 2014. **30**: p. 111-39.
15. Wichner, W. and R. Schekman, *Membrane fusion.* Nat Struct Mol Biol, 2008. **15**(7): p. 658-664.
16. Kielian, M. and F.A. Rey, *Virus membrane-fusion proteins: more than one way to make a hairpin.* Nat Rev Microbiol, 2006. **4**(1): p. 67-76.
17. Barrett, C.T. and R.E. Dutch, *Viral Membrane Fusion and the Transmembrane Domain.* Viruses, 2020. **12**(7).
18. Blijleven, J.S., et al., *Mechanisms of influenza viral membrane fusion.* Semin Cell Dev Biol, 2016. **60**: p. 78-88.

19. Grigory B. Melikyan, R.M.M., * Michael G. Roth,† and Fredric S. Cohen*‡, *A Point Mutation in the Transmembrane Domain of the Hemagglutinin of Influenza Virus Stabilizes a Hemifusion Intermediate That Can Transit to Fusion.* Mol Biol Cell, 2000. **11**: p. 3765-3775.

20. Hui Qiao, R.T.A., † Grigory B. Melikyan,‡ Fredric S. Cohen,‡ and Judith M. White*†, *A Specific Point Mutant at Position 1 of the Influenza Hemagglutinin Fusion Peptide Displays a Hemifusion Phenotype.* Mol Biol Cell, 1999. **10**: p. 2759-2769.

21. Ebel, H., T. Benecke, and B. Vollmer, *Stabilisation of Viral Membrane Fusion Proteins in Prefusion Conformation by Structure-Based Design for Structure Determination and Vaccine Development.* Viruses, 2022. **14**(8).

22. Jahn, R. and R.H. Scheller, *SNAREs--engines for membrane fusion.* Nat Rev Mol Cell Biol, 2006. **7**(9): p. 631-43.

23. Yavuz, H., et al., *Arrest of trans-SNARE zippering uncovers loosely and tightly docked intermediates in membrane fusion.* J Biol Chem, 2018. **293**(22): p. 8645-8655.

24. Lu, X., et al., *Membrane fusion induced by neuronal SNAREs transits through hemifusion.* J Biol Chem, 2005. **280**(34): p. 30538-41.

25. Reese, C., F. Heise, and A. Mayer, *Trans-SNARE pairing can precede a hemifusion intermediate in intracellular membrane fusion.* Nature, 2005. **436**(7049): p. 410-4.

26. Yoon, T.Y. and M. Munson, *SNARE complex assembly and disassembly.* Curr Biol, 2018. **28**(8): p. R397-R401.

27. Zito, F., et al., *United we stand: Adhesion and molecular mechanisms driving cell fusion across species.* Eur J Cell Biol, 2016. **95**(12): p. 552-562.

28. Benjamin Podbilewicz and J.G. White, *Cell Fusions in the Developing Epithelia of C.elegans.* Developmental Biology, 1994. **161**: p. 408-424.

29. Mohler, W.A., et al., *The Type I Membrane Protein EFF-1 Is Essential for Developmental Cell Fusion.* Developmental Cell, 2002. **2**: p. 355-362.

30. Sapir, A., et al., *AFF-1, a FOS-1-regulated fusogen, mediates fusion of the anchor cell in C. elegans.* Dev Cell, 2007. **12**(5): p. 683-98.

31. Avinoam, O. and B. Podbilewicz, *Eukaryotic cell-cell fusion families.* Curr Top Membr, 2011. **68**: p. 209-34.

32. Perez-Vargas, J., et al., *Structural basis of eukaryotic cell-cell fusion.* Cell, 2014. **157**(2): p. 407-419.

33. Avinoam, O., et al., *Conserved Eukaryotic Fusogens Can Fuse Viral Envelopes to Cells.* Science, 2011. **332**: p. 589-592.

34. Palfreyman, M.T. and E.M. Jorgensen, *In Vivo Analysis of Membrane Fusion*, in *eLS*. 2015. p. 1-21.

35. Millay, D.P., et al., *Myomaker is a membrane activator of myoblast fusion and muscle formation.* Nature, 2013. **499**(7458): p. 301-5.

36. Sampath, S.C., S.C. Sampath, and D.P. Millay, *Myoblast fusion confusion: the resolution begins.* Skelet Muscle, 2018. **8**(1): p. 3.

37. Bi, P., et al., *Control of muscle formation by the fusogenic micropeptidemyomixer.* Science, 2017. **356**: p. 323-327.

38. Quinn, M.E., et al., *Myomerger induces fusion of non-fusogenic cells and is required for skeletal muscle development.* Nat Commun, 2017. **8**: p. 15665.

39. Zhang, Q., et al., *The microprotein Minion controls cell fusion and muscle formation.* Nat Commun, 2017. **8**: p. 15664.

40. Ciechonska, M. and R. Duncan, *Reovirus FAST proteins: virus-encoded cellular fusogens.* Trends Microbiol, 2014. **22**(12): p. 715-24.

41. Gamage, D.G., et al., *Phosphatidylserine orchestrates Myomerger membrane insertions to drive myoblast fusion.* Proc Natl Acad Sci U S A, 2022. **119**(38): p. e2202490119.

42. Leikina, E., et al., *Myomaker and Myomerger Work Independently to Control Distinct Steps of Membrane Remodeling during Myoblast Fusion.* Dev Cell, 2018. **46**(6): p. 767-780 e7.

43. von Besser, K., et al., *Arabidopsis HAP2 (GCS1) is a sperm-specific gene required for pollen tube guidance and fertilization.* Development, 2006. **133**(23): p. 4761-9.

44. Mori, T., et al., *GENERATIVE CELL SPECIFIC 1 is essential for angiosperm fertilization.* Nat Cell Biol, 2006. **8**(1): p. 64-71.

45. Clark, T., *HAP2/GCS1: Mounting evidence of our true biological EVE?* PLoS Biol, 2018. **16**(8): p. e3000007.

46. Pinello, J.F., Y. Liu, and W.J. Snell, *MAR1 links membrane adhesion to membrane merger during cell-cell fusion in Chlamydomonas.* Dev Cell, 2021. **56**(24): p. 3380-3392 e9.

47. Wong, J.L. and M.A. Johnson, *Is HAP2-GCS1 an ancestral gamete fusogen?* Trends Cell Biol, 2010. **20**(3): p. 134-41.

48. Fedry, J., et al., *The Ancient Gamete Fusogen HAP2 Is a Eukaryotic Class II Fusion Protein.* Cell, 2017. **168**(5): p. 904-915 e10.

49. Pinello, J.F., et al., *Structure-Function Studies Link Class II Viral Fusogens with the Ancestral Gamete Fusion Protein HAP2.* Curr Biol, 2017. **27**(5): p. 651-660.

50. Valansi, C., et al., *Arabidopsis HAP2/GCS1 is a gamete fusion protein homologous to somatic and viral fusogens.* J Cell Biol, 2017. **216**(3): p. 571-581.

51. Zhang, J., et al., *Species-specific gamete recognition initiates fusion-driving trimer formation by conserved fusogen HAP2.* Nat Commun, 2021. **12**(1): p. 4380.

52. Brukman, N.G., et al., *How cells fuse.* J Cell Biol, 2019. **218**(5): p. 1436-1451.

53. Pinello, J.F. and T.G. Clark, *HAP2-Mediated Gamete Fusion: Lessons From the World of Unicellular Eukaryotes.* Front Cell Dev Biol, 2021. **9**: p. 807313.

54. Moi, D., et al., *Discovery of archaeal fusexins homologous to eukaryotic HAP2/GCS1 gamete fusion proteins.* Nat Commun, 2022. **13**(1): p. 3880.

55. Bhakta, H.H., F.H. Refai, and M.A. Avella, *The molecular mechanisms mediating mammalian fertilization.* Development, 2019. **146**(15).

56. Brukman, N.G., et al., *A novel function for the sperm adhesion protein IZUMO1 in cell-cell fusion.* J Cell Biol, 2023. **222**(2).

57. Bianchi, E. and G.J. Wright, *Find and fuse: Unsolved mysteries in sperm-egg recognition.* PLoS Biol, 2020. **18**(11): p. e3000953.

58. Inoue N., et al., *The immunoglobulin superfamil protein Izumo is required for sperm to fuse with eggs.* Nature, 2005. **434**(7030): p. 234-38.

59. Aydin, H., et al., *Molecular architecture of the human sperm IZUMO1 and egg JUNO fertilization complex.* Nature, 2016. **534**(7608): p. 562-5.

60. Satouh, Y., et al., *Visualization of the moment of mouse sperm-egg fusion and dynamic localization of IZUMO1.* J Cell Sci, 2012. **125**(Pt 21): p. 4985-90.

61. Matsumura, T., et al., *Sperm IZUMO1 Is Required for Binding Preceding Fusion With Oolemma in Mice and Rats.* Front Cell Dev Biol, 2021. **9**: p. 810118.

62. Bianchi, E., et al., *Juno is the egg Izumo receptor and is essential for mammalian fertilization.* Nature, 2014. **508**(7497): p. 483-7.

63. Vondrakova, J., et al., *MAIA, Fc receptor–like 3, supersedes JUNO as IZUMO1 receptor during human fertilization.* Science Advances, 2022. **8**.

64. Brukman, N.G., X. Li, and B. Podbilewicz, *Fusexins, HAP2/GCS1 and Evolution of Gamete Fusion.* Front Cell Dev Biol, 2021. **9**: p. 824024.

65. Bianchi, E. and G.J. Wright, *Izumo meets Juno: preventing polyspermy in fertilization.* Cell Cycle, 2014. **13**(13): p. 2019-20.

66. Bianchi, E. and G.J. Wright, *Sperm Meets Egg: The Genetics of Mammalian Fertilization.* Annu Rev Genet, 2016. **50**: p. 93-111.

67. Ohto, U., et al., *Structure of IZUMO1-JUNO reveals sperm-oocyte recognition during mammalian fertilization.* Nature, 2016. **534**(7608): p. 566-9.

68. Inoue, N., et al., *Molecular dissection of IZUMO1, a sperm protein essential for sperm-egg fusion.* Development, 2013. **140**(15): p. 3221-9.

69. K Miyado, et al., *Requirement of CD9 on the egg plasma membrane for fertilization.* Science, 2000. **287**(5451): p. 321-324.

70. Kaji, K., et al., *The gamete fusion process is defective in eggs of Cd9-deficient mice 2000.* Nature Genetics, 2000. **24**: p. 279-282.

71. Le Naour, F., et al., *Severely reduced female fertility in CD9-deficient mice.* Science, 2000. **287**: p. 319-21.

72. Vance, T.D.R., et al., *SPACA6 ectodomain structure reveals a conserved superfamily of gamete fusion-associated proteins.* Commun Biol, 2022. **5**(1): p. 984.

73. Inoue, N., T. Saito, and I. Wada, *Unveiling a novel function of CD9 in surface compartmentalization of oocytes.* Development, 2020. **147**(15).

74. Lamas-Toranzo, I., et al., *TMEM95 is a sperm membrane protein essential for mammalian fertilization.* Elife, 2020. **9**.

75. Noda, T., et al., *Sperm proteins SOF1, TMEM95, and SPACA6 are required for sperm-oocyte fusion in mice.* Proc Natl Acad Sci U S A, 2020. **117**(21): p. 11493-11502.

76. Tang, S., et al., *Human sperm TMEM95 binds eggs and facilitates membrane fusion.* Proc Natl Acad Sci U S A, 2022. **119**(40): p. e2207805119.

77. Inoue, N., Y. Hagihara, and I. Wada, *Evolutionarily conserved sperm factors, DCST1 and DCST2, are required for gamete fusion.* Elife, 2021. **10**.

78. Fujihara, Y., et al., *Spermatozoa lacking Fertilization Influencing Membrane Protein (FIMP) fail to fuse with oocytes in mice.* Proc Natl Acad Sci U S A, 2020. **117**(17): p. 9393-9400.

79. Hernandez-Falco, M., et al., *The Role of Sperm Proteins IZUMO1 and TMEM95 in Mammalian Fertilization: A Systematic Review.* Int J Mol Sci, 2022. **23**(7).

80. Noda, T., et al., *Sperm membrane proteins DCST1 and DCST2 are required for sperm-egg interaction in mice and fish.* Commun Biol, 2022. **5**(1): p. 332.

81. Kroft, T.L., E.J. Gleason, and S.W. L'Hernault, *The spe-42 gene is required for sperm-egg interactions during C. elegans fertilization and encodes a sperm-specific transmembrane protein.* Dev Biol, 2005. **286**(1): p. 169-81.

82. Wilson, K.L., et al., *Sperm plasma membrane breakdown during Drosophila fertilization requires sneaky, an acrosomal membrane protein.* Development, 2006. **133**(24): p. 4871-9.

83. Grote, E., *Cell Fusion Assays for Yeast Mating Pairs.* 2008.

84. Bender, A. and G.F. Sprague, Jr., *Pheromones and pheromone receptors are the primary determinants of mating specificity in the yeast Saccharomyces cerevisiae.* Genetics Society of America, 1989. **121**: p. 463-476.

85. Duina, A.A., M.E. Miller, and J.B. Keeney, *Budding yeast for budding geneticists: a primer on the Saccharomyces cerevisiae model system.* Genetics, 2014. **197**(1): p. 33-48.

86. Shermann, F., *Getting Started with Yeast* Methods Enzymol., 2003. **350**: p. 3-41.

87. Merlini, L., O. Dudin, and S.G. Martin, *Mate and fuse: how yeast cells do it.* Open Biol, 2013. **3**(3): p. 130008.

88. Clark-Cotton, M.R., K.C. Jacobs, and D.J. Lew, *Chemotropism and Cell-Cell Fusion in Fungi.* Microbiol Mol Biol Rev, 2022. **86**(1): p. e0016521.

89. Sieber, B., J.M. Coronas-Serna, and S.G. Martin, *A focus on yeast mating: From pheromone signaling to cell-cell fusion.* Semin Cell Dev Biol, 2022.

90. Betz, R., V.L. MacKay, and W. Duntze, *α-factor from Saccharomyces cerevisiae- Partial characterization of a mating hormone produced by cells of mating type a.* J Bacteriol., 1977. **132**(2): p. 462-472.

91. Hagen, D.C., G. MCCaffery, and G.F. Sprague, Jr., *Evidence the yeast STE3 gene encodes a receptor for the peptide pheromone a factor: Gene sequence and implications for the structure of the presumed receptor.* Proc Natl Acad Sci, 1986. **83**: p. 1418-1422.

92. Jenness, D.D. and P. Spatrick, *Down regulation of the α-Factor pheromone receptor in S.cerevisiae.* Cell, 1986. **46**: p. 345-353.

93. Michaelis, S. and J. Barrowman, *Biogenesis of the Saccharomyces cerevisiae pheromone α-factor, from yeast mating to human disease.* Microbiol Mol Biol Rev, 2012. **76**(3): p. 626-51.

94. Jacobs, K.C. and D.J. Lew, *Pheromone Guidance of Polarity Site Movement in Yeast.* Biomolecules, 2022. **12**(4).

95. Bardwell, L., *A walk-through of the yeast mating pheromone response pathway.* Peptides, 2004. **25**(9): p. 1465-76.

96. Dohlman, H.G. and J.E. Slessareva, *Pheromone Signaling Pathways in Yeast.* Sci, STKE, 2006.

97. Tedford, K., et al., *Regulation of the mating pheromone and invasive growth responses in yeast by two MAP kinase substrates.* Cell Press, 1997. **7**(4): p. 228-238.

98. Herskowitz, I., *MAP kinase pathways in yeast: for mating and more.* Cell Press, 1995. **80**(2): p. 187-197.

99. Dorer, R., et al., *Genetic Analysis of Default Mating Behavior in Saccharomyces cerevisiae.* Genetics Society of America, 1997. **146**: p. 39-55.

100. Erdman, S., et al., *Pheromone-regulated genes required for yeast mating differentiation.* J Cell Biol, 1998. **140**(3): p. 461-83.

101. Sprague, G.F., Jr., and J. Thorner, *Pheromone Response and Signal Transduction during the Mating Process of Saccharomyces cerevisiae. In The Molecular Biology of the Yeast Saccharomyces.* Cold Spring Harbor Laboratory, Cold Spring Harbor, NY, 1992: p. 657–744.

102. Bagnat, M. and K. Simons, *Cell surface polarization during yeast mating.* Proc Natl Acad Sci U S A, 2002. **99**(22): p. 14183-8.

103. Mathelie-Guinlet, M., et al., *Single-cell fluidic force microscopy reveals stress-dependent molecular interactions in yeast mating.* Commun Biol, 2021. **4**(1): p. 33.

104. Zhao, H., et al., *Interaction of alpha-agglutinin and a-agglutinin, Saccharomyces cerevisiae sexual cell adhesion molecules.* J Bacteriol, 2001. **183**(9): p. 2874-80.

105. Lipke, P.N., D. Wojciechowicz, and J. Kurjan, *AG alpha 1 is the structural gene for the Saccharomyces cerevisiae alpha-agglutinin, a cell surface glycoprotein involved in cell-cell interactions during mating.* Mol Biol Cell, 1989. **9**(8): p. 3155-65.

106. Huberman, L.B. and A.W. Murray, *A model for cell wall dissolution in mating yeast cells: polarized secretion and restricted diffusion of cell wall remodeling enzymes induces local dissolution.* PLoS One, 2014. **9**(10): p. e109780.

107. Cappellaro, C., V. Mrsa, and W. Tanner, *New Potential Cell Wall Glucanases of Saccharomyces cerevisiae and Their Involvement in Mating.* J Bacteriol, 1998. **180**(19): p. 5030-5037.

108. Gammie, A.E., V. Brizzio, and M.D. Rose, *Distinct Morphological Phenotypes of Cell Fusion Mutants.* Mol Biol Cell, 1998. **9**: p. 1395-1410.

109. Nelson, B., et al., *Fus1p Interacts With Components of the Hog1p Mitogen-Activated Protein Kinase and Cdc42p Morphogenesis Signaling Pathways to Control Cell Fusion During Yeast Mating.* Genetics Society of America, 2003. **166**: p. 67-77.

110. Santos, B. and M. Snyder, *Specific protein targeting during cell differentiation: polarized localization of Fus1p during mating depends on Chs5p in Saccharomyces cerevisiae.* Eukaryot Cell, 2003. **2**(4): p. 821-5.

111. Barale, S., D. McCusker, and R.A. Arkowitz, *The exchange factor Cdc24 is required for cell fusion during yeast mating.* Eukaryot Cell, 2004. **3**(4): p. 1049-61.

112. Barale, S., D. McCusker, and R.A. Arkowitz, *Cdc42p GDP/GTP cycling is necessary for efficient cell fusion during yeast mating.* Mol Biol Cell, 2006. **17**(6): p. 2824-38.

113. Ydenberg, C.A., R.A. Stein, and M.D. Rose, *Cdc42p and Fus2p act together late in yeast cell fusion.* Mol Biol Cell, 2012. **23**(7): p. 1208-18.

114. Stein, R.A., J.A. Smith, and M.D. Rose, *An Amphiphysin-Like Domain in Fus2p Is Required for Rvs161p Interaction and Cortical Localization.* G3 (Bethesda), 2015. **6**(2): p. 337-49.

115. Smith, J.A., A.E. Hall, and M.D. Rose, *Membrane curvature directs the localization of Cdc42p to novel foci required for cell-cell fusion.* J Cell Biol, 2017. **216**(12): p. 3971-3980.

116. Trueheart, J. and G.R. Fink, *The yeast cell fusion protein FUS1 i O-glycosylated and spans the plasma membrane.* Cell Biology, 1989. **86**: p. 9916-9920.

117. Hall, A.E. and M.D. Rose, *Cell fusion in yeast is negatively regulated by components of the cell wall integrity pathway.* Mol Biol Cell, 2019. **30**(4): p. 441-452.

118. Grote, E., *Secretion is required for late events in the cell-fusion pathway of mating yeast.* Cell Science, 2010. **123**: p. 1902-1912.

119. Jin, H., J.M. McCaffery, and E. Grote, *Ergosterol promotes pheromone signaling and plasma membrane fusion in mating yeast.* J Cell Biol, 2008. **180**(4): p. 813-26.

120. Heiman, M.G. and W. P., *Prm1p, a Pheromone-regulated Multispanning Membrane Protein, Facilitates Plasma Membrane Fusion during Yeast Mating.* The Journal of Cell Biology, 2000. **151**(3): p. 719-730.

121. Olmo, V.N. and E. Grote, *Prm1 functions as a disulfide-linked complex in yeast mating.* J Biol Chem, 2010. **285**(4): p. 2274-83.

122. Olmo, V.N. and E. Grote, *Prm1 targeting to contact sites enhances fusion during mating in Saccharomyces cerevisiae.* Eukaryot Cell, 2010. **9**(10): p. 1538-48.

123. Jin, H., et al., *Prm1 prevents contact-dependent lysis of yeast mating pairs.* Eukaryot Cell, 2004. **3**(6): p. 1664-73.

124. Aguilar, P.S., A. Engel, and W. P., *The Plasma Membrane Proteins Prm1 and Fig1 Ascertain Fidelity of Membrane Fusion during Yeast Mating.* Molecular Biology of the Cell, 2007. **18**: p. 547-556.

125. Fleissner, A., S. Diamond, and N.L. Glass, *The Saccharomyces cerevisiae PRM1 homolog in Neurospora crassa is involved in vegetative and sexual cell fusion events but also has postfertilization functions.* Genetics, 2009. **181**(2): p. 497-510.

126. Fu, C. and J. Heitman, *PRM1 and KAR5 function in cell-cell fusion and karyogamy to drive distinct bisexual and unisexual cycles in the Cryptococcus pathogenic species complex.* PLoS Genet, 2017. **13**(11): p. e1007113.

127. Curto, M.A., et al., *Membrane organization and cell fusion during mating in fission yeast requires multipass membrane protein Prm1.* Genetics, 2014. **196**(4): p. 1059-76.

128. Engel, A., P.S. Aguilar, and P. Walter, *The Yeast Cell Fusion Protein Prm1p Requires Covalent Dimerization to Promote Membrane Fusion.* Mol Biol Cell, 2010. **18**: p. 547-556.

129. Clemente-Ramos, J.A., et al., *The tetraspan protein Dni1p is required for correct membrane organization and cell wall remodelling during mating in Schizosaccharomyces pombe.* Mol Microbiol, 2009. **73**(4): p. 695-709.

130. Iida, H., Y. Yagawa, and Y. Anraku, *Essential role for induced Ca2+ influx followed by [Ca2+]i rise in maintaining viability of yeast cells late in the mating pheromone response pathway. A study of [Ca2+]i in single Saccharomyces cerevisiae cells with imaging of fura-2.* Journal of Biological Chemistry, 1990. **265**(22): p. 13391-13399.

131. Muller, E.M., et al., *Fig1p facilitates Ca2+ influx and cell fusion during mating of Saccharomyces cerevisiae.* J Biol Chem, 2003. **278**(40): p. 38461-9.

132. Cyert, M.S. and C.C. Philpott, *Regulation of cation balance in Saccharomyces cerevisiae.* Genetics, 2013. **193**(3): p. 677-713.

133. Julius, D., et al., *Isolation of the putative structural gene for the lysine-arginine-cleaving endopeptidase required for processing of yeast prepro-alpha-factor.* Cell, 1984. **37**(3): p. 1075-1089.

134. Fuller, R.S., A. Brake, and J. Thorner, *Yeast prohormone processing enzyme (KEX2 gene product) is a Ca2+-dependent serine protease. Proc Natl Acad Sci U S A 86(5):1434-8.* Proc Natl Acad Sci, 1989. **86**: p. 1434-1438.

135. Heiman, M.G., A. Engel, and P. Walter, *The Golgi-resident protease Kex2 acts in conjunction with Prm1 to facilitate cell fusion during yeast mating.* J Cell Biol, 2007. **176**(2): p. 209-22.

136. David Julius, L.B., * Anthony Brake,** and G.S.a.J. Thorner*, *Yeast alpha-factor is processed from a larger precursor polypeptide - The essential role of a membrane-bound dipeptidyl aminopeptidase.* Cell, 1983. **32**: p. 839-852.

137. Fuller, R.S., R.E. Sterne, and J. Thorner, *Enzymes required for yeast prohormone processing.* Ann Rev Physiol, 1988. **50**: p. 345-362.

138. Henderson, C.M. and D.E. Block, *Examining the role of membrane lipid composition in determining the ethanol tolerance of Saccharomyces cerevisiae.* Appl Environ Microbiol, 2014. **80**(10): p. 2966-72.

139. Jorda, T. and S. Puig, *Regulation of Ergosterol Biosynthesis in Saccharomyces cerevisiae.* Genes (Basel), 2020. **11**(7).

140. Aguilar, P.S., et al., *Structure of sterol aliphatic chains affects yeast cell shape and cell fusion during mating.* Proc Natl Acad Sci U S A, 2010. **107**(9): p. 4170-5.

141. Weichert, M., et al., *Accumulation of specific sterol precursors targets a MAP kinase cascade mediating cell-cell recognition and fusion.* Proc Natl Acad Sci U S A, 2016. **113**(42): p. 11877-11882.

142. Mohammadi, S., et al., *Scope and limitations of yeast as a model organism for studying human tissue-specific pathways.* BMC Syst Biol, 2015. **9**: p. 96.

143. Oren-Suissa, M. and B. Podbilewicz, *Evolution of programmed cell fusion: common mechanisms and distinct functions.* Dev Dyn, 2010. **239**(5): p. 1515-28.

144. Michael Knop, K.S., Gislene Pereira, Wolfgang Zachariae, Barbara Winsor, Kim Nasmyth, Elmar Schiebel, *Epitope tagging of yeast genes using a PCR-based strategy more tags and improved practical routines.* Yeast, 1999. **15**(10B): p. 963-972.

145. Janke, C., et al., *A versatile toolbox for PCR-based tagging of yeast genes: new fluorescent proteins, more markers and promoter substitution cassettes.* Yeast, 2004. **21**(11): p. 947-62.

146. Cohen, Y. and M. Schuldiner, *Advanced methods for high-throughput microscopy screening of genetically modified yeast libraries.* Methods Mol Biol, 2011. **781**: p. 127-59.

147. Tong, A.H.Y. and C. Boone, *Synthetic Genetic Array Analysis in Saccharomyces cerevisiae.* Humana Press Inc., 2006. **313**: p. 171-191.

148. Salzman, V., et al., *Quantitation of yeast cell-cell fusion using multicolor flow cytometry.* Cytometry A, 2015. **87**(9): p. 843-54.

149. Trueheart, J., J.D. Boeke, and G.R. Fink, *Two Genes Required for Cell Fusion during Yeast Conjugation: Evidence for a Pheromone-Induced Surface Protein.* Molecular and Cellular Biology, 1987. **7**(7): p. 2316-2328.

150. Maxwell, G.H. and P. Water, *Prm1p, a Pheromone-regulated Multispanning Membrane Protein, Facilitates Plasma Membrane Fusion during Yeast Mating.* The Journal of Cell Biology, 2000. **151**(3): p. 719-730.

151. Aguilar, P.S., A. Engel, and P. Walter, *The plasma membrane proteins Prm1 and Fig1 ascertain fidelity of membrane fusion during yeast mating.* Mol Biol Cell, 2007. **18**(2): p. 547-56.

152. Nolan, S., et al., *FUS1 regulates the opening and expansion of fusion pores between mating yeast.* Mol Biol Cell, 2006. **17**(5): p. 2439-50.

153. Brizzio, A., et al., *Cell Fusion during Yeast Mating Requires High Levels of a-Factor Mating Pheromone.* The Journal of Cell Biology, 1996. **135**(6): p. 1727-1739.

154. Zhang, M., D. Bennett, and S.E. Erdman, *Maintenance of Mating Cell Integrity Requires the Adhesin Fig2p.* Eukaryotic Cell, 2002. **1**(5): p. 811-822.

155. Futai, M., et al., *Luminal acidification of diverse organelles by V-ATPase in animal.* The Journal of Experimental Biology, 2000. **203**: p. 107-116.

156. Willer, T., et al., *Protein O-mannosylation is crucial for cell wall integrity, septation and viability in fission yeast.* Mol Microbiol, 2005. **57**(1): p. 156-70.

157. Marianne A.A.van Berkel, et al., *The Saccharomyces cerevisiae CWH8 gene is required for full levels of dolichol-linked oligosaccharides in the endoplasmic reticulum for efficient N-glucosylation.* Glycobiology, 1999. **9**(3): p. 243-253.

158. Claude Nuoffer, et al., *Determinants for glycophospholipid anchoring of the Saccharomyces cerevisiae GAS1 protein to the plasma membrane.* Molecular and Cell Biology, 1991. **11**(1): p. 27-37.

159. David Feldheim, K.Y., Arie Admon, and a.R. Schekman, *Structural and Functional Characterization of Sec66p, a New Subunit of the Polypeptide Translocation Apparatus in the Yeast Endoplasmic Reticulum.* Mol Biol Cell, 1993. **4**: p. 931-939.

160. Bonangelino, C.J., E.M. Chavez, and J.S. Bonifacino, *Genomic Screen for Vacuolar Protein Sorting Genes in Saccharomyces cerevisiae.* Mol Biol Cell, 2002. **13**: p. 2486-2501.

161. Cotter, K., et al., *Recent Insights into the Structure, Regulation, and Function of the V-ATPases.* Trends Biochem Sci, 2015. **40**(10): p. 611-622.

162. Nelson, H. and N. Nelson, *Disruption of genes encoding subunits of yeast vacuolar H+-ATPase causes conditional lethality.* Cell Biology, 1990. **87**: p. 3503-3507.

163. Ohya, Y., N. Umemoto, I. Tanida, A. Ohta, H. Iida, and Y. Anraku, *Calcium-sensitive cls mutants of Saccharomyces cerevisiae showing a Pet- phenotype are ascribable to defects of vacuolar membrane H.* The Journal of Biological Chemistry, 1991. **266**: p. 13971-13977.

164. Sambade, M., et al., *A genomic screen for yeast vacuolar membrane ATPase mutants.* Genetics, 2005. **170**(4): p. 1539-51.

165. Diakov, T.T. and P.M. Kane, *Regulation of vacuolar proton-translocating ATPase activity and assembly by extracellular pH.* J Biol Chem, 2010. **285**(31): p. 23771-8.

166. Jacquier, N., et al., *Expression of oleosin and perilipins in yeast promotes formation of lipid droplets from the endoplasmic reticulum.* J Cell Sci, 2013. **126**(Pt 22): p. 5198-209.

167. Kanneganti, V., R. Kama, and J.E. Gerst, *Btn3 is a negative regulator of Btn2-mediated endosomal protein trafficking and prion curing in yeast.* Mol Biol Cell, 2011. **22**(10): p. 1648-63.

168. Breitling, J. and M. Aebi, *N-linked protein glycosylation in the endoplasmic reticulum.* Cold Spring Harb Perspect Biol, 2013. **5**(8): p. a013359.

169. Chasse, S.A., et al., *Genome-scale analysis reveals Sst2 as the principal regulator of mating pheromone signaling in the yeast Saccharomyces cerevisiae.* Eukaryot Cell, 2006. **5**(2): p. 330-46.

170. Jeronimo, C. and F. Robert, *The Mediator Complex: At the Nexus of RNA Polymerase II Transcription.* Trends Cell Biol, 2017. **27**(10): p. 765-783.

171. Soutourina, J., *Transcription regulation by the Mediator complex.* Nat Rev Mol Cell Biol, 2018. **19**(4): p. 262-274.

172. Zhu, X., et al., *Mediator tail subunits can form amyloid-like aggregates in vivo and affect stress response in yeast.* Nucleic Acids Res, 2015. **43**(15): p. 7306-14.

173. Chan, R.K. and C.A. Otte, *Isolation and Genetic Analysis of Saccharomyces cerevisiae Mutants Supersensitive to G1 Arrest by a Factor and alpha Factor Pheromones* Mol Biol Cell, 1981. **2**(1): p. 11-20.

174. Proszynski, T.J., K. Simons, and M. Bagnat, *O-glycosylation as a sorting determinant for cell surface delivery in yeast* Mol Biol Cell, 2004. **15**(4): p. 1533-1543.

175. Gelin-Licht, R., et al., *Translational control as a novel regulator of gradient sensing and chemotropism in yeast.* bioRxiv, 2021.

176. Jackson, C.L. and L.H. Hartwell, *Courtship in S. cerevisiae- Both cell types choose mating partners by responding to the strongest pheromone signal.* Cell, 1990. **63**: p. 1039-1051.

177. Stevens, T.H., *Structure, function and regulation of the vacuolar (H+)-ATPase.* Rev Cell Dev Biol, 1997. **13**: p. 779-808.

178. Y.E., O. and P.M. Kane, *Mutations in the yeast KEX2 gene cause a VMA- like phenotype: a possible role for the Kex2 endoprotease in vacuolar acidification.* Molecular and Cellular Biology, 1998. **18**: p. 1534-1543.

179. Velivela, S.D. and P.M. Kane, *Compensatory Internalization of Pma1 in V-ATPase Mutants in Saccharomyces cerevisiae Requires Calcium- and Glucose-Sensitive Phosphatases.* Genetics, 2018. **208**(2): p. 655-672.

180. Wang, L., et al., *Structures of a Complete Human V-ATPase Reveal Mechanisms of Its Assembly.* Mol Cell, 2020. **80**(3): p. 501-511 e3.

181. Li, S.C., et al., *Vacuolar H+-ATPase works in parallel with the HOG pathway to adapt Saccharomyces cerevisiae cells to osmotic stress.* Eukaryot Cell, 2012. **11**(3): p. 282-91.

182. Milgrom, E., et al., *Loss of vacuolar proton-translocating ATPase activity in yeast results in chronic oxidative stress.* J Biol Chem, 2007. **282**(10): p. 7125-36.

183. Kane, P.M., *The where, when, and how of organelle acidification by the yeast vacuolar H+-ATPase.* Microbiol Mol Biol Rev, 2006. **70**(1): p. 177-91.

184. Plant, P.J., et al., *Alternative mechanisms of vacuolar acidification in H(+)-ATPase-deficient yeast.* J Biol Chem, 1999. **274**(52): p. 37270-9.

185. Perez-Castineira, J.R., et al., *A plant proton-pumping inorganic pyrophosphatase functionally complements the vacuolar ATPase transport activity and confers bafilomycin resistance in yeast.* Biochem J, 2011. **437**(2): p. 269-78.

186. Desfougeres, Y., et al., *Organelle acidification negatively regulates vacuole membrane fusion in vivo.* Sci Rep, 2016. **6**: p. 29045.

187. Kontani, K., I.P. Moskowitz, and J.H. Rothman, *Repression of cell-cell fusion by components of the C. elegans vacuolar ATPase complex.* Dev Cell, 2005. **8**(5): p. 787-94.

188. Smurova, K. and B. Podbilewicz, *Endocytosis regulates membrane localization and function of the fusogen EFF-1.* Small GTPases, 2017. **8**(3): p. 177-180.

189. Li, S.C. and P.M. Kane, *The yeast lysosome-like vacuole: endpoint and crossroads.* Biochim Biophys Acta, 2009. **1793**(4): p. 650-63.

190. Ryan, M., L.A. Graham, and T.H. Stevens, *Voa1p Functions in V-ATPase Assembly in the Yeast Endoplasmic Reticulum. .* Mol Biol Cell, 2008. **19**: p. 5131-5142.

191. Pittet, M., et al., *The N-glycosylation defect of cwh8Delta yeast cells causes a distinct defect in sphingolipid biosynthesis.* Glycobiology, 2006. **16**(2): p. 155-64.

192. James, A.W., R. Gowsalya, and V. Nachiappan, *Dolichyl pyrophosphate phosphatase-mediated N-glycosylation defect dysregulates lipid homeostasis in Saccharomyces cerevisiae.* Biochim Biophys Acta, 2016. **1861**(11): p. 1705-1718.

193. Zhang, Y.Q., et al., *Requirement for ergosterol in V-ATPase function underlies antifungal activity of azole drugs.* PLoS Pathog, 2010. **6**(6): p. e1000939.

194. Vasanthakumar, T., et al., *Structural comparison of the vacuolar and Golgi V-ATPases from Saccharomyces cerevisiae.* Proc Natl Acad Sci U S A, 2019. **116**(15): p. 7272-7277.

195. Santos-Pereira, C., L.R. Rodrigues, and M. Corte-Real, *Emerging insights on the role of V-ATPase in human diseases: Therapeutic challenges and opportunities.* Med Res Rev, 2021. **41**(4): p. 1927-1964.

196. Aitchison, J.D. and M.P. Rout, *The yeast nuclear pore complex and transport through it.* Genetics, 2012. **190**(3): p. 855-83.

197. M Künzler, J.T., C Sette, E Hurt, and J Thorner, *Mutations in the YRB1 gene encoding yeast ran-binding-protein-1 that impair nucleocytoplasmic transport and suppress yeast mating defects.* Genetics, 2001. **157**(3): p. 1089-1105.

198. Shimada, Y., M.P. Gulli, and M. Peter, *Nuclear sequestration of the exchange factor Cdc24 by Far1 regulates cell polarity during yeast mating.* Nat Cell Biol, 2000. **2**(2): p. 117-124.

199. Kawasaki, M.-S., D. Botstein, and Y. Ohya, *Identification of Functional Connections Between Calmodulin and the Yeast Actin Cytoskeleton.* Genetics Society of America, 1998. **150**: p. 43-58.

200. Burda, B. and M. Aebi, *The dolichol pathway of N-linked glycosylation.* Biochimica et Biophysica Acta, 1999. **1426**: p. 239-257.

201. Szkopifiska, A., et al., *The deficiency of sterol biosynthesis affects synthesis of glycosyl derivates of dolichyl phosphatates.* **FEMS Microbiology Letters**, 1993. **112**: p. 325*328.

202. Fei, W., et al., *Genome-wide analysis of sterol-lipid storage and trafficking in Saccharomyces cerevisiae.* Eukaryot Cell, 2008. **7**(2): p. 401-14.

203. Huang, J., et al., *Lipid Droplet Metabolism Across Eukaryotes: Evidence from Yeast to Humans.* Journal of Evolutionary Biochemistry and Physiology, 2020. **56**(5): p. 396-405.

204. Leber, R., et al., *Dual Localization of Squalene Epoxidase, Erg1p, in Yeast Reflects a Relationship between the Endoplasmic Reticulum and Lipid Particles. .* Mol Biol Cell, 1998. **9**: p. 375–386.

205. Fernandez, F., et al., *The CWH8 gene encodes a dolichyl pyrophosphate phosphatase with a luminally oriented active site in the endoplasmic reticulum of Saccharomyces cerevisiae.* J Biol Chem, 2001. **276**(44): p. 41455-64.

206. Heller, L., P. Orlean, and W.L. Adair, Jr., *Saccharomyces cerevisiae sec59 cells are deficient in dolichol kinase activity.* Proc Natl Acad Sci, 1992. **89**: p. 7013-7016.

207. Wu, B., et al., *Synthesis of a Comprehensive Polyprenol Library for Evaluation of Bacterial Enzyme Lipid Substrate Specificity.* European J Org Chem, 2013. **2013**(36): p. 8162-8173.

208. Carlson, M., *Genetics of transcriptional regulation in yeast - connections to the RNA polymerase II CTD.* Annu. Rev. Cell Dev, Biol., 1997. **13**: p. 1-23.

209. Biddick, R. and E.T. Young, *Yeast mediator and its role in transcriptional regulation.* C R Biol, 2005. **328**(9): p. 773-82.

210. Verger, A., D. Monte, and V. Villeret, *Twenty years of Mediator complex structural studies.* Biochem Soc Trans, 2019. **47**(1): p. 399-410.

211. Richter, W.F., et al., *The Mediator complex as a master regulator of transcription by RNA polymerase II.* Nat Rev Mol Cell Biol, 2022. **23**(11): p. 732-749.

212. Niederberger, T., et al., *MC EMiNEM maps the interaction landscape of the Mediator.* PLoS Comput Biol, 2012. **8**(6): p. e1002568.

213. Allen, B.L. and D.J. Taatjes, *The Mediator complex: a central integrator of transcription.* Nat Rev Mol Cell Biol, 2015. **16**(3): p. 155-66.

214. Nishizawa, M., et al., *Yeast Gal11 protein mediates the transcriptional activation signal of two different transacting factors, Gal4 and general regulatory factor I repressor activator site binding protein 1 translation upstream factor.* Proc Natl Acad Sci, 1990. **87**: p. 5373-5377.

215. Piruat, J.I., S. Chavez, and A. Aguilera, *The Yeast HRSl Gene Is Involved in Positive and Negative Regulation of Transcriptionand Shows Genetic Characteristics Similarto SIN 4and GAL11.* Genetics Society of America, 1997. **147**: p. 1585-1594.

216. Nelson, C., et al., *Srb10 Cdk8 regulates yeast filamentous growth by phosphorylating the transcription factor Ste12.* letters to nature, 2003. **421**: p. 187-190.

217. Zhou, W., et al., *Binding and Regulation of Transcription by Yeast Ste12 Variants To Drive Mating and Invasion Phenotypes.* Genetics, 2020. **214**(2): p. 397-407.

218. White, J.M. and M.D. Rose, *Yeast mating: Getting close to membrane merger.* Current Biology, 2001. **11**: p. R16-R20.

219. William James, A., et al., *Crosstalk between protein N-glycosylation and lipid metabolism in Saccharomyces cerevisiae.* Sci Rep, 2019. **9**(1): p. 14485.

220. Dudin, O., et al., *A systematic screen for morphological abnormalities during fission yeast sexual reproduction identifies a mechanism of actin aster formation for cell fusion.* PLoS Genet, 2017. **13**(4): p. e1006721.

221. Weichert, M., et al., *Plasma Membrane Fusion Is Specifically Impacted by the Molecular Structure of Membrane Sterols During Vegetative Development of Neurospora crassa.* Genetics, 2020. **216**(4): p. 1103-1116.

222. Barbaux, S., et al., *Sperm SPACA6 protein is required for mammalian Sperm-Egg Adhesion/Fusion.* Sci Rep, 2020. **10**(1): p. 5335.

223. Rush, J.S., et al., *Identification and characterization of a cDNA encoding a dolichyl pyrophosphate phosphatase located in the endoplasmic reticulum of mammalian cells.* J Biol Chem, 2002. **277**(47): p. 45226-34.

Publications and conferences

Publications

Hagemeier A., Kratzenberg L., Hernandez J.M., A genetic interaction network involved in cell-cell fusion during the mating of *S. cerevisiae*. **Manuscript in preparation.**

Conferences

Jun 2022: **Cell-Cell Fusion Gordon Research Conference**

Easton, MA, USA

Contribution: Poster presentation

Title: Discovery of novel cell fusion mutants during the mating of *Saccharomyces cerevisiae*

Apr 2021: **8th IMPRS-LM Student's Symposium**

Max Planck Institute of Molecular Physiology, Dortmund

Contribution: Virtual poster presentation

Title: A genetic interaction network for cell fusion during the mating of *Saccharomyces cerevisiae*

Aug 2019: **29th International Conference on Yeast Genetics and Molecular Biology**

Gothenburg, Sweden

Contribution: Poster presentation

Title: Uncovering genes involved in cell-cell fusion during the mating of yeast

Acknowledgements

I am profoundly grateful to Dr. Matias Hernandez for recognizing my potential and offering me the opportunity to join his research group. Throughout my PhD journey, his unwavering support and open-door policy have been invaluable. I have always felt his genuine desire to bring out the best in me, pushing me to exceed my own expectations. His mentorship has been instrumental in my growth as a researcher, constantly reminding me to look at the bigger picture and to approach challenges with resilience and creativity.

I sincerely thank Prof. Dr. Stefan Raunser for serving as my first referee and creating a motivating and inspiring atmosphere within the department. I also like to express my appreciation for the financial support that has enabled me to carry out my work effectively.

Many thanks to Prof. Dr. Stefan Westermann for his support as both my second referee and mentor during the TAC meetings. I thank for his guidance, constructive feedback and insightful suggestions towards the project.

I would like to extend my heartfelt thanks to my closest lab mates Dr. Sheila Mainye, Dr. Anson Shek, Diana Ludwig and Lisa Kratzenberg. I am grateful for the support, laughter, and shared experiences we have had. Thank you for being a part of my journey and for making it truly memorable.

Many thanks to all my colleagues in Department 3 for creating a welcoming and supportive atmosphere throughout my time. Special thanks to the former Neumann-Group & all members of the “Happy Office”, Nathalie Bleimling, Dr. Sebastian Tacke, Dr. Alexander Belyy and Dr. Sabrina Pospich.

I would like to extend my heartfelt gratitude to Dr. Raphael Gasper-Schoenenbruecher for his open ear, Davide Tamborrini for being a constant source of inspiration and Dr. Farid Ghasemalizadeh for his exceptional kindness and sense of humor.

Thanks to the IMPRS coordinators Dr. Lucia Sironi and Christa Hornemann. Their support has been invaluable in shaping my academic career, and I am truly grateful for their contributions.

Lastly, I would like to express my deepest gratitude to my friends and family for being my unwavering support system throughout my PhD journey. Your love, encouragement, and understanding have been a constant source of strength for me.